INAUGURAL – DISSERTATION

zur

Erlangung der Doktorwürde

der

Naturwissenschaftlich-Mathematischen

Gesamtfakultät

der

Ruprecht-Karls-Universität

Heidelberg

vorgelegt von

Kirill Yu. Monakhov (M.Sc.)

aus Moskau, Russland

Tag der mündlichen Prüfung: 2. Juli 2010

Experimental and Theoretical Study of the Polynuclear Bismuth Compounds – Dimers, Clusters, Molecular Self-Assemblies and Polyhedral Cage Molecules

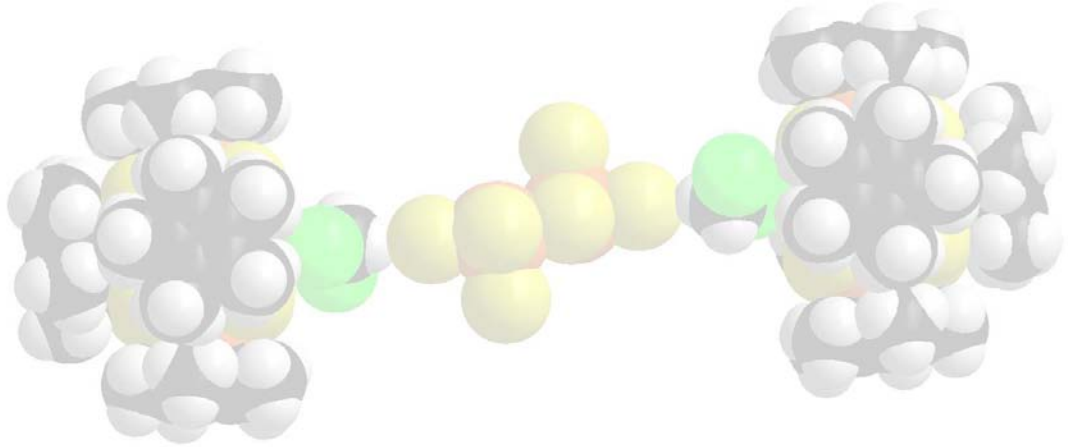

Gutachter: Prof. Dr. Gerald Linti

Prof. Dr. Hans-Jörg Himmel

Die vorliegende Arbeit wurde in der Zeit von November 2007 bis Mai 2010 am Institut für Anorganische Chemie der Ruprecht-Karls-Universität Heidelberg unter Anleitung von Herrn Prof. Dr. Gerald Linti durchgeführt.

Meinen Eltern und Großeltern, meinem Bruder,
Mariam und ihrer Mutter Irène gewidmet

«Die wahre Wissenschaft und das wahre Studium des Menschen ist der Mensch»

Pierre Charron,
»Le traité de la sagesse«

List of Publications

Following topics of this thesis are prepared to be published:

11. Aromaticity of indium and bismuth cluster compounds.
G. Linti, K. Yu. Monakhov, M. Bühler, T. Zessin, *Graduate College 850 Book* **2010**, manuscript in preparation.

10. Molecular self-assemblies based on $(C_5Me_5)BiX_2$ units (X = halogen): synthesis, X-ray crystal structures and quantum chemical study.
K. Yu. Monakhov, T. Zessin, G. Linti, manuscript in preparation.

9. Seven-vertex cage cluster $Bi_4[\mu_3\text{-}Fe(CO)_3]_3$ with π-coordinated aromatic ligands and inverted sandwich behavior in the crystal.
K. Yu. Monakhov, T. Zessin, G. Linti, manuscript in preparation.

Following topics of this thesis have been published during the doctorate period:

8. Cubane-like bismuth-iron cluster: synthesis, X-ray crystal structure and theoretical characterization of $[Bi_4Fe_8(CO)_{28}]^{4-}$ anion.
K. Yu. Monakhov, T. Zessin, G. Linti, *Eur. J. Inorg. Chem.* **2010**, in print.

7. Reduction *vs.* metathesis in the reactions of bismuth tribromide with bulky lithium silanide – an experimental and theoretical study.
K. Yu. Monakhov, T. Zessin, G. Linti, *Eur. J. Inorg. Chem.* **2010**, 322–332.

6. Theoretical study of structure, bonding and electronic behavior of low-valent bismuth cyclopentadienyl and pentamethylcyclopentadienyl half-sandwich compounds.
K. Yu. Monakhov, G. Linti, *Inorg. Chem.* **2009**, *48*, 6986–6996.

Following topics based on works in the group 13 metals have been published or submitted:

5. Linked cluster compounds "transition metal - group 13 metals": synthesis, structure characterization and DFT study.
E. V. Grachova, G. Linti, K. Yu. Monakhov, T. Zessin, *Eur. J. Inorg. Chem.* **2010**, submitted.

4. Synthesis and structure of Tri- and octaindium compounds.
G. Linti, M. Bühler, K. Yu. Monakhov, T. Zessin, *Dalton Trans.* **2009**, 8071–8078.

Following topics have been published during the master period:

3. Synthesis and solution behavior of the trinuclear palladium(II) unsaturated carboxylate complexes *triangle*-$Pd_3[\mu\text{-}OCO(R')C{=}CHMe]_6$ (R' = Me, H), and X-ray structure of palladium(II) tiglate (R' = Me).
   T. A. Stromnova, K. Yu. Monakhov, J. Cámpora, P. Palma, E. Carmona, E. Álvarez, *Inorg. Chim. Acta* **2007**, *360*, 4111–4116.

2. A quantum-chemical study of donor-acceptor properties of carboxylic acids and their anions, and evaluation of the effect of these properties on geometric and spectroscopic parameters of palladium(II) carboxylates.
   K. Yu. Monakhov, T. A. Stromnova, *Russ. J. Gen. Chem.* **2007**, *77*, 1841–1849; **2008**, *77*, 1896–1903 (Engl. Transl.).

1. Palladium(I) carbonyl carboxylate clusters *cyclo*-$[Pd_2(\mu\text{-}CO)_2(\mu\text{-}OCOR)_2]_n$ (*n* = 2 or 3): structure and reactivity.
   T. A. Stromnova, O. N. Shishilov, M. V. Dayneko, K. Yu. Monakhov, A. V. Churakov, L. G. Kuz'mina, J. A. K. Howard, *J. Organomet. Chem.* **2006**, *691*, 3730–3736.

Talks and Poster Presentations

1. K. Yu. Monakhov, T. Zessin, G. Linti. – "Polyhedral bismuth cages stabilized by organic and inorganic ligands". // *Challenges in Inorganic and Materials Chemistry*, 20–23 July **2010**, Hong Kong, China.

2. K. Yu. Monakhov, G. Linti. – "Theoretical study of structure, bonding and electronic behavior of low-valent bismuth cyclopentadienyl and pentamethylcyclopentadienyl half-sandwich compounds". // *Summer School in Computational Chemistry*, 22–26 September **2009**, Essen, Germany.

3. K. Yu. Monakhov, G. Linti, E. V. Grachova. – "The problem of metal centers interaction in mixed-metal bridging complexes containing transition metal and group 13 metal". // *XXIVth International Chugaev Conference on Coordination Chemistry*, 15–19 June **2009**, St. Petersburg, Russia. Book of Abstracts, p. 414.

4. K. Yu. Monakhov, G. Linti. – "The precursors for the synthesis of indium and bismuth silyl-substituted compounds". // *VIth International Congress of Young Chemists*, 15–19 October **2008**, Cracow, Poland. Book of Abstracts, p. 131.

5. K. Yu. Monakhov, G. Linti. – "Theoretical investigation of Bi···C_5R_5 (R = H, Me) interactions in bismuth (I, III, V) cyclopentadienyl and pentamethylcyclopentadienyl complexes". // *44th Symposium on Theoretical Chemistry*, 23–27 September, **2008**, Ramsau am Dachstein, Austria. Book of Abstracts, P-15.

6. K. Yu. Monakhov, T. A. Stromnova. – "Prochiral palladium carboxylates: synthesis, structures and properties". // *XXIIIth International Chugaev Conference on Coordination Chemistry*, 4–7 September **2007**, Odessa, Ukraine. Book of Abstracts, pp. 540–541.

7. K. Yu. Monakhov, T. A. Stromnova. – "Unsaturated carboxylic acids as polyfunctional ligands in chemistry of the platinum metals". // *The XIVth International Scientific Conference for Undergraduate and Postgraduate Students, and Young Scientists «Lomonosov-2007»*, 11–14 April **2007**, Moscow, Russia. Book of Abstracts, p. 252.

Danksagung

Zuallererst möchte ich mich ganz herzlich bei meinem Doktorvater **Prof. Dr. Gerald Linti** für die interessante Themenstellung und die wissenschaftlichen Freiheiten, für das fortwährende Interesse an meiner Arbeit und die wissenschaftliche Förderung bedanken.

Auch bedanke ich mich bei meinen Laborkollegen, namentlich **Thomas Zessin, Philipp Butzug, Dominik Scheid, Marc Herrmann, Dr. Tobias Adamczyk**, **Dr. Annekathrin Seifert** und **Dr. Ovidiu Feier-Iova** für ein produktives und angenehmes Arbeiten und für das freundliche Arbeitsklima. Insbesondere möchte ich **Thomas** und **Philipp** für ihre Hilfe bei den alltäglichen Problemen im Labor und für das Messen und die Lösung der Röntgenstrukturen „*Vielen Dank*“ sagen.

Frau Dr. Elena Grachova (Department of Chemistry, St. Petersburg State University) und **Herrn Dr. Alexander A. Auer** (Atomistic Modeling Group, Max Planck Institute for Iron Research in Düsseldorf) danke ich für die hilfsreichen Diskussionen zu meiner Chemie und die wertvollen Ratschläge. Bei **Frau Dr. Elena Grachova** bedanke ich mich nochmals für eine produktive Zusammenarbeit im Bereich Übergangsmetalle und Hauptgruppenelemente.

Herzlichen Dank an **Frau Karin Stelzer** und **Frau Marlies Schönebeck-Schilli** für die groβe Hilfe und Unterstützung bei allen Verwaltungsangelegenheiten.

Vielen Dank auch allen, die direkt oder indirekt zum Gelingen der Arbeit beigetragen haben: meinem Forschungspraktikanten **Johannes Straub**; allen Mitarbeitern der chemischen Institute, insbesondere **Herrn Dr. Jürgen Gross** und seinen Mitarbeitern für die Massenspektrometrie-daten; **Frau Beate Termin** für das Messen der NMR-Spektren; dem gesamten **Arbeitskreis „Comba“** für eine gute Atmosphäre am Institut für Anorganische Chemie und ihre Hilfsbereitschaft; allen **Mitgliedern des Graduiertenkollegs 850** für eine schöne gemeinsame Zeit im Studium.

Des Weiteren bedanke ich mich bei dem **Graduiertenkolleg 850 der Deutschen Forschungsgemeinschaft** für das Stipendium.

Schließlich gilt mein ganz besonders herzlicher Dank meinen Eltern **Natalia** und **Yuri Monakhov**, meinem Bruder **Artem**, meinen Groβeltern, meiner schönen Freundin **Mariam Mainguy** und ihrer Mutter **Irène Mainguy**, die mir durch ihre moralische Unterstützung während meiner wissenschaftlichen Arbeit in Heidelberg geholfen haben.

Contents

Abbreviations and Symbols

av.	average	M	metal
Bu	butyl	Me	methyl CH_3
Cp	cyclopentadienyl	Mes	mesityl $C_6H_2(CH_3)_3$
Cp*	pentamethylcyclopentadienyl	ml	milliliter
deg	degree	mmol	millimole
E	element	Ph	phenyl C_6H_5
eq.	equation	pm	picometer
eV	electron volt	R	substituent
Et	ethyl C_2H_5	r.t.	room temperature
Fig.	Figure	r_{vdw}	van der Waals radii
g	gram	Tab.	Table
h	hour(s)	*t*Bu	*tert*-butyl
*i*Pr	isopropyl	thf	tetrahydrofuran
K	Kelvin degree	X	halogen
kcal/mol	kilocalorie per mole	°	degree (temperature and angle)
kJ/mol	kilojoule per mole	~	approximately
L	ligand	τ	dihedral angle

Elemental Analysis (EA)		*Nuclear Magnetic Resonance (NMR)*	
calcd.	calculated	δ	chemical shift
Infrared Spectroscopy (IR)		m	multiplet
m	medium	ppm	parts per million
s	strong	s	singlet
$\tilde{\nu}$	frequency (in cm^{-1})	TMS	tetramethylsilane $SiMe_4$
w	weak	*Ultraviolet-Visible Spectrophotometry (UV/Vis)*	
Mass Spectrometry (MS)		λ	wavelength
EI	Electron Ionization	CT	Charge Transfer
ESI	Electron Spray Ionization	LMCT	Ligand–Metal Charge Transfer
LIFDI	Liquid Injection Field Desorption/Ionization	MMCT	Metal–Metal Charge Transfer
		nm	nanometer
M^+	molecular ion		
m/z	mass-to-charge ratio		

Quantum Chemical Calculations			
DFT	Density Functional Theory	NHO	Natural Hybrid Orbital
G	Gauss	NICS	Nucleus-Independent Chemical Shift
HOMO	Highest Occupied Molecular Orbital	NLMO	Natural Localized Molecular Orbital
IP	Ionization Potential	NPA	Natural Population Analysis
LP	Lone Pair	OOv	Order of Orbital Overlapping
LUMO	Lowest Unoccupied Molecular Orbital	TD-DFT	Time-Dependent Density Functional Theory
NBO	Natural Bond Orbital	WBI	Wiberg Bond Index

Abstract

In the framework of this thesis, the polynuclear bismuth chemistry has been investigated from different perspectives with the main focus on four types of the chemical bonding. Thus, the section of bismuth–bismuth bonding affects redox/metathesis reactions of $BiBr_3$ with bulky lithium silanide $Li(thf)_3SiPh_2tBu$ in three different ratios, leading to the formation of a Bi–Bi bonded compound, $(tBuPh_2Si)_4Bi_2$ as one of the reaction products. The quantum chemical study has been mainly performed to shed light on the processes of oligomerisation of $R_2Bi^{\cdot}$ radicals and bismuth dimers. That is a major challenge in the context of "thermochromicity" and "closed-shell interactions" in inorganic chemistry of organobismuth compounds with homonuclear Bi–Bi bonds. The section of bismuth–transition-metal bonding gives a deep insight into the structures, the chemical bonding and the electronic behavior of heteronuclear bulky Bi–Fe cage-like clusters, cubic $[Bi_4Fe_8(CO)_{28}]^{4-}$ and seven-vertex $[Bi_4Fe_3(CO)_9]$, on the experimental and theoretical level. The section of bonding in bismuth–cyclopentadienyl compounds represents a detailed theoretical and experimental study of molecular systems based on cyclopentadienyl bismuth units such as $(C_5R_5)Bi^{2+}$, $[(C_5R_5)Bi]_n$ and $(C_5R_5)BiX_2$ (R = H, Me; X = F, Cl, Br, I; n = 1−4) in order to develop an effective adjustment of their electronic and bonding behavior and then, to be able to manipulate highly fluxional $Bi–C_5R_5$ bonds. The experimental part of this section emphasizes the theoretical results by observation of the unprecedented nanoscopic supramolecular architecture $[\{(C_5Me_5)_5Bi_5Br_9\}\{(CH_2Cl_2)(BiBr_4)\}]_2$, cationic molecule $[(C_5Me_5)_5Bi_6Cl_{12}]^+$ and zig-zag polymer chains $[(C_5Me_5)BiX_2]_\infty$ (X = Br, I). The section of icosahedral and macroicosahedral bismuthanediide oligomers is a conceptual approach to understand the structures and the electronic properties of highly symmetric molecules such as $[R_nBi_nM_{2n-4}]^{4-}$ (n = 12, 32, ...) on the theoretical level. The obtained results open the way to their endohedral chemistry. To sum up, unique structural and bonding features of the molecular assemblies based on C_5Me_5-substituted bismuth halides, as well as the observed Bi−arene π-complexations and inverted sandwich behavior found in the crystal cell of a Bi–Fe cluster, are an important step in the development of supramolecular chemistry and crystal engineering of the compounds of the heavy group 15 elements. Furthermore, the bismuth cage and cluster chemistry has taken one step forward. The largest cluster of the bismuth–iron family (Bi_4Fe_8) and the spherical aromaticity of seven-vertex Bi_4Fe_3 structure have been observed. The new examples of a Bi_4 tetrahedron, stabilized by transition-metal groups, as well as bismuth's square pyramidal (Bi_5) nido-polyhedron-like and octahedral (Bi_6) deltahedron-like cages, stabilized by C_5Me_5 and halo ligands, have been discovered. A new chapter in the theoretical chemistry of highly symmetric bismuth cage molecules (Bi_{12}, Bi_{32}) has been opened.

Zusammenfassung

In der vorliegenden Arbeit wurde die polynukleare Chemie des Bismuts von verschiedenen Winkeln mit dem Schwerpunkt auf vier Typen der chemischen Bindung untersucht. So behandelt das Kapitel "Bismut-Bismut-Bindung" die Redox-Metathese-Reaktionen von $BiBr_3$ mit dem sterisch anspruchsvollen Lithiumsilanid $Li(thf)_3SiPh_2tBu$ in drei verschiedenen Verhältnissen, die zur Bildung eines Bi–Bi verknüpften Produkts $(tBuPh_2Si)_4Bi_2$ unter anderen führten. Die quantenchemische Untersuchung wurde hauptsächlich durchgeführt, um Licht auf die Oligomerizationsprozesse von $R_2Bi^{\cdot}$ Radikalen und Bismut-Dimeren zu werfen. Diese sind eine große Herausforderung im Kontext von "Thermochromie" und "geschlossenen Schale-Wechselwirkungen" in der anorganischen Chemie der Organobismut-Verbindungen mit homonuklearen Bi–Bi Bindungen. Das Kapitel "Bismut-Übergangsmetall-Bindung" gibt einen tieferen Einblick in die Strukturen, die chemische Bindung und das elektronische Verhalten von heteronuklearen voluminösen Bi–Fe-Clustern, das kubische $[Bi_4Fe_8(CO)_{28}]^{4-}$ und das siebeneckenverknüpfte $[Bi_4Fe_3(CO)_9]$, auf einem experimentellen und theoretischen Niveau. Das Kapitel "Bindung in Cyclopentadienyl-Bismut-Verbindungen" stellt eine eingehende theoretische und experimentelle Untersuchung an molekularen Systemen dar. Basierend auf den Cyclopentadienyl-Bismut-Einheiten wie $(C_5R_5)Bi^{2+}$, $[(C_5R_5)Bi]_n$ und $(C_5R_5)BiX_2$ (R = H, Me; X = F, Cl, Br, I; n = 1−4) wird versucht, die Regulierung derer Elektronen- und Bindungsverhaltens zu verstehen, um auf diese Weise die stark fluktuierenden Cyclopentadienyl-Bismut-Bindungen gezielt manipulieren zu können. Der experimentelle Teil dieses Kapitels betont die theoretischen Ergebnisse durch Beobachtung der beispiellosen nanoskopischen supramolekularen Architektur $[\{(C_5Me_5)_5Bi_5Br_9\}\{(CH_2Cl_2)(BiBr_4)\}]_2$, des Moleküles $[(C_5Me_5)_5Bi_6Cl_{12}]^+$ und der Zick-Zack-Kettenpolymer-Verknüpfungen $[(C_5Me_5)BiX_2]_\infty$ (X = Br, I). Das Kapitel "ikosaedrische und makroikosaedrische Bismutandiide-Oligomere" ist ein konzeptioneller Ansatz, um die Strukturen und die elektronischen Eigenschaften der hoch symmetrischen Bismutmoleküle wie $[R_nBi_nM_{2n-4}]^{4-}$ (n = 12, 32, ...) auf einem theoretischen Niveau zu verstehen. Aufgrund der erhaltenen Ergebnisse wird der Weg frei gemacht für deren endohedrische Chemie. Fazit ziehend, sind einzigartige Struktur- und Bindungsbesonderheiten bei zwischenmolekularen Wechselwirkungen der cyclopentadienylsubstituierten Bismuthalogenide, sowie der Bismut-Aromaten-π-Komplexe. Beispiel ist das invertierte "Sandwich"-Verhalten eines Bi–Fe Clusters in Kristall. Dies stellt einen wichtigen Schritt in der Entwicklung supramolekularer Chemie der Verbindungen der schweren Elemente der 15. Gruppe dar. Darüber hinaus hat die Bismutkäfig- und Bismutcluster-Chemie einen Schritt nach vorne getan. Das größte Cluster der Bismut-Eisen-Familie (Bi_4Fe_8) und die sphärische

Aromatizität von siebeneckenverknüpfter Bi_4Fe_3-Struktur wurden beobachtet. Die neuen Beispiele eines Bi_4 Tetraeders, das durch Übergangsmetall-Gruppen stabilisierbar ist, sowie der nido-polyederartigen quadratischpyramidalen (Bi_5) und oktaedrischen (Bi_6) Bismutkäfige, die durch Pentamethylcyclopentadienyl- und Halogen-Liganden stabilisierbar sind, wurden entdeckt. Ein neues Kapitel in der theoretischen Chemie von hoch symmetrischen Bismut-Käfigmolekülen (Bi_{12}, Bi_{32}) wurde eröffnet.

Chapter 1. Introduction

1.1 The heaviest element (Bi) of the group 15 elements and its chemistry

Bismuth [bisemutum (new latin), Bismut (german)] is a chemical element group 15 that has the symbol Bi, atomic number 83 and electron configuration $[Xe]4f^{14}5d^{10}6s^{2}6p^{3}$. Bismuth is a brittle metal with a white, silver-pink hue. Although, bismuth has been known since ancient times (the Incas used it along with the usual copper and tin in a special bronze alloy for knives[1]), no one person is credited with its discovery. The name bismuth was probably taken from two German words, "weiße Masse", meaning "white mass". The phrase describes how the element appears in nature. Later the name was shortened to Bismut, and then to bisemutum, before bismuth came into common use. Thus, bismuth belongs to post-transition metal-element category and is the most naturally diamagnetic of all metals. Of any metal, Bi has the second lowest thermal conductivity (after mercury). Its electronegativity is 2.02 (Pauling scale). The melting and boiling points of Bi are 271.3°C and boiling point is 1580°C, respectively. Its density is 9.80 grams per cubic centimeter. Bismuth is generally considered to be the last naturally occurring stable, non-radioactive element on the periodic table, although it is actually slightly radioactive, with an extremely long half-life. Its toxicity is much lower than that of its neighbors in the periodic table such as lead (Pb), tin (Sn), tellurium (Te), antimony (Sb), and polonium (Po). Bismuth is also an element with the heaviest stable isotope, ^{209}Bi.

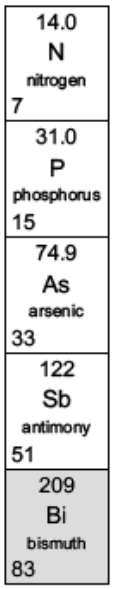

Unfortunately, chemistry of bismuth has received much less attention in comparison with that of nitrogen (N), phosphor (P), arsenic (As), and antimony (Sb). Only last two and a half decades have been revealed an increasing interest in the investigation of the inorganic and organometallic chemistry of the heaviest element of the group 15 elements (bismuth), having atomic weight of 208.98040(1) $g \cdot mol^{-1}$.[2] Thus, during this time the number of bismuth compounds structurally characterized by X-ray crystal structure diffraction analysis has considerably increased. In very fine review on the structural aspects of known crystallographically studied bismuth compounds, published in *Chemical Reviews* in 1999, the authors (Silvestru, Breunig and Althaus – picture on the right) have pointed out the diversity of bismuth coordination chemistry, which is mainly possible due to the potential for normal covalent as well as coordinative bonds, the latter being the result of the bismuth Lewis acidicity.[3]

In its compounds, Bi is able to display various oxidation states (+3 and +5 are the most common, but formal +1 are also known) and coordination numbers up to 10.

Thus, for the Bi in the formal oxidation state +3 and +1, five valence electrons of the bismuth atom may be involved in bonding to other elements in different ways: (i) using the p orbitals of the valence shell to achieve three covalent Bi–Q (here, Q = same or different atoms or group of atoms) bonds, where all of these or only some of these have either σ-character or/and π-character [examples: R_3Bi, R_2BiX, $R_2Bi–BiR_2$, RBi=BiR etc.]; (ii) using the remaining lone pair of electrons, which has a basically s orbital contribution [examples: $R_3Bi–TMG$ $R_2Bi–(TMG)_2$, $XBi–(TMG)_2$ etc., where TMG is transition metal group and R is an organic substituent]. It is important to remark the stereochemical activity of the lone pair orbital of s type at the Bi atom in case of Bi(III) and Bi(I) compounds is sometimes questionable.

In this matter, the octet rule at Bi is fulfilled. The resulting geometry environment around the bismuth center, where Bi displays the formal oxidation state +3, is trigonal pyramidal. It might be regarded as being consistent with valence shell electron pair repulsion (VSEPR) theory predictions.[4] This model in chemistry predicts that bonding (sigma bonds only) and nonbonding electron pairs in a molecule will adopt a geometry (the shape of individual molecules) in which the distance between the electron pairs is maximized from one another in order to minimize the electrostatic repulsions. This will result in a molecular geometry with the lowest possible energy. The theory developed by Gillespie and Nyholm also allows us to predict which hybridization the central atom takes in bonding to other atoms. The number of electron

pairs surrounding an atom, both bonding and nonbonding, is called its steric number.

Interesting, an almost trigonal planar BiQ_3 arrangement was found in one inorganic "bismuthinidene" derivate, which contains some multiple bond character in the angular BiQ_2 system.[5] For the purposes of VSEPR theory, the multiple electron pairs in a multiple bond are treated as though they were a single "pair".

Due to the Lewis acidic character at the Bi center, additional intra- or intermolecular contacts are usually established in the presence of donor molecules or ions, thus increasing the coordination number.[3] According to the "semibonding concept" introduced by Alcock, the bonds at the Bi atom might be generally described in terms of primary and secondary bonds.[6] Here, the primary bonds are normal covalent bonds with bond lengths close to the sum of the covalent radii for the two elements involved. The secondary bonds are interactions with interatomic distances significantly longer than a covalent bond but shorter than the sum of the van der Waals radii for the two elements concerned. The covalent and van der Waals radii of the bismuth element are 152 and 240 pm, respectively. When the secondary bonds lie almost *trans* to the primary bonds a trend could be usually observed. Thus, the *trans* influence is reflected in the length of the bismuth–element distances. A shorter secondary bond corresponds to a longer related primary bond, a feature which was considered to be consistent with the use of Bi–Q σ*-antibonding orbitals as acceptor orbitals for a BiQ_3 unit.[7] In some cases the lengths of secondary and primary bonds are similar. Alternatively, the hypervalent bismuth compounds might be described using the three-center four-electron model.[8] i.e., the use of a single p orbital of Bi to form two covalent bonds.[3]

As is depicted in Figure A, with 1–3 donor atoms available for additional interactions, in most cases the resulting coordination polyhedron around the Bi atom becomes trigonal bipyramidal (seesaw structure; **a**), octahedral (square pyramidal; **b**), or octahedral (**c**), corresponding to 10-Bi-4, 12-Bi-5, and 14-Bi-6 systems, respectively (*N*–Bi–*L* designation: *N* = number of formal valence shell electrons about a Bi atom; *L* = the number of ligands).[9] Interesting, various degrees of distortion from the ideal polyhedra have been observed, here.

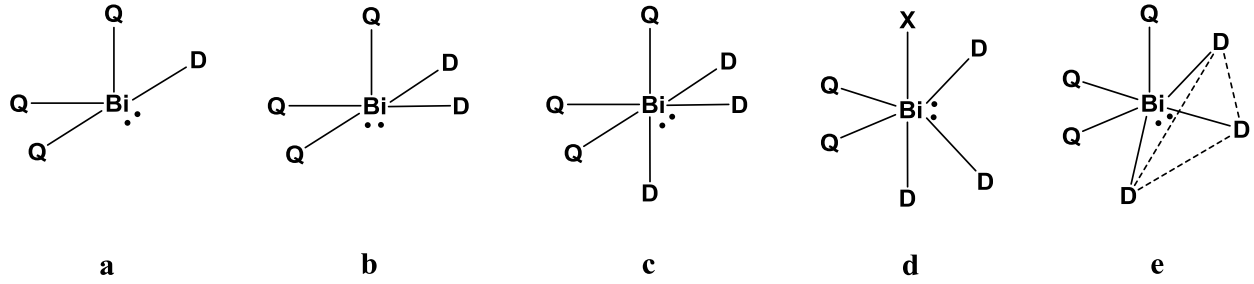

Figure A. Coordination polyhedra around the Bi atom.

Furthermore, distortions from regular octahedron (**c**) to pentagonal bipyramid (opened edge; **d**) or capped octahedron (opened face; **e**) were established (Figure A).

Interesting geometry situations are also found in the cases of four- and five-coordinate bismuth compounds. Thus, the geometries generally observed fit with those predicted by the simple VSEPR theory for AB_4E_1 (seesaw) and AB_5E_0 / AB_5E_1 (trigonal bipyramidal / square pyramidal) systems, respectively, when a model based on the availability of vacant d orbitals is used to form dsp^3 and d^2sp^3 hybrid orbital sets. The distortions also fit with VSEPR theory, here. Thus, for the AB_4E_1 structure, the equatorial bond angle is less than 120º and the axial groups are displaced toward the equatorial ones as expected for an electrostatic repulsion between the nonbonding lone pair and the bonding pairs of electrons (**f**; Figure B).[3] Besides, an opposite displacement of the axial groups away from the equatorial ones (**g**; Figure B) was also established for other 10-Bi-4 compounds.[10]

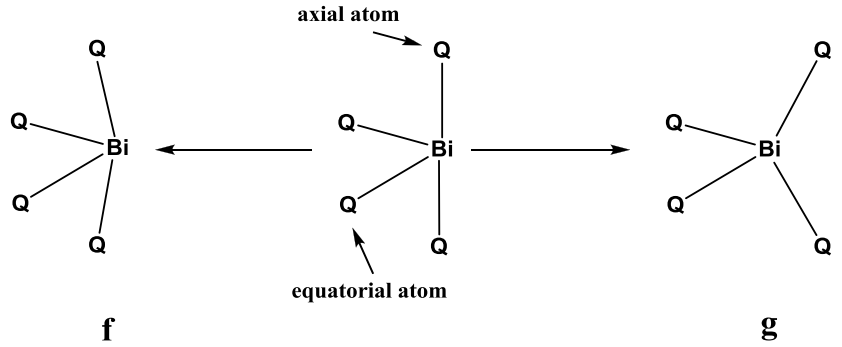

Figure B. Distortions from the ideal seesaw structure of four-coordinative bismuth compounds.

In compounds containing Bi in the formal oxidation state +5, all valence shell electrons are involved in bonds, i.e. the central atom has five bonding pairs of electrons. As a result, there is no remaining lone pair at the central atom. In this case, the most common coordination polyhedron is trigonal bipyramidal (Figure C, left).[11] However, various degrees of distortion depending on the nature of compound have been established. Thus, the square pyramidal geometries are also observed for pentaorganobismuth (V) derivates (Figure C, center).[12]

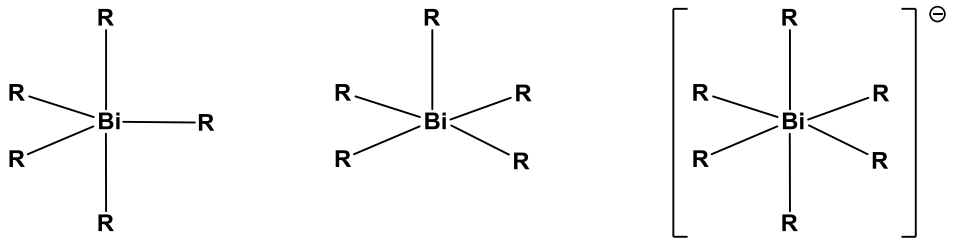

Figure C. Trigonal bipyramidal (left), square pyramidal (center) and octahedral (right) geometries of bismuth(V) complexes.

Moreover, the Lewis acidic character of the Bi(V) center is responsible for the possibility of increasing the coordination number to six, resulting in distorted octahedral geometries of $[R_6Bi]^-$ anions (Figure C, right).[11a,13]

The increasing interest to the bismuth chemistry arises by the following practical reasons together with the fundamental ones: (i) emerging importance of the bismuth compounds in the development of new thermoelectric materials, new electronic materials, and novel polymeric materials; (ii) industrial uses as precursors in advanced material science (superconductors, photorefractive systems, sol-gel processes, production of thin films by chemical vapor deposition etc.)[14] and catalysts (e.g., Bi–molybdate materials in the SOHIO process for acrylonitrile synthesis and more generally to catalyze amination and oxidation reactions as well as unique property of $n MoO_3/Bi_2O_3$ phases to act as catalysts for the allylic oxidation of propene);[15] (iii) bioactivity (treatment of a variety of gastrointestinal disorders,[16] antitumor,[17] antimicrobial and antibacterial activity[16d,18]) and development of new pharmaceutical materials (N. Burford; Dalhousie University, Canada; picture on the right);[19] (iiii) uses in organic syntheses (e.g. phenylation agent or mild oxidizing agents).[20]

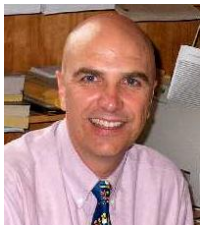

All above-mentioned reasons require a more extensive understanding of bismuth fundamental chemistry on the synthetic, structural and theoretical level.

1.2 Nomenclature of bismuth compounds

BiH_3 and compounds derived from it by substituting one, two or three hydrogen atoms by hydrocarbyl groups: R_3Bi, $RBiH_2$, R_2BiH ($R \neq H$) are called primary, secondary and tertiary bismuthines, respectively. A specific bismuthine is preferably named as a substituted bismuthane, e.g. Me_3Bi trimethylbismuthane. The fragments $[R_2Bi]^-$ are $[RBi]^{2-}$ are named as bismuthanides and bismuthanediides, respectively. All of compounds with the bismuth–bismuth bonds can be also separated into some groups under following names: (i) dibismuthanes, $(R_2Bi)_2$; (ii) *n*-bismuthanes, *cyclo*-$(RBi)_n$ ($n \geq 3$) and *bicyclo*-$(R_{n-2}Bi_n)$, (iii) dibismuthenes, RBi=BiR.

1.3 Element–element relationships

1.3.1 What is cluster?

The phrase "cluster" was coined by F. A. Cotton in the 1960s to describe compounds containing metal–metal bonds.[21] Despite that this definition exists about 50 years, it provokes many questions up to now. A metal atom cluster as defined by Cotton is still a very broad term,

because non-metal atoms can also be part of the cluster core (for example, fullerene and borane clusters). There are also other definitions of metal cluster. The latter is a compound containing a group of two or more metal atoms where direct and substantial metal–metal bonding is present[22] or cluster is a compound in which two or more metal atoms aggregate so as to be within bonding distance of one another and each metal atom is bonded to at least two other metal atoms.

Frank Albert Cotton (1930–2007)

The main cluster types are (i) "naked" clusters containing no stabilizing ligands, (ii) metalloid clusters[23] where more metal–metal bonds than metal–ligand bonds are involved and (iii) those with ligands.

Metal cluster compounds bridge the gap between the solid-state chemistry of the metals and the metal complexes in which each metal ion is completely surrounded by and bonded to a set of ligands or ions. The latter group comprises the classical coordination chemistry of metal ions. Interest in metal cluster compounds arises from unique features of their chemistry: (i) cluster compounds provide models for studying fundamental reactions on surfaces; (ii) there is a hope that cluster compounds may provide entry to new classes of catalysts that may be tailored to specific syntheses and may thus be more selective than existing processes; (iii) the nature of the bonding in cluster compounds is an area wherein experiment and theory are continuously challenging each other; (iiii) the systematic synthesis of mixed metal clusters may provide for the development of new types of supported catalysts.

1.3.2 What are poly-, homo- and heteronuclear metal compounds?

The term "polynuclear" refers to a compound with more than one metal atom; "homonuclear" refers to a compound with the identities of the metal centers and "heteronuclear" refers to a compound with at least two different metal elements.

1.3.3 Bonding concept by Lipscomb

In the 1950s, William Lipscomb used the fundamental concept of three-center two-electron bonding[24] to develop a topological model that explained the structures of the known neutral boron hydrides. In Figure D, it is presented for all boron analogs. The description of the bonding in the boranes involved: (i) 3-center 2-electron (3c2e) B–H–B hydrogen bridges; (ii) 3-center 2-electron (3c2e) B–B–B bonds; (iii) 2-center 2-electron (2c2e) terminale bonds (in B–B, B–H and BH_2). The styx number was introduced to aid in electron counting where s = count of 3c2e B–H–B bonds; t = count of 3c2e B–B–B bonds, y = count of 2c2e B–B bonds and x = count of 2c2e BH_2 groups. Bonding concept by Lipscomb is used very successful for the main group element (E) chemistry up to date (Figure D). The balance equations in cluster compounds are thus submitted to the formels $3t + 2y = 3n$ (orbital balance for $[E_nR_n]^{m-}$) and $2t + 2y = 2n +$ m

(electron balance for $[E_nR_n]^{m-}$).

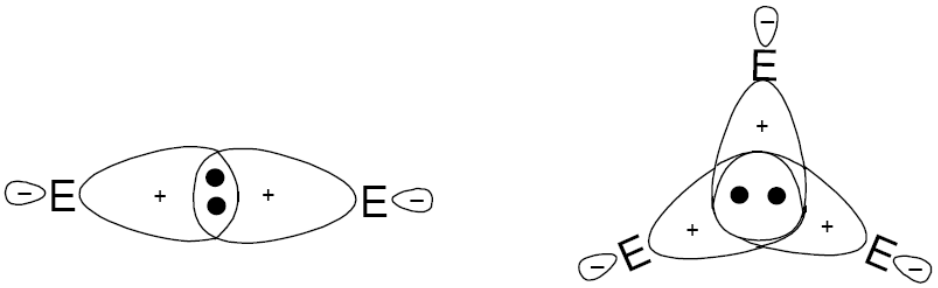

Figure D. Valence bonds description of EE-2c2e bonding (links) and EEE-3c2e bonding (right).

1.3.4 Topologies of clusters

In the 1970s, the electron counting rules originally formulated by K. Wade and further evolved by Mingos and others opened a way to predicting structures and topologies of clusters by counting the skeleton electrons. Although, the ground rules of polyhedral skeletal electron pair theory[25] were developed by Wade to aid the prediction of the structures of borane and carborane cluster compounds, these rules, based on a molecular orbital treatment of the bonding, are available up to date for main group element and transition metal clusters. Thus, $2n + m$ cluster electrons (n = number of cluster atoms) with $m = 2$ lead to *closo*-clusters. This means that the cluster-forming atoms are the corners of a trigonal-bipyramid, an octahedron, a pentagonal-bipyramid and so on. With $m = 4, 6, 8, \ldots$, clusters that are missing one, two, three or more corners with respect to a *closo*-cluster are predicted, the so-called *nido*-, *arachno*- and *hypho*-clusters, respectively. For $m = 0, -2, -4, \ldots$, one-fold, two-fold, three-fold, … capped clusters are to be expected.[26]

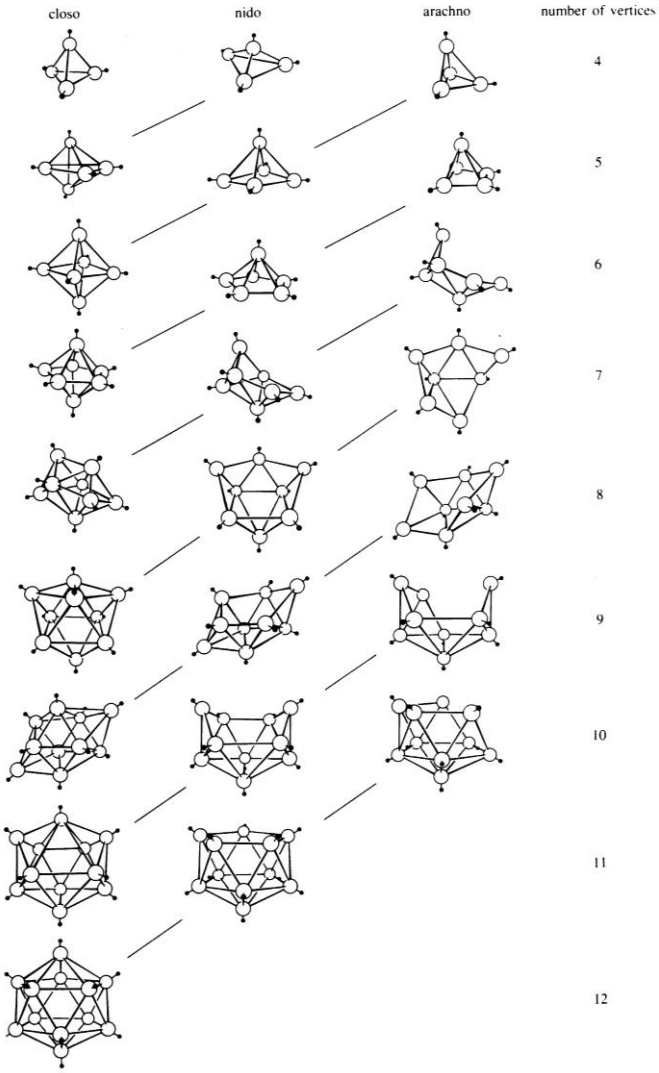

Generally, the skeletal electron pair theory counts for the four types of polyhedral cluster are:

(i) 2*n*+2 bonding electrons, *n* vertex *closo n*+1 bonding orbitals;

(ii) 2*n*+4 bonding electrons, *n* vertex *nido n*+2 bonding orbitals;

(iii) 2*n*+6 bonding electrons, *n* vertex *arachno n*+3 bonding orbitals;

(iiii) 2*n*+8 bonding electrons, *n* vertex *hypho n*+4 bonding orbitals.

1.3.5 Principle of isolobality

The principle of isolobality as a means of understanding the electronic structure and reactivity of compounds has advanced by Hoffmann[27]. Thus, two species are isolobal if they have similar number, symmetry properties, approximate energies, and occupation by electrons of their frontier orbitals. For example, the groups BH, AlR, CH^+, CR^+ and NR^{2+} are isolobal to each other.

1.3.6 Principle of isoelectronicity

Two species are isoelectronic (a group of ions, atoms, or molecules) if they the same total number of electrons and the same number of atoms whose atomic masses are greater than that of hydrogen (heavy atoms). As consequence, they tend to have similar electronic structures, similar chemical properties, and heavy-atom geometries.

1.3.7. Theoretical and computational approach

The term "theoretical chemistry" may be defined as the mathematical description of chemistry. Many chemical and physical-chemical problems can be solved on the theoretical level using the computational chemistry, which uses the results of theoretical chemistry, incorporated into efficient computer programs. The computational chemistry is also a great alternative to experiment in making accurate predictions of observed chemical phenomena as well as hitherto unobserved ones.

The quantum chemical studies of inorganic and organometallic molecular systems benefit well from applying different methods, approaches and theories to the structure and chemical bonding questions as well as the questions of energetic, electronic, and spectroscopic behavior of these compounds. The *ab initio*, density functional, semi-empirical and empirical methods, as well as molecular mechanics, chemical and molecular dynamics can be applied, here. Use of the first two methods, based on the respective theories, is the most popular among the chemists in the above-mentioned questions.

The term "*ab initio*" is latin for "from the beginning". This name is given to computations which are derived directly from theoretical principles, with no inclusion of experimental data. The most common type of *ab initio* electronic structure calculation is the Hartree Fock (HF) scheme, in which the primary approximation is called the central field approximation. This means that

the Coulombic electron-electron repulsion is not specifically taken into account. However, it is net effect is included in the calculation. This is a variational calculation, meaning that the approximate energies calculated are all equal to or greater than the exact energy. The second approximation in HF calculations is that the wave function must be described by some functional form, which is only known exactly for a few one electron systems. The functions, used most often, are linear combinations of Slater type orbitals (STO) or Gaussian type orbitals (GTO). The wave function is formed from linear combinations of atomic orbitals or more often from linear combinations of basis functions. A number of types of calculations begin with a HF calculation, then correct for the explicit electron-electron repulsion, referred to as electronic correlation. Møller–Plesset perturbation theory (MP*n*, where *n* is the order of correction), the Generalized Valence Bond (GVB) method, Multi-Configurations Self Consistent Field (MCSCF), Configuration Interaction (CI) and Coupled Cluster theory (CC) are referred to as correlated calculations. Here, MP*n*, CI and CC are examples of the post-HF methods.[28]

An alternative *ab initio* method is Density Functional Theory (DFT) in which the total energy is expressed in terms of the total one-electron density, rather than the wavefunction. In this type of calculation, there is an approximate Hamiltonian and an approximate expression for the total electron density. Here, the properties of a many-electron system can be determined by using functionals, i.e. functions of another function, which in this case is the spatially dependent electron density. Hence, the name DFT comes from the use of functionals of the electron density. The DFT bases on two Hohenberg-Kohn (H-K) theorems. The first H-K theorem asserts that an electronic density, that depends on only three spatial coordinates, determines all ground-state properties of the system, that is, $E = E(n_0)$, where n_0 is the ground-state density of the system. This theorem can be extended to the time-dependent domain to develop time-dependent density functional theory (TD-DFT), which can be used to describe excited states. The second H-K theorem shows that there exists a variational principle for the above energy density functional $E(n)$. Namely, if n' is not the ground state density of the above system, then $E(n') > E(n_0)$. Interesting, the original H-K theorems held only for non-degenerate ground states in the absence of a magnetic field, although they have since been generalized to encompass these. While DFT in principle gives a good description of ground state properties, practical applications of DFT are based on approximations for the exchange-correlation potential. This potential describes the effects of the Pauli principle and the Coulomb potential beyond a pure electrostatic interaction of the electrons. A common approximation is the local density approximation (LDA) which locally substitutes the exchange-correlation energy density of an inhomogeneous system by that of an electron gas evaluated at the local density.[29]

1.4 Aim of the thesis

The highlights of this thesis are the experimental and theoretical investigations of novel polynuclear bismuth compounds displaying unusual structures and exhibiting interesting chemical bonding and electronic behavior as well as new connectivities. Sterically demanding silyl and cyclopentadienyl ligands as well as transition metal carbonyls and alkali metals were regarded as stabilizing and protecting agents at the bismuth atoms. The X-ray diffraction as well as spectroscopic and spectrometric methods was used for the characterization of new observed compounds. Quantum chemical calculations were applied to study the experimentally observed bismuth molecular systems and their computational models on the theoretical level using different methods and approaches. Molecular, supramolecular and cluster chemistry and mainly molecular systems, where bismuth forms polyhedral cages, are subject of this thesis.

1.5 References

[1] R. B. Gordon, J. W. Rutledge, *Science* **1984**, *223*, 585.

[2] *Chemistry of Arsenic, Antimony and Bismuth*; Norman, N. C., Ed.; Blackie Academic and Professional: London, **1998**.

[3] C. Silvestru, H. J. Breunig, H. Althaus, *Chem. Rev.* **1999**, *99*, 3277.

[4] R. J. Gillespie, I. Hargittai, *The VSEPR Model of Molecular Geometry*; Allyn and Bacon: New York, **1991**.

[5] S. J. Davies, N. A. Compton, G. Huttner, L. Zsolnai, S. E. Garner, *Chem. Ber.* **1991**, *124*, 2731.

[6] (a) N. W. Alcock, *Adv. Inorg. Chem. Radiochem.* **1972**, *15*, 1; (b) N. W. Alcock, *Bonding and Structure: Structural Principles in Inorganic and Organic Chemistry*; Ellis Horwood: Chichester, **1990**.

[7] (a) G. A. Fisher, N. C. Norman, *Adv. Inorg. Chem.* **1994**, *41*, 233; (b) N. C. Norman, *Phosphorus, Sulfur Silicon* **1994**, *87*, 167.

[8] G. A. Landrum, R. Hoffmann, *Angew. Chem.* **1998**, *110*, 1989.

[9] C. W. Perkins, J. C. Martin, A. J. Arduengo, W. Lau, A. Algeria, J. K. Kochi, *J. Am. Chem. Soc.* **1980**, *102*, 7753.

[10] W. Clegg, N. A. Compton, R. J. Errington, G. A. Fisher, D. C. R. Hockless, N. C. Norman, A. G. Orpen, S. E. Stratford, *J. Chem. Soc., Dalton Trans.* **1992**, 3515.

[11] (a) S. Wallenhauer, K. Seppelt, *Angew. Chem.* **1994**, *106*, 1044; *Angew. Chem. Int. Ed.* **1994**, *33*, 976; (b) B. Neumüller, K. Dehnicke, *Angew. Chem.* **1994**, *106*, 1803; *Angew. Chem. Int. Ed.* **1994**, *33*, 1726.

[12] A. Schmuck, J. Buschmann, J. Fuchs, K. Seppelt, *Angew. Chem.* **1987**, *99*, 1206; *Angew. Chem. Int. Ed.* **1987**, *26*, 1180.

[13] S. Wallenhauer, D. Leopold, K. Seppelt, *Inorg. Chem.* **1993**, *32*, 3948.

[14] (a) H. Maeda, Y. Tamaka, M. Fukutomi, T. Asano, *Jpn. J. Appl. Phys.* **1988**, *27*, L209; (b) T. Asaka, Y. Okazawa, T. Hirayama, K. Tachikawa, *Jpn. J. Appl. Phys.* **1990**, *29*, L280; (c) S. Katayama, M. Sekine, *J. Mater. Res.* **1991**, *6*, 36; (d) B. A. Vaarstra, J. C. Huffman, W. E. Streib, K. G. Caulton, *Inorg. Chem.* **1991**, *30*, 3068; (e) R. D. Rogers, A. H. Bond, S. Aguinaga, *J. Am. Chem. Soc.* **1992**, *114*, 2960; (f) R. D. Rogers, A. H. Bond, S. Aguinaga, A. Reyes, *J. Am. Chem. Soc.* **1992**, *114*, 2967; (g) S. R. Breeze, S. Wang, L. K. Thompson, *Inorg. Chim. Acta* **1996**, *250*, 163; (h) E. Moya, L. Contreras, C. Zaldo, *J. Opt. Soc. Am.* **1988**, *B5*, 1737; (i) S. Wang, D. B. Mitzi, G. A. Landrum, H. Genin, R. Hoffmann, *J. Am. Chem. Soc.* **1997**, *119*, 724; (j) P. Majewski, *Adv. Mater.* **1994**, *6*, 460; (k) J. F. Scott, F. M. Ross, C. A. Paz de Araujo,

M. C. Scott, M. Huffman, *Mater. Res. Soc. Bull.* **1996**, *21*, 33; (l) A. Ekstrand, M. Nygren, G. Westin, *J. Sol-Gel Sci. Technol.* **1997**, *8*, 697; (m) F. Soares-Carvalho, P. Thomas, J. P. Mercurio, B. Frit, S. Parola, *J. Sol-Gel Sci. Technol.* **1997**, *8*, 759.

[15] (a) C. Coin, T. Zevaco, E. Dunach, M. Postel, *Bull. Soc. Chim. Fr.* **1996**, *133*, 913; (b) G. W. Keulks, L. D. Krenzke, T. M. Notermann, *Adv. Catal.* **1978**, *27*, 183; (c) R. K. Grasselli, J. D. Burrington, *Adv. Catal.* **1981**, *30*, 133; (d) R. K. Grasselli, J. D. Burrington, *Ind. Engl. Chem. Prod. Res. Dev.* **1984**, *23*, 394; (e) J. Belagem, J. A. Osborn, J. Kress, *J. Mol. Catal.* **1994**, *86*, 267; (f) R. K. Grasselli, in: G. Ertl, H. Knozinger, J. Weitkamp (Eds.), *Handbook of Heterogeneous Catalysis*; VCH Verlagsgesellschaft mbH, Weinheim, **1997**, 2302; (g) Y. H. Jang, W. A. Goddard III, *Top. Catal.* **2001**, *15*, 273; (h) T. A. Hanna, *Coord. Chem. Rev.* **2004**, *248*, 429.

[16] (a) C. F. Baxter, *Chem. Br.* **1992**, *28*, 445; (b) P. J. Sadler, H. Sun, *J. Chem. Soc., Dalton Trans.* **1995**, 1395; (c) E. Asato, K. Katsura, M. Mikuriya, U. Turpeinen, I. Mutikainen, J. Reedijk, *Inorg. Chem.* **1995**, *34*, 2447; (d) N. Burford, S. O. J. Veldhuyzen van Zamen, L. Agocs, L. Best, T. S. Cameron, G. B. Yhard, J. M. Curtis, *Gastroenterology* **1994**, *106*, A59; (e) R. LeBlanc, S. O. J. Veldhuyzen van Zamen, N. Burford, L. Agocs, D. J. Leddin, *Gastroenterology* **1995**, *108*, A860.

[17] P. Köpf-Maier, T. Klapötke, *Inorg. Chim. Acta* **1988**, *152*, 49.

[18] (a) T. Klapötke, *J. Organomet. Chem.* **1987**, *42*, 940; (b) M. S. Zhou, A. L. Tan, Y. Xu, C.-F. Lam, P.-H. Leung, K. F. Mok, L.-L. Koh, T. S. A. Hor, *Polyhedron* **1987**, *16*, 2381.

[19] G. G. Briand, N. Burford, *Chem. Rev.* **1999**, *99*, 2601.

[20] (a) H. Suzuki, T. Ikegami, Y. Matano, *Tetrahedron Lett.* **1994**, *35*, 8197; (b) H. Suzuki, T. Ikegami, *J. Chem. Res.* **1996**, 24; (c) M. Postel, E. Duñach, *Coord. Chem. Rev.* **1996**, *155*, 127; (d) T. Arnauld, D. H. R. Barton, E. Doris, *Tetrahedron* **1997**, *53*, 4137; (e) N. M. Leonard, L. C. Wieland, R. S. Mohan, *Tetrahedron* **2002**, *58*, 8373.

[21] (a) F. A. Cotton, *Quart. Rev. Chem. Soc.* **1966**, *20*, 389; (b) F. A. Cotton, *J. Chem. Educ.* **1983**, *60*, 713.

[22] D. M. P. Mingos, *Introduction to cluster chemistry*; Prentice Hall in Englewood Cliffs, N.J., **1990**, p. 571.

[23] A. Schnepf, G. Stößer, H. Schnöckel, *J. Am. Chem. Soc.* **2000**, *122*, 9178.

[24] (a) R. E. Dickerson, W. N. Lipscomb, *J. Chem. Phys.* **1957**, *27*, 212; (b) W. N. Lipscomb, *Boron Hydrides*, W. A. Benjamin, New York, **1963**; (c) W. N. Lipscomb in *Boron Hydride Chemistry*; E. L. Muetterties, Ed., Academic Press, New York, **1975**, 30.

[25] (a) K. Wade, *Chem. Commun.* **1971**, 792; (b) D. M. P. Mingos, *Nature* **1972**, *336*, 99; (c) K. Wade, *Adv. Inorg. Chem. Radiochem.* **1976**, *18*, 1; (d) R. W. Rudolph, *Acc. Chem. Res.* **1976**, *9*, 446; (e) R. E. Williams, *Adv. Inorg. Chem. Radiochem.* **1976**, *18*, 67; (f) D. M. P. Mingos, *Acc. Chem. Res.* **1984**, *17*, 311.

[26] G. Linti, H. Schnöckel, W. Uhl, N. Wiberg in *Molecular Clusters of the Main Group Elements*; (Hrsg.: M. Driess, H. Nöth), Wiley-VCH, Weinheim, **2004**, 126.

[27] R. Hoffmann, *Angew. Chem.* **1982**, *94*, 752; *Angew. Chem. Int. Ed.* **1982**, *21*, 711.

[28] (a) R. G. Parr, *Int. J. Quantum Chem.* **1990**, *37*, 327; (b) I. N. Levine, *Quantum Chemistry*; Englewood Cliffs, New Jersey: Prentice Hall, **1991**, 455; (c) C. J. Cramer, *Essentials of Computational Chemistry*; Chichester: John Wiley & Sons, Ltd. **2002**, 191; (d) F. Jensen, *Introduction to Computational Chemistry*; Chichester, England: John Wiley and Sons, **2007**, 98.

[29] (a) R. G. Parr, W. Yang, *Density-Functional Theory of Atoms and Molecules*; New York: Oxford University Press., **1989**; (b) T. Ziegler, *Chem. Rev.* **1991**, *91*, 651; (c) R. Dreizler, E. Gross, *Density Functional Theory*; Plenum Press, New York, **1995**; (d) W. Koch, M. C. Holthausen, *A Chemist's Guide to Density Functional Theory*; Wiley-VCH, Weinheim, Ed. 2, **2002**.

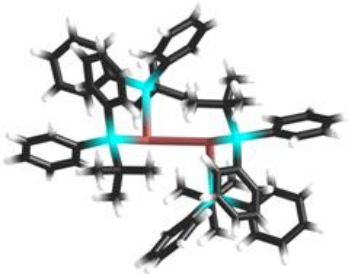

(tBuPh$_2$Si)$_4$Bi$_2$

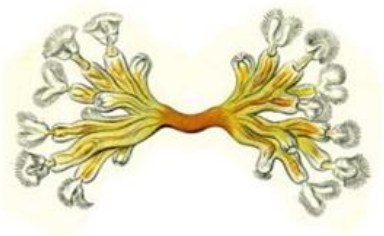

Alcyonella flabellum

Chapter 2. Bismuth–Bismuth Bonding

2.1 Introduction

2.1.1 Dibismuthanes

The history of discovery of the first organometallic compound with a homonuclear Bi–Bi single bond dates back to the 1930s, when Paneth reported that the reaction between methyl radicals and a heated bismuth mirror gave a trace of a violet solid which melted to a yellow liquid prior to decomposition. Thus, Paneth assigned the violet compound the structure of $Me_2Bi–BiMe_2$.[1] The next fifty years after this pioneering work of Paneth the groups of Ashe,[2] Becker,[3] Calderazzo[4] and Breunig[5] were able to develop efficient syntheses for $R_2Bi–BiR_2$ species where R is alkyl or aryl group. All of these compounds with a homonuclear single bond between two bismuth atoms contain Bi in the oxidation state +2.

Friedrich Adolf Paneth
(1887-1958)

Whereas the synthetic approaches to $R_2Bi–BiR_2$ compounds are studied in the best way for dibismuthanes containing Bi–C bonds, those to dibismuthanes containing Bi–Si, Bi–N and Bi–P bonds are not well developed yet and the examples of such bonding are still rare. Thus, a general synthetic pathway for many tetraalkyl-substituted dibismuthanes implies the fission of trialkyl bismuthanes with sodium in liquid ammonia, and oxidation of the resulting dialkyl sodium bismuthides with a 1,2-dihaloethane.[2,6] There are some other interesting pathways to alkyl- and

aryl-substituted dibismuthanes: (i) elimination of hydrogen from secondary bismuthines, R_2BiH at low temperatures.[7]; (ii) reduction of diorgano bismuth halides by sodium or magnesium; (iii) decomposition of cyclobismuthanes.[8]

The molecular structures of dibismuthanes in the crystalline state display two pyramidal diorganobismuth moieties linked through Bi–Bi single bonds (Figure A). The values for the Bi–Bi bond lengths usually are close to 300 pm (Table A). Variations depend on a volume of the substituents on bismuth. The bond angles of Bi are not far from 90° when the sterical repulsion between the organic substituents is weak. In this matter, the usual conformation of dibismuthanes in the crystals is *trans* (Figure A).

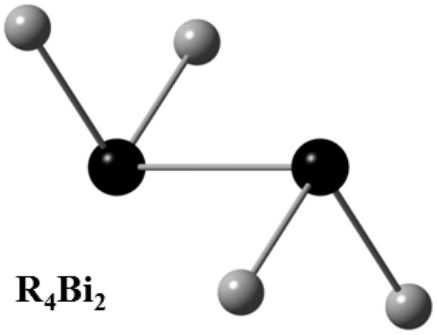

Figure A. Molecular view of dibismuthanes, $R_2Bi–BiR_2$ exhibiting a *trans* conformation.

As was earlier remarked by Breunig (University of Bremen, Germany; picture on the right), under the influence of bulky groups or bidentate ligands deviations from the ideal *trans*-conformation occur. It is expressed in the deviations from the ideal value for the dihedral angle $\tau = 180°$ (Table A). The angle τ is here determined as LP–Bi–Bi–LP where LP assumes direction of the lone pair of electrons of Bi.[9]

Table A. Selected structural data of dibismuthanes*.

Compound	Bi–Bi [pm]	Bi···Bi [pm]	τ [deg]	References
Ph_4Bi_2	299.0		180	[4,10]
$(Me_3Si)_4Bi_2$	303.5	380.4	180	[11]
$[(HC=CMe)_2]_2Bi_2$	299.0	366.0	180	[12]
Mes_4Bi_2	308.7		180	[13]
$[(Me_3Si)_2CH]_4Bi_2$	305.3		164	[14]
$[2\text{-}(Me_2NCH_2)C_6H_4]_4Bi_2$	306.6		132	[15]

* For Me_4Bi_2 preliminary structural data are available only.[16]

The compounds $R_2Bi–BiR_2$ have very specific properties, which depend on steric protection of the bismuth centers. Thus, these compounds can be separated into thermolabile and thermoinert species as well as thermochromic and nonthermochromic species. Here, the compounds with little steric protection are thermolabile, decomposing rapidly at r.t. with formation of R_3Bi and elemental bismuth. In contrast, the bulky ligands protecting a Bi–Bi bond lead to thermoinerticity of species by its stabilization. For example, a compound containing four mesityl ligands is stable up to 170 °C in an inert atmosphere, whereas tetramethyl-substituted this one has a half life of approx. 6 h in dilute benzene solution. The situation with thermochromicity of $R_2Bi–BiR_2$ compounds also looks very interesting. Thus, there are a few examples of $R_2Bi–BiR_2$, which display fascinating color changes with variation of the temperature. The term "thermochromic" dibismuthanes has been used for those which show a bathochromic shift between fluid (red or orange colors) and solid phases (violet or green colors).[17] Such dibismuthane molecules are associated through close intermolecular Bi···Bi contacts forming extended bismuth chains (Figure B). These intermolecular contact distances lie between the bond lengths of Bi–Bi single bonds and the sum of van der Waals radii of two bismuth atoms (480 pm). Thermochromicity of $R_2Bi–BiR_2$ compounds was observed for these with R = Me[16], Me_3Si[11] and R_2 = $(MeC=CH)_2$[12]. The compounds Ph_4Bi_2,[4,10] Mes_4Bi_2,[13] $[(Me_3Si)_2CH]_4Bi_2$[14] and $[2\text{-}(Me_2NCH_2)C_6H_4]_4Bi_2$[15] belong to nonthermochromic species.

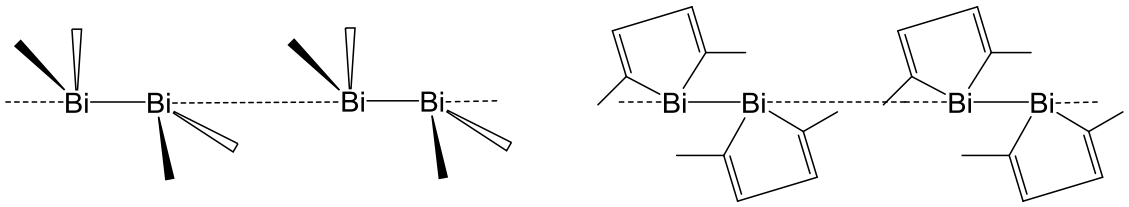

Figure B. Oligomerization of dibismuthanes R_4Bi_2 (R = Me, Me_3Si) (left) and $[(HC=CMe)_2]_2Bi_2$ (right) to chains observed in the crystal.

The dibismuthanes with little steric protection have a tendency to dissociation. The fission of the Bi–Bi bond with formation of R_2Bi radicals has been considered as the first step of thermal or photochemical decomposition reactions of tetramethyl dibismuthane.[18] In contrast, no dissociation was observed for $Ph_2Bi–BiPh_2$ in toluene.[10]

2.1.2 Monovalent organobismuth compounds

In 1997, Tokitoh (picture on the right) et al. reported in *Science* synthesis and crystal structure of the first organometallic compound with a homonuclear bismuth–bismuth double bond, RBi=BiR where R is C_6H_2-2,4,6-$[CH(SiMe_3)_2]_3$ (Tbt).[19] This species became the first representative of a class of the

organobismuth(I) compounds. The crystal structures of following monovalent compounds, *cyclo*-$(RBi)_4$, exhibiting the Bi–Bi single bonds, have been discovered by the groups of Breunig [R = $(Me_3Si)_2CH$][20] and Linti [R = *t*Bu_3Si, $(Me_3Si)_3Si$][21] in 1998 and 2002, respectively. In 2002, Linti (picture on the left) et al. also reported the largest compound of the family of Bi–Bi bonded species, *bicyclo*-R_6Bi_8 where R is $(Me_3Si)_3Sn$.[21a] Latter remains the largest one up to now. The structural views of all above-mentioned compounds are presented in Figure C.

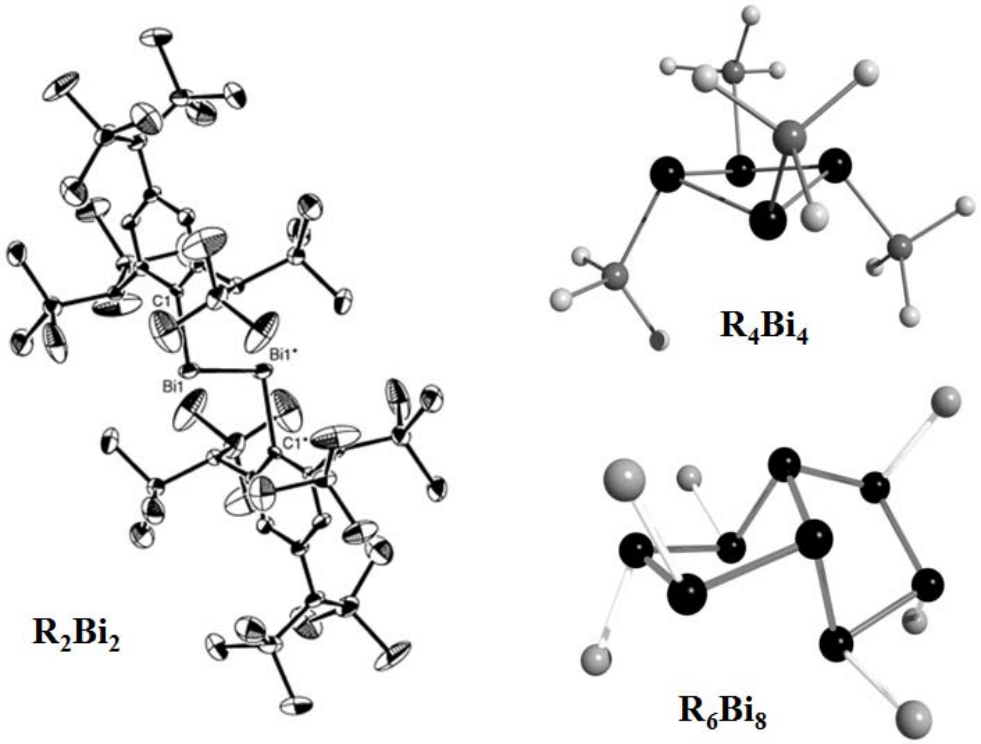

Figure C. Survey of organobismuth(I) compounds with homonuclear bismuth–bismuth bonds.

All stable dibismuthenes known up to now are formed only with extremely bulky aryl groups (Scheme A), which have proven very useful in the stabilization of multiple Bi–Bi bonds.[19,22] Synthetic pathways to dibismuthenes containing Bi–C bonds include deselenation of a bismuth selenium heterocycle, elimination of an aromatic hydrocarbon from a primary bismuthane, elimination of a distibene from a bismastibene and reduction of organo bismuth dihalides. In hydrocarbons dibismuthenes form red or purple solutions. UV-Vis spectra of these compounds show strong absorptions between 500 and 530 nm for the π-π* transitions of the Bi=Bi unit. In the crystal state (Table B), dibismuthenes are in the *trans* form and have a center of symmetry in the middle of the Bi=Bi bond, and thus, the planar aryl rings are parallel. In addition, sterically well-protected dibismuthenes containing Bi–C bonds are thermally more stable than many dibismuthanes. A lone pair of electrons at each Bi atom is inert.[19]

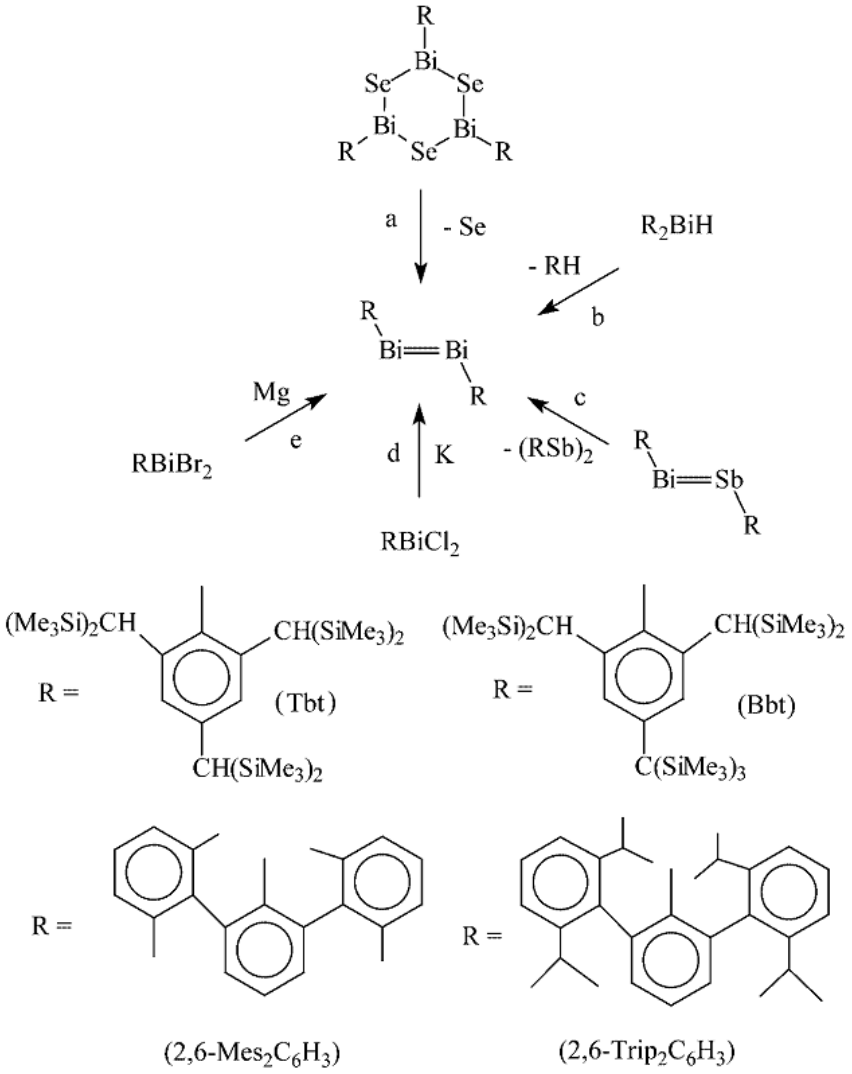

Scheme A. Synthetic pathways leading to the formation of dibismuthenes: (a) R = Tbt,[19] (b) R = 2,6-$Mes_2C_6H_3$,[22c,d] (c) R = Bbt,[22e] (d) R = 2,6-$Trip_2C_6H_3$,[22d] (e) R = Bbt.[22e] [Reprinted from ref. 9. (f) is not shown, here.]

Table B. Selected structural data of dibismuthenes R_2Bi_2, *cyclo*-bismuthanes R_4Bi_4 and *bicyclo*-bismuthane R_6Bi_8.

Compound	Bi–Bi [pm]	Bi–Bi–E [deg] (E = C, Si, Sn)	Bi–Bi–Bi [deg]	References
trans-Tbt_2Bi_2	282.1	100.5		[19]
trans-(2,6-$Mes_2C_6H_3)_2Bi_2$	283.3	92.5		[22d]
$[(Me_3Si)_2CH]_4Bi_4$	297.0 – 304.4	93.9 – 109.4	79.0 – 79.9	[20]
$[2\text{-}(Me_2NCH_2)C_6H_4]_4Bi_4$	300.9 – 302.2	92.3 – 101.7	76.8 – 79.5	[15]
$[(Me_3C)_2Si]_4Bi_4$	301.3 – 303.8	100.3 – 108.9	88.0 – 88.1	[21b]
$[(Me_3Si)_3Si]_4Bi_4$	301.3 – 303.0	99.4 – 103.1	84.7 – 87.4	[21a]
$[(Me_3Si)_3Sn]_6Bi_8$	297.2 – 301.9	90.4 – 101.7	89.4 – 105.3	[21a]

Three and four membered bismuth rings of Breunig, *cyclo*-$(RBi)_3$ and *cyclo*-$(RBi)_4$, respectively, containing medium demanding alkyl ligands [R = $(Me_3Si)_2CH$] in *cis,trans*-configurations are formed by reduction of $RBiCl_2$ with magnesium filings in thf.[20] In solution there is equilibrium between these two organobismuth rings, that is shifted in favor of *cyclo*-$(RBi)_4$ when the solution is cooled. As consequence, grown crystals are observed exclusively of the cyclotetramer (Table B). Interesting, the ring compounds have very different colors by dissolution of the crystals in hydrocarbons. Whereas solutions of *cyclo*-$(RBi)_4$ are intensive green, benzene solutions containing *cyclo*-$(RBi)_3$ are red. As was remarked by Breunig, such bismuth ring-ring transformation (Scheme B) is fully reversible following the Le Châtelier's principle.[9]

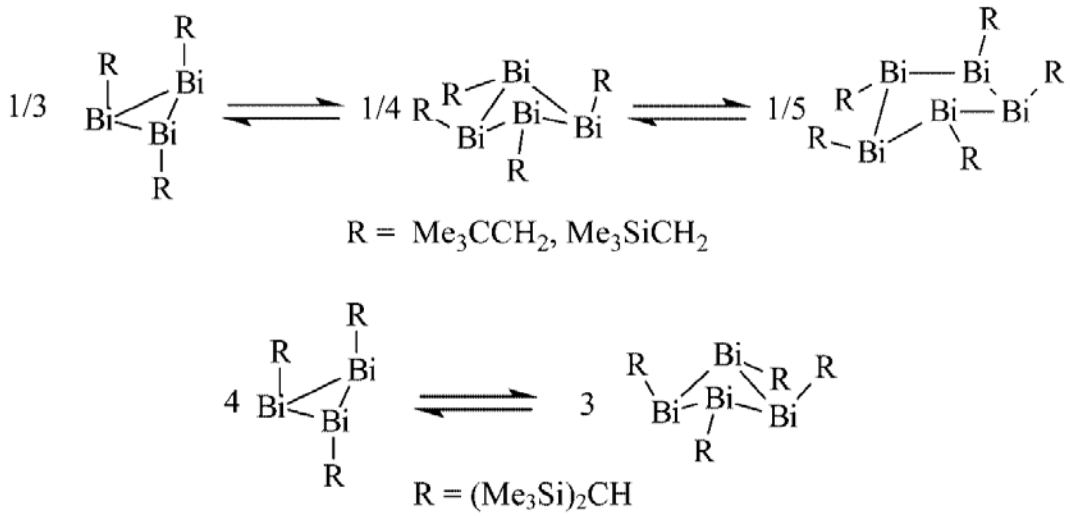

Scheme B. Ring-ring equilibria of Breunig's cyclobismuthanes.[9]

Analogous situation with a transformation of the ring systems has been observed by Breunig et al. for cyclobismuthanes with neopentyl (R = Me_3CCH_2) and trimethylsilylmethyl (R = Me_3SiCH_2) substituents.[8,23] These ring forms are thermally unstable and extremely air sensitive, but at low temperatures in an inert atmosphere they can be handled with reasonable effort. The preparative strategy leading to the formation of *cyclo*-$(RBi)_n$ (n = 3, 5) was to avoid purification steps and therefore pure starting materials and a clean low temperature ring formation process was required (Scheme C). According to the NMR- and X-ray studies, the neopentyl and trimethylsilylmethyl bismuth rings form a system consisting of the cyclotrimers, cyclotetramers and cyclopentamers in solution (Scheme B). Unfortunately, a full single crystal structure determination was not achieved. However, Breunig suggests that the solid phase should consist of cyclopentamers. He explicates, the ring system follows the Le Châtelier's principle which favors smaller rings on the cost of larger rings on dilution and vice versa.[9]

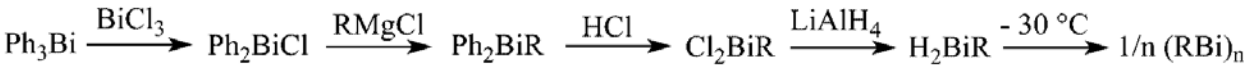

Scheme C. Synthesis of cyclobismuthanes (n = 3, 5) with neopentyl (R = Me_3CCH_2) and trimethylsilylmethyl (R = Me_3SiCH_2) substituents.[9]

Breunig et al. also reported very interesting four membered bismuth ring stabilized by bulky 2-(Me_2NCH_2)C_6H_4 groups. These potentially bidentate ligands already served in the sterical and coordinative protection of a dibismuthane (Table A). The cyclobismuthane $(RBi)_4$ has been observed here on reaction of $RBiCl_2$ with sodium in liquid ammonia or by elimination of RH from R_2BiH.[15] As well as in a case with bismuth rings containing $(Me_3Si)_2CH$ groups, the several types of these being in equilibrium has been formed in these reactions. Thus, they exist as a ring system containing the tetramer and the trimer. Even though both rings are present in solution, the crystals contain exclusively the cyclotetramer (Table B). The crystal structure of this consists of a folded all-*trans* tetrabismuthane. The dimethylamino groups are coordinated *trans* to the Bi–Bi bonds. The coordination at Bi is pseudo trigonal bipyramidal. The orientation of the aryl groups leads to a propeller-like arrangement.

As described above, bulky silyl [R = *t*Bu_3Si, $(Me_3Si)_3Si$] and stannyl [R = $(Me_3Si)_3Sn$] substituents have been used by Linti et al. for the stabilization of bismuth rings.[21] These are observed on reactions of $BiBr_3$ with corresponding alkali metal silanides or stannyl alkali metal reagent (Scheme D).

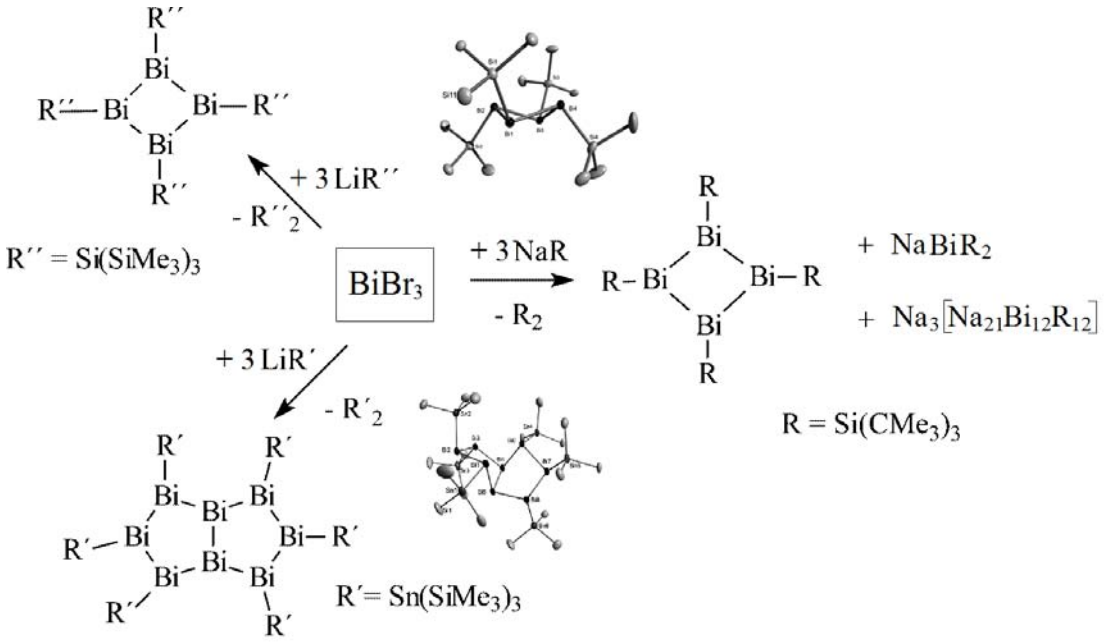

Scheme D. Synthetic pathways leading to the formation of Linti's silyl-substituted *cyclo*-bismuthanes and stannyl-substituted *bicyclo*-bismuthane R_6Bi_8.[9,21]

Interesting, such alkali metal species serve not only as source for the substituents on the bismuth atoms but also as reducing agents. The structures of Linti's silyl-substituted cyclotetrabismuthanes, *cyclo*-$(RBi)_4$, where the rings contain a folded Bi_4 core with the silyl groups in the *all-trans*-configuration, are similar to the analogous four membered ring with the bis(trimethylsilylmethyl) substituent [R = $(Me_3Si)_2CH$] reported by Breunig (Table B). The compound R_6Bi_8 in the crystal state displays a bicyclo[3.3.0]octane-like core consisting of eight bismuth atoms.[21a] The bicyclo system Bi_8 is formed from two condensed, much folded five membered rings in *cis*-linking. The tris(trimethylsilyl)stannyl groups, coordinated to the neighboring bismuth atoms, are all *trans*-standing.

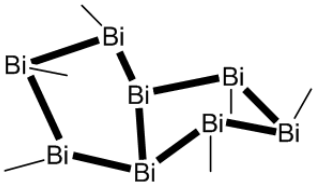

In contrast to very thermolabile and air sensitive alkyl-substituted *cyclo*-bismuthanes, these ones with Bi–Si bonds are thermoinert. Being remarkably stable red compounds, silyl-substituted cyclotetrabismuthanes do not decompose when heated in benzene for weeks or are exposed to sun light.

As was shown by above-mentioned studies of the compounds with homonuclear bismuth–bismuth bonds, steric demand of the substituents plays a very important role for the protection and stabilization of the Bi–Bi bonds.

In conclusion to the parts 2.1.1 and 2.1.2, one can take the words of Breunig into account that it is necessary to broaden and develop the field of organometallic compounds with Bi–Bi bonds and increase the number of known structural types.[9]

On the basis of above-described topics, the following interesting questions arise: (i) because there is unnumerous number of examples of homonuclear bismuth–bismuth bonding stabilized by silyl groups, which bulky silanides can else be used synthetically to access this kind of bonding? (ii) whether the terms "thermolability" and the "thermochromicity" can be applied to the new observed bismuth-bismuth compounds protected by voluminous silyl groups in this case? (iii) because the problem of oligomerisation of alkyl- and silyl-substituted $R_2Bi^{\cdot}$ radicals and dibismuthanes has attracted and attracts special interest, what could shed light on this process and what kind of structural and energetic differences are there between bismuth compounds with alkyl and silyl ligands? (iiii) is a lone pair of electrons at Bi stereochemically active or inert?

2.1.3 References

[1] (a) F. A. Paneth, *Trans. Faraday Soc*. **1934**, *30*, 179; (b) F. A. Paneth, H. Loleit, *J. Chem. Soc*. **1935**, 366.

[2] A. J. Ashe, III, *Organometallics* **1982**, *1*, 1408.

[3] G. Becker, M. Rößler, *Z. Naturforsch.* **1982**, *37b*, 91.

[4] F. Calderazzo, A. Morvillo, G. Pelizzi, R. Poli, *J. Chem. Soc.Chem. Commun.* **1983**, 507.

[5] H. J. Breunig, D. Müller, *Angew. Chem. Int. Ed.* **1982**, *21*, 439.

[6] H. J. Breunig, D. Müller, *Z. Naturforsch.* **1983**, *38b*, 125.

[7] (a) L. Balázs, H. J. Breunig, E. Lork, *Z. Naturforsch*. **2005**, *60b*, 1; (b) G. Balazs, H. J. Breunig, E. Lork, *Organometallics* **2002**, *21*, 2584.

[8] G. Balázs, L. Balázs, H. J. Breunig, E. Lork, *Organometallics* **2003**, *22*, 2919.

[9] H. J. Breunig, *Z. Anorg. Allg. Chem.* **2005**, *631*, 621.

[10] F. Calderazzo, R. Poli, G. Pelizzi, *J. Chem. Soc. Dalton Trans.* **1984**, 2365.

[11] O. Mundt, G. Becker,M. Rössler, C.Witthauer, *Z. Anorg. Allg.Chem.* **1983**, *506*, 42.

[12] A. J. Ashe, J. W. Kampf, D. B. Puranik, S. M. Al-Taweel, *Organometallics* **1992**, *11*, 2743.

[13] L. Balázs, H. J. Breunig, E. Lork, *Z. Naturforsch*. **2005**, *60b*, 1.

[14] G. Balázs, H. J. Breunig, E. Lork, *Organometallics* **2002**, *21*, 2584.

[15] L. Balázs, H. J. Breunig, E. Lork, C. Silvestru, *Eur. J. Inorg. Chem.* **2003**, 1361.

[16] O. Mundt, H. Riffel, G. Becker, A. Simon, *Z. Naturforsch.* **1988**, *43b*, 952.

[17] (a) A. J. Ashe, III, *Adv. Organomet. Chem.* **1990**, *30*, 77; (b) H. J. Breunig, *The chemistry of organic arsenic, antimony and bismuth compounds*; Ed. S. Patai, J. Wiley & Sons, Chichester, **1994**, 441.

[18] A. J. Ashe, III, E. G. Ludwig, J. Oleksyszyn, *Organometallics* **1983**, *2*, 1859.

[19] N. Tokitoh, Y. Arai, R. Okazaki, S. Nagase, *Science* **1997**, *277*, 78.

[20] H. J. Breunig, R. Rösler, E. Lork, *Angew. Chem. Int. Ed.* **1998**, *37*, 3175.

[21] (a) G. Linti, W. Köstler, *Z. Anorg. Allg. Chem.* **2002**, *628*, 63; (b) G. Linti, W. Köstler, H. Pritzkow, *Eur. J. Inorg. Chem*. **2002**, 2643.

[22] (a) N. Tokitoh, *J. Organomet. Chem.* **2000**, *611*, 217; (b) C. Jones, *Coord. Chem. Rev*. **2001**, *215*, 151; (c) N. J. Hardman, B. Twamley, P. P. Power, *Angew. Chem. Int. Ed*. **2000**, *39*, 2771; (d) B. Twamley, C. D. Sofield, M. M. Olmstead, P. P. Power, *J. Am. Chem. Soc.* **1999**, *121*, 3357; (e) T. Sasamori, N. Takeda, N. Tokitoh, *Chem. Commun.* **2000**, 1353.

[23] (a) L. Balazs, H. J. Breunig, E. Lork, *Angew. Chem. Int. Ed.* **2002**, *41*, 2309; (b) H. J. Breunig, L. Balazs, *Organometallics* **2004**, *23*, 304; (c) L. Balazs, H. J. Breunig, E. Lork, *Z. Anorg. Allg. Chem*. **2004**, *630*, 1937.

2.2 Silyl-substituted bismuth compounds

2.2.1 Introduction

The chemistry of silyl-substituted bismuth compounds is an object of intensive study in the last years, because of the interesting behavior of these compounds in synthetic reactions and the following applications and the ability of these compounds to form interesting structural motives. Only seventeen examples of such species, whose structures have been determined by X-ray diffraction, are well-known up to now. Primarily, these are homonuclear[1-3] (four examples) and heteronuclear[1,3,5-11] complexes (thirteen examples) containing silyl groups of various steric requirements [$SiMe_3$, Si*t*Bu_3, $Si(SiMe_3)_3$], which play a stabilizing role, here. In these compounds, bismuth displays the oxidation states +1, +2 and +3. Homo- and heteronuclear silyl-substituted bismuth complexes could be obtained by different synthetic strategies: (a) metalation of trisilylbismuthane with alkyllithium,[1] (b) conversion of lithium bis(trisilylbismuthane) with 1,2-dibromoethane,[1] (c) conversion of sodium potassium bismuthide with 1,2-dichlorotetramethyl-disilane,[2] (d) reduction of bismuth halides with alkali metal silanides[3] and with silyl-substituted lithium phosphanides[4] {the formation of the silyl-substituted bismuth complexes from the reactions of $Ar'BiCl_2$ [Ar' = 2,6-(2,6-*i*Pr_2-C_6H_3)$_2$-C_6H_3] with potassium silanides was not observed},[12] (e) dehydrosilylation of group 13 diorganohydrides with trisilylbismuthane,[5,6,9] (f) heterometallic addition of trisilylbismuthane to group 13 trialkyl compounds,[6-8] (g) conversion of trisilylbismuthane with copper(I) *tert*-butoxide and trialkylphosphanes,[10] and (h) metathesis reaction of a heterometallic aluminum-bismuth adduct with a trialkyl indium-pyridine adduct.[11]

The redox and metathesis conversions of bismuth tribromide with the lithium silanide $Li(thf)_3SiPh_2$*t*Bu[13] in various ratios, resulting in a stable silyl-substituted dibismuthane and a disilylbismuth halide, are performed, herein. Quantum chemical calculations are applied on simplified model compounds of silyl- and alkyl-substituted bismuthanes to obtain an insight into the possibility of forming $(R_3Si)_3Bi$ structures, the stability of the silyl-substituted $(H_3Si)_2E\cdot$ radicals against dimerization as well as the instability of $[(H_3Si)_2E]_2$ molecules towards dissociation in the series of pnicogens E = P, As, Sb, Bi. In addition, the oligomerization of $n(H_3A)_2Bi^{\cdot}$ radicals (A = C, Si; *n* = 2–4), the bonding and orbital situations as well as the electronic excitations in the dibismuthane and its oligomerized forms are studied with the use of density functional (DFT), time-dependent density functional (TD-DFT), and conventional *ab initio* theory to get an insight into the nature of Bi–Bi and Bi···Bi interactions, which have been observed in the fluid and crystalline phase.

2.2.2 Reduction *vs.* metathesis in the reactions of $BiBr_3$ with $Li(thf)_3SiPh_2tBu$

2.2.2.1 Syntheses and spectroscopic characterization of $(tBuPh_2Si)_4Bi_2$ and $(tBuPh_2Si)_2BiBr$

The reactions of $BiBr_3$ with $Li(thf)_3SiPh_2tBu$ (**1**) in the corresponding ratios in the solvent toluene yield the silyl-substituted bismuthanes $(tBuPh_2Si)_4Bi_2$ (**2**) and $(tBuPh_2Si)_2BiBr$ (**3**) (Scheme 1). Thus, the intended salt metathesis reaction of $BiBr_3$ with three equivalents of **1** leads to a redox process under the applied conditions (warming from –78 °C to r.t. during the reaction), resulting in the dibismuthane $(tBuPh_2Si)_4Bi_2$ (**2**) and the disilane $(tBuPh_2Si)_2$. During the reaction the color of the solution changes from green to red-brown. Workup allows isolation of **2** as dark-red crystals soluble in toluene. The ^{29}Si NMR spectrum of the dark-red solution contains two signals: singlets for the silicon atoms of dibismuthane (15.9 ppm) and disilane (–2.16 ppm).

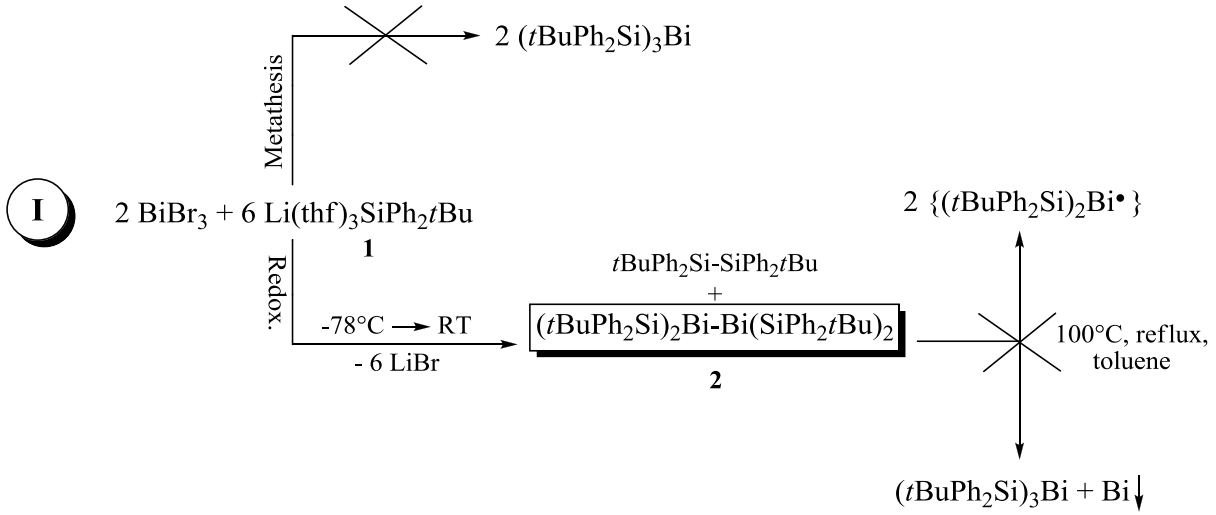

Scheme 1. Reaction pathways I and II leading to the formation of bismuthanes **2** and **3**.

The formation of $(tBuPh_2Si)_3Bi$ was not observed. This is probably due to steric reasons, which will be discussed later.

Heating of **2** under reflux at 100 °C for 3 h did not lead to disproportionation into elemental bismuth and $(tBuPh_2Si)_3Bi$ or to dissociation of **2** into corresponding radicals. As a result, **2** could be observed in the reaction solution again as a thermodynamically stable compound. This high thermostability may be related to the relatively short Bi–Bi distance in **2**.

The reaction of $BiBr_3$ with **1** in a 1:2 and 1:1 ratio gives the disilylbismuth halide $(tBuPh_2Si)_2BiBr$ (**3**) together with **2**. Here, after workup of the reaction mixture, red crystals of **3**

were isolated from the dark-green hexane solution as well as from the red toluene solution only. The ^{29}Si NMR spectra of the solutions show singlets at –4.19 and –6.10 ppm, respectively. In addition, both solutions contain **2**, which forms here predominantly (ratio ca. 2.5:1 according to ^{29}Si NMR signals). Interestingly, the dark-green solution is more stable than that of red color, which decomposes with formation of elemental bismuth after short periods of time at low temperature (–20 °C) or much faster at room temperature. In our opinion, the dark-green oily solution should contain a form of **3** oligomerized via weak Br–Bi···Br intermolecular contacts (like Mes_2BiBr,[14] for example; Figure A), which are broken upon crystallization of the oligomer to give **3**. However, no crystals could be isolated from this solution.

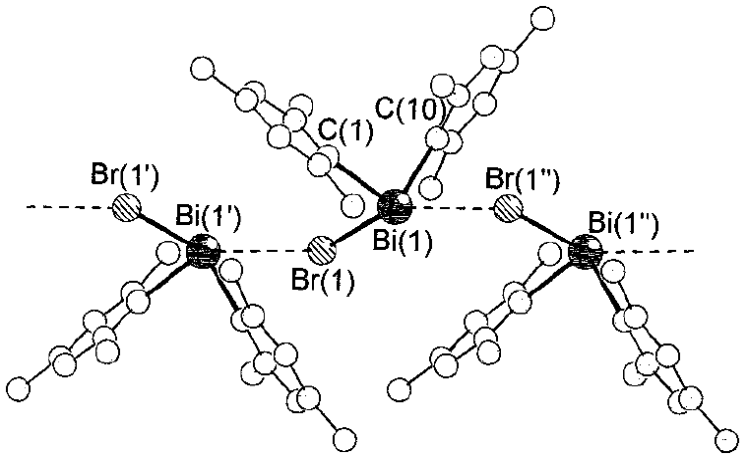

Figure A. Polymeric association in the crystal of Mes_2BiBr ($d_{Br–Bi\cdots Br}$ = 379.5 pm).[14,22]

2.2.2.2 X-ray crystal structure of $Li(thf)_3SiPh_2tBu$

Tris(tetrahydrofuran)lithium(*tert*-butyldiphenylsilanide)lithium [$Li(thf)_3SiPh_2tBu$ (**1**)] was synthesized by starting from the reaction of chloro-*tert*-butyldiphenylsilane, $tBuPh_2SiCl$, with lithium granulate in tetrahydrofuran solution according to the literature procedure.[13] The compound was crystallized from a *n*-hexane/thf mixture at –20 °C. Compound **1** crystallizes in the monoclinic crystal system, space group $P2_1/n$ (Table 3). Figure 1 shows the molecular structure of **1** in the solid state. The asymmetric unit contains three independent molecules of **1**. The crystal structure displays monomer silanide units, where the lithium ions are surrounded by three thf molecules and a silicon atom in a tetrahedral geometry. They differ only in the slight disorder of coordinated thf molecules and in the rotational conformation of the $(thf)_3Li$ and the $SiPh_2tBu$ units. For the $C_{Bu}SiLiO$, torsional angle values of 37°, 39°, and 49° are observed. The Si–Li bond lengths in the three independent molecules [266.0(5), 267.5(5), 269.0(5) pm] are fairly similar. This is in the typical range, as compared to other thf adducts of monomeric lithium silanides {262.7 pm in $Li(thf)_3SiPh(NEt_2)_2$,[15] 266.9 pm in $Li(thf)_3Si(SiMe_3)_3$,[16] 267.2

pm in $Li(thf)_3SiPh_3$,[16] 267.8 and 268.2 pm in $Li(thf)_3SiPh_2(NEt_2)$,[15] 271.7 pm in $Li(thf)_3Si\textit{t}Bu_3$,[17,18] 273.2 pm in $Li(thf)_3SiPh_2(NPh_2)$,[19] and 276.0 pm in $Li(thf)_3Si(SiMe_2SiMe_3)_3$[20]}. A computational analysis of structure, energetic and molecular properties of **1** and its derivates can be found in the appendix to chapter 2.2.

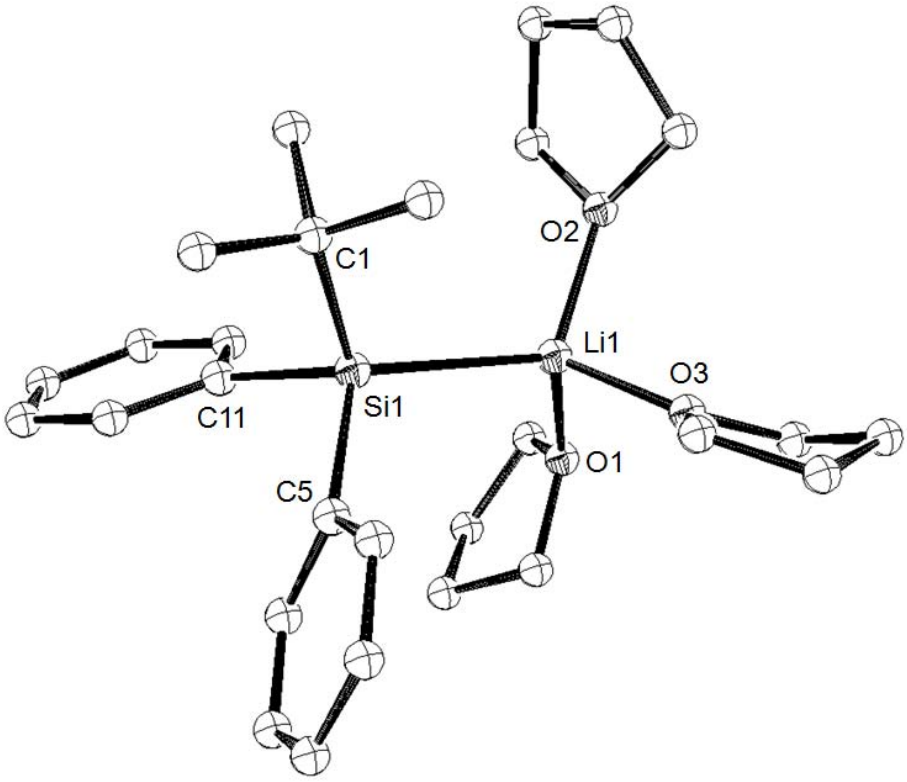

Figure 1. Molecular structure of lithium silanide **1** (crystal; the thermal ellipsoids are given at the 30 % probability level; hydrogen atoms are omitted for clarity). Only one of the three independent molecules is shown. Selected bond lengths [pm] and angles [°]: Si1–Li1 267.5(5), Si1–C5 192.0(4), Si1–C11 192.7(4), Si1–C1 195.8(5), O1–Li1 198.1(8), O2–Li1 196.1(8), O3–Li1 192.4(8), C5–Si1–C11 99.8(2), C5–Si1–C1 106.3(2), C11–Si1–C1 102.2(2), O3–Li1–O2 105.1(3), O3–Li1–O1 99.1(4), O2–Li1–O1 106.8(3).

2.2.2.3 X-ray crystal structure of $(tBuPh_2Si)_4Bi_2$

Compound **2**, $(\textit{t}BuPh_2Si)_4Bi_2$ crystallizes in the triclinic crystal system, space group $P\bar{1}$, $Z = 2$ (Figure 2). The solid-state molecular structure shows a dibismuthane with a Bi–Bi bond length of 300.6 pm. The $Si_2Bi–BiSi_2$ core is in the semi-eclipsed conformation, where each bismuth atom is surrounded by two *tert*-butyldiphenylsilyl ($\textit{t}BuPh_2Si$) groups. Two silyl-containing dibismuthanes of similar structural type, but with less bulky silyl (Me_3Si) or alkyl [$(Me_3Si)_2CH$] groups, have been reported up to now.[1,21] The Bi–Bi distance in **2** is shorter by 2.9 pm and 4.7 pm than in anti-periplanar molecules $(Me_3Si)_4Bi_2$ ($d_{Bi–Bi}$ = 303.5 pm)[1] and $[(Me_3Si)_2CH]_4Bi_2$

($d_{Bi–Bi}$ = 305.3 pm),[21] respectively. Finally, it is 3.4 pm shorter than the sum of the covalent radii ($\Delta\Sigma r_{cov}$ = 304 pm). The Bi–Si bond lengths in **2** are $d_{Bi–Si}$ = 268.6 – 270.8 pm, which is expected from the covalent radii of bismuth and silicon [r_{cov}(Si) = 0.5$r_{(Si–Si)}$, $r_{(Si–Si)}$ = 238.6 pm in (tBuPh$_2$Si)$_2$; see the appendix to chapter 2.2].

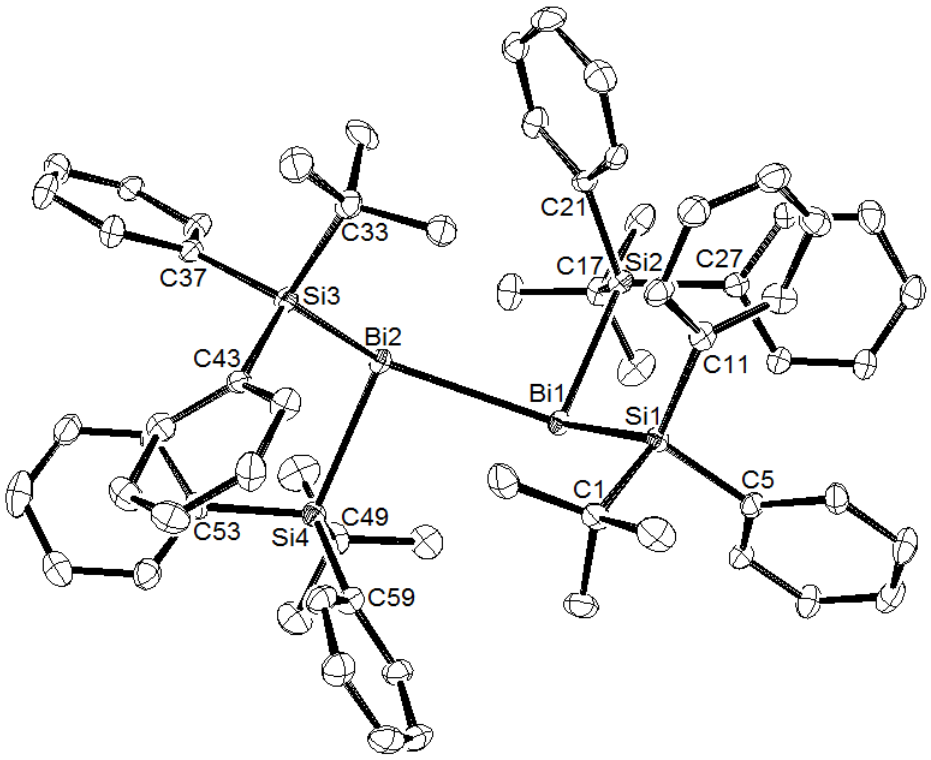

Figure 2. Molecular structure of **2** (crystal; the thermal ellipsoids are given at the 30 % probability level; hydrogen atoms are omitted for clarity). Selected bond lengths [pm] and angles [°]: Bi1–Bi2 300.6(8), Bi1–Si2 268.9(2), Bi1–Si1 270.8(2), Bi2–Si4 268.6(3), Bi2–Si3 268.7(3), Si1–C11 187.8(9), Si1–C1 190.2(9), Si1–C5 191.4(9), Si2–C21 186.4(8), Si2–C27 187.1(9), Si2–C17 190.7(8), Si3–C43 187.5(8), Si3–C37 189.6(8), Si3–C33 191.3(10), Si4–C53 187.5(9), Si4–C59 188.3(8), Si4–C49 192.3(9), Si2–Bi1–Si1 101.6(7), Si2–Bi1–Bi2 93.9(6), Si1–Bi1–Bi2 124.6(6), Si4–Bi2–Si3 101.8(8), Si4–Bi2–Bi1 95.0(6), Si3–Bi2–Bi1 124.3(5), C11–Si1–C1 113.6(4), C11–Si1–C5 108.4(4), C1–Si1–C5 106.3(4), C11–Si1–Bi1 118.4(2), C1–Si1–Bi1 107.5(3), C5–Si1–Bi1 101.3(3), C21–Si2–C27 106.5(4), C21–Si2–C17 113.3(4), C27–Si2–C17 106.6(4), C21–Si2–Bi1 115.7(3), C27–Si2–Bi1 107.4(2), C17–Si2–Bi1 106.9(3), C43–Si3–C37 106.9(4), C43–Si3–C33 113.2(4), C37–Si3–C33 106.5(4), C43–Si3–Bi2 117.7(3), C37–Si3–Bi2 102.6(3), C33–Si3–Bi2 108.8(3), C53–Si4–C59 106.9(4), C53–Si4–C49 106.7(4), C59–Si4–C49 113.4(4), C53–Si4–Bi2 107.9(3), C59–Si4–Bi2 115.0(3), C49–Si4–Bi2 106.6(3), Si1–Bi1–Bi2–Si3 4.6(9), Si2–Bi1–Bi2–Si3 –102.4(8), Si1–Bi1–Bi2–Si4 –103.3(8), Si2–Bi1–Bi2–Si4 149.8(8).

The molecules of **2** can be regarded as isolated ones with a shortest intermolecular Bi···Bi distance of 1000 pm. In $(Me_3Si)_4Bi_2$, aggregation via Bi···Bi contacts (380.4 pm) was observed.[1,22] This leads to a moderate elongation of the Bi–Bi bond in the dibismuthane unit. The quantum chemical calculations, which will be discussed later, provide evidence for this.

The space-filling representations of the silyl-substituted molecules **2** and $[(Me_3Si)_2Bi]_2$ in Figure 3 show that bulky *t*BuPh$_2$Si groups of **2** more effectively surround the reactive Bi–Bi bond. Such effective steric protection of the bismuth centers in **2** can be regarded as one of the main reasons of the stability of this compound.

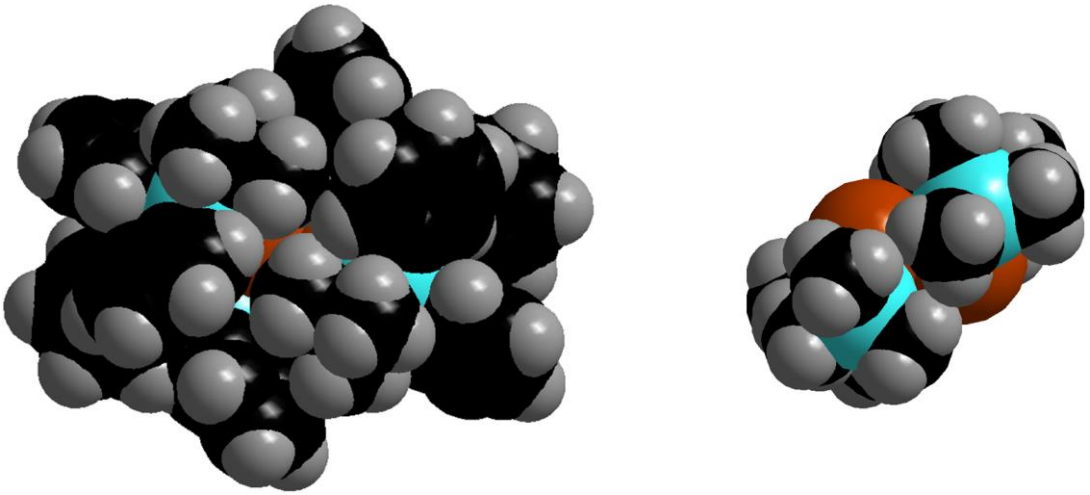

Figure 3. Space-filling models of silyl-substituted dibismuthanes **2** (left) and $[(Me_3Si)_2Bi]_2$ (right).

The bond angles around bismuth lie in the wide range of 94–125°, resulting in a sum of angles at the bismuth centers (Bi^{sum}) of 320.1° (Bi_1) and 321.0° (Bi_2). The dihedral angle τ between Si–Bi–Si planes is 84.1° (Figure 4). Thus, all of these angles are evidence of steric strain in **2**.

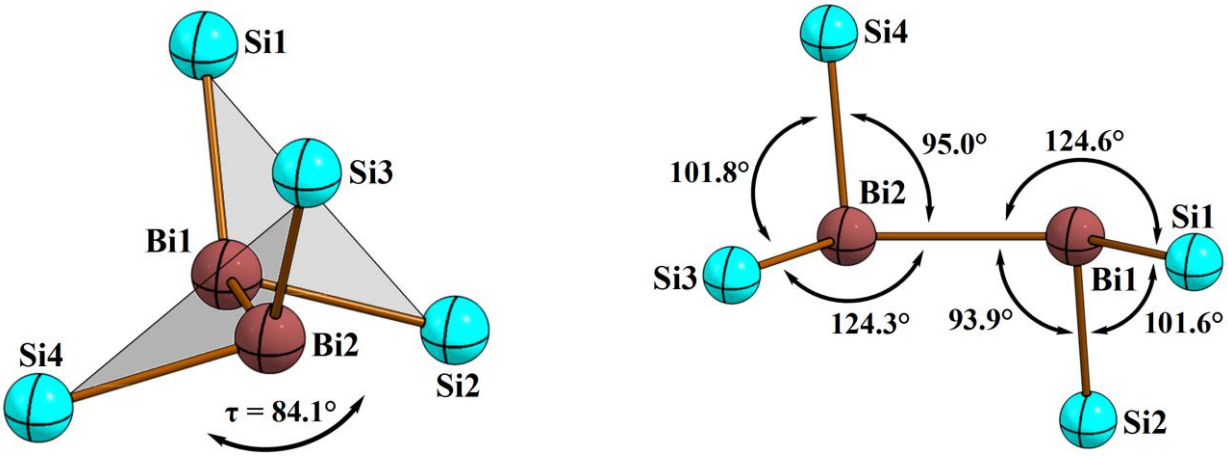

Figure 4. The core of dibismuthane **2**. Views along the Bi–Bi bond.

2.2.2.4 X-ray crystal structure of (tBuPh$_2$Si)$_2$BiBr

Compound **3**, (*t*BuPh$_2$Si)$_2$BiBr crystallizes in the orthorhombic crystal system, space group $P2_12_12_1$, $Z = 4$ (Figure 5). Its solid-state structure is similar to [(Me$_3$Si)$_2$CH]$_2$BiCl,[23] which is described as a mixed-substituted monomeric diorganobismuth halide with a pyramidal environment around the bismuth center. The Bi–Si bond lengths in **3** are 267.8 pm and 269.6 pm, which are similar to the Bi-Si distances in **2**. The Bi–Br distance is 266.7 pm. The Si–Bi–Si angle is 100.22°. As in [(Me$_3$Si)$_2$CH]$_2$BiCl, we observed a slight dissimilarity of the R–Bi–X angles (Si–Bi–Br = 96.97° and 98.70°). Such slight distortions in the Bi–Si bond lengths and Si–Bi–Br angles may be related to steric strain in **3**. In addition, the total sum of angles at the bismuth center (Bi^{sum}) is 295.9°. This is a smaller deviation than that in **2** from the expected structure of R$_3$Bi with bond angles of 90° each.

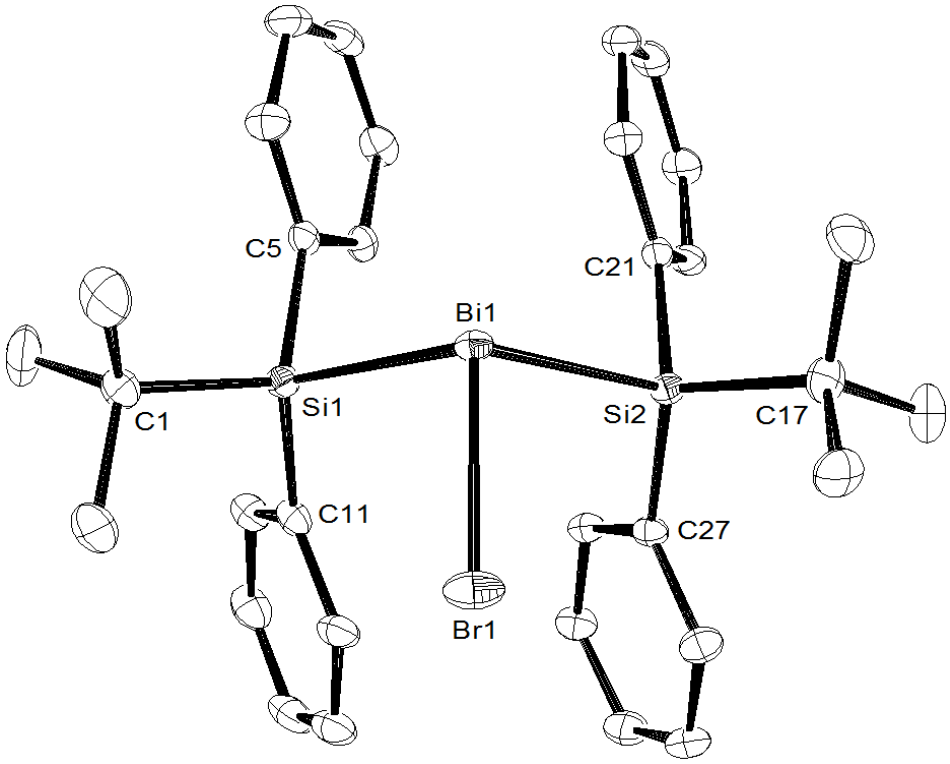

Figure 5. Molecular structure of **3** (crystal; the thermal ellipsoids are given at the 30 % probability level; hydrogen atoms are omitted for clarity). Selected bond lengths [pm] and angles [°]: Br1–Bi1 266.7(7), Bi1–Si1 267.8(1), Bi1–Si2 269.6(1), Si1–C11 186.8(5), Si1–C5 187.4(4), Si1–C1 191.0(5), Si2–C27 186.3(4), Si2–C21 186.9(4), Si2–C17 189.8(5), Br1–Bi1–Si1 98.7(3), Br1–Bi1–Si2 97.0(3), Si1–Bi1–Si2 100.2(3), C11–Si1–C5 111.7(2), C11–Si1–C1 107.7(2), C5–Si1–C1 112.9(2), C11–Si1–Bi1 117.2(1), C5–Si1–Bi1 98.4(1), C1–Si1–Bi1 108.8(2), C27–Si2–C21 110.8(2), C27–Si2–C17 113.2(2), C21–Si2–C17 108.0(2), C27–Si2–Bi1 114.4(1), C21–Si2–Bi1 103.1(1), C17–Si2–Bi1 106.7(2).

As can be seen from the space-filling model of **3** (Figure 6), there is a vacant site on the bismuth atom, which is assigned to the lone pair (LP) on the bismuth atom. Through this LP, intermolecular interactions like Br–Bi···Br in the oligomerized form are enabled.

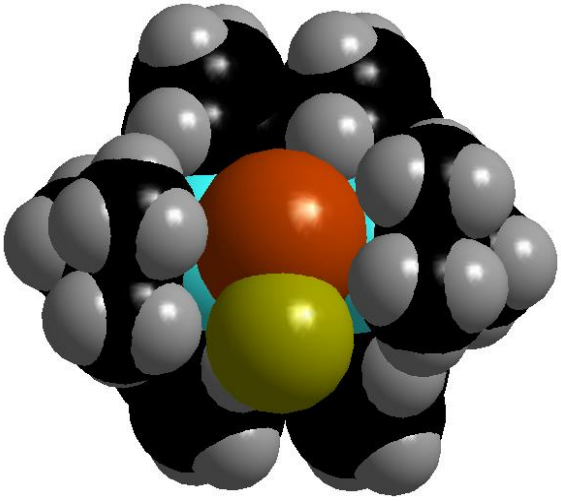

Figure 6. Space-filling models of disilylbismuth bromide **3**.

2.2.3 Quantum chemical study of bismuthanes and dibismuthanes

2.2.3.1 Pyramidal $(R_3Si)_3Bi$ structures

The possibility of forming $(R_3Si)_3E$ (E = metal element of main group) structures may be related to a "hybridization sp valence orbitals effect" of the metal, to the presence of the lone pair on the metal atom and its type, an orientation of the lone pair, and as a consequence the repulsive interactions of the R_3Si groups around metal center. Thus, according to the natural localized molecular orbitals (NLMO) analysis at the MP2(full) level on the DFT-optimized geometry of the simplified electrostatic model $(H_3Si)_3Bi$, the bismuth atom uses 9.3 % s and 90.4 % p orbitals for bonding with silyl groups [$s^{8.3\%}p^{91.4\%}$ according to the natural bond orbital (NBO)]. The lone pair of electrons on Bi possesses 74.6 % s and 25.4 % p character (according to the NLMO). As a result, the $(H_3Si)_3Bi$ structure shows a pyramidal environment around Bi (Figure 7), where the Si-Bi-Si angles are 89°. In NBO evaluations, the Bi–Si bonds are more weakly polarized toward Si atoms (ca. 50.7 %). In this manner, the valence sp hybrid orbitals at Bi are adapted for a nucleophilic attack of only moderately bulky alkyl or silyl anions like $[(Me_3Si_2)AH]^-$ (A = C) or $[AMe_3]^-$ (A = Si) to form $(R_3A)_3Bi$.[24] Increased steric bulk of substituents leads to an increase in the Bi–Si bond lengths [267.0 pm for $(H_3Si)_3Bi$; 267.8 pm for $(Me_3Si)_3Bi$; 273.2 – 275.9 pm for $(i\text{Pr}_3Si)_3Bi$] and the Si–Bi–Si angles [89.0° for $(H_3Si)_3Bi$, 96.8° for $(Me_3Si)_3Bi$, 107.1 – 109.7° for $(i\text{Pr}_3Si)_3Bi$], and, consequently, to more steric strain in the molecule. Here, $(t\text{BuPh}_2Si)_3Bi$ is a good example. Thus, according to the DFT-optimized

geometry of the tertiary bismuthane (*t*BuPh$_2$Si)$_3$Bi, the Bi–Si bond lengths and the Si–Bi–Si angles lie between 273.3 and 275.1 pm, and 99.6 and 109.8°, respectively. Such relatively large deviations in the Bi–Si distances and the Si–Bi–Si angles may be related to repulsive interactions of the silyl substituents in (*t*BuPh$_2$Si)$_3$Bi. Therefore, three bulky *t*BuPh$_2$Si ligands may be hardly coordinated to the bismuth centre on the way of experimentally described reactions here, whereas for indium (for example), displaying a planar structural motive in the solid state, this is accessible [synthesis and X-ray crystal structure of In(SiPh$_2$*t*Bu)$_3$ can be found in the appendix to chapter 2.2].[25]

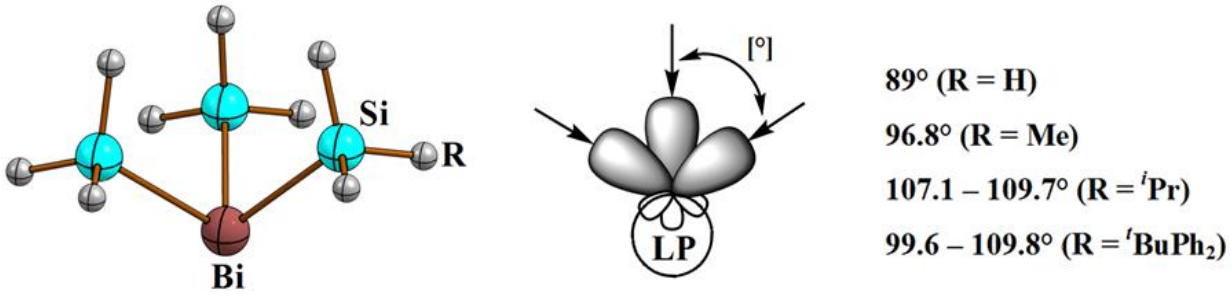

Figure 7. DFT-optimized structure for (R$_3$Si)$_3$Bi (R = H, Me, *i*Pr, *t*BuPh$_2$) molecules and view of sp valence orbitals of metal.

2.2.3.2 Pnicogen radicals (H$_3$Si)$_2$E$^{\cdot}$ and their dimers

Formation of persistent radicals (R')$_2$E$^{\cdot}$ (R' = alkyl or amide) of group 15 elements is well known. Thus, the phosphanyl and arsinyl radicals,[26,27] generated in solution by reaction of the dialkyl- or diamidophosphorus(III) or -arsenic(III) monochlorides with an electron-rich olefin, or under photolytic conditions by melting or vaporizing of the dipnicogens [here, (PR'$_2$)$_2$], have been observed in solution as well as in the gas phase and characterized by ESR spectroscopy, gas-phase electron diffraction (GED), and X-ray crystal analysis. In addition, the participation of the group 15 p elements in the formation of the silyl radicals is established. For example, homolysis of tris(triethylsilyl)antimony leads to antimony and free triethylsilyl radicals.[28] In case of bismuth, the formation of its (R')$_2$Bi$^{\cdot}$ radicals has been observed in the gas phase. Thus, the signals for (R')$_2$Bi$^+$ ions [R' = (Me$_3$Si$_2$)CH or 2,6-(Me$_2$NCH$_2$)$_2$C$_6$H$_3$] could be detected by EI mass spectrometry.[21,29] The probable formation of the bismuth radicals in liquid ammonia was reported by Gilman.[30] Di-*p*-tolylbismuth halide and sodium reacted to yield an intensely green colored solution. The homolytic cleavage of the Bi–Bi single bond should depend on the steric bulk of the ligands. In our case, a bismuth cation [(*t*BuPh$_2$Si)$_2$Bi]$^+$ was observed in toluene solution by LIFDI mass spectrometry, indicating homolytic dissociation of the dibismuthane and subsequent ionization.

Herein, the stability of the silyl-substituted $(H_3Si)_2E^{\cdot}$ radicals towards dimerization, and thus, the instability of $[(H_3Si)_2E]_2$ molecules towards dissociation in the series of pnicogens E = P, As, Sb, Bi are discussed on the basis of the bond association and dissociation energies, respectively, as well as on the basis of the total charge transfer on the pnicogen atoms during both of these processes.

Upon traveling downward within group E, the bond length E–E in the $[(H_3Si)_2E]_2$ compounds becomes longer and the natural population analysis (NPA) pnicogen charge becomes more positive (Table 1, Figure 8). This is in line with the increasing covalent radii and decreasing electronegativity of the homologous elements. The relatively small increase in the Bi–Bi bond length compared to that in the Sb–Sb bond length may be related to "relativistic effects", which result in a decrease in the atom sizes and a shortening of the E–E bond. Upon dimerization of the pnicogen radicals, the association energies for $[(H_3Si)_2E]_2$ decrease within the group (Table 1, Figure 9).

Table 1. Intramolecular properties. Computed structural and bond strength parameters, and calculated charges and energies for molecules $[(H_3Si)_2E]_2$ (E = P, As, Sb, Bi) of C_{2h} symmetry.

Parameter	$(H_3Si)_2E–E(SiH_3)_2$			
	E = P	E = As	E = Sb	E = Bi
d(E–E)[a]	225.7	247.6	285.6	301.4
Q_{NPA}[b]	–0.3990	–0.2568	+0.0002	+0.0741
ΔQ_{ct}(as)[c]	–0.350	–0.320	–0.283	–0.234
ΔQ_{ct}(dis)[c]	+0.350	+0.320	+0.283	+0.234
WBI[c]	0.995	0.980	0.974	0.970
OOv[d]	0.761	0.722	0.719	0.658
ΔE_{as}[e]	–215.4	–188.8	–155.8	–141.3
ΔE_{dis}[e]	215.4	188.8	155.8	141.3

[a] E–E bond lengths [pm] were computed at the PBE0/BS-I level of theory. [b] The NPA pnicogen charges *e* were computed at the MP2(full)/BS-II//PBE0/BS-I level. [c] Total charge transfers (ΔQ_{ct}) *e* upon association (as) and dissociation (dis) and the Wiberg bond index (WBI) for E–E were calculated at the MP2(full)/BS-II//PBE0/BS-I level. [d] Order of overlapping (OOv) of the valence sp orbitals of the pnicogens was computed at the MP2(full)/BS-II//PBE0/BS-I level. [e] E–E bond association (ΔE_{as}) and bond dissociation (ΔE_{dis}) energies [kJ/mol] were calculated at the MP4(SDQ)/BS-II//PBE0/BS-I level.

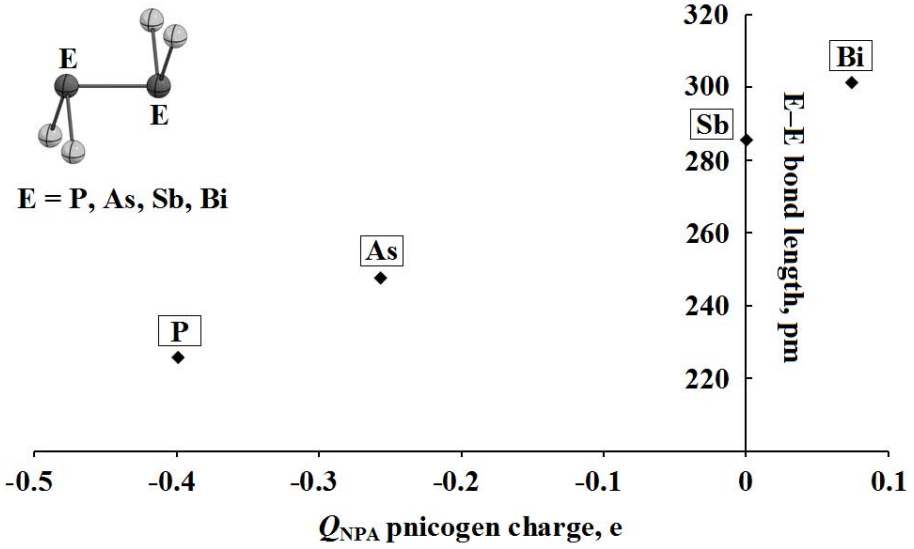

Figure 8. Calculated bond lengths and NPA pnicogen charges for $[(H_3Si)_2E]_2$ (E = P, As, Sb, Bi).

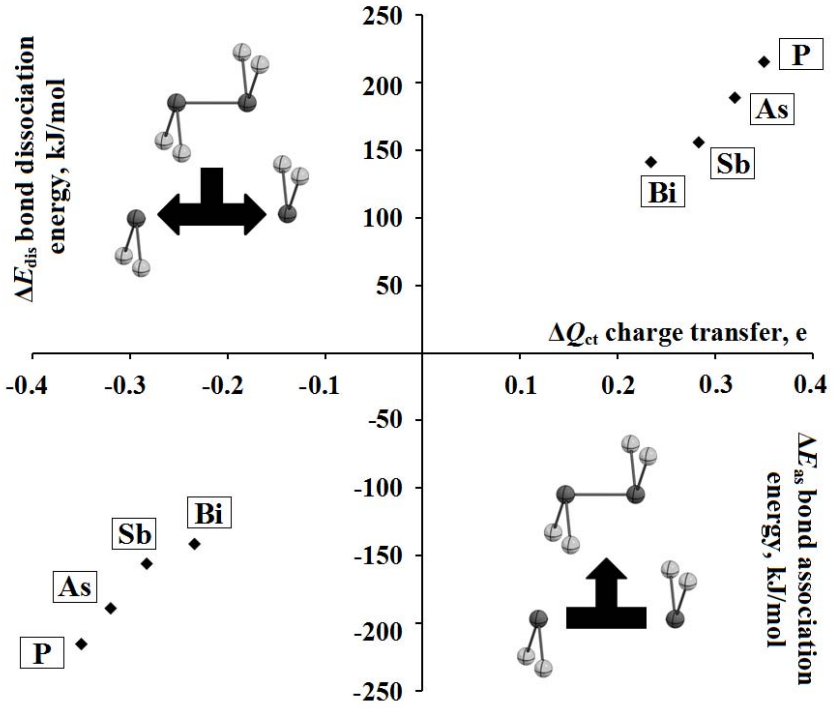

Figure 9. Calculated E–E bond association energies for $(H_3Si)_2E^{\cdot}$ and E–E bond dissociation energies for $[(H_3Si)_2E]_2$ (E = P, As, Sb, Bi) and corresponding total charge transfers on the pnicogen atoms.

In addition, the total intramolecular charge transfer for the lighter elements becomes more negative; this corresponds to a better stabilization of the molecules by the formation of E–E bonds. As a consequence, the instability of the E–E bond increases within the group, which is expressed in a decrease in the bond dissociation energies of $[(H_3Si)_2E]_2$ molecules. Here, as expected, the longer the bond length, the less is the bond energy. The total charge transfer also

indicates that the Bi–Bi bond is the most flexible among the E–E bonds of other pnicogens. The E–E bond strengths for $[(H_3Si)_2E]_2$ molecules (P–P > As–As > Sb–Sb > Bi–Bi), on the basis of the Wiberg bond indexes (WBIs) and the effective overlapping of orbitals, provide evidence for results described above (Table 1). As a result, the $[(H_3Si)_2Bi]_2$ dimers possess the lowest stability among these compounds of pnicogens. An increase in stability of the bismuth species might be achieved by the steric bulk of the silyl substituents. For example, dibismuthanes R_4Bi_2 with little and moderate steric protection [R = Me, Et, $SiMe_3$, $CH(SiMe_3)_2$] are thermolabile and have a tendency toward disproportionation into elemental bismuth and tertiary bismuthanes $(R_3A)_3Bi$. In contrast to this, bismuthane molecules R_yBi_x (x, y = 2–4) with bulky groups [R = Ph, Mes, Si*t*Bu, $Si(SiMe_3)_3$; in our case R = *t*$BuPh_2$] are stabilized with respect to thermal decomposition.[1,3,4,31]

2.2.3.3. N-merization of $n(H_3A)_2Bi^{\cdot}$ radicals and oligomerization of dimers

The *n*-merization of $(H_3A)_2Bi^{\cdot}$ radicals into $[(H_3A)_2Bi]_n$ (A = C, Si; n = 2–3) and the oligomerization associated with the formation of the systems $n[(H_3A)_2Bi]_2$ (A = C, Si; n = 2) via intermolecular Bi···Bi contacts were evaluated by means of structure, charge, and energy calculations (Table 2, Figure 10). According to DFT computations, the intramolecular Bi-Bi bond lengths in $n[(H_3A)_2Bi]_2$ elongate upon oligomerization. In $[(H_3A)_2Bi]_3$ a 3c3e bond is to be formulated. The tetramers $n[(H_3A)_2Bi]_2$ (n = 2) are a model for the oligomerization observed for R_4Bi_2 compounds in the liquid and crystalline phase. Here, rectangle and chain oligomerization has to be distinguished. Thus, the Bi_2 unit is retained and only weak intermolecular Bi···Bi contacts appear. The intermolecular Bi···Bi distances in $n[(H_3A)_2Bi]_2$ are shorter than the sum of van der Waals radii of Bi in the chain oligomerization and longer in case of the distorted rectangle oligomerization. As can be seen, the NPA bismuth charges in the silyl-substituted molecules are much lower than those in the alkyl-substituted molecules. This corresponds to better donor properties of the silyl substituents and leads to a shrinking of the covalent radius of bismuth in the alkyl derivatives. The different electronegativity of C and Si atoms, better polarization of the Bi–C bonds, which are highly polarized toward carbon atoms (ca. 70 %) here, as well as two highly positive charges on neighboring Bi atoms should lead to an elongation of the intermolecular $Bi^{+Q}\cdots{}^{+Q}Bi$ bond. As a result, the repulsive van der Waals force between two alkyl-substituted dimers (A = C) dominates (Table 2). All in all, this is well expressed for the chain oligomerization. However, the distorted rectangle oligomerization reveals an inverse situation: here, the intermolecular Bi···Bi distances between alkyl-substituted dimers are slightly shorter than those between the silyl-substituted dimers. This phenomenon will be discussed later.

Table 2. Intermolecular properties. Computed structural parameters and calculated charges and energies for molecules $[(H_3A)_2Bi]_2$ (A = C, Si).

Parameter	$[(H_3A)_2Bi]_n$				$n[(H_3A)_2Bi]_2$			
	n = 2		n = 3		n = 2 (rectangle)		n = 2 (chain)	
	A = C	A = Si	A = C	A = Si	A = C	A = Si	A = C	A = Si
Bi1–Bi2[a]	299.9	301.4	319.4	320.2	301.4	302.5	300.8	302.6
Bi2–Bi3			319.3	319.5			392.2	379.9
Bi3–Bi4					301.4	302.5	300.7	302.5
Bi1–Bi3					424.2	429.5		
Bi2–Bi4					425.3	431.5		
Q_{NPA}[b]	+0.814	+0.074	+0.849	+0.127	+0.799[av]	+0.044[av]	+0.828	+0.099
			+0.773[d]	–0.019[d]	+0.799[av]	+0.041[av]	+0.793[e]	+0.028[e]
ΔE_{mer}[c]	–130.5	–141.3	–130.4	–153.2	–277.2	–301.7	–272.4	–303.1
ΔE_{inter}[c]					–16.2	–19.1	–11.5	–20.6
E_n[c]	–65.2	–70.6	–43.5	–51.1	–69.3	–75.4	–68.1	–75.8

[a] Bi–Bi bond lengths and intermolecular Bi···Bi contacts [pm] were computed at the PBE0/BS-I level of theory. [b] The NPA charges e at Bi were computed at the MP2(full)/BS-II//PBE0/BS-I level. [c] Energies of n-merization of $(H_3A)_2Bi^{\cdot}$ radicals and energies of intermolecular contacts (ΔE_{mer} and ΔE_{inter}, respectively) [kJ/mol], as well as energy gains per radical unit (E_n) were calculated at the MP4(SDQ)/BS-II//PBE0/BS-I level. [d] NPA charge on the central Bi atom in the trimer. [e] NPA charges on intermolecular interaction centers of bismuth.

The increase in the energy gain (E_n) per radical $(H_3A)_2Bi^{\cdot}$ unit for $[(H_3A)_2Bi]_n$ and $n[(H_3A)_2Bi]$ (A = C, Si) molecules listed in Table 2 indicates increased stabilization of the corresponding systems. Therefore, the silyl-substituted molecules spend more energy *per* radical unit than alkyl-substituted ones gain. The energies of the intermolecular Bi···Bi contacts (ΔE_{inter}) in the tetramers $n[(H_3A)_2Bi]_2$ (n = 2) show that for A = C the distorted rectangle oligomerization is more preferred (about 1.4 times more in the exothermic energy) over chain formation, whilst for A = Si the chain oligomerization is slightly more preferred. As one of the reasons, this inversion barrier at bismuth may be related to better delocalization of two high charges on Bi for A = C via the distorted rectangle, even though the Bi···Bi distances in the rectangle formation are longer than the sum of van der Waals radii of Bi. Such an effect is more weakly expressed for A = Si. An appreciable increase in the exothermic energies ΔE_{inter} with the

increase in the number of $n[(H_3A)_2Bi]_2$ molecules *per* chain (n = 3) was not observed. Thus, the exchange of H atoms for Me groups in anti-periplanar $[(H_3Si)_2Bi]_2$ should lead to a stronger shift to chain formation on the basis of an increase in the steric strain in the molecule.

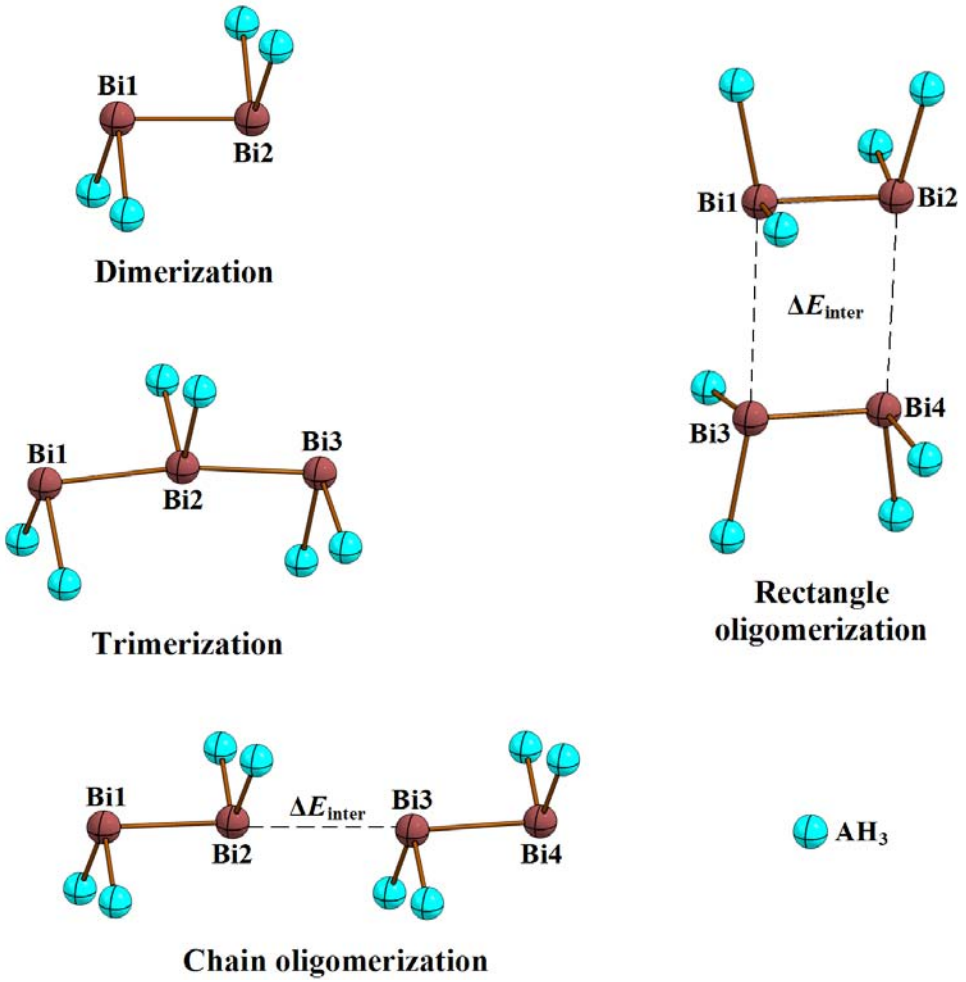

Figure 10. General view of DFT-optimized structures of $[(H_3A)_2Bi]_n$ (A = C, Si) molecules (hydrogen atoms are omitted for clarity).

The forms of the oligomerization, described above for the gas phase, have been experimentally observed for $(R_2Bi)_2$ [R = Me, $SiMe_3$; R_2 = $(CMe{=}CH)_2$; chain][1,32] and $\{[(Me_3Si)_2CH]_2Bi\}_2$[21] (rectangle). Here, it is necessary to remark that rectangle formation for the $\{[(Me_3Si)_2CH]_2Bi\}_2$ molecule was established in the liquid phase by NMR spectroscopy as a dynamic process of an exchange of the $[(Me_3Si)_2CH]_2Bi$ units between associated molecules, whereas in the crystalline phase, only chain formation for alkyl- and silyl-substituted dibismuthanes is well-known.[1,32] While the results, obtained in the gas phase for the silyl-substituted dibismuthane molecules, are in line with their experimental behavior in the crystalline phase {see $[(Me_3Si)_2Bi]_2$[1]}, the alkyl-substituted derivatives reveal various behavior. In addition, in the gas phase the intramolecular Bi-Bi bond length and the intermolecular Bi···Bi distance in the chained molecule $n[(H_3A)_2Bi]_2$

(A = C; *n* = 2) are 300.8 and 392.2 pm, respectively, whereas in the crystalline phase experimentally observed Bi–Bi bond length and Bi···Bi distance are 312 and 358 pm, respectively. Interestingly, the lengthening of the intramolecular Bi···Bi distance in the chained $R_4Bi_2\cdots Bi_2R_4$ (R = H) system to a value of 312 pm (in accordance with experimentally observed Bi–Bi bond lengths for R = Me in the crystalline phase) leads to a shortening in the intermolecular Bi···Bi distance, and as consequence, to an increase of about 11 % in energy of intermolecular contacts.[33] All in all, such a difference in structure and energy behavior in the gas, liquid, and crystalline phases may be related to the temperature factor, phase transitions, as well as to an influence of the solvent molecules. All of these possible reasons demand additional investigations on such factor-dependent systems. In addition, the chain and rectangle oligomerization should strongly depend on steric strain and rigidity of the ligands. In this manner, an increase in steric strain and rigidity of the substituents on the metal atoms should lead to a moderate shift into chain formation or no oligomerization. As a result, the types of oligomerization represented above are not expected for the molecules with effectively protecting silyl (like *t*$BuPh_2Si$) or alkyl ligands (see Figure 3, too).

2.2.3.4 NBO analysis

The charges (Q_{NPA}) on the bismuth atoms (natural electron configuration $6s^{1.78}6p^{3.13}$) in $[(H_3Si)_2Bi]_2$, obtained by natural population analysis (NPA) at the MP2(full) level, are slightly positive (+0.074e). The NPA bismuth charge in $(H_3Si)_2BiBr$ is much more positive than in $[(H_3Si)_2Bi]_2$, Q_{NPA} = +0.521e. The results of the NBO evaluations for $[(H_3Si)_2Bi]_2$ show that the bonding between bismuth centers (Bi–Bi; WBI = 0.97) is mainly carried out by p-p orbital overlap ($s^{5.0\%}p^{94.5\%}d^{0.5\%}$). This overlap corresponds to the hybrid HOMO of NBO type, which indicates a σ bond between the bismuth atoms (50 %) (Figure 11).

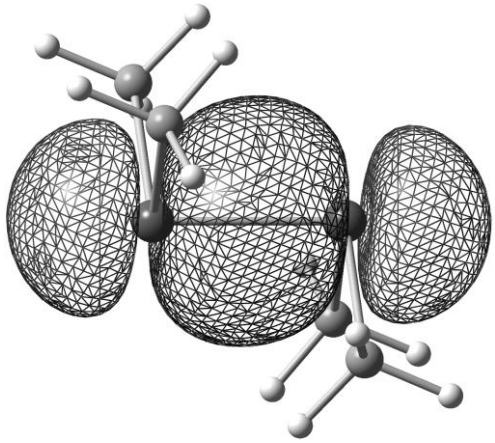

Figure 11. Graphical representation of the NBO hybrid HOMO of the model $(H_3Si)_2Bi–Bi(SiH_3)_2$.

As a result, the $[(H_3Si)_2Bi]_2$ molecule is apolar with a dipole moment of 0 Debye. The hybrid HOMO–1, HOMO–2, HOMO–3, and HOMO–4 contain the main contributions from the Bi–Si interactions, whereas the HOMO–5 and HOMO–6 are metal lone pairs of mainly s character ($s^{78.5\%}p^{21.5\%}$; NLMO analysis provides the same result). In the polar molecule $(H_3Si)_2BiBr$ (dipole moment ca. 4 Debye), the lone pair NHO at Bi is of type s ($s^{80.1\%}p^{19.9\%}$), too.

2.2.3.5. Results from molecular orbital theory

Figure 12 presents the frontier molecular orbitals of $[(H_3Si)_2Bi]_2$ obtained by means of canonical MO theory, which were computed at the MP4(SDQ)/BS-II//PBE0/BS-I level. Thus, according to the atomic orbital population of MOs, the components of HOMO–1 and LUMO come mainly from p orbitals of bismuth, while the HOMO contains the large s lone pair orbital parts of bismuth.

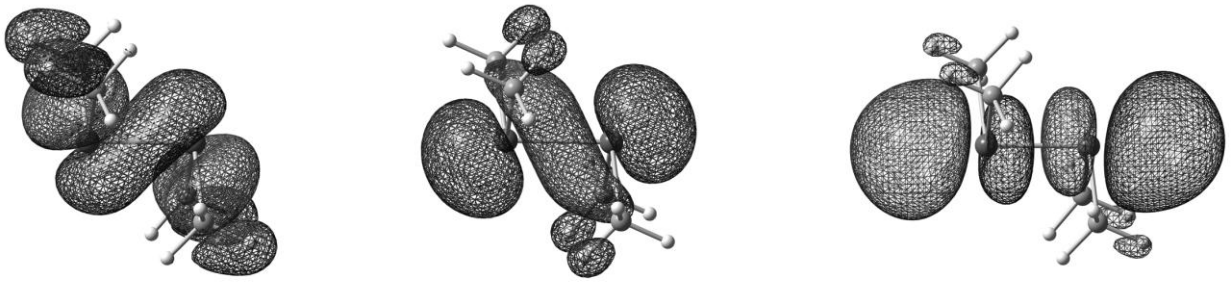

Figure 12. Graphical representation of the frontier canonical molecular orbitals of $(H_3Si)_2Bi–Bi(SiH_3)_2$ (± 0.02 isosurface value).

According to results of MO theory, the s LPs on Bi in model compound $[(H_3Si)_2Bi]_2$ with non-overloaded silyl substituents correspond to the HOMO. Interactions through these LPs are known and were observed in the reactions of tBu$_3$M with Bi_2Et_4, resulting in Lewis acid-base adducts $[Et_4Bi_2][Mt Bu_3]_2$ (where M = Al, Ga).[34] An increase in steric protection of the substituents should lead to a decrease in activity of the s LPs, and accordingly to an increase in stereochemical inert character. Therefore, the stereochemically active role of the LPs of bismuth in **2** is expressed very weakly. The s LP of **3** corresponds to the HOMO, too.

Interestingly, the $\Delta E_{HOMO–LUMO}$ gap for $[(H_3Si)_2Bi]_n$ decreases upon oligomerization (Figure 13). Thus, delocalization of p electrons of $(H_3Si)_2Bi^{\cdot}$ radicals (ΔE = 9.43 eV) in the Bi–Bi bond (the Bi–Bi stretching frequency is 127 cm^{-1}) leads to the reduction of ΔE toward 8.73 eV (n = 2). The Bi–Bi chain-oligomerized forms, $n[(H_3Si)_2Bi]_2$, have gaps of 7.75 eV (n = 2) and 7.24 eV (n = 3), accordingly. The values of the first ionization potentials (IP = E_{HOMO}; on the basis of the Koopman's theorem) and the energy values of the lowest unoccupied molecular

orbitals decrease, accordingly. According to DFT-optimized geometries of the $n[(H_3Si)_2Bi]_2$ systems (n = 1 – 3), the interaction between intermolecular Bi centers in the chain provides a moderate elongation of the intramolecular Bi–Bi bond in the dibismuthane unit from 301.4 pm for n = 1 through 302.5/302.6 pm for n = 2 toward 302.6/302.7 and 303.9 pm (central unit) for n = 3. In addition, this leads to a shorting of the intermolecular Bi···Bi contacts from 379.9 pm for n = 2 toward 378.2 pm (average) for n = 3.

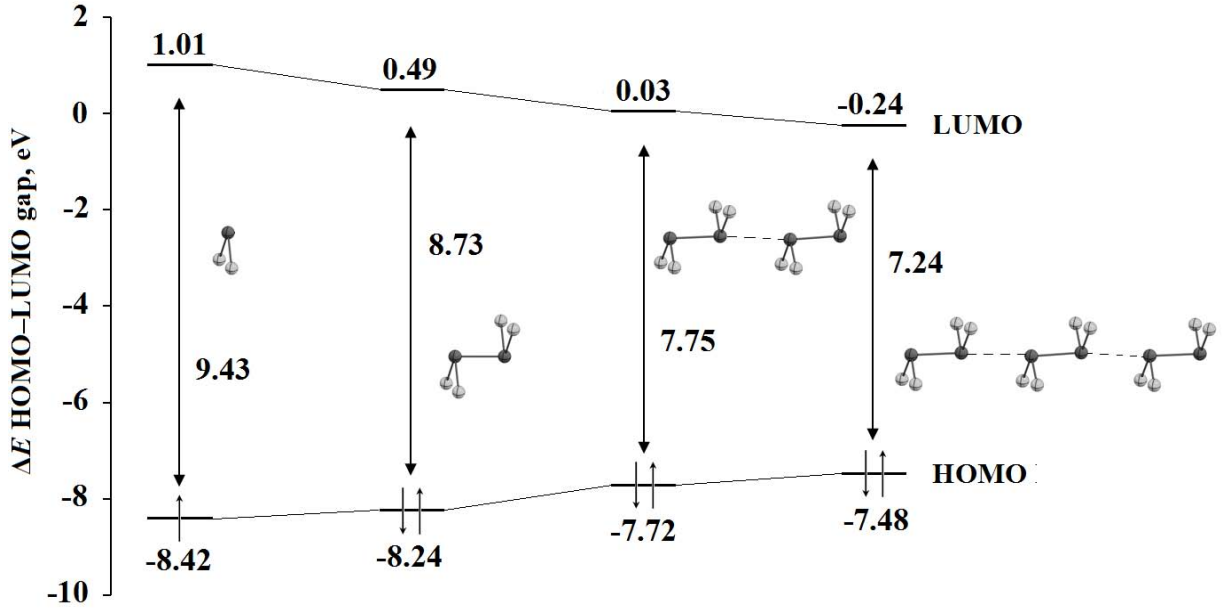

Figure 13. Changes in the HOMO–LUMO energy gap for $n(H_3Si)_2Bi^{\cdot}$ (n = 1–2) and $n[(H_3Si)_2Bi]_2$ (n = 2 – 3) systems upon n-merization and chain oligomerization, respectively.

As can be seen in Figure 14, the intermolecular interactions in the chained $[(H_3Si)_2Bi]_2\cdots[Bi(SiH_3)_2]_2$ molecule correspond to the bonding HOMO–1 (s LP orbitals that are bound together) and HOMO–3 (p-type orbitals that are bound together) and the LUMO with overlapping intermolecular p* orbitals, whereas the HOMO and the HOMO–2 are intermolecular antibonding in nature and correspond to the intramolecular interactions in each dimer molecule $[(H_3Si)_2Bi]_2$ (as described in Figure 12). As a result of the $[(H_3Si)_2Bi]_2\cdots[Bi(SiH_3)_2]_2$ intermolecular interaction, the charges on the bismuth interacting centers are reduced from +0.074e in dimer $[(H_3Si)_2Bi]_2$ to +0.028e in oligomer $[(H_3Si)_2Bi]_2\cdots[Bi(SiH_3)_2]_2$, whereas the charges on the non-interacting bismuth centers become slightly more positive +0.099e, accordingly. This induced dipole causes an electrostatic attraction between these two nonpolar molecules. Thus, the dipole moment of $[(H_3Si)_2Bi]_2$ is 0 Debye, whereas that of $[(H_3Si)_2Bi]_2\cdots[Bi(SiH_3)_2]_2$ becomes more positive, 0.46 Debye. In addition, such Bi···Bi intermolecular attraction is very weak (0.04) according to the WBI. This

fact and the small charges involved here, as well as the absence of other intermolecular contacts, point to the London dispersion force.

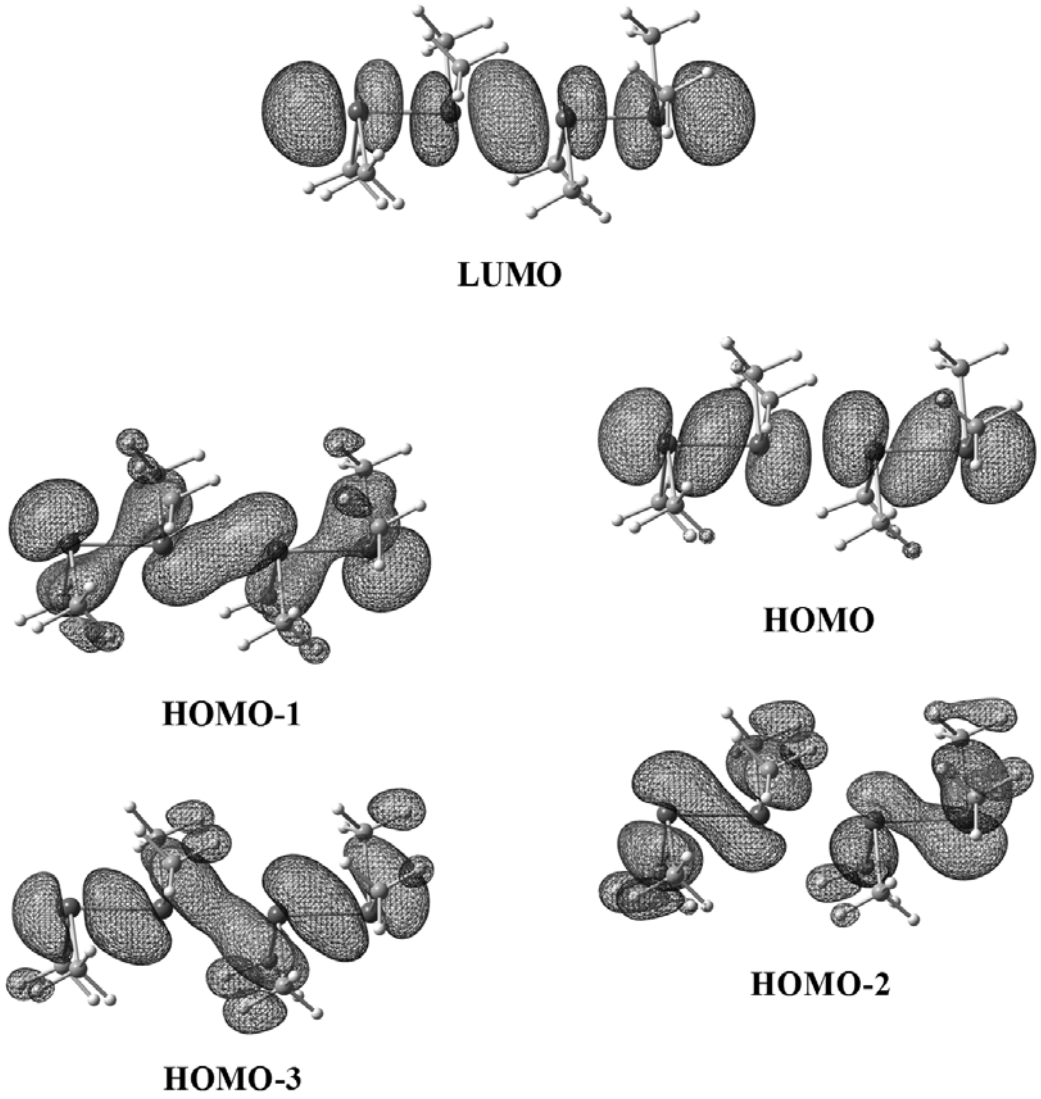

Figure 14. Graphical representation of the frontier canonical molecular orbitals of $[(H_3Si)_2Bi]_2\cdots[Bi(SiH_3)_2]_2$ upon oligomerization (± 0.02 isosurface value).

2.2.3.6 TD-DFT computations

According to time-dependent (TD) DFT computations of vertical electronic transitions in $[(H_3Si)_2Bi]_2$, the lowest energy $S_0 \rightarrow S_1$ electronic transition corresponds to the HOMO→LUMO and HOMO–1→LUMO excitations with a predominantly $n_{Bi(s,p)} \rightarrow n^*_{Bi(p)}$ character. The transitions are in the near UV region (301 nm, 4.12 eV, 33 223 cm^{-1}). Such electron transfer can be described as metal-metal charge transfer (MMCT excitation). Intermolecular interaction of s LPs of the Bi–Bi bond in the bismuth chain-oligomerized form (Figures 14) leads to a bathochromic shift toward lower frequencies.

The lowest energy electronic transitions for $n[(H_3Si)_2Bi]_2$ are 301 (n = 1), 347 (n = 2), and 391 nm (n = 3). This fits well with the results described above (Figure 13). Experimentally, a change in color is observed for $[(Me_3Si)_2Bi]_2$[1] upon transition between the fluid phase {red $[(Me_3Si)_2Bi]_2$} and the crystalline phase {green $n[(Me_3Si)_2Bi]_2$, where n is the number of molecules in the Bi chain}. These results are in contrast to those obtained for **2**, which is "nonthermochromic" dibismuthane. In addition, a maximum absorption band for the compounds with more bulky silyl ligands should be shifted to lower energy, too. The absorption spectrum of **2** in toluene provides evidence for this. Thus, the observed lowest energy absorption maximum lies at 465 nm (2.67 eV, 21 505 cm^{-1}) in the visible spectral region and is close to the value of the $S_0 \rightarrow S_1$ electronic transition (the HOMO→LUMO and HOMO–2→LUMO excitations) determined computationally by using the fixed structure of **2** from X-ray crystallography (418 nm, 2.97 eV, 23 923 cm^{-1}).

2.2.4 Conclusions

By the reactions of $BiBr_3$ with various amounts of the bulky lithium silanide **1**, the formation of Bi–Bi bonded product **2** could be observed. However, **2** was isolated only from the redox reaction in 1:3 ratio, as a main product. The formation of tertiary bismuthane $(t\text{BuPh}_2\text{Si})_3\text{Bi}$ was not observed. This is probably due to steric reasons. Accordingly, no oligomerization of **2** is observed. This is in contrast to the observation that $(Me_3Si)_4Bi_2$ is "thermochromic",[1] where oligomerization via Bi···Bi contacts is observed (Figure B). In all reactions, both metathesis and redox processes were observed. These led to the formation of Bi–Br bonded product **3** simultaneously with **2**.

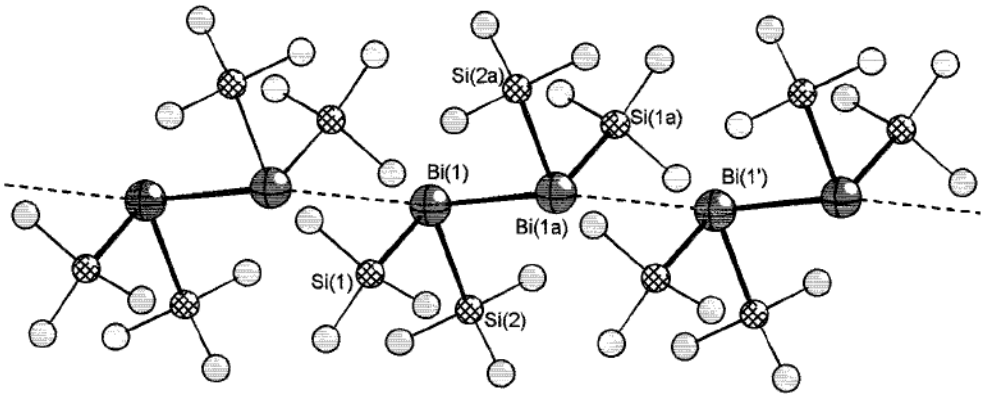

Figure B. Chain oligomerization in the crystal of $(Me_3Si)_2Bi–Bi(SiMe_3)_2$.[1,22]

The bulky $SiPh_2tBu$ ligand is a valuable source, which should promote the radicalization processes in the reactions of trigonal pyramidal structural units (like EX_3) of the group 15 elements (E = P, As, Sb, Bi) with alkali metal silanide $M(sol)_nSiPh_2tBu$ (M = Li, Na, K; n = 0–

3) on the basis of the shape of the silyl substituents (steric factor) and "hybridization sp valence orbital effect" of the corresponding element E (electronic factor).

Dibismuthanes such as **2** are potentially useful and important starting reagents for further synthetic applications. On one hand, dibismuthanes may react via the s LPs of Bi as σ-donor, to form Lewis acid-base adducts;[34] on the other hand, the more sterically demanding alkyl or silyl groups (like those in **2**) are, the less stereochemically active or quite inert these orbitals are. Finally, such compounds with Bi–Bi bonds open a way to ring systems or to bismuth species in its +1 oxidation state, for example.[31b] Sterically protecting ligands should play a key role and determine all probabilities of reaction of the complexes.

2.2.5 References

[1] (a) O. Mundt, G. Becker, M. Rössler, C. Witthauer, *Z. Anorg. Allg. Chem.* **1983**, *506*, 42; (b) (b) G. Becker, O. Mundt in *Unkonventionelle Wechselwirkungen in der Chemie metallischer Elemente*, VCH, Weinheim, **1992**, 199.

[2] G. M. Kollegger, H. Siegl, K. Hassler, K. Gruber, *Organometallics* **1996**, *15*, 4337.

[3] (a) G. Linti, W. Köstler, *Z. Anorg. Allg. Chem.* **2002**, *628*, 63; (b) G. Linti, W. Köstler, H. Pritzkow, *Eur. J. Inorg. Chem.* **2002**, 2643.

[4] C. von Hänisch, D. Nikolova, *Eur. J. Inorg. Chem.* **2006**, 4770.

[5] S. Schulz, M. Nieger, *Angew. Chem.* **1999**, *111*, 1020; *Angew. Chem. Int. Ed.* **1999**, *38*, 967.

[6] A. Kuczkowski, F. Thomas, S. Schulz, M. Nieger, *Organometallics* **2000**, *19*, 5758.

[7] A. Kuczkowski, S. Schulz, M. Nieger, *Eur. J. Inorg. Chem.* **2001**, 2605.

[8] A. Kuczkowski, S. Schulz, M. Nieger, P. R. Schreiner, *Organometallics* **2002**, *21*, 1408.

[9] F. Thomas, S. Schulz, M. Nieger, *Organometallics* **2002**, *21*, 2793.

[10] D. Fenske, A. Rothenberger, S. Wieber, *Z. Anorg. Allg. Chem.* **2003**, *629*, 929.

[11] F. Thomas, S. Schulz, H. Mansikkamäki, M. Nieger, *Angew. Chem.* **2003**, *115*, 5800; *Angew. Chem. Int. Ed.* **2003**, *42*, 5641.

[12] R. Wolf, J. Fischer, R. C. Fischer, J. C. Fettinger, P. P. Power, *Eur. J. Inorg. Chem.* **2008**, 2515.

[13] B. K. Campion, R. H. Heyn, T. D. Tilley, *Organometallics* **1993**, *12*, 2584.

[14] K. H. Ebert, R. E. Schulz, H. J. Breunig, C. Silvestru, I. Haiduc, *J. Organomet. Chem.* **1994**, *470*, 93.

[15] C. Strohmann, O. Ulbrich, D. Auer, *Eur. J. Inorg. Chem.* **2001**, 1013.

[16] (a) H. V. R. Dias, M. M. Olmstead, K. Ruhlandt-Senge, P. P. Power, *J. Organomet. Chem.* **1993**, *462*, 1; (b) A. Heine, R. Herbst-Irmer, G. M. Sheldrick, D. Stalke, *Inorg. Chem.* **1993**, *32*, 2694.

[17] N. Wiberg, K. Ameluxen, H.-W. Lerner, H. Schuster, H. Nöth, I. Krossing, M. Schmidt-Ameluxen, T. Seifert, *J. Organomet. Chem.* **1997**, *542*, 1.

[18] H.-W. Lerner, I. Sänger, F. Schödel, K. Polborn, M. Bolte, M. Wagner, *Z. Naturforsch., Teil B* **2007**, *62*, 1285.

[19] A. Kawachi, K. Tamao, *J. Am. Chem. Soc.* **2000**, *122*, 1919.

[20] Y. Apeloig, M. Yuzefovich, M. Bendikov, D. Bravo-Zhivotovskii, D. Bläser, R. Boese, *Angew. Chem. Int. Ed.* **2001**, *40*, 3016.

[21] G. Balázs, H. J. Breunig, E. Lork, *Organometallics* **2002**, *21*, 2584.

[22] C. Silvestru, H. J. Breunig, H. Althaus, *Chem. Rev.* **1999**, *99*, 3277.

[23] H. Althaus, H. J. Breunig, R. Rösler, E. Lork, *Organometallics* **1999**, *18*, 328.

[24] B. Murray, J. Hvoslef, H. Hope, P. P. Power, *Inorg. Chem.* **1983**, *22*, 3421.

[25] G. Linti, M. Bühler, K. Yu. Monakhov, T. Zessin, *Dalton Trans.* **2009**, 8071.

[26] (a) S. L. Hinchley, C. A. Morrison, D. W. H. Rankin, C. L. B. Macdonald, R. J. Wiacek, A. H. Cowley, M. F. Lappert, G. Gundersen, J. A. C. Clyburne, P. P. Power, *Chem. Commun.* **2000**, 2045; (b) S. L. Hinchley, C. A. Morrison, D. W. H. Rankin, C. L. B. Macdonald, R. J. Wiacek, A. Voigt, A. H. Cowley, M. F. Lappert, G. Gundersen, J. A. C. Clyburne, P. P. Power, *J. Am. Chem. Soc.* **2001**, *123*, 9045.

[27] (a) M. J. S. Gynane, A. Hudson, M. F. Lappert, P. P. Power, H. Goldwhite, *J. Chem. Soc., Dalton Trans.* **1980**, 2428; (b) P. P. Power, *Chem. Rev.* **2003**, *103*, 789.

[28] N. S. Vyazankin, G. A. Razuvaev, O. A. Kruglaya, G. S. Semchikova, *J. Organomet. Chem.* **1966**, *6*, 474.

[29] L. Balázs, H. J. Breunig, E. Lork, A. Soran, C. Silvestru, *Inorg. Chem.* **2006**, *45*, 2341.

[30] (a) H. Gilman, H. L. Yablunky, *J. Am. Chem. Soc.* **1941**, *63*, 212; (b) H. Gilman, H. L. Yale, *Chem. Rev.* **1942**, *30*, 281.

[31] (a) A. J. Ashe III, E. G. Ludwig Jr., J. Oleksyszyn, *Organometallics* **1983**, *2*, 1859; (b) H. J. Breunig, *Z. Anorg. Allg. Chem.* **2005**, *631*, 621.

[32] (a) O. Mundt, H. Riffel, G. Becker, A. Simon, *Z. Naturforsch., Teil B* **198**8, *43*, 952; (b) A. J. Ashe III, J. W. Kampf, D. B. Puranik, S. M. Al-Taweel, *Organometallics* **1992**, *11*, 2743.

[33] K. W. Klinkhammer, P. Pyykkö, *Inorg. Chem.* **1995**, *34*, 4134.

[34] A. Kuczkowski, S. Schulz, M. Nieger, *Angew. Chem.* **2001**, *113*, 4351; *Angew. Chem. Int. Ed.* **2001**, *40*, 4222.

2.3 Appendix to chapter 2.2

2.3.1 Evaluation of the effects of an solvent complexation on the geometric, bonding, electronic and energetic characteristics of lithium *tert*-butyldiphenylsilanides

The tailor-made alkali metal silanides are of great importance as transfer reagents to organometallic systems. Therefore, quantum chemical understanding of their geometric, bonding, electronic and energetic properties based on the silicon–alkali-metal interactions is important. To try to clarify the nature and behavior of Si–Li bond in lithium *tert*-butyldiphenylsilanides, $Li(thf)_xSiPh_2tBu$ (x = 0 – 3) (Figure A), to evaluate the effect of thf complexation at lithium centers, and to analyze the stability of these systems, quantum chemical calculations were applied.

Table A. Influence of HF exchange components in the DFT functionals on the geometric values of $Li(thf)_3SiPh_2tBu$ (basis set is def2-TZVP).

Parameter	Experimental values	DFT functionals with HF exchange components				
		BP86	TPSSH	B3LYP	PBE0	BHLYP
		0%	10%	20%	25%	50%
Si–Li [pm]	266.0 / 267.5 / 269.0	269.2	270.1	268.7	266.8	266.7
$O–Li_{av}$ [pm]	197.3 / 195.5 / 195.6	203.8	203.1	202.3	200.7	198.6
Si_{sum} [°]	309.9 / 308.3 / 308.4	312.6	311.2	312.4	312.2	312.0
Li_{sum} [°]	313.0 / 311.0 / 305.6	308.5	310.3	307.4	309.0	307.2

The initial geometries of lithium *tert*-butyldiphenylsilanides were fully optimized with different DFT functional with 0% – 50% Hartree-Fock (HF) exchange to obtain better correlation with the experimental structural data. The BP86 (0% HF), TPSSH (10%), B3LYP (20% HF), PBE0 (25% HF) and BHLYP (50% HF) were employed (Table A). The results, obtained with the BHLYP functional, were very close to the experimental values; therefore, all following structural calculations were carried out using the BHLYP functional. DFT structure optimizations were performed with the Turbomole program, adopting the multiple "M3" grid size for the density fitting and a SCF convergence criterion of 1×10^{-7} E_h. As Gaussian AO basis for all atoms, large all-electron triple ζ split valence (TZVP) sets of def2-type were employed (Basis Set System I, which is denoted BS-I). The hybrid exchange-correlation functional B3LYP and 6-311+G(d,p) basis sets for all atoms were used for all other "non-structural" calculations with the Gaussian 03 program package. The results are summarized in Tables B, C, and D. Upon thf complexation at Li, heterolytic bond dissociation energy decreases, whereas homolytic bond dissociation energy moderately increases.

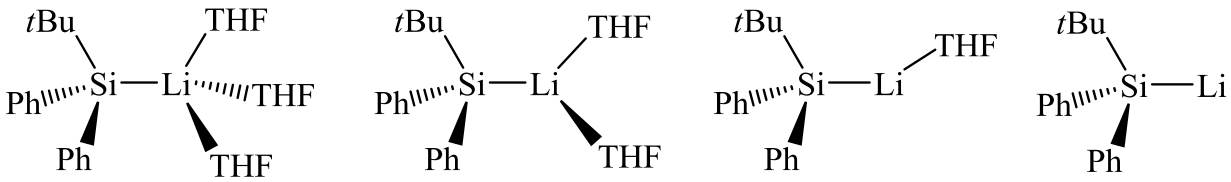

1-3THF **1**-2THF **1**-THF **1**

Figure A. Donor and free solvent-containing systems of lithium *tert*-butyldiphenylsilanides.

Table B. Calculated structural parameters of lithium *tert*-butyldiphenylsilanides.

Parameter	Experimental	Calculated values [a]			
	values of **1**·3THF	**1**·3THF	**1**·2THF	**1**·THF	**1**
Si–Li [pm]	266.0 / 267.5 / 269.0	266.7	257.3	251.0	248.7
O–Li^{av} [pm]	197.3 / 195.5 / 195.6	198.6	191.2	185.5	
C–Si–C[b] [°]	309.9 / 308.3 / 308.4	312.0	314.3	317.3	319.8
Δr_{Si-Li}[c] [pm]		18.0	8.6	2.3	
$r_{(Si-THF_{plane})}^{av}$ [pm]	388.7 / 391.7 / 396.5[d]	353.2	367.8	433.1	

[a] Structural parameters calculated at the BHLYP/def2-TZVP level of theory. [b] Total sum of the bond angles at the Si centre. [c] Change of the distance Si–Li obtained from **1**·*n*THF – **1** [pm]. [d] Si–O(av) distances [pm].

Table C. Important calculated values for the complexes obtained from the NBO analysis at the B3LYP/6-311+G(d,p)//BHLYP/def2-TZVP level.

Parameter		**1**·3THF	**1**·2THF	**1**·THF	**1**
NEC[a]	Li	$2s^{0.20\%}$	$2s^{0.23\%}$	$2s^{0.26\%}$	$2s^{0.25\%}$
	Si	$3s^{1.20\%}3p^{2.07\%}$	$3s^{1.18\%}3p^{2.09\%}$	$3s^{1.15\%}3p^{2.10\%}$	$3s^{1.14\%}3p^{2.12\%}$
i_{Si-Li}[b]		78.2	75.6	72.7	74.0
Overlap / WBI[c]		0.142/0.193	0.307 / 0.269	0.380 / 0.363	0.384 / 0.404
LP NHO[d] at Si		$s^{47.46\%}p^{52.53\%}$	$s^{46.14\%}p^{53.84\%}$	$s^{44.49\%}p^{55.48\%}$	$s^{43.02\%}p^{56.92\%}$
Occupancy[e]		1.765	1.739	1.696	1.686
ρ_L[f]		98.4	98.2	98.0	97.6

[a] Natural electron configuration. [b] Degree of ionicity [%] [c] Atom-atom overlap-weighted NAO bond order and Wiberg bond index of the Si–Li bond. [d] Lone pair natural hybrid orbital at the silicon atom. [e] Occupancy of lone pair orbital [*e*]. [f] Accuracy of calculation picture [%].

Table D. Important calculated values for lithium *tert*-butyldiphenylsilanides obtained from the single point calculations at the B3LYP/6-311+G(d,p)//BHLYP/def2-TZVP level.

Parameter	**1**·3THF	**1**·2THF	**1**·THF	**1**
$E_{stabilization}$ [a]	43.56	52.40	57.30	45.74
$-\Delta E_{complexation}$ [b]	194.4	161.7	98.8	
$-\Delta D_{homolytic}$ [c]	233	237	212	170
$-\Delta D_{heterolytic}$ [c]	331	396	485	579
$-IP$ [d]	3.81	4.09	4.36	4.86
$\Delta E_{HOMO-LUMO}$ [e]	3.08	3.31	3.39	3.12
μ [f]	10.0	10.0	11.0	6.16

[a] Delocalization energy of LP_{Si} into lithium 2s-orbitlal [kcal/mol]. [b] Complexation energy of thf molecules on the Li centre [kJ/mol]. [c] Bond dissociation energies [kJ/mol]. [d] Ionization potential [eV]. [e] Energy of HOMO–LUMO gap [eV]. [f] Dipole moment of molecule [Debye].

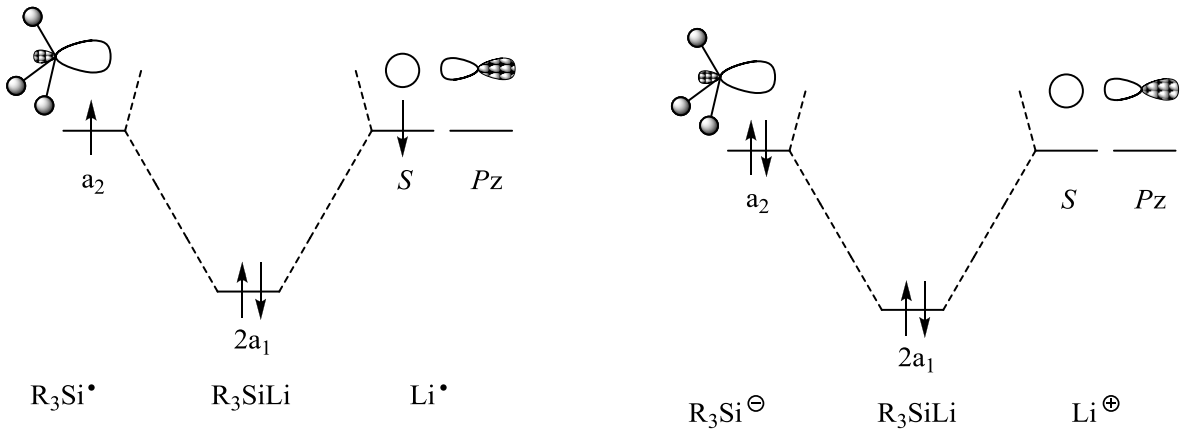

Figure B. Qualitative orbital interaction diagrams of lithium *tert*-butyldiphenylsilanides based on homolytic (left) and heterolytic (right) approaches. [The important aspects of the carbon–lithium bonding are discussed in *Lithium Chemistry*: *A Theoretical and Experimental Overview*, A.-M. Sapse, P.v.R. Schleyer (Eds.), Wiley-Interscience Publications, New York, **1995**.]

2.3.2 Synthesis and X-ray crystal structure of $In(SiPh_2tBu)_3$

If the bulky silanide $Li(thf)_3SiPh_2tBu$ was reacted with indium(III) chloride, $In(SiPh_2tBu)_3$ was obtained (eq. 1). The formation of $(SiPh_2tBu)_2$ hints to redox reactions, but no other indium species could be detected.

$$InCl_3 + 3\ Li(thf)_3SiPh_2tBu \xrightarrow[-\ 3\ LiCl]{thf} In(SiPh_2tBu)_3 \qquad (1)$$

$In(SiPh_2tBu)_3$ forms yellow prisms of the triclinic system, space group $P\bar{1}$. The indium atom is a surrounded trigonal planar [In(1) resides only 16 pm above the plane through the Si atoms] (Figure C). The average In–Si distance is 260.7 pm, which is shorter than in $(thf)In(SiPh_3)_3$and $In\{Si(SiMe_3)_3\}_3$. This is due to the higher coordination number in $(thf)In(SiPh_3)_3$ and the even more bulky substituent in $In\{Si(SiMe_3)_3\}_3$, respectively. The steric strain imposed by the $SiPh_2tBu$ substituents is visible in the different In–Si distances. Variations in the Si–C distances and In–Si–C angles to the *t*Bu groups are in line with this too. The Si–C bonds involving the *ipso*-carbon atoms of the phenyl groups are all nearly equal [188.1(3)–188.8(4) pm]. This might be due to the orientation of these substituents. The butyl groups are in the $InSi_3$ plane (with regard to the In–C bonds), whilst the phenyl rings are oriented topside and below this plane.

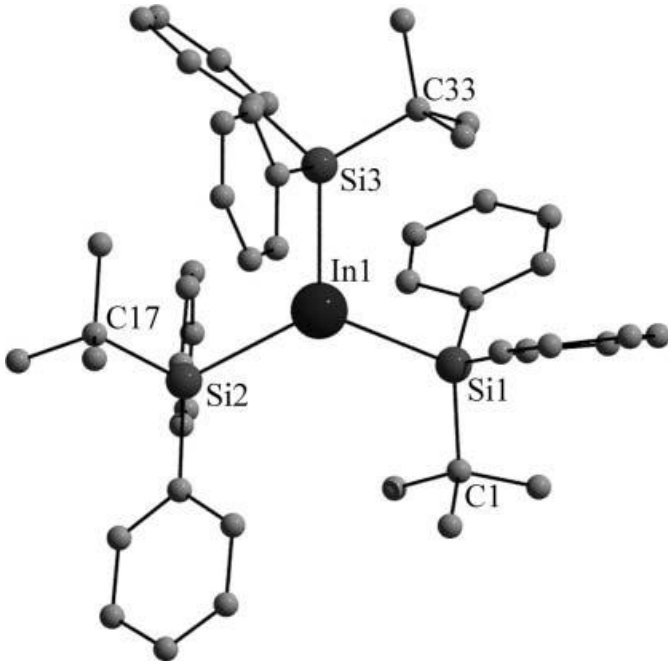

Figure C. View of a molecule of $In(SiPh_2tBu)_3$ (hydrogen atoms have been omitted for clarity). Selected distances [pm] and angles [°]: In(1)–Si(1) 257.9(1), In(1)–Si(2) 261.4(1), In(1)–Si(3) 262.7(1), Si(1)–C(1) 188.8(4), Si(2)–C(17) 190.4(3), Si(3)–C(33) 191.4(3); Si(1)–In(1)–Si(2) 123.1(3), Si(2)–In(1)–Si(3) 116.4(4), Si(3)–In(1)–Si(1) 119.4(4), In(1)–Si(1)–C(1) 118.4(1), In(1)–Si(2)–C(17) 114.9(1), In(1)–Si(3)–C(33) 119.1(1).

2.3.3 X-ray crystal structure of (*t*BuPh$_2$Si)$_2$

The molecular structure of (*t*BuPh$_2$Si)$_2$ in the solid state is shown in Figure D. Disilane crystallizes as dimer *t*BuPh$_2$Si–SiPh$_2$*t*Bu in the monoclinic crystal system, space group $P2_1/c$. Around the central Si–Si bond are located *t*BuPh$_2$ groups in *trans*-configuration. The Si–Si bond is 238.6 pm and slightly longer than the sum of the covalent Si–Si radii ($\Delta\Sigma r_{cov}$ = 234 pm), but shorter than that in Ph*t*Bu$_2$Si–Si*t*Bu$_2$Ph (249.7 pm), Ph$_3$Si–SiPh$_3$ (251.7 pm) and *t*Bu$_3$Si–Si*t*Bu$_3$ (269.0 pm). The significant deviations of the Si–Si bond lengths in these disilanes may be related to the repulsive interactions of protected organic substituents (*t*Bu$_x$Ph$_y$) that should lead to the electron repulsion of the silicon centers.

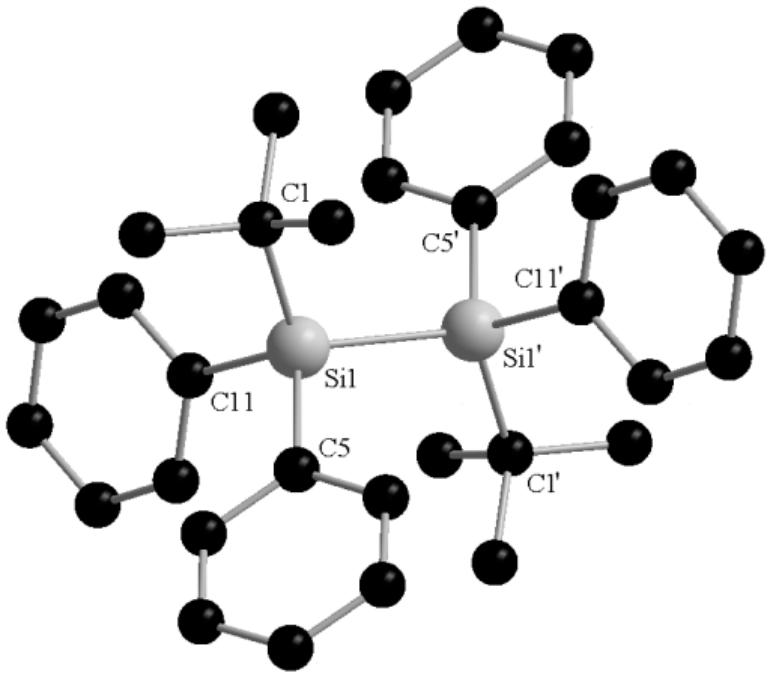

Figure D. View of a molecule of [*t*BuPh$_2$Si]$_2$ (hydrogen atoms have been omitted for clarity. Selected bond lengths [pm] and angles [deg]: Si(1)–C(5) 188.6(3), Si(1)–C(11) 189.4(3), Si(1)–C(1) 191.3(3), Si(1)–Si(1') 238.6(2), C(5)–Si(1)–C(11) 105.8(1), C(5)–Si(1)–C(1) 106.1(1), C(11)–Si(1)–C(1) 111.7(1).

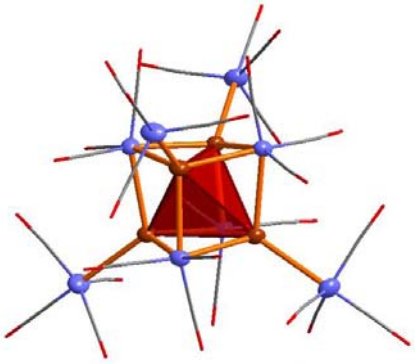

$[Bi_4Fe_8(CO)_{28}]^{4-}$

Tympaniscus tripodiscus

Chapter 3. Bismuth–Transition-Metal Bonding

3.1 Introduction

3.1.1 A short view into the bismuth–transition-metal chemistry

Bismuth–transition-metal (Bi–TM) chemistry is an object of intensive studies of the last three decades. A wide range of investigations on the Bi–TM species is available in the literature.[1–6] This class of compounds has received attention as part of the general interest in main group–transition metal clusters. Thus, the most number of examples containing the Bi–TM bonds is mainly known for the compounds where TM is metal of the group 6 d-elements (Mo and W) or this one of the groups 8 and 9 d-elements (Fe and Co, respectively). The number of compounds with the Bi–Cr, Bi–Mn and Bi–Ni bonds is much smaller. A few structural examples of Bi–Zr[7], Bi–Cu[8] and Bi–Zn[9] bonded systems are available, too. Recently, the report on Bi–Re bonding have also been published.[10] The experimental studies of bonding between bismuth and platinum group metals are mainly concerned with the Bi–Ru (7 crystal structures are

		chromium 24 Cr 51.996	manganese 25 Mn 54.938	iron 26 Fe 55.845	cobalt 27 Co 58.933	nickel 28 Ni 58.693	copper 29 Cu 63.546	zinc 30 Zn 65.39
zirconium 40 Zr 91.224		molybdenum 42 Mo 95.94		ruthenium 44 Ru 101.07	rhodium 45 Rh 102.91	palladium 46 Pd 106.42		
		tungsten 74 W 183.84	rhenium 75 Re 186.21	osmium 76 Os 190.23	iridium 77 Ir 192.22	platinum 78 Pt 195.08		

bismuth 83 Bi 208.98

available)[11] and Bi–Rh (7 crystal structures are available)[11d,12] systems. The examples of other bismuth–platinum-group-metals compounds are very rare or not known (2 crystal structures are available for Bi–Os bonding;[13] one structure is available for Bi–Ir;[14] 1 crystal structure is available for Bi–Pd[15] and Bi–Pt,[16] each).

3.1.2 General synthetic strategies

In general synthetic considerations, some strategies for generating the Bi–TM bonds can be summarized:

(1) simple salt elimination reactions, i.e. reactions of bismuth halo complexes with anionic or neutral TM complexes;

(2) substitution reactions;

(3) heterometallic addition or Lewis acid-base interactions;

(4) reactions of TM hydrides with bismuth alkyl compounds;

(5) pyrolysis reactions of organo-bismuth complexes with TM compounds;

(6) deoxygenation of bismuth oxides by TM carbonyls, i.e. addition of $NaBiO_3$ to the base reaction solution by methodology of Hieber which consisted of $Fe(CO)_5$ dissolved in basic aqueous solution, where obvious active species involved are the anions $[HFe(CO)_4]^-$ and $[Fe(CO)_4]^{2-}$.[3,17]

3.1.3 General structural view

In a general structural view, the different coordination geometries around the Bi atom in the Bi–TM compounds such as pyramidal, tetrahedral, trigonal bipyramidal and some other relatively rare structures have been observed by X-ray diffraction. Figure A represents the most common and structural examples.

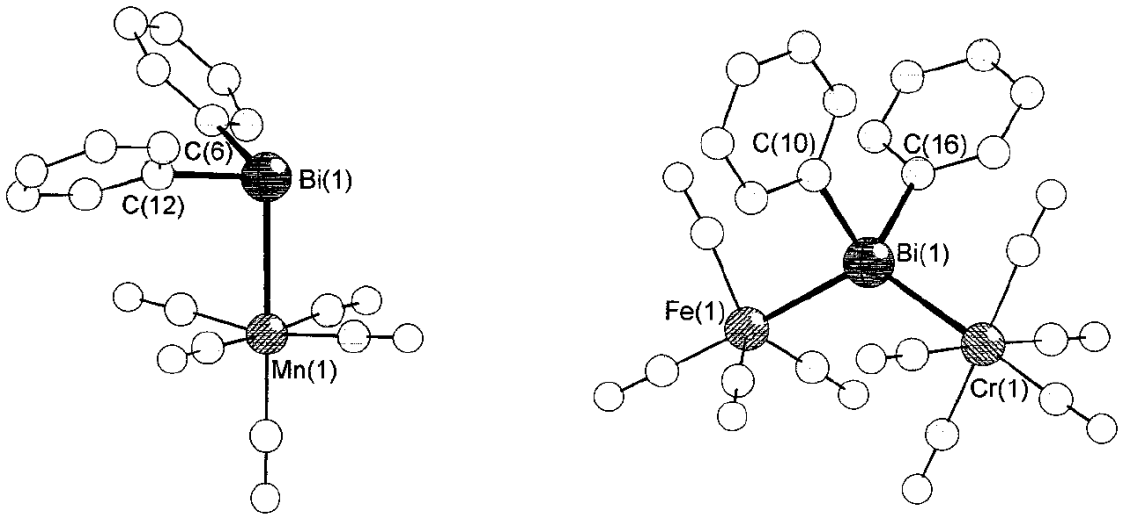

Figure A. Molecular structures of neutral $Ph_2BiMn(CO)_5$[18] (left) with pyramidal $C_2Bi(TM)$ core and anionic $[Ph_2Bi]\{Cr(CO)_5\}\{Fe(CO)_4\}$[19] with tetrahedral $C_2Bi(TM)_2$ core (right).

3.1.4 Bismuth–transition-metal classes

All known Bi–TM compounds can be separated into four classes with reference to the bismuth element upon a structural factor: monomers, dimers and clusters as well as compounds where the bismuth atoms form cages (tetrahedra and other deltahedra) stabilized by d-transition-metal fragments. The structural and electronic features as well as the synthetic and catalytic potential of the above-mentioned classes of Bi–TM compounds are an interesting area and target of chemistry. It is already well-known that heterobimetallic complexes containing bismuth have been shown to be good precursors to heterobimetallic nanostructured materials.[20]

The class "dimers" contains only a few examples of Bi–Bi bonded cores connected to d-transition-metal fragments. Here, formally multiple bonds between the Bi atoms are present. Up to now, X-ray crystal structures have been determined for the five complexes $[\{W(CO)_5\}_2Bi_2\{CH_2tBu\}_2]$ (**I**),[21] $[\{W(CO)_5\}_2\{Bi_2(CH_2SiMe_3)_2\}]$ (**II**),[21] $[Bi_2(C_6H_3\text{-}2,6\text{-}Mes_2)_2\{Zr(C_5H_5)_2\}$ (**III**),[7] $[Bi_2\{2,6\text{-}(2,6\text{-}iPr_2\text{-}C_6H_3)_2\text{-}C_6H_3\}_2]\{Fe(CO)_4\}$[22] (**IV**) and $[Bi_2\{2,6\text{-}(2,4,6\text{-}Me_3\text{-}C_6H_2)_2C_6H_3\}_2]\{Fe(CO)_4\}$[22] (**V**) (Scheme A). The compounds **I** and **II** are formed by conversion of *cyclo*-$(RBi)_n$ (R: R' = Me_3CCH_2 and R" = Me_3SiCH_2; n = 3, 5) with $W(CO)_5$thf. A metallocene-complexed dibismuthene **III** can be prepared by the sodium metal reduction of $(C_5H_5)_2ZrCl_2$ with (Ar')$BiCl_2$ (Ar' = C_6H_3-2,6-Mes_2). The compounds **IV** and **V** are observed on reaction of Ar*$BiCl_2$ [Ar*: Ar" = 2,6-(2,6-$^iPr_2$-$C_6H_3)_2$-C_6H_3 or Ar"' = 2,6-(2,4,6-Me_3-$C_6H_2)_2$-C_6H_3, respectively] with $Na_2[Fe(CO)_4]$.

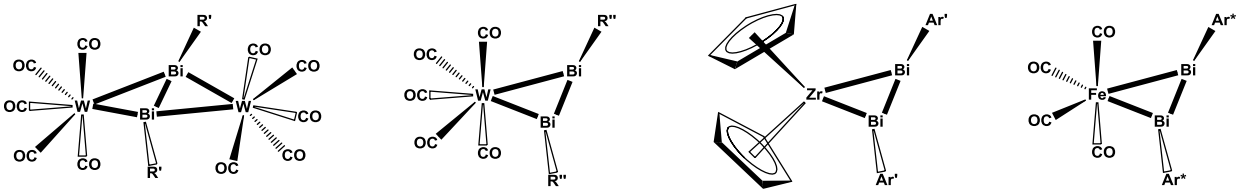

I **II** **III** **IV, V**

Scheme A. Survey of **I** – **V** transition-metal-fragment-complexed dibismuthenes.

The class "clusters" as well as this one "monomers" contain many interesting and surprising structures and coordination geometries.[1–6] Unfortunately, the Bi–TM cluster cage chemistry is still not so well developed. The recent works, published by Sevov (University of Notre Dame, USA; picture on the right) et al. in 2001 and 2007 in *Journal of the American Chemical Society* on the Bi–TM (TM = Cr, Mo, Ni) clusters (Figure B) where the Bi–TM atoms form joint deltahedral cages, have shown a considerable interest in this area of chemistry.[23]

In addition, numerous exceptions to the classic Wade's rules, which are very useful for

rationalizing bonding and predicting structures of simple cluster molecules, can be found for the complicated Bi–TM cluster systems where the bonding requirements (electronegativity and overlap) of two different types of elements are quite dissimilar.[24]

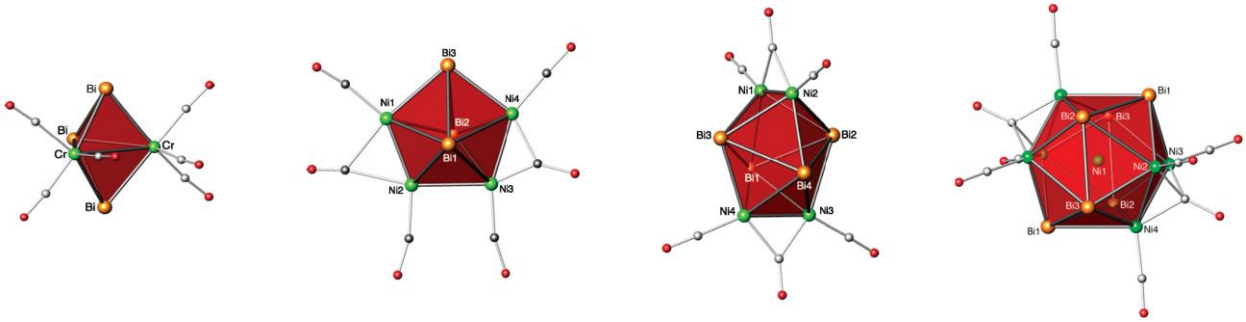

Figure B. Molecular views of trigonal bipyramidal cluster $[Bi_3M_2(CO)_6]^{3-}$ (M = Cr, Mo) (left), pentagonal bipyramidal cluster $[Bi_3Ni_4(CO)_6]^{3-}$ (center-left), bisdisphenoidal cluster $[Bi_4Ni_4(CO)_6]^{2-}$ (center-right), icosahedral cluster $[Ni_x@\{Bi_6Ni_6(CO)_8\}]^{4-}$ (right).

A considerable attention of this thesis is mainly concentrated on bismuth cage chemistry. The Bi–TM compounds, where the bismuth atoms are placed in such a manner to form polyhedral cages (tetrahedra or other deltahedra) stabilized by d-transition-metal fragments, are still very rare and their chemistry is extremely underdeveloped. The clusters known up to now amaze by their structures and chemical bonding. In addition, such kind of compounds has a high potential to exhibit unique physical-chemical properties.

3.1.5 References

[1] N. C. Norman, *Chem. Soc. Rev.* **1988**, *17*, 269.

[2] N. A. Compton, R. J. Errington, N. C. Norman, *Adv. Organomet. Chem.* **1990**, *31*, 91.

[3] K. H. Whitmire, *J. Clust. Sci.* **1991**, *2*, 231.

[4] K. H. Whitmire, *Adv. Organomet. Chem.* **1998**, *42*, 1.

[5] C. Silvestru, H. J. Breunig, H. Althaus, *Chem. Rev.* **1999**, *99*, 3277.

[6] S. Roggan, C. Limberg, *Inorg. Chim. Acta* **2006**, *359*, 4698.

[7] Y. Wang, B. Quillian, X.-J. Yang, P. Wei, Z. Chen, C. S. Wannere, P. v. R. Schleyer, G. H. Robinson, *J. Am. Chem. Soc.* **2005**, *127*, 7672.

[8] D. Fenske, A. Rothenberger, S. Wieber, *Z. Anorg. Allg. Chem.* **2003**, *629*, 929.

[9] J. M. Goicoechea, S. C. Sevov, *Angew. Chem. Int. Ed.* **2006**, *45*, 5147.

[10] R. D. Adams, W. C. Pearl, Jr., *Inorg. Chem.* **2009**, *48*, 9519.

[11] (a) H. G. Ang, C. M. Hay, B. F. G. Johnson, J. Lewis, P. R. Raithby, A. J. Whitton, *J. Organomet. Chem.* **1987**, *330*, C5; (b) C. M. Hay, B. F. G. Johnson, J. Lewis, P. R. Raithby, A. J. Whitton, *J. Chem. Soc., Dalton Trans.* **1988**, 2091; (c) B. F. G. Johnson, J. Lewis, P. R. Raithby, A. J. Whitton, *Chem. Commun.* **1988**, 401; (d) E. V. Dikarev, T. G. Gray, Bo Li, *Angew. Chem. Int. Ed.* **2005**, *44*, 1721.

[12] (a) E. V. Dikarev, Bo Li, A. Yu. Rogachev, H. Zhang, M. A. Petrukhina, *Organometallics* **2008**, *27*, 3728; (b) E. V. Dikarev, Bo Li, H. Zhang, *J. Am. Chem. Soc.* **2006**, *128*, 2814.

[13] H. G. Ang, C. M. Hay, B. F. G. Johnson, J. Lewis, P. R. Raithby, A. J. Whitton, *J. Organomet. Chem.* **1987**, *330*, C5.

[14] W. Kruppa, D. Bläser, R. Boese, G. Schmid, *Z. Naturforsch. B* **1982**, *37*, 209.

[15] J. L. Stark, B. Harms, I. Guzmann-Jimenez, K. H. Whitmire, R. Gautier, J.-F. Halet, J.-Y. Saillard, *J. Am. Chem. Soc.* **1999**, *121*, 4409.

[16] M. N. Bochkarev, G. A. Razuvaev, L. N. Zakharov, Yu. T. Struchkov, *J. Organomet. Chem.* **1980**, *199*, 205.

[17] (a) W. Hieber, J. Gruber, *Z. Anorg. Allg. Chem.* **1958**, *296*, 91; (b) W. Hieber, J. Gruber, F. Lux, *Z. Anorg. Allg. Chem.* **1959**, *300*, 275; (c) W. Hieber, W. Beck, *Z. Anorg. Allg. Chem.* **1960**, *305*, 265.

[18] J. Cassidy, K. H. Whitmire, *Inorg. Chem.* **1991**, *30*, 2788.

[19] R. E. Bachman, K. H. Whitmire, *Inorg. Chem.* **1995**, *34*, 1542.

[20] (a) R. Raja, R. D. Adams, D. A. Blom, W. C. Pearl, Jr., E. Gianotti, J. M. Thomas, *Langmuir* **2009**, *25*, 7200; (b) T. Ould-Ely, J. H. Thurston, K. H. Whitmire, *Compt. Rend. Chim.*

2005, *8*, 1906; (c) J. H. Thurston, T. Ould-Ely, D. Trahan, K. H. Whitmire, *Chem. Mater.* **2003**, *15*, 4407.

[21] (a) L. Balázs, H. J. Breunig, *Angew. Chem.* **2002**, *114*, 2411; *Angew. Chem. Int. Ed.* **2002**, *41*, 2309; (b) G. Balázs, L. Balazs, H. J. Breunig, E. Lork, *Organometallics* **2003**, *22*, 2919.

[22] R. Wolf, J. Fischer, R. C. Fischer, J. C. Fettinger, P. P. Power, *Eur. J. Inorg. Chem.* **2008**, 2515.

[23] (a) J. M. Goicoechea, M. W. Hull, S. C. Sevov, *J. Am. Chem. Soc.* **2007**, *129*, 7885; (b) L. Xu, A. Ugrinov, S. C. Sevov, *J. Am. Chem. Soc.* **2001**, *123*, 4091.

[24] T. A. Albright, K. Ae. Yee, J. Y. Saillard, S. Kahlal, J.-F. Halet, J. S. Leigh, K. H. Whitmire, *Inorg. Chem.* **1991**, *30*, 1179.

3.2 Cubane-like bismuth–iron cluster

3.2.1 Introduction

The tetrahedral cluster Bi_4 is a high-temperature modification, which exists only in liquid or in the gas phase. Matrix isolation studies[1] and quantum-chemical calculations[2] are available. Tetrahedral Bi_4 is stabilized in the solid state using transition metal fragments. The hybrid Zintl-metal carbonyl cluster anion $[Bi_4Fe_4(CO)_{13}]^{2-}$ has been discovered by Whitmire (Rice University, USA; picture on the right) et al.[3] Other examples of such bismuth-transition-metal (Bi–TM) clusters are rare, up to now. The structural and electronic features of this class of molecules as well as the synthetic pathways to these are an interesting area and target of chemistry. The Bi–TM heteronuclear cluster systems (Scheme 1) could be obtained by different synthetic strategies: (a) carbonylation of $[n\text{Bu}_4\text{N}][\text{BiFe}_3(\text{CO})_{10}]$ to form **I**;[3] (b) pyrolysis of $[\text{Bi}\{\text{Co}(\text{CO})_4\}_3]$ or photolysis of $[\text{Bi}\{\text{Co}(\text{CO})_4\}_2\text{Fe}(\text{CO})_2\text{Cp}]$ to form **II**;[4,5] (c) conversion of $[\{\text{Cp}''(\text{CO})_2\text{Fe}\}\text{BiCl}_2]$ ($\text{Cp}'' = \eta^5\text{-C}_5\text{H}_3t\text{Bu}_2$) with $Na_2[Fe(CO)_4]$ to form **III**;[5] (d) conversion of $Pd(PPh_2Me)_4$ with Ph_2BiBr to form **IV**.[6]

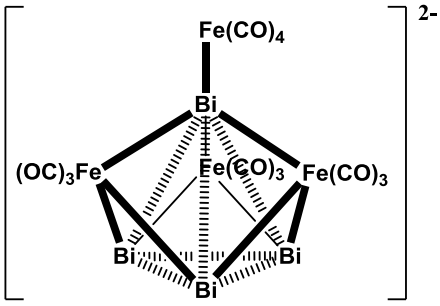

I

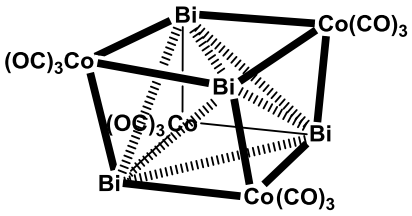

II

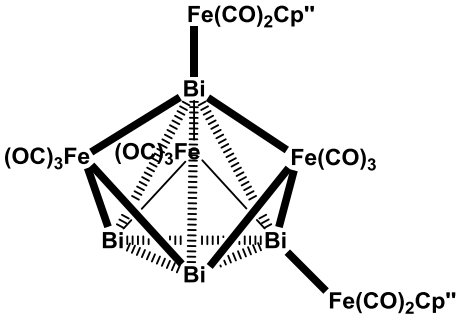

III

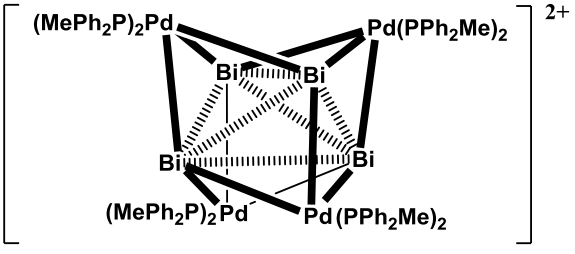

IV

Scheme 1. Survey of **I** – **IV** bismuth-transition-metal clusters displaying Bi_4 core.

The question of whether the Bi_4 cores in these compounds, taking in account different molecular

symmetry, has bonding Bi–Bi interactions ($d_{Bi–Bi}$ = 314 – 353 pm) was a subject of intensive discussions. For example, polyhedral bismuth polycations such as trigonal bipyramidal Bi_5^{3+} and square pyramidal Bi_5^{+} clusters as well as the distorted Bi_6^{2+} octahedron, square-antiprismatic Bi_8^{2+}, tricapped trigonal prismatic Bi_9^{5+} and pentagonal-antiprismatic Bi_{10}^{4+} clusters have been isolated in intermetallic phases as naked units with the closest Bi–Bi contacts.[7] An example of a Bi_4N_4 cubane cluster core with significant longer Bi···Bi separations ($d_{Bi–Bi}$ = 344 – 364 pm) is also known.[8]

In this part, an unusual synthetic method of the formation of the bismuth–iron metal complex $[n\text{Bu}_4\text{N}]_4[\text{Bi}_4\text{Fe}_8(\text{CO})_{28}]$, displaying a cuboid cluster shape, where eight carbonyl iron fragments are involved in bonding to a Bi_4 cluster core, is presented. In addition, DFT quantum chemical calculations are performed for anionic portion of the Bi–Fe complex and its derivates to get an insight into the geometric and electronic structures, the chemical bonding as well as into stability and aromaticity of these species.

3.2.2 Synthesis of $[n\text{Bu}_4\text{N}]_4[\text{Bi}_4\text{Fe}_8(\text{CO})_{28}]$

The reaction (eq. 1) of $Bi_4[Si(SiMe_3)_3]_4$[9] (**1**) with eight equivalents of $Na_2[Fe(CO)_4]$ and an excess of $n\text{Bu}_4\text{NCl}$ in the solvent thf leads to a redox process under the applied conditions (warming from –78°C to r.t. during the reaction), resulting in compound $[n\text{Bu}_4\text{N}]_4[\text{Bi}_4\text{Fe}_8(\text{CO})_{28}]$ (**2**). During the reaction a gradual deepening of the dark-red color of the solution was observed. Workup allows isolation of **2** as thf soluble black crystals. The anion portion $[\text{Bi}_4\text{Fe}_8(\text{CO})_{28}]^{4-}$ (**2a**) of **2** is the largest cluster of the bismuth-iron family. Reaction does not take place without the addition of the ammonium salt, which means activation of $[Fe(CO)_4]^{2-}$ via exchange of the cation. The bismuth silicon bonds are cleaved with formation of $[Si(SiMe_3)_3]_2$ and other products.

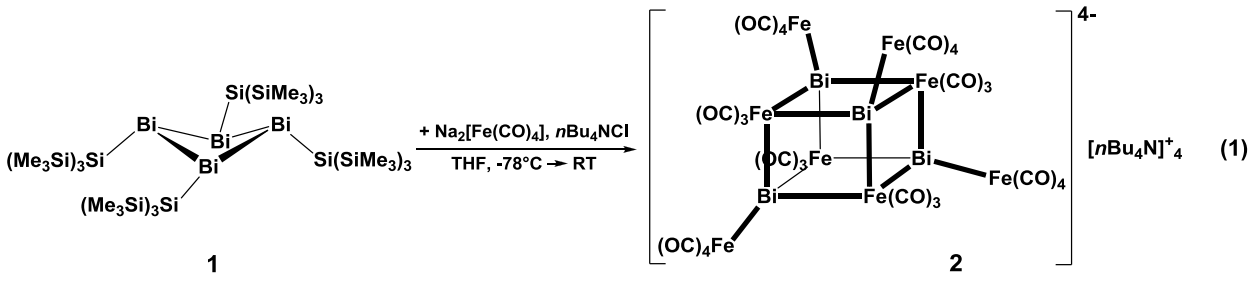

(1)

3.2.3 X-ray crystal structure of $[n\text{Bu}_4\text{N}]_4[\text{Bi}_4\text{Fe}_8(\text{CO})_{28}]$

2 crystallizes together with six thf molecules in the orthorhombic space group *Pba*2. Four $[n\text{Bu}_4\text{N}]^+$ cations are the counterions for the tetranion **2a** molecule. The C_2 symmetric cluster core of **2a** (Figure 1) is a distorted Bi_4Fe_4 cube.

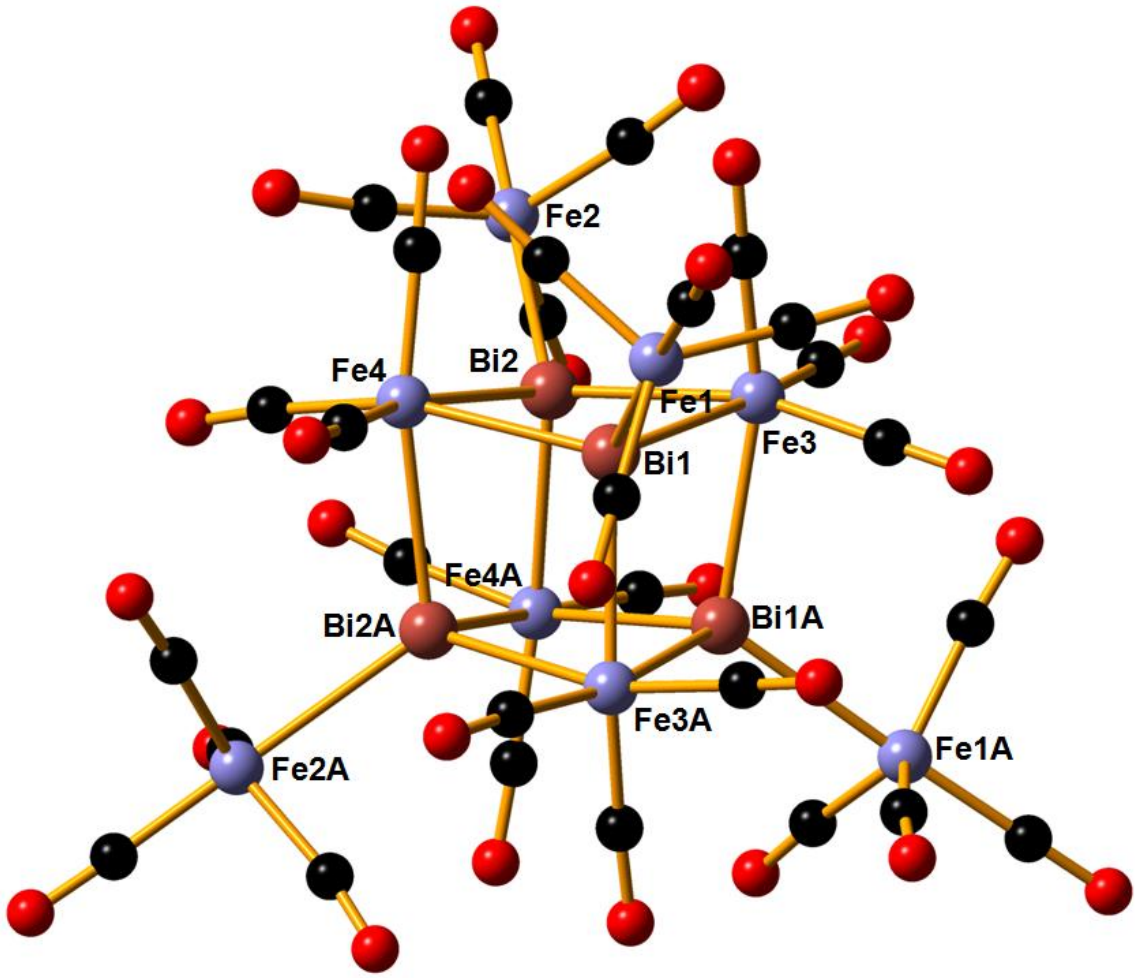

Figure 1. View of cluster molecule **2a**. Selected bond lengths [pm] and angles [°]: Bi(1)–Bi(1A) 343.5(8), Bi(1)–Bi(2) 343.8(8), Bi(1)–Bi(2A) 343.7(8), Bi(2)–Bi(1A) 343.7(8), Bi(2)–Bi(2A) 342.8(9), Bi(1A)–Bi(2A) 343.8(8), Bi(1)–Fe(1) 271.9(2), Bi(2)–Fe(2) 272.4(2), Bi(1A)–Fe(1A) 271.9(2), Bi(2A)–Fe(2A) 272.4(2), Bi(1)–Fe(3) 271.8(2), Bi(1)–Fe(3A) 270.8(2), Bi(1)–Fe(4) 272.7(1), Bi(2)–Fe(3) 271.6(2), Bi(2)–Fe(4A) 272.1(2), Bi(2)–Fe(4) 270.6(2), Bi(1A)–Fe(3) 270.8(2), Bi(1A)–Fe(3A) 271.8(2), Bi(1A)–Fe(4A) 272.7(2), Bi(2A)–Fe(4) 272.1(2), Bi(2A)–Fe(3A) 271.6(2), Bi(2A)–Fe(4A) 270.6(2), Bi(1)–Fe(4)–Bi(2) 78.5(5), Bi(2)–Fe(3)–Bi(1) 78.5(5), Bi(1A)–Fe(3A)–Bi(2A) 78.5(5), Bi(2A)–Fe(4A)–Bi(1A) 78.5(5), Bi(1A)–Fe(3A)–Bi(1) 78.5(4), Bi(1)–Fe(3)–Bi(1A) 78.5(4), Bi(1)–Fe(3A)–Bi(2A) 78.6(5), Bi(2A)–Fe(4)–Bi(1) 78.2(5), Bi(2A)–Fe(4)–Bi(2) 78.3(4), Bi(2)–Fe(4A)–Bi(2A) 78.3(4), Bi(2)–Fe(3)–Bi(1A) 78.6(5), Bi(1A)–Fe(4A)–Bi(2) 78.2(5), Fe(3)–Bi(1)–Fe(4) 100.1(6), Fe(4)–Bi(2)–Fe(3) 100.7(5), Fe(3A)–Bi(2A)–Fe(4A) 100.7(5), Fe(4A)–Bi(1A)–Fe(3A) 100.2(6), Fe(3A)–Bi(1)–Fe(3) 100.4(4), Fe(3)–Bi(1A)–Fe(3A) 100.4(4), Fe(3A)–Bi(2A)–Fe(4) 100.5(5), Fe(4)–Bi(1)–Fe(3A) 100.5(6), Fe(4)–Bi(2)–Fe(4A) 100.6(5), Fe(4A)–Bi(2A)–Fe(4) 100.6(5), Fe(4A)–Bi(2)–Fe(3) 100.5(5), Fe(3)–Bi(1A)–Fe(4A) 100.5(6).

The building Bi_4 tetrahedron is nearly ideal [d_{Bi-Bi} = 342.8 – 343.8 pm]. The neutral bismuth-cobalt complex **II** has a similar cluster core with shorter Bi–Bi distances [d_{Bi-Bi} = 331.6 – 337.6 pm].[4,5] Three other examples, **I**, **III** and **IV**, display more distorted Bi_4 tetrahedra. The Bi–Bi distances are lying in the regions 313.9 – 347.3[3], 308.9 – 353.0[5] and 320.1 – 350.9[6] pm, respectively. All of these Bi–Bi distances lie in an interval comparable with the closest Bi–Bi contacts of 307.1 – 352.9 pm in the pure crystalline element.[10] The four tetrahedral Bi_4 faces of **2a** and **II** are capped by $Fe(CO)_3$ and $Co(CO)_3$ moieties in a μ_3 fashion, respectively. The Bi–Fe bond lengths in **2a** [d_{Bi-Fe} = 270.6 – 272.7 pm] are slightly shorter than the Bi–Co bonds in **II** [d_{Bi-Co} = 274.2 – 276.3 pm].[4,5] The special structural feature of **2a** are the four $Fe(CO)_4$ fragments coordinated in a μ_1 fashion to four Bi atoms. The Bi–Fe bond lengths [d_{Bi-Fe} = 271.9 – 272.4 pm] are nearly equal to the bridging ones. This is, on the first glance, unexpected, but indicates a low basicity of the bismuth atoms via the lone pair. This is in line with the ligand behavior of P_4.[11] In **I**[3] the terminal Bi–Fe-bond [d_{Bi-Fe} = 275.2 pm] is even longer than in **2a**, whilst the bridging ones are in a similar range [d_{Bi-Fe} = 269.9 – 275.3 pm]. In complex **II** these four bismuth tops are left bare. The Bi–Fe–Bi bond angles [approx. 78°] in **2a** are smaller than the 90° angles of a cube, whereas the Fe–Bi–Fe bond angles [approx. 100°] are larger.

3.2.4 Theoretical characterization of $[Bi_4Fe_8(CO)_{28}]^{4-}$ anion and its derivates

DFT quantum chemical calculations (Table 1 – 3) were performed for **2a** as well as $\{Bi_4[\mu_3\text{-}Fe(CO)_3]_4\}^{4-}$ (**2aa**) and $\{Bi_4[\mu_3\text{-}Fe(CO)_3]_4\}^{2+}$ (***closo*-2ab**, ***arachno*-2ab**). The last two species were used as model compounds for the cluster system **2a**. The four μ_1-coordinated $Fe(CO)_4$ fragments were removed either as neutral fragment, isolobal to an oxygen atom or partially negatively in order to obtain models with negative or positive charge in the remaining Bi_4Fe_4 cores (Scheme 2).

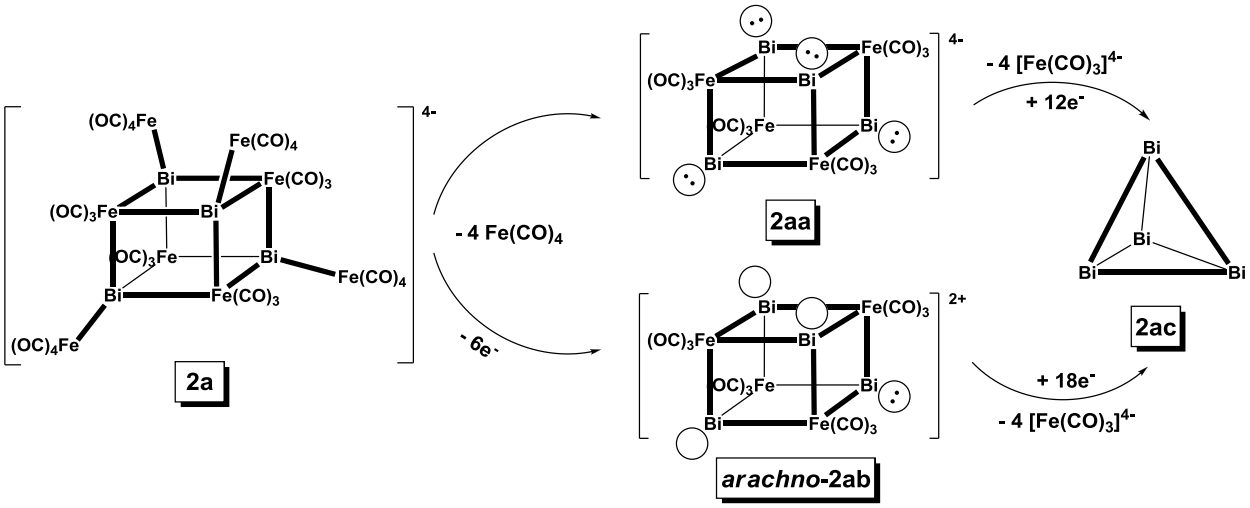

Scheme 2. Simplification of **2a** (24 SEC) into **2aa** (24 SEC), ***arachno*-2ab** (18 SEC) and **2ac** (12 SEC) upon elimination of μ_1-$Fe(CO)_4$ and μ_3-$Fe(CO)_3$ fragments.

Skeletal electron counts (SEC) for **2a** and **2aa** show that the clusters belong to cubane classes on the basis of the isolobality principle (Scheme 3). Thus, **2a** and **2aa** providing 12 skeletal electron pairs are structural analogs to cubane C_8H_8. $\{Bi_4[\mu_3\text{-}Fe(CO)_3]_4\}^{2+}$ providing only 9 skeletal electron pairs should adopt a structure analogously to *closo*-borane $B_8H_8^{2-}$ (Scheme 3).[12] Really, a cubane-like cluster structure (***arachno*-2ab**) of $\{Bi_4[\mu_3\text{-}Fe(CO)_3]_4\}^{2+}$ is slightly less energetically favored by 21 kJ/mol (ΔE_{rel} + ZPE) in comparison to ***closo*-2ab**. Such unsignificant energy difference between these two structures may be related to that that stella quadrangula structure[13a] (tetracapped tetrahedron; ***arachno*-2ab**) is allowed to be on the basis that the t_1 set on the Bi_4 tetrahedron is well able to stabilize the capping Fe_4 t_1 set.[13b] For example, the cubane-like $[Bi_4Pd_4(PPh_2Me)_8]^{2+}$ cluster[6] and the *closo*-deltahedron $[Bi_4Ni_4(CO)_6]^{2-}$ bisdisphenoid[14], isoelectronic with these two **2ab** clusters, were synthesized and described.

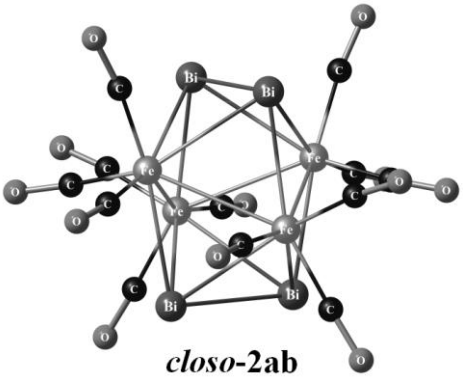

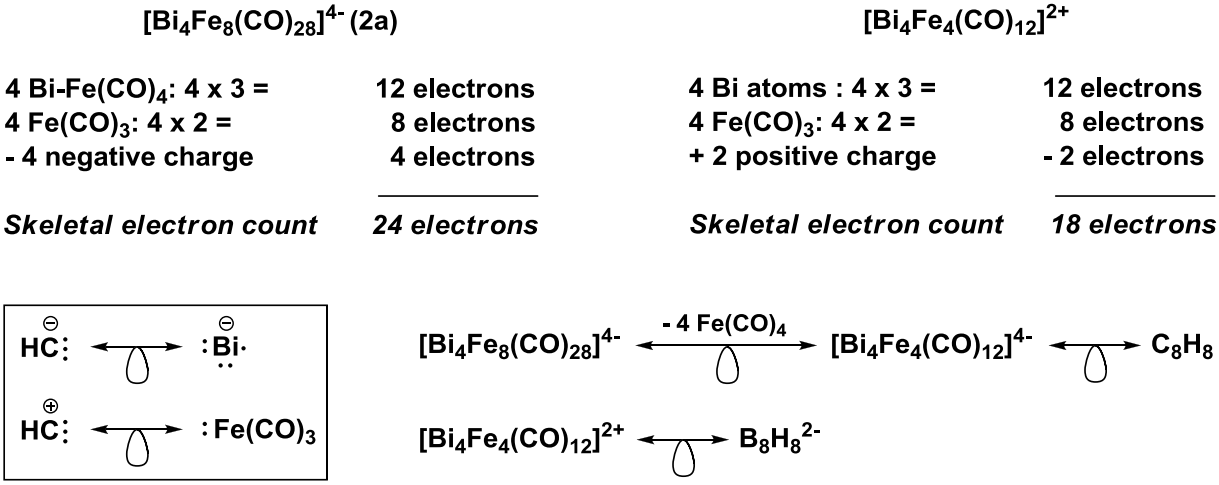

Scheme 3. Wade's electron counting for **2a** and **2aa** as well as for the cluster $\{Bi_4[\mu_3\text{-}Fe(CO)_3]_4\}^{2+}$, and isolobality between given species and carbon and boron structural analogs.

The DFT optimized geometry of **2a** is very close to the experimental one of **2** (Table 1). The calculated Bi–Fe–Bi and Fe–Bi–Fe bond angles for **2aa** and ***arachno*-2ab** demonstrate more distorted cubic structures in comparison to **2a** (Figure 2). This fact can be well correlated with the electrostatic repulsions and attractions within these clusters on the basis of the charges on the metal atoms (Table 2), indicating a high degree of the ionic character of the Bi–Fe bonds. Thus, more positive charges on the Bi atoms and less negative charges on these of μ_3-Fe lead to an elongation of Bi–Bi distances and to a shortening of Bi–μ_3-Fe bonds in **2a**.

Table 1. Selected theoretical structural parameters (LSDA/BS-I level; bond lengths in pm and bond angles in degrees) for anionic cluster **2a** and its simplified derivates **2aa**, ***arachno*-2ab** and **2ac**. Structural data of **2a**, obtained from X-ray crystal structure analysis of **2**, are given for comparison.

Parameter	$[Bi_4Fe_8(CO)_{28}]^{4-}$ **2a**	$[Bi_4Fe_4(CO)_{12}]^{4-}$ **2aa**	$[Bi_4Fe_4(CO)_{12}]^{2+}$ ***arachno*-2ab**	Bi_4 **2ac**	Experimental Data for **2**
Bi–Bi	341.2 – 341.6	332.4 – 332.7	319.6 – 320.2	297.3	342.8 – 343.8
Bi–μ_3-Fe	268.7 – 269.1	276.9 – 277.1	267.5 – 267.7		270.6 – 272.7
Bi–μ_1-Fe	269.2 – 269.3				271.9 – 272.4
Bi–Fe–Bi	78.7 – 78.9	73.7 – 73.8	73.3 – 73.5		78.2 – 78.6
Fe–Bi–Fe	100.1 – 100.3	104.1 – 104.2	104.2 – 104.5		100.1 – 100.7

Interesting, the cubes **2a** and ***arachno*-2ab** have smaller size than **2aa**. While the height and the wide of **2a** are 266.6 pm, the values of these parameters for ***arachno*-2ab** and **2aa** are 262.6 pm and 272.0 pm, respectively. Such change of the cluster size may be related to the strength of metal–ligand interactions, i.e. for the contraction of the cubes **2a** and ***arachno*-2ab** the Bi–μ_3-Fe attraction forces are responsible. First, the Bi–μ_3-Fe distances in **2a** and ***arachno*-2ab** clusters are very close to each other and shorter than these in **2aa** (Table 1) where the Bi–μ_3-Fe repulsion forces prevail. Secondly, computed WBI values and overlap populations for the Bi–μ_3-Fe bonds exhibit stronger bonding character of these for **2a** and ***arachno*-2ab** species than for **2aa** (Table 2), as consequence.

Table 2. Selected theoretical data obtained from the NBO analysis at the MW1PW91/BS-II level for anionic cluster **2a** and its simplified derivates **2aa**, ***arachno*-2ab** and **2ac**.

Parameter	$[Bi_4Fe_8(CO)_{28}]^{4-}$ **2a**	$[Bi_4Fe_4(CO)_{12}]^{4-}$ **2aa**	$[Bi_4Fe_4(CO)_{12}]^{2+}$ ***arachno*-2ab**	Bi_4 **2ac**
WBI_{Bi-Bi}[a]	0.112	0.233	0.272	0.992
WBI_{Bi-Fe}	0.615 (μ_3)[b]	0.556	0.673	
	0.565 (μ_1)[c]			
OOv_{Bi-Bi}[d]	+0.213	+0.288	+0.299	+0.581
OOv_{Bi-Fe}	+0.636 (μ_3)	+0.601	+0.708	
	+0.616 (μ_1)			
Q_{NPA}[e] (Bi)	+1.285	+0.926	+1.141	0
Q_{NPA} (Fe)	–2.244 (μ_3)	–2.345	–2.098	
	–1.921 (μ_1)			

[a] Wiberg bond index. [b] For bonding between Bi and μ_3-coordinated iron carbonyl. [c] For bonding between Bi and μ_1-coordinated iron carbonyl. [d] Order of orbital overlapping. [e] NPA charge on the metal atom [e].

This interesting observation lies in line with this one, pointed out by Sarasa et al. for M_4X_4 structures in transition metal chemistry (M = Ti, V; X = N, P, As).[15] The Bi–μ_1-Fe bonds in **2a** are slightly more elongate with regard to the Bi–μ_3-Fe bonds and consequently weaker. The bonding to four μ_1-Fe(CO)$_4$ fragments in **2a** is carried out via lone pairs of Bi. The lone pair of electrons on each Bi atom in **2aa** possesses 79.4 % and 81.5 % s character according to the NBO and NLMO analysis, respectively. Four μ_1-Fe(CO)$_4$ groups are involved in 2c2e bonding to three-valent Bi atoms, here. As a consequence, the negative charge is localized within cluster **2a**. The NBO analysis for ***arachno*-2ab** finds one nonbonded lone pair (LP) orbital on Bi (s 63.2 %; s 80.6 % according to the NLMO) and three unfilled nonbonded lone pair (LP*) orbitals of s type. This may result in the Jahn-Teller-type distortion of the cube as has been discussed by Whitmire, Saillard et al.[6]

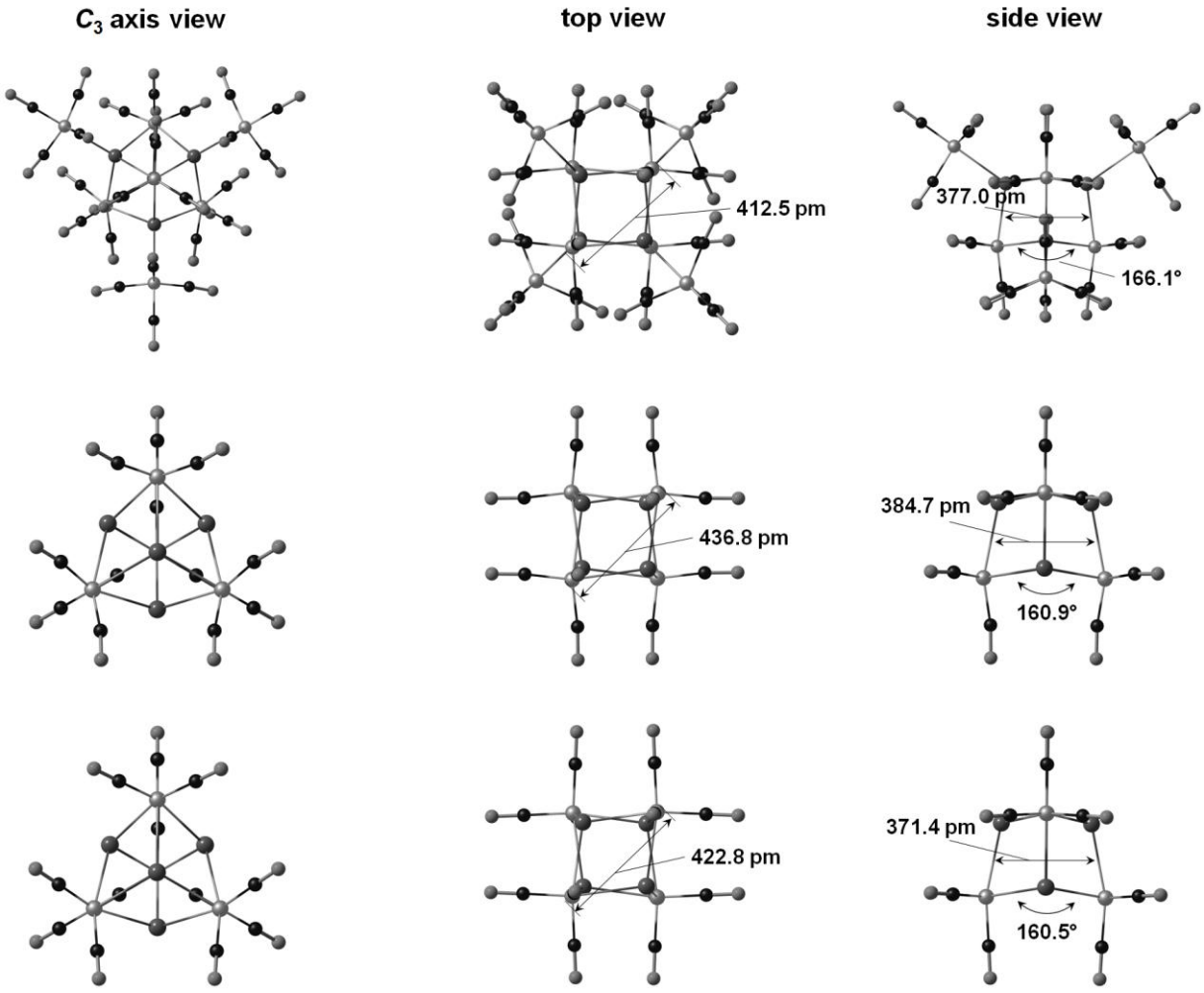

Figure 2. DFT optimized structures of the clusters **2a** (top), **2aa** (middle) and ***arachno*-2ab** (bottom) representing stationary points (global minima for **2a** and **2aa** and local minimum for **2ab**) on their potential energy surfaces. The number of imaginary frequencies for all structures is 0.

Formally, removal of four μ_3-coordinated iron carbonyl fragments from **2aa** and ***arachno*-2ab** leads to the neutral Bi_4 tetrahedron (**2ac**; 6 skeletal electron pairs) as a building block of all represented species (Scheme 2). [A calculation of strain energy of Bi_4 cluster core and its molecular orbital relationships with *arachno*-Bi_4 core can be found in the appendix to chapter 3.2.] Monotonous shortening of Bi–Bi distances, observed in direction of **2a** → **2aa** → ***arachno*-2ab** → **2ac** (Table 1), is accompanied by an increase in the Bi–Bi bonding strength according to the WBI values and order of orbital overlapping (Table 2). These bonding characteristics indicate that the bonding along the edges of Bi_4 tetrahedron is very weak or completely absent in **2a** (about 85 % of ionic character).

The relatively large value of HOMO–LUMO gap computed for **2a** predicts higher stability of latter than its derivate **2aa** where four Bi tops are left bare (Table 3). For the cationic cluster ***arachno*-2ab** the HOMO–LUMO gap is comparable to that of **2a**. This is in line with the higher positive charge on the bismuth atoms in **2a** and ***arachno*-2ab**. In spite of this, the charge reconstruction by an elimination of four $Fe(CO)_4$ groups from the cluster **2a** to give ***arachno*-2ab** is energetically ungained (ΔE_{rel} = +3102 kJ/mol), whereas the μ_1 coordination of iron carbonyl fragments to ***arachno*-2ab** is vice versa. Analogically, the elimination process of four $Fe(CO)_4$ groups from **2a** to give its derivate **2aa** is endothermic (ΔE_{rel} = +1638 kJ/mol). The charge reconstruction of **2aa** toward ***arachno*-2ab** is endothermic (ΔE_{rel} = +1465 kJ/mol), too.

Table 3. Stretching vibrations of the carbonyl groups of anionic cluster **2a** and its simplified derivates **2aa** and ***arachno*-2ab** calculated at the LSDA/BS-I level; selected energy values and GIAO-NICS values from MW1PW91/BS-II computations for closed-shell **2a**, **2aa**, ***arachno*-2ab** and **2ac**.

Parameter	$[Bi_4Fe_8(CO)_{28}]^{4-}$ **2a**	$[Bi_4Fe_4(CO)_{12}]^{4-}$ **2aa**	$[Bi_4Fe_4(CO)_{12}]^{2+}$ ***arachno*-2ab**	Bi_4 **2ac**
$\tilde{\nu}_{CO}$[a]	2074, 2053, 2022, 2017, 1993, 1988	1954, 1912	2168, 2131	
HLG[b]	2.86	1.96	2.92	4.44
NICS[c]	+23.7	–12.3	–19.4	–37.4

[a] Stretching vibrations [cm^{-1}] of the carbonyl groups. [b] Energy of the HOMO–LUMO gap [eV]. [c] NICS value [ppm] at the cage center of cluster.

The infrared (IR) spectra of **2** in thf solution and in solid state as well as the IR spectra computed for the gas-phase structures of the clusters **2a**, **2aa** and ***arachno*-2ab** are a precedent for the discussions. Thus, the IR spectrum of the saturated thf solution of **2** displays six bands of different strength for the CO vibrations (2004w, 1977s, 1957s, 1934m, 1919m, 1899m cm^{-1}).

The same number of stretching vibrations of the carbonyl groups (2008w, 1994w, 1976m, 1915s, 1895s, 1878s cm^{-1}) was observed for the solid state of **2**. The computed IR spectrum for the cluster anion **2a** predicts three bands of stretching vibrations of the $Fe(CO)_3$ carbonyl groups at 2074, 2022 and 2017 cm^{-1} and three these ones of the $Fe(CO)_4$ fragments at 2053, 1993 and 1988 cm^{-1}. The computed spectra of **2aa** and ***arachno*-2ab** show two bands of these vibrations, only (Table 3). The stretching modes of the CO groups for cationic ***arachno*-2ab** are shifted to higher wave numbers in comparison to anionic clusters **2a** and **2aa**.

According to the nucleus-independent chemical shifts (NICS) computations, the "naked" Bi_4 cage [d(Bi–Bi)$_{theor}$ = 297.3 pm (**a**)] demonstrates spherical aromaticity (NICS ~ –37 ppm), as is well-known.[2b,16] For a swollen up tetrahedron with fixed Bi–Bi distances similar to those in **2a** [d(Bi–Bi) = 342.8 – 343.8 pm (**b**)] no significant decrease of aromaticity (NICS –32.3 at the cage center) is expected. The Bi–Bi bonds are weakened only marginally by the elongation from **a** to **b** (WBI = 0.986). For this reason one would anticipate similar diatropic character of anionic clusters **2a** and **2aa** as well as cationic cluster ***arachno*-2ab** containing tetracapped Bi_4 core as building block.

Thus, NICS computations (Table 3) show that **2aa** and ***arachno*-2ab** exhibit diatropic NICS values of –12.3 and –19.4 ppm, respectively, providing aromaticity of these species despite the fact that the WBI values for the Bi–Bi separations are here 0.233 (**2aa**) and 0.272 (***arachno*-2ab**), only (Table 2). In contrast, the positive NICS value of +23.7 ppm was observed at the cage center of **2a** that is an evidence for paratropic ring current associated with antiaromaticity.

The NICS values at the cage centers of **2aa** and ***arachno*-2ab** are strongly reduced with regard to "naked" Bi_4 tetrahedron. Such large difference in the NICS values of these species may be related to an influence of d-electrons of μ_3-coordinated iron carbonyl fragments and the partially ionic character of the Bi–Fe bonds on the electronic density picture within the cluster. Besides, the strength of the diatropic ring current should depend on the size of a cluster π orbital (π molecular orbital subsystem), responsible for the spherical aromaticity of the cage. To understand from which cluster π orbital (Bi_4 vs. Fe_4) this aromaticity comes and to get more insight into the different magnetic shielding behavior of **2a**, **2aa** and ***arachno*-2ab** clusters the molecular orbitals (MOs) of these were analyzed. Figure 3 shows the correlations between cluster π orbitals placed within the Bi_4 and Fe_4 cages of the clusters **2aa** and ***arachno*-2ab**. Thus, the a_1 (s, π)-orbital of Bi_4 (HOMO-9) in **2aa** is a cluster π orbital. The later is reduced compared to the size of the (d, π)-orbital (cluster π orbital) of Fe_4 (HOMO-23), whereas the share of analogical π orbitals of Bi_4 (HOMO-3) and Fe_4 (HOMO-20) in ***arachno*-2ab** are similar. The antiaromatic character of **2a** is shown in the tetrahedral-shaped orbital within Bi_4 tetrahedron

(HOMO-17), whilst the cluster π orbital within Fe_4 cage (HOMO-39) retains its integrity (Figure 3).

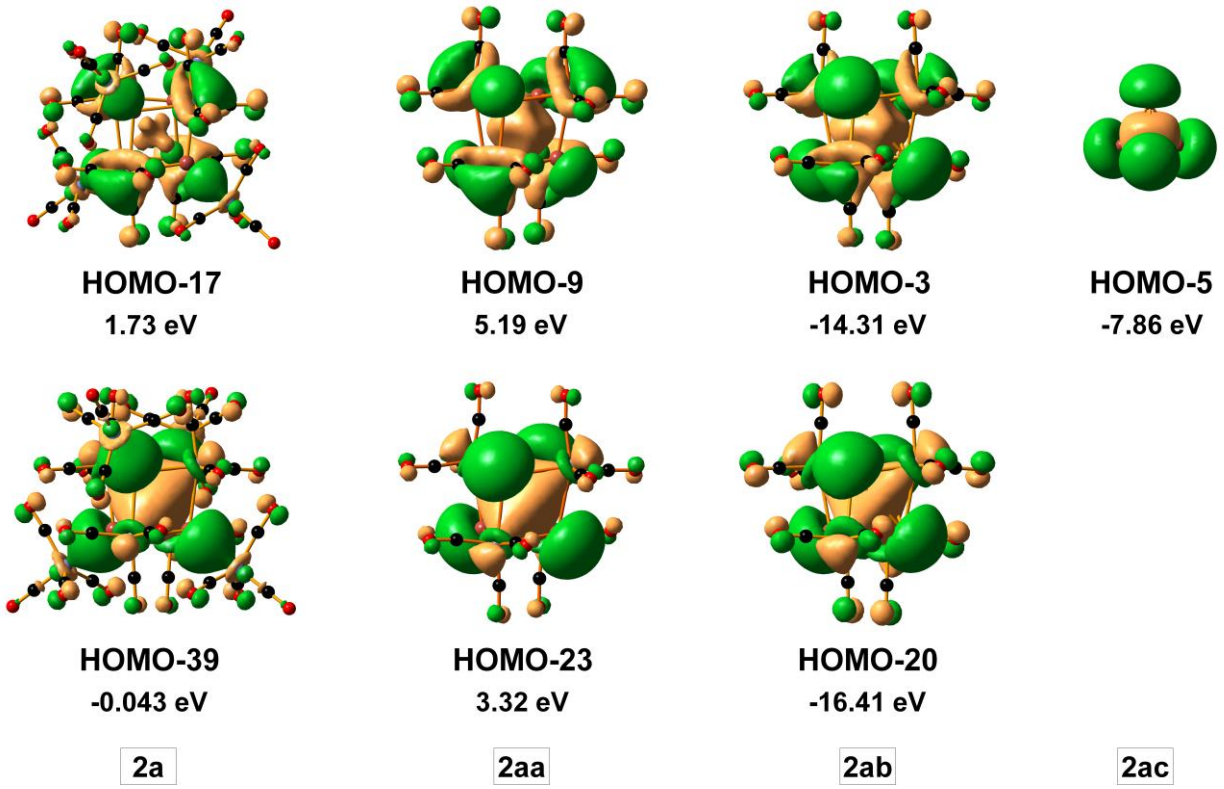

Figure 3. π Molecular orbital subsystems of Bi_4 (top) and Fe_4 (bottom) within **2a**, **2aa**, ***arachno*-2ab** and **2ac** species (±0.02 isosurface value). The eigenvalues of these MOs were computed at the MPW1PW91/BS-II level (positive eigenvalues are typical for DFT calculations of highly negative charged species).

Such magnetic deshielding of **2a** to positive NICS value (+23.7 ppm) may be mainly related to an involving of s-type lone pairs of Bi_4 in the interactions with the μ_1-$Fe(CO)_4$ fragments. This μ_1 coordination leads to the strong change in the electronic structure within the cluster. All of these results suggest that namely the cluster π orbitals contributed by Bi_4 tetrahedra are responsible for the aromatic character of the discussed species where the lone pairs of Bi_4 play a key role. The size of these internal-caged π orbitals also explains the difference in the degree of spherical aromaticity of **2aa** (–12.3 ppm) and ***arachno*-2ab** (–19.4 ppm). Finally, it is interesting to remark that ***arachno*-2ab** has slightly larger HOMO–LUMO gap separation in comparison to ***closo*-2ab** (HLG is 2.45 eV). This may be related to less aromatic character of the latter, exhibiting the NICS value of –14.0 ppm at the cage center.

3.2.5 Conclusions

By the reaction of **1** with $Na_2[Fe(CO)_4]$ and nBu$_4$NCl the formation of cluster **2** was observed. The Zintl anion (**2a**) of latter is an unprecedented cluster displaying Bi–Fe cubane shape and being the largest cluster of the bismuth-iron family. Electrophilic cluster anion **2a** is antiaromatic, whereas its hypothetical derivates, **2aa** and ***arachno*-2ab**, are spherically aromatic in their nature. The synthetic availability of these is a challenge in the bismuth-transition metal chemistry. In addition, cubane-like **2a** and its models might be valuable single-source molecular precursors to polycrystalline E_nTM_m materials (E = heavy group 15 element; TM = transition metal).[6] A Bi_2Fe ion observed in thf solution of **2** by ESI mass spectrometry predicts a presence of such capability. Whether these unique compounds are really practical for synthetic applications will depend on their improved availability.

3.2.6 References

[1] V. E. Bondybey, J. H. English, *J. Chem. Phys.* **1980**, *73*, 42.

[2] (a) H. Zhang, K. Balasubramanian, *J. Chem. Phys.* **1992**, *97*, 3437; (b) A. Hirsch, Z. Chen, H. Jiao, *Angew. Chem.* **2001**, *113*, 2916; *Angew. Chem. Int. Ed.* **2001**, *40*, 2834; (c) I. Krossing in *Molecular Clusters of the Main Group Elements* (Eds.: M. Driess, H. Nöth), Wiley-VCH, Weinheim, **2004**, 209.

[3] (a) K. H. Whitmire, M. R. Churchill, J. C. Fettinger, *J. Am. Chem Soc.* **1985**, *107*, 1056; (b) K. H. Whitmire, T. A. Albright, S.-K. Kang, M. R. Churchill, J. C. Fettinger, *Inorg. Chem.* **1986**, *25*, 2799.

[4] G. Ciani, M. Moret, A. Fumagalli, S. Martinengo, *J. Organomet. Chem.* **1989**, *362*, 291.

[5] T. Gröer, M. Scheer, *Organometallics* **2000**, *19*, 3683.

[6] J. L. Stark, B. Harms, I. Guzman-Jimenez, K. H. Whitmire, R. Gautier, J.-F- Halet, J.-Y. Saillard, *J. Am. Chem Soc.* **1999**, *121*, 4409.

[7] (a) S. Ulvenlund, K. Stahl, L. Bengtsson-Kloo, *Inorg. Chem.* **1996**, *35*, 223; (b) M. Ruck, *Z. Anorg. Allg. Chem.* **1998**, *624*, 521; (c) J. Beck, C. J. Brendel, L. Bengtsson-Kloo, B. Krebs, M. Mummert, A. Stankowski, S. Ulvenlund, *Chem. Ber.* **1996**, *129*, 1219; (d) A. Hershaft, J. D. Corbett, *Inorg. Chem.* **1963**, *2*, 979; (e) M. Ruck, V. Dubenskyy, T. Söhnel, *Angew. Chem.* **2003**, *115*, 3086; *Angew. Chem. Int. Ed.*, **2003**, *42*, 2978.

[8] J. F. Bickley, A. D. Bond, F. Garcia, K. Jantos, G. T. Lawson, M. McPartlin, A. Steiner, D. S. Wright, *J. Chem. Soc., Dalton Trans.*, **2002**, 4629.

[9] G. Linti, W. Köstler, *Z. Anorg. Allg. Chem.* **2002**, *628*, 63.

[10] P. Cucka, C. S. Barrett, *Acta Crystallogr.* **1962**, *15*, 865.

[11] (a) I. Krossing, L. Van Wullen, *Chem. Eur. J.* **2002**, *8*, 700; (b) I. de Los Rios, J.-R. Hamon, P. Hamon, C. Lapinte, L. Toupet, A. Romerosa, M. Peruzzini, *Angew. Chem. Int. Ed.* **2001**, *40*, 3910; (c) M. Di Vaira, P. Frediani, S. Seniori Costantini, M. Peruzzini, P. Stoppioni, *Dalton Trans.* **2005**, 2234; (d) P. Barbaro, M. Di Vaira, S. Seniori Costantini, M. Peruzzini, P. Stoppioni, *Chem. Eur. J.* **2007**, *13*, 6682.

[12] L. J. Guggenberger, *Inorg. Chem.* **1969**, *8*, 2771.

[13] (a) C. Zheng, R. Hoffmann, D. R. Nelson, *J. Am. Chem. Soc.* **1990**, *112*, 3784; (b) T. A. Albright, K. A. Yee, J.-Y. Saillard, S. Kahlal, J.-F. Halet, J. S. Leigh, K. H. Whitmire, *Inorg. Chem.* **1991**, *30*, 1179.

[14] J. M. Goicoechea, M. W. Hull, S. C. Sevov, *J. Am. Chem Soc.* **2007**, *129*, 7885.

[15] J. P. Sarasa, J. M. Poblet, M. Bénard, *Organometallics* **2000**, *19*, 2264.

[16] Z. Chen, R. B. King, *Chem. Rev.* **2005**, *105*, 3613.

3.3 Bismuth–iron cluster with π-coordinated aromatic ligands

3.3.1 Introduction

This part continues an experimental and theoretical study of the Bi–Fe cage cluster compounds providing unusual bonding situations and physical-chemical properties. The highlight is a Bi–Fe cluster with π-coordinated aromatic ligands of arene type. Here, different synthetic methods of the formation of neutral compound $[Bi_4Fe_3(CO)_9]$ (**1**) exhibiting unique type of bismuth–arene (Bi···Ar) π-intermolecular interactions in the crystal [**1**·2(C_6H_5Me)] are presented. In addition, DFT quantum chemical calculations are performed to get an insight into the geometric and electronic structures, the chemical bonding as well as into stability and aromaticity of these species.

Arene complexes of bismuth, where the aromatic hydrocarbons coordinated as ligands to the bismuth atoms, have been known since the 1960s. However, the first structures were elucidated only in the end of the 1980s, when arene complexes of bismuth trichloride (η^6-1,3,5-$Me_3C_6H_3$)$BiCl_3$ and (μ-η^6-C_6Me_6)($BiCl_3$)$_2$ were structurally characterized.[1–3] In general, two coordination geometries around the bismuth atom were observed, regardless of the nature of the anionic ligands and the arene molecule, i.e. distorted octahedral and pentagonal bipyramidal (Figure A).[3]

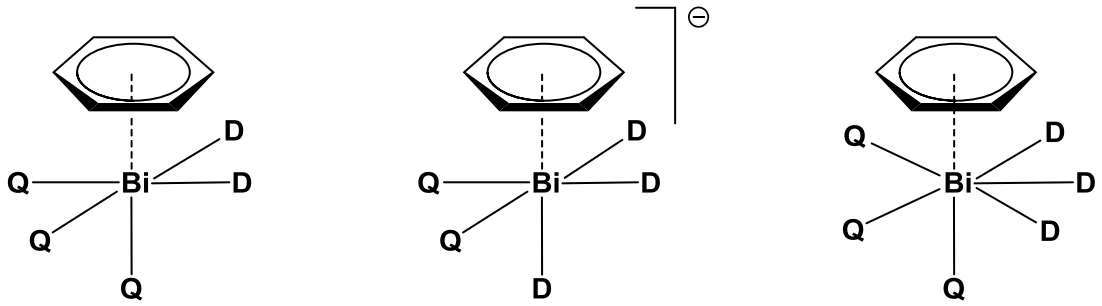

Figure A. Octahedral (left, center) and pentagonal bipyramidal (right) geometries around the bismuth atom.

Although, the weak bismuth–arene interactions (classed so, due to the excessively long Bi–C bond lengths) were established for triphenylbismuthane Ph_3Bi, pentafluorophenoxy-substituted compounds $[Bi(OC_6F_5)_2(\mu\text{-}OC_6F_5)]_2$,[4] trifluoroacetate-substituted dibismuthane $[Bi_2(\mu\text{-}O_2CCF_3)_4]_2$,[5] two triorgano bismuth compounds $[Bi(OSiPh_2tBu)_3]_2$ and $[Bi(CH_2C_6H_4Cl\text{-}2)_3]_2$,[6] and few examples of bismuth–transition-metal bonding, the Bi···Ar interactions are mainly well-known for the neutral bismuth halides BiX_3.[3] The hapticity is there generally six, i.e. the bismuth atoms occupy positions above or/and below the center of the arene rings. These complexes are the bismuth analogues of the so-called "Menshutkin" complexes of antimony

trihalides with arenes. But, by virtue of the η^6-bonding, bismuth–arene complexes differ markedly from the "Menshutkin" complexes, in which there is no central coordination.[1,7]

Nikolai A. Menshutkin (1842–1907)

The intermolecular distances in all of these compounds in solid state are in the range from 270 to 400 pm.

Some common features concerning the coordination environment of the metal atom in bismuth–arene complexes investigated by X-ray diffraction have been pointed out by Silvestru, Breunig and Althaus in *Chemical Reviews*. Thus, each bismuth atom has three primary (short) bonds and two or three secondary (longer) bonds (or interactions) to halide or oxygen atoms, thus leading to different degrees of association in the crystal. The C_6 aromatic system is placed *trans* to a primary Bi–Q bond with trans Q–Bi···$Ar_{centroid}$ angles in the range of 153.4 – 168.5°.[3] Only one exception was found up to now here. This is ionic $[(\eta^6\text{-}C_6Me_6)BiCl_2][AlCl_4]$[8] which has only two primary Bi–Cl bonds. The typical Bi–$Ar_{centroid}$ distances lie between 272 and 329 pm. These reflect the acid–base properties of the arene donors and the bismuth acceptors. The increase of Lewis basicity of the arenes in the series C_6H_6, $Me_2C_6H_4$, $Me_3C_6H_3$, C_6Me_6 as well as an increase of the acidity of the bismuth center (cf. $BiCl_3$ vs. $BiCl_2^+$) leads to shorter arene–bismuth bonds.[3] Relatively recently, weak bismuth–arene interactions have been reported in the scientific literature, again. Thus, two bismuth–arene complexes have been observed by Mehring et. all, where the Bi···$Ar_{centroid}$ distances could be established for $[Bi(OSiPh_2tBu)_3]_2$ (334.0 pm) and $[Bi(CH_2C_6H_4Cl\text{-}2)_3]_2$ (365.9 pm) (Figure B).[6]

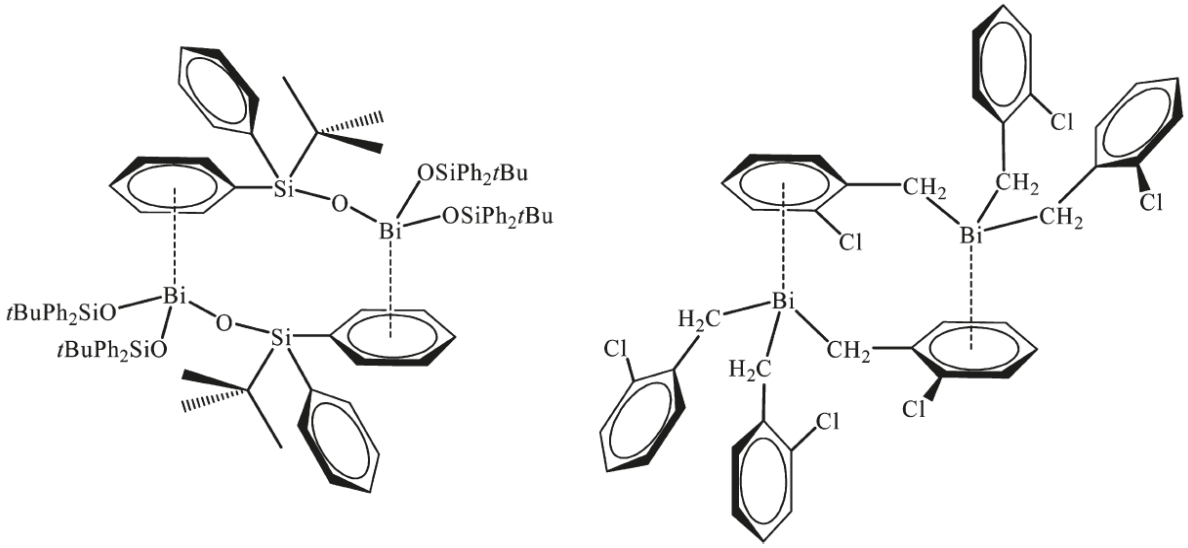

Figure B. Molecular structures of $[Bi(OSiPh_2tBu)_3]_2$ (left) and $[Bi(CH_2C_6H_4Cl\text{-}2)_3]_2$ (right).[6]

3.3.2 Synthesis of $[Bi_4Fe_3(CO)_9]$

The reactions (eq. 1) of two equivalents of $BiBr_3$ with three equivalents of $Na_2[Fe(CO)_4]$ as well as one equivalent of $(C_5Me_5)BiI_2$ (see chapter 4) with one equivalent of $Na_2[Fe(CO)_4]$ in the solvent thf (warming from –78°C to r.t. during the reaction) lead to $[Bi_4Fe_3(CO)_9]$ (**1**). In the latter case, not only substitution of the iodine atoms takes place, but the reaction proceeds analogously to that of $BiBr_3$ in a 2:3 stoichiometry. During the reactions the color of the mixture changes from dark-green to dark-brown. Workup allows isolation of **1**·2(C_6H_5Me) as toluene soluble red-brown crystals.

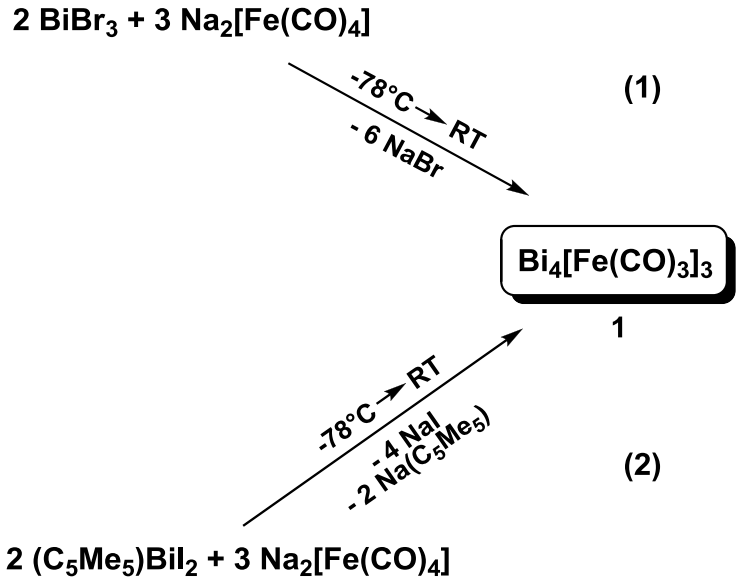

3.3.3 X-ray crystal structure of $[Bi_4Fe_3(CO)_9]\cdot 2(C_6H_5Me)$

1 crystallizes together with two toluene molecules in the monoclinic space group $P2_1/n$ (Figure 2, Table 1). The symmetry of metal core Bi_4Fe_3 is C_{3v}. The building Bi_4 tetrahedron is slightly distorted [d_{Bi-Bi} = 317.0 – 323.9 pm]. The neutral bismuth-cobalt complex $[Bi_4Co_4(CO)_{12}]$ (**II**) has a similar distortion of Bi_4 core but with longer Bi–Bi distances of d_{Bi-Bi} = 331.6 – 337.6 pm.[9,10] The complexes $[Bi_4Fe_4(CO)_{13}]^{2-}$ (**I**),[11] $[Bi_4\{Fe_3(CO)_9\}\{Fe(CO)_2Cp''\}_2]$ (Cp'' = η^5-$C_5H_3tBu_2$) (**III**)[10] and $[Bi_4Pd_4(PPh_2Me)_8]^{2+}$ (**IV**)[12] display more distorted Bi_4 tetrahedra. The Bi–Bi distances are lying in the regions 313.9 – 347.3, 308.9 – 353.0 and 320.1 – 350.9 pm, respectively. The anion bismuth-iron complex $[Bi_4Fe_8(CO)_{28}]^{4-}$ has a nearly ideal built Bi_4 core with Bi–Bi distances of d_{Bi-Bi} = 342.8 – 343.8 pm. All of these Bi–Bi distances lie in an interval comparable with the closest Bi–Bi contacts of 307.1 – 352.9 pm in the pure crystalline element.[13] Three of the four faces of the tetrahedral Bi_4 core in **1** are capped by $Fe(CO)_3$ moieties in a μ_3 fashion, while the fourth is left bare. Thus, the Bi_4Fe_3 core can be deduced from a Bi_4Fe_4 disphenoid by removing one Fe atom. Such coordination structure is analogously to

that in **I** and **III**. The Bi–Fe bond lengths in **1** [$d_{Bi–Fe}$ = 262.3 – 276.3 pm] are in the same region as those in **I** ($d_{Bi–Fe}$ = 269.9 – 275.3 pm) and **III** ($d_{Bi–Fe}$ = 264.7 – 278.2 pm). The Bi–Fe–Bi bond angles (70.2 – 73.9°) in **1** are smaller than the 90° angles of a cube, whereas the Fe–Bi–Fe bond angles (99.6 – 107.3°) are larger.

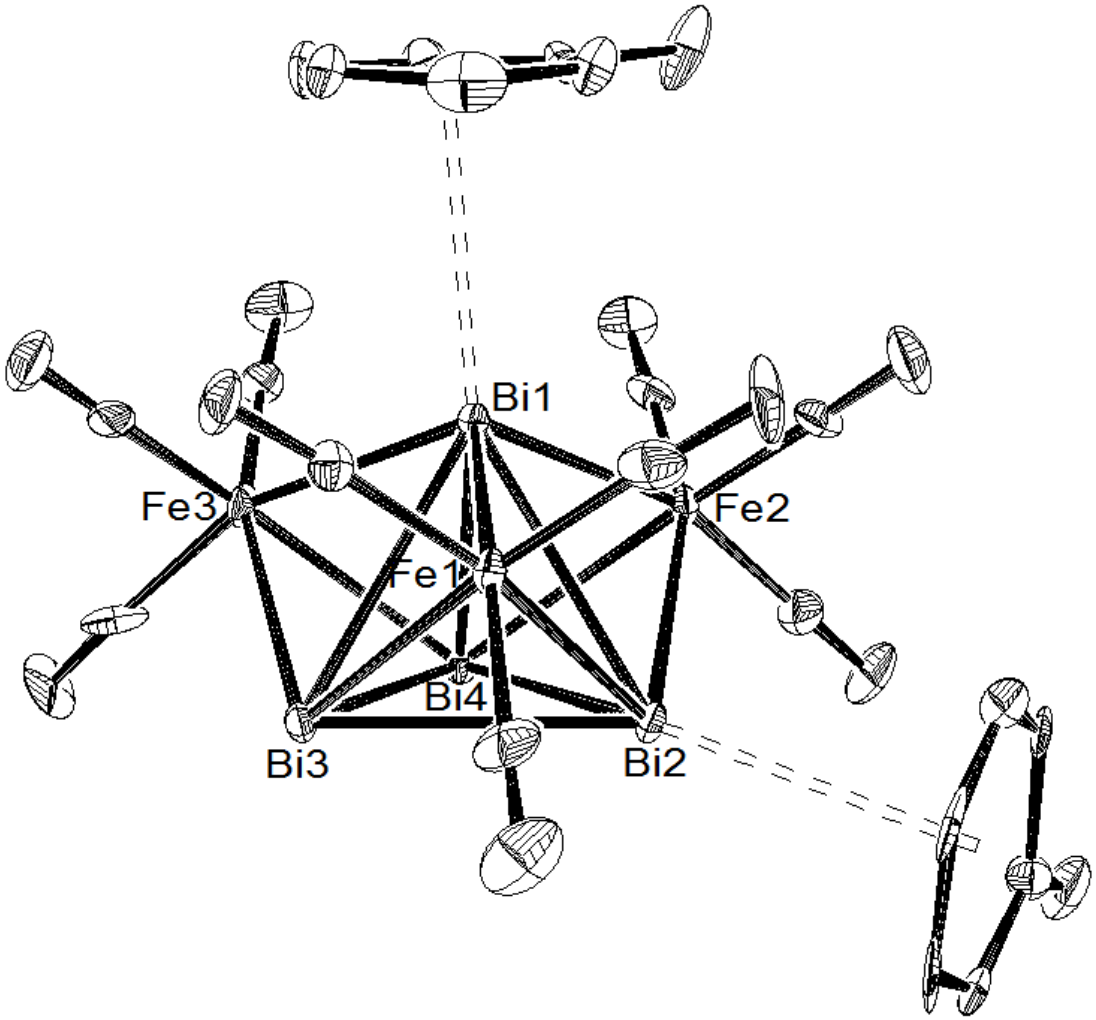

Figure 1. Molecular structure of **1**·2(C_6H_5Me) (crystal; the thermal ellipsoids are given at the 30% probability level; hydrogen atoms are omitted for clarity). Selected bond lengths [pm] and angles [°]: Bi1–Bi2 323.9(7), Bi1–Bi3 323.1(7), Bi1–Bi4 321.0(6), Bi2–Bi3 320.1 (6), Bi2–Bi4 317.0(7), Bi3–Bi4 318.7(7), Bi1–Fe1 263.3(6), Bi1–Fe2 262.9(4), Bi1–Fe3 262.3(4), Bi2–Fe1 275.7(4), Bi2–Fe2 276.0(5), Bi3–Fe1 274.7(4), Bi3–Fe3 274.7(5), Bi4–Fe2 275.1(4), Bi4–Fe3 276.3(4), Bi1···$C_6H_5Me_{(centroid)}$ 324.8(8), Bi2···$C_6H_5Me_{(centroid)}$ 342.6(5), Bi3–Fe3–Bi1 73.9(5), Bi3–Fe3–Bi4 70.7(5), Bi3–Fe1–Bi1 73.8(5), Bi4–Fe3–Bi1 73.1(5), Bi4–Fe2–Bi1 73.2(5), Bi4–Fe2–Bi2 70.2(5), Bi2–Fe2–Bi1 73.9(5), Bi2–Fe1–Bi1 73.9(5), Bi2–Fe1–Bi3 71.1(5), Fe1–Bi3–Fe3 99.9(6), Fe3–Bi1–Fe1 106.2(6), Fe3–Bi4–Fe2 100.2(6), Fe3–Bi1–Fe2 107.3(7), Fe2–Bi2–Fe1 99.6(6), Fe2–Bi1–Fe1 106.4(6).

The solid state structure of the cluster **1** also displays two toluene molecules [**1**·2(C_6H_5Me)], which are attached to two Bi atoms in $\eta^6(\pi)$ coordination modes [$d_{Bi–Arene(centroid)}$ = 324.8 and 342.6 pm]. The Bi–C_{arene} distances lie in the range of 345.4 – 364.6 pm for Bi1···C_6H_5Me contacts and 353.6 – 382.0 pm for Bi2···C_6H_5Me these ones. Such metal-arene π-complexations of bismuth with the aromatic hydrocarbon are the result of weak intermolecular interactions.

The space-filling representation of the cluster **1** containing two π-coordinated toluene molecules [**1**·2(C_6H_5Me)] shows that C_6H_5Me molecules effectively protect only two Bi atoms of the Bi_4 tetrahedron (Figure 2). This gives the possibility to further coordination.

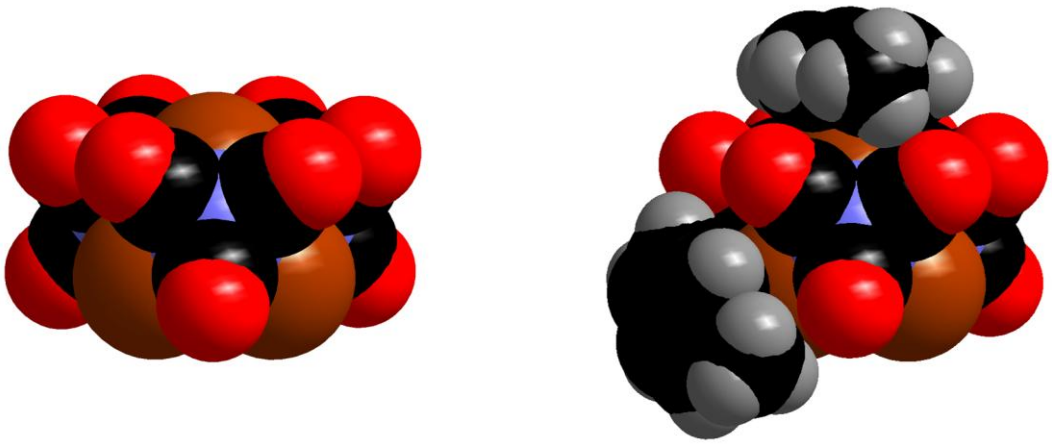

Figure 2. Space-filling models of **1** (left) and **1**·2(C_6H_5Me) (right) in the crystal.

Thus, it is one of few examples of weak intermolecular interactions of Bi with the aromatic hydrocarbon established for its cluster compounds in the solid state. The weak interactions between Bi and the aromatic carbon atoms were also found in the compounds $(Ph_2Bi)_2[Fe(CO)_4]$[14] where $d_{Bi–C(Arene)}$ = 345–373 pm and $[W_2(CO)_8(\mu\text{-}\eta^2\text{-}Bi_2)\{\mu\text{-}MeBiW(CO)_5\}](\eta^3\text{-}C_6H_6)$[15] where $d_{Bi–C(Arene)}$ = 352–374 pm (Figure C).

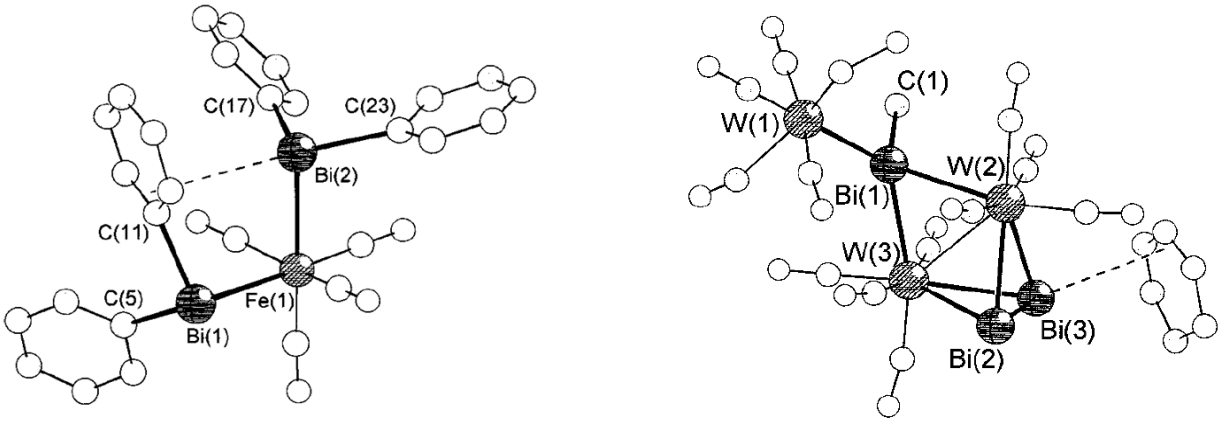

Figure C. Molecular structures of $(Ph_2Bi)_2[Fe(CO)_4]$[14] (left) and $[W_2(CO)_8(\mu\text{-}\eta^2\text{-}Bi_2)\{\mu\text{-}MeBiW(CO)_5\}](\eta^3\text{-}C_6H_6)$[15] (right).[3]

In addition, **1**·2(C_6H_5Me) shows other interesting features in the crystal cell. This displays an inverted sandwich behavior, providing unique type of intermolecular interactions between the [$Bi_4Fe_3(CO)_9$]·2(C_6H_5Me) cluster units through neighbor π-coordinated C_6H_5Me aromatic rings (double-side arene coordination). Here, the observed contacts of 350.4 pm are longer than the distances of the other bismuth–arene π-coordinations in the single cluster unit **1**·2(C_6H_5Me) (Figure 3). Thus, the clusters are connected via three of the four Bi atoms to form a 2D network.

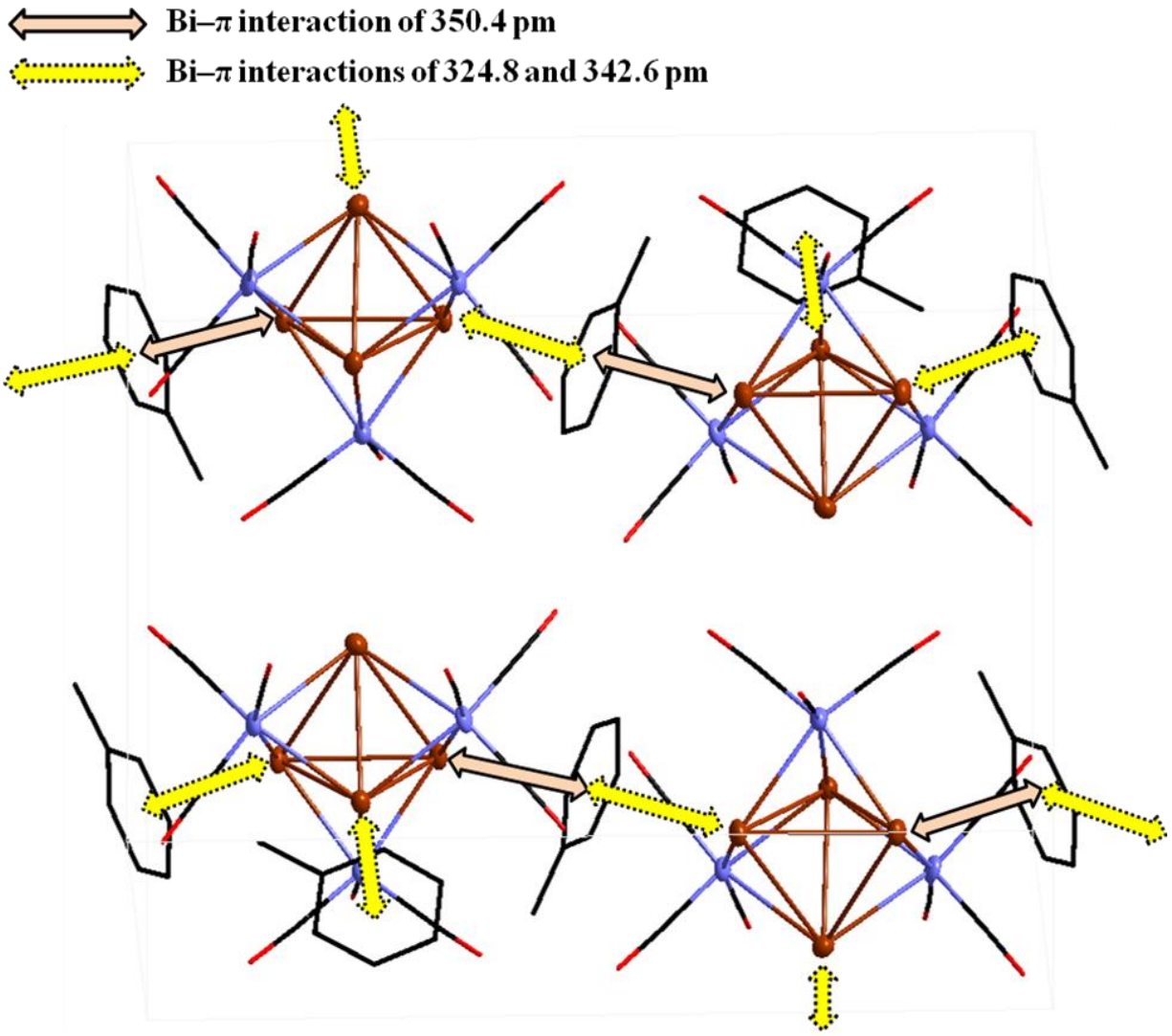

Figure 3. Slice from the two-dimensional network of **1**·2(C_6H_5Me) in the crystal cell showing bismuth–arene π-coordinations.

A similar type of intermolecular double-side arene coordinations were found in the bismuth–hexamethylbenzene adducts, bismuth halide complex (μ-η^6-C_6Me_6)($BiCl_3$)$_2$[1,16] and trifluoroacetate-substituted dibismuthane (μ-η^6-C_6Me_6)[Bi_2(μ-O_2CCF_3)$_4$]$_2$.[5] In the crystals of (μ-η^6-C_6Me_6)($BiCl_3$)$_2$, the centric η^6 coordination of a C_6 aromatic ligand is further extended in a

spectacular way. The crystals consist of tetrameric $(BiCl_3)_4$ units each containing four crystallographically equivalent metal centers coordinated by a hexamethylbenzene ligand. The distorted pentagonal bipyramidal coordination of the metal center is completed by a η^6-C_6Me_6 ligand placed in a apical position, *trans* to the μ^3-Cl atom (Figure D, left).[3] Besides, the centers of the arene molecules form crystallographic inversion centers with the consequence that an identical bismuth halide unit is found on the other side of the ring (Figure D, center). The coordination sphere of the bismuth atoms in $(\mu$-η^6-$C_6Me_6)[Bi_2(\mu$-$O_2CCF_3)_4]_2$ is completed by arene molecules placed *trans* to the Bi–Bi bond on each side of the dinuclear moiety, resulting in an octahedral geometry. Hence, the chain polymeric structure with collinear Bi atoms and arene centers is the result of the π-donation pattern of the C_6Me_6 molecules which exhibit interactions with bismuth atoms on both sides of the aromatic ring (Figure D, right).[3]

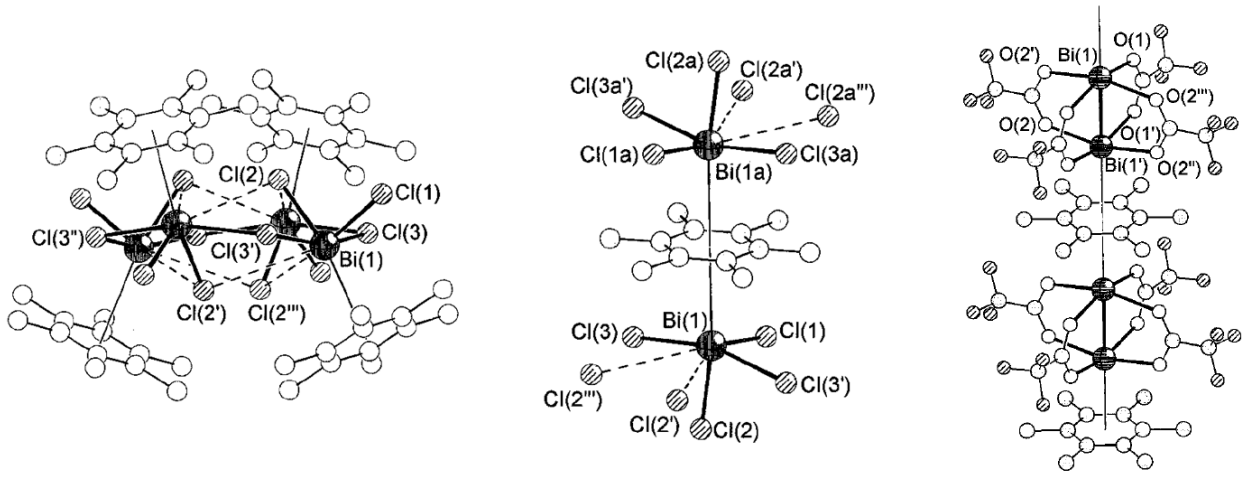

Figure D. Tetranuclear Bi_4Cl_{12} core (left) and double-side arene coordination in the crystal of $(\mu$-η^6-$C_6Me_6)(BiCl_3)_2$[1,16] (center), and polymeric association in the crystal of $(\mu$-η^6-$C_6Me_6)[Bi_2(\mu$-$O_2CCF_3)_4]_2$[5] (right).[3]

3.3.4 Theoretical characterization of $[Bi_4Fe_3(CO)_9]$ and $[Bi_4Fe_3(CO)_9]\cdot 2(C_6H_5Me)$

According to the Wade's electron counting rule, skeletal electron count (SEC) for $[Bi_4Fe_3(CO)_9]$ (**1**) is 18. Hence, with 9 skeletal electrons pairs the shape of **1** corresponds to a *nido*-polyhedral cluster (n+2 where n = 7). As a consequence, the cluster **1** displays a seven-vertex *nido*-structure derived from a disphenoid.

DFT quantum chemical calculations (Table 1 – 3) were performed for **1** as well as $[Bi_4Fe_3(CO)_9]\cdot 2(C_6H_5Me)$ [$\mathbf{1}\cdot 2(C_6H_5Me)$]. Thus, the DFT optimized geometry of **1** is close to the experimental one of $\mathbf{1}\cdot 2(C_6H_5Me)$ (Table 1, Figure 4). The addition of two toluene molecules to **1** [$\mathbf{1}\cdot 2(C_6H_5Me)$], however, leads to relatively strong distortion of Bi_4 tetrahedron and less significant distortions of Bi–μ_3-Fe distances and the Bi–Fe–Bi and Fe–Bi–Fe angles.

Such distortions may be elucidated by quite short intermolecular Bi···C_6H_5Me contacts (about 40 pm shorter than those observed by X-ray diffraction), which are relatively bad described by non-dispersion corrected DFT functionals. In addition, by virtue of the η^6-bonding modes, the experimentally observed structure **1**·2(C_6H_5Me) reveals interesting difference from the calculated this one, in which η^2-bonding modes of the arene rings were observed. Here, the Bi–C_{arene} distances lie in the range of 265.4 – 361.3 pm for Bi_{top}···C_6H_5Me contacts and 284.6 – 369.4 pm for Bi···C_6H_5Me these ones (Table 1, Figure 4).

Table 1. Selected theoretical structural parameters (LSDA/BS-I level; bond lengths in pm and bond angles in degrees) for clusters [$Bi_4Fe_3(CO)_9$] (**1**) and **1**·2(C_6H_5Me). Structural data of latter, obtained from X-ray crystal structure analysis, are given for comparison.

Parameter	Calculated values		Experimental values
	1	**1**·2(C_6H_5Me)	**1**·2(C_6H_5Me)
Bi–Bi	317.7 – 319.9	309.6 – 330.1	317.0 – 323.9
Bi–μ_3-Fe	260.4 – 269.5	258.0 – 276.4	262.3 – 276.3
Bi–Fe–Bi	72.3 – 74.3	69.4 – 77.2	70.2 – 73.9
Fe–Bi–Fe	100.7 – 105.6	96.9 – 107.6	99.6 – 107.3
Bi···C_6H_5Me		284.8, 299.5	324.8, 342.6

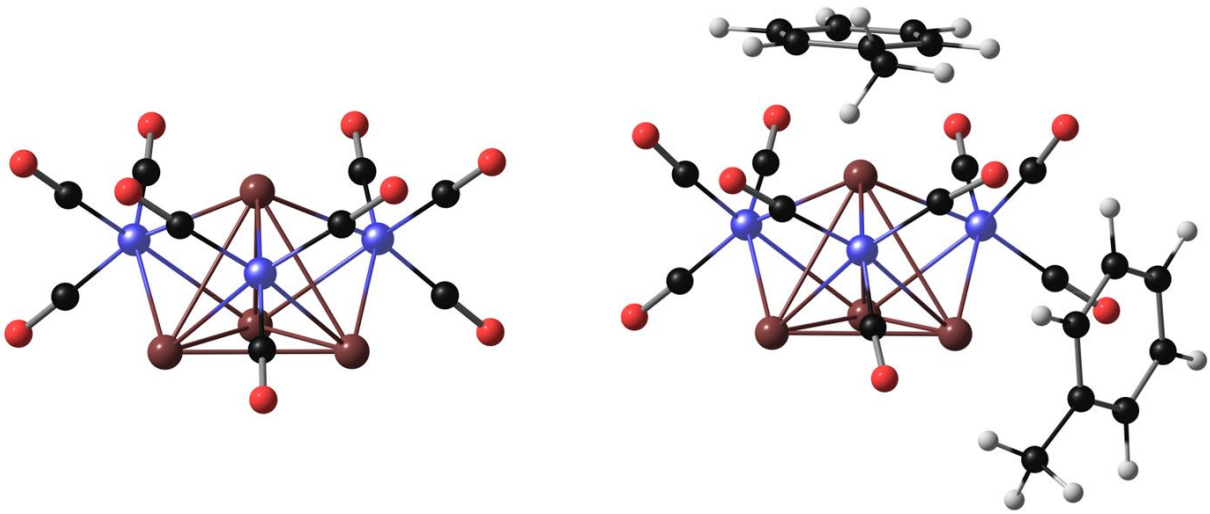

$[Bi_4Fe_3(CO)_9]$ **$[Bi_4Fe_3(CO)_9]\cdot2(C_6H_5Me)$**

1 **$1\cdot2(C_6H_5Me)$**

Figure 4. DFT optimized structures of the clusters **1** and **1**·2(C_6H_5Me) representing global minima on their potential energy surfaces. The number of imaginary frequencies (NImag) for all structures is 0.

According to the NBO analysis (Table 2), the DFT calculated geometry of **1** can be well correlated with the electrostatic repulsions and attractions within this cluster on the basis of the charge distribution on the metal atoms, indicating a relatively high degree of the ionic character for the Bi–Bi (in the range of 50 – 70 %) und Bi–Fe (in the range of 35 – 50 %) bonds (Figure 5). Here, the contributions of more positive charge localized on the Bi_{top} atom of Bi_4 tetrahedron [in comparison to other three positive charges on the Bi atoms forming trigon (3Bi)] and negative charge on the μ_3-Fe atoms in the cluster bonding arise an elongation of Bi_{top}–3Bi (319.9 pm; $d_{Bi–Bi}$ = 317.7 pm) distances and a shortening of Bi_{top}–μ_3-Fe (260.4 pm; $d_{3Bi–3Fe}$ = 269.5 pm) bonds in **1** (Figure 5). It is accompanied by a decrease in the Bi_{top}–3Bi bonding strength [in comparison to this one of the Bi atoms forming trigon (3Bi)] according to the WBI values and order of orbital overlapping as well as an increase in the Bi_{top}–3Fe bonding strength and order of orbital overlapping [in comparison to these ones of 3Bi–3Fe] (Table 2). Thus, the bonding characteristics indicate that the bonding along the edges of Bi_{top}–3Bi tetrahedron in **1** is very weak, whereas the trigon-forming Bi atoms seem to be bonded. This fact will be further examined by molecular orbital (MO) theory.

Table 2. Selected theoretical data obtained from the NBO analysis at the MW1PW91/BS-II level for clusters **1**.

$WBI_{Bi–Bi}$ [a]	$WBI_{Bi–Fe}$	$+OOv_{Bi–Bi}$ [d]	$+OOv_{Bi–Fe}$	Q_{NPA} [e] (Bi)	Q_{NPA} (Fe)
0.258 (Bi_{top}–3Bi)	0.701 (Bi_{top}–3Fe)	0.276 (Bi_{top}–3Bi)	0.746 (Bi_{top}–3Fe)	+1.240 (Bi_{top})	–2.309
0.473 (3Bi)	0.656 (3Bi–3Fe)	0.417 (3Bi)	0.671(3Bi–3Fe)	+0.793	

[a] Wiberg bond index. [b] For bonding between Bi and μ_1-coordinated iron carbonyl. [c] For bonding between Bi and μ_3-coordinated iron carbonyl. [d] Order of orbital overlapping. [e] NPA charge on the metal atom [e].

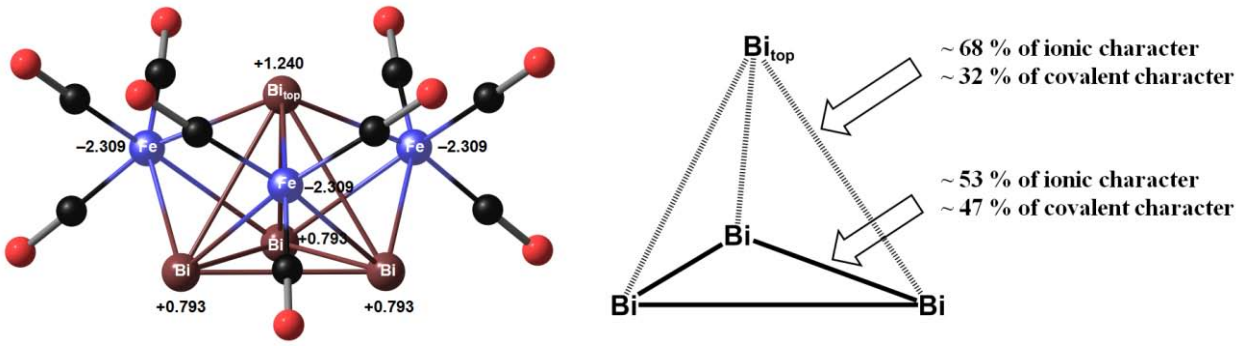

Figure 5. NPA charges on the metal atoms computed on the DFT optimized structure of the cluster **1** (left) and chemical bonding in Bi_4 tetrahedron of **1** (right).

The natural bond orbital analysis (NBO) of **1** shows an interesting feature of the latter. Whereas,

only one nonbonded lone pair (LP) orbital predominantly of s type (57.7%) was found on the Bi_{top} atom, the NBO analysis for each trigon-forming Bi atom finds a pair of LP and LP* orbitals, i.e. one nonbonded LP orbital mainly of s type (83.4 %) and one unfilled nonbonded LP* orbital mainly of p type (93.7%).

According to the nucleus-independent chemical shifts (NICS) computations, seven-vertex structures **1** and **1**·2(C_6H_5Me) exhibit diatropic NICS values of –18.6 and –15.0 ppm, respectively, providing aromaticity of these species. As is well-known, the "naked" Bi_4 cage [d(Bi–Bi)$_{theor}$ = 297.3 pm] demonstrates spherical aromaticity with NICS ~ –37 ppm.[17] The NICS values computed at the Bi_4 cage centers of the clusters **1** and **1**·2(C_6H_5Me) are strongly reduced with regard to "naked" Bi_4 tetrahedron (Table 3). Such large difference in the NICS values may be related here to an influence of d-electrons of μ_3-coordinated iron carbonyl fragments and the partially ionic character of the Bi–Fe bonds on the electronic density picture within the cluster.

Table 3. Selected energy values and GIAO-NICS values from MW1PW91/BS-II computations for clusters **1** and **2**.

Parameter	**1**	**1**·2(C_6H_5Me)
HLG[a]	2.46	2.82
NICS[b]	–18.6 (Bi_4Fe_3), –20.6 (Bi_4)	–15.0 (Bi_4Fe_3), –20.0 (Bi_4)

[a] Energy of the HOMO–LUMO gap [eV]. [b] NICS value [ppm] at the cage center of cluster.

To get more insight into the electronic and magnetic shielding behavior of **1**, the canonical molecular orbitals (MOs) of this cluster were analyzed. Thus, according to Figure 6 the LP of electrons of the bismuth atoms take considerable place in the two degenerate frontier MO's, HOMO and HOMO-1. The HOMO-3 orbital displays (p, σ)-bonding in the Bi_{trigon}-core of the seven-vertex cluster **1**. The HOMO-6 and the HOMO-17 correspond to π molecular orbital subsystems of Bi_4 and Fe_3 cages, respectively. Here, the a_1 (s, π)-orbital is a cluster π orbital of Bi_4 (HOMO-6; picture on the right) and the (d, π)-orbital is this one of Fe_3 (HOMO-17). As was shown by the previous study of the aromaticity of cluster $[Bi_4Fe_8(CO)_{28}]^{4-}$ and its derivates, namely the cluster π orbitals contributed by Bi_4 tetrahedra are responsible for the aromatic character of the whole species where the lone

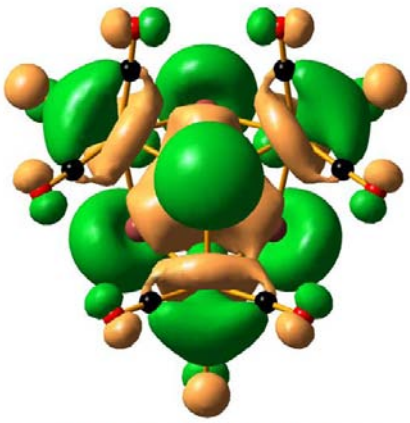

π molecular orbital subsystem of Bi_4 within a seven-vertex cage corresponding to cluster a_1 (s, π)-orbital.

pairs of Bi_4 play a key role. Besides, the size of the internal-caged π orbitals explains the differences in the degree of spherical aromaticity of the clusters. Thus, the spherical aromaticity of **1**·2(C_6H_5Me) is slightly less than this one of **1** because of intermolecular interactions of the bismuth atoms with the aromatic hydrocarbon.

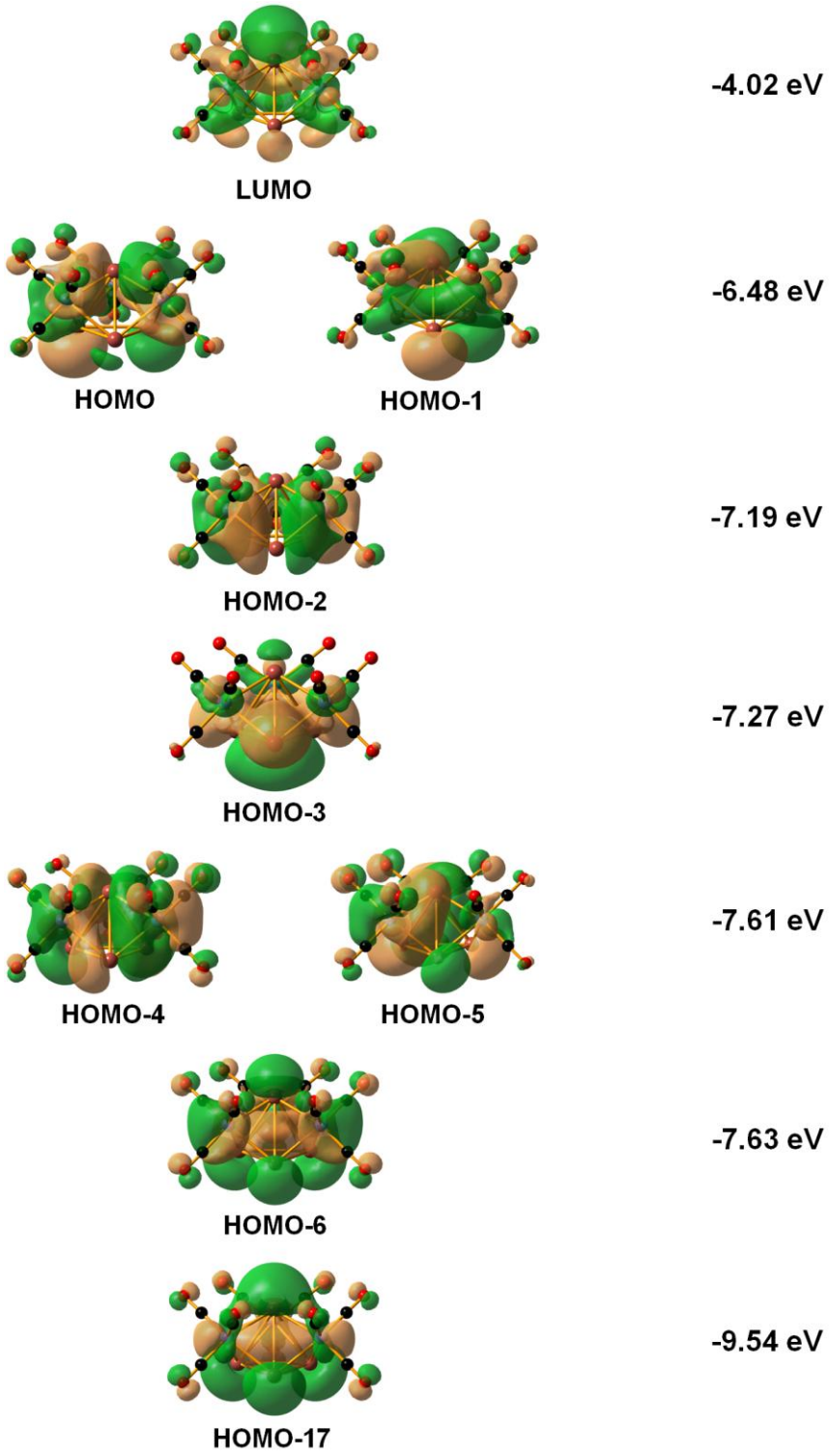

Figure 6. Selected molecular orbitals of **1** (±0.02 isosurface value). The eigenvalues of the MOs were computed at the MPW1PW91/BS-II level.

The results obtained from the NBO analysis and the MO theory indicate that the cluster **1** may act as Lewis acid-base compound via frontier LP and LP* orbitals. The relatively large value of HOMO–LUMO gap computed for **1** predicts its high stability (Table 3).

3.3.5 Conclusions

The reactions of $BiBr_3$ and $(C_5Me_5)BiI_2$ with three and one equivalents of $Na_2[Fe(CO)_4]$, respectively, yield the cluster **1** displaying in the crystal a seven-vertex *nido*-structure [**1**·2(C_6H_5Me)]. The bismuth−arene π-complexations and inverted sandwich behavior in the crystal cell of the latter were observed, here. As a result, it is one of few examples of weak intermolecular interactions of bismuth with the aromatic hydrocarbon established for its cluster compounds. This discovery can be important in term of development of supramolecular chemistry of bismuth's cluster compounds. In addition, **1** provides a spherical aromaticity, which slightly decreases upon coordination of two C_6H_5Me molecules. Being based on the structural and electronic feature of **1**, this cluster has a potential to be useful for synthetic applications using Lewis acid-base interaction scheme.

3.3.6 References

[1] A. Schier, J. M. Wallis, G. Müller, H. Schmidbaur, *Angew. Chem.* **1986**, *98*, 742; *Angew. Chem. Int. Ed.* **1986**, *25*, 757.

[2] H. Schmidbaur, J. M. Wallis, R. Nowak, B. Huber, G. Müller, *Chem. Ber.* **1987**, *120*, 1837.

[3] C. Silvestru, H. J. Breunig, H. Althaus, *Chem. Rev.* **1999**, *99*, 3277.

[4] C. M. Jones, M. D. Burkart, R. E. Bachman, D. L. Serra, S.-J. Hwu, K. H. Whitmire, *Inorg. Chem.* **1993**, *32*, 5136.

[5] W. Frank, V. Reiland, G. J. Reiss, *Angew. Chem.* **1998**, *110*, 3154; *Angew. Chem. Int. Ed.* **1998**, *37*, 2984.

[6] A. A. Auer, D. Mansfeld, C. Nolde, W. Schneider, M. Schürmann, M. Mehring, *Organometallics*, **2009**, *28*, 5405.

[7] (a) H. H. Perkampus in *Wechselwirkungen von π-Elektronensystemen mit Metall-halogeniden*; Springer, Berlin, **1973**; b) D. Mootz, V. Händler, *Z. Anorg. Allg. Chem.* **1986**, *533*, 23.

[8] W. Frank, J. Weber, E. Fuchs, *Angew. Chem.* **1987**, *99*, 68; *Angew. Chem. Int. Ed.* **1987**, *26*, 75.

[9] G. Ciani, M. Moret, A. Fumagalli, S. Martinengo, *J. Organomet. Chem.* **1989**, *362*, 291.

[10] T. Gröer, M. Scheer, *Organometallics* **2000**, *19*, 3683.

[11] (a) K. H. Whitmire, M. R. Churchill, J. C. Fettinger, *J. Am. Chem Soc.* **1985**, *107*, 1056; (b) K. H. Whitmire, T. A. Albright, S.-K. Kang, M. R. Churchill, J. C. Fettinger, *Inorg. Chem.* **1986**, *25*, 2799.

[12] J. L. Stark, B. Harms, I. Guzman-Jimenez, K. H. Whitmire, R. Gautier, J.-F- Halet, J.-Y. Saillard, *J. Am. Chem Soc.* **1999**, *121*, 4409.

[13] P. Cucka, C. S. Barrett, *Acta Crystallogr.* **1962**, *15*, 865.

[14] J. Cassidy, K. H. Whitmire, *Inorg. Chem.* **1991**, *30*, 2788.

[15] (a) A. M. Arif, A. H. Cowley, N. C. Norman, M. Pakulski, *J. Am. Chem. Soc.* **1985**, *107*, 1062; (b) A. M. Arif, A. H. Cowley, N. C. Norman, M. Pakulski, *Inorg.Chem.* **1986**, *25*, 4836.

[16] H. Schmidbaur, R. Nowak, A. Schier, J. M. Wallis, B. Huber, G. Müller, *Chem. Ber.* **1987**, *120*, 1829.

[17] (a) A. Hirsch, Z. Chen, H. Jiao, *Angew. Chem.* **2001**, *113*, 2916; *Angew. Chem. Int. Ed.* **2001**, *40*, 2834; (b) Z. Chen, R. B. King, *Chem. Rev.* **2005**, *105*, 3613.

3.4 Appendix to chapter 3.2

3.4.1 Strain energies of *arachno*-Bi_4 and *nido*-Bi_4 cluster cores and their molecular orbital relationships

According to model homodesmotic reactions[1] (equations 1 and 2) involving cyclobismuthane $Bi_4(SiH_3)_4$ and tetrahedron Bi_4, strain energy [ΔE_{str} was calculated as E (Product) – E (Reagents)] of bismuth cluster cores (*arachno*-Bi_4 and *nido*-Bi_4, respectively) increases by ring closure of *arachno*-Bi_4 (Scheme A). Thus, calculated value of 0.7 kcal/mol for the reaction 1, depicted in Scheme A, indicates that this process is slightly endothermic ($\Delta E > 0$), whereas value of –30.7 kcal/mol for the reaction 2 provides the relief of strain that corresponds to exothermic process ($\Delta E < 0$). As a result, the strain energy ΔE_{str} of Bi_4 (30.7 kcal/mol) is larger than this one estimated for tetrahedral P_4 (19.7 kcal/mol) and much less than ΔE_{str} of C_4H_4 (141 kcal/mol), for comparison.[1] Such relatively low strain in E_4 pnicogen tetrahedrons is a result of presence of bent E–E "banana"-bonds in a valence bond description.[2]

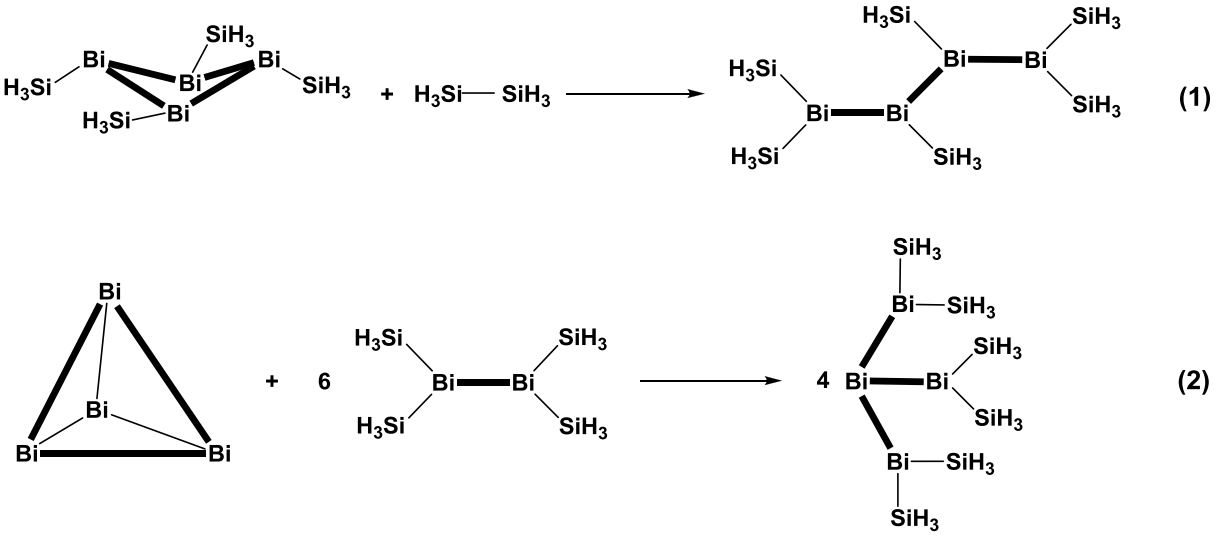

Scheme A. Homodesmotic reactions involving cyclobismuthane $Bi_4(SiH_3)_4$ and tetrahedral Bi_4. Energy and structure calculations were carried out at the MP4(SDQ)/BS-I//PBE0/def2-SV(P) level, here.

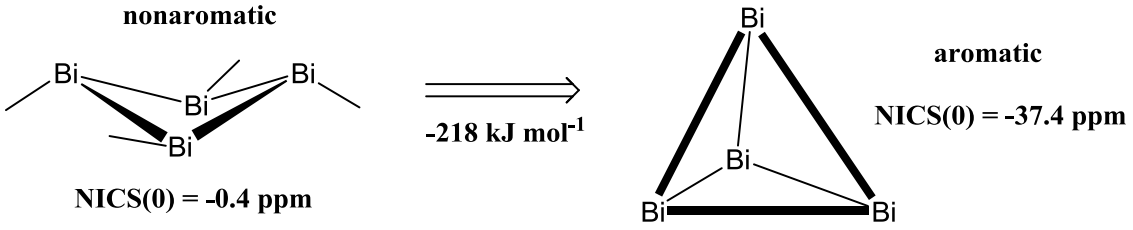

Scheme B. Electronic and energy relationships between *arachno*-Bi_4H_4 and *nido*-Bi_4 clusters. ΔE_{rel} is given between bare *arachno*-Bi_4 and *nido*-Bi_4 cores.

Deprotonation leads to the deformation of Bi_4 rings into Bi_4 tetrahedron and, as consequence, results in magnetic shielding into more negative NICS values, i.e. causes increase of aromaticity (Scheme B). The MO-picture shows delocalized cluster bonding orbitals (Figure A).

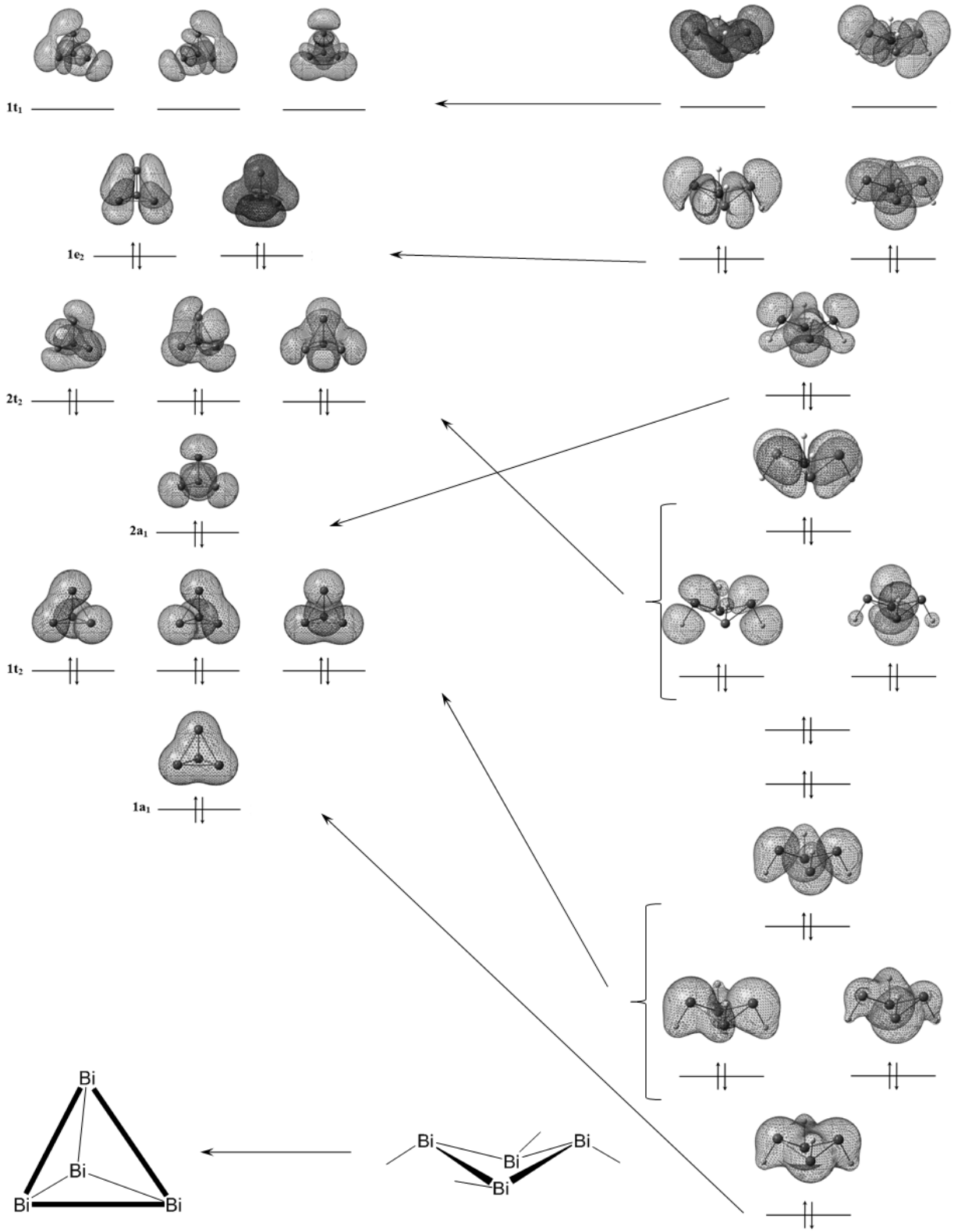

Figure A. Molecular orbital relationships between Bi_4 and Bi_4H_4 clusters in the $^1A_1$ ground state.

3.4.2 References

[1] (a) D. S. Warren, B. M. Gimarc, *J. Am. Chem. Soc.* **1992**, *114*, 5378; (b) S. Nagase, *Angew. Chem. Int. Ed.* **1989**, *28*, 329.

[2] I. Krossing in *Molecular Clusters of the Main Group Elements* (Eds.: M. Driess, H. Nöth), Wiley-VCH, Weinheim, **2004**, 209.

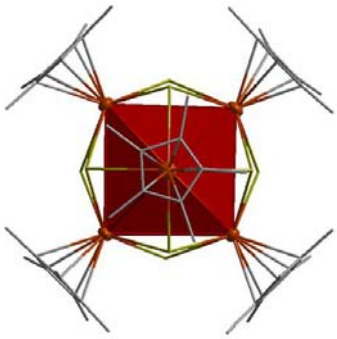

$[(C_5Me_5)_5Bi_5Br_9]^+$

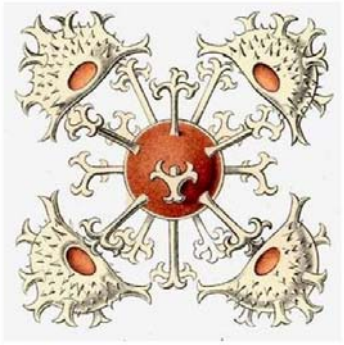

Staurastrum spinosum

Chapter 4. Bonding in Bismuth–Cyclopentadienyl Compounds

4.1 Introduction

4.1.1 Cyclopentadienyl ligands in organometallic chemistry of main group elements

The considerable importance of cyclopentadienyl (C_5R_5) ligands in organometallic chemistry of the group 13−15 p-elements is conditional, not at least, on their capability to be potentially leaving groups in the Metalorganic Chemical Vapor Deposition (MOCVD) process, where organometallic compounds may act as single source precursors to the production of thin films by CVD.[1] On the other hand, compounds containing cyclopentadienyl rings display a variety of metal oxidation states and consequently many variations in electronic structure and behavior. Thus, C_5R_5 group are also very well "electron-buffer" substituents. The flexibility in bonding enables the C_5R_5 group ideally to adjust to the electronic situation at the respective central atom. Main group elements interact with the C_5R_5 ligands in a variety of fashions which are specified structurally in terms of the position of the element with respect to the pentagonal cylinder defined by the C_5 perimeter (Figure A).[2]

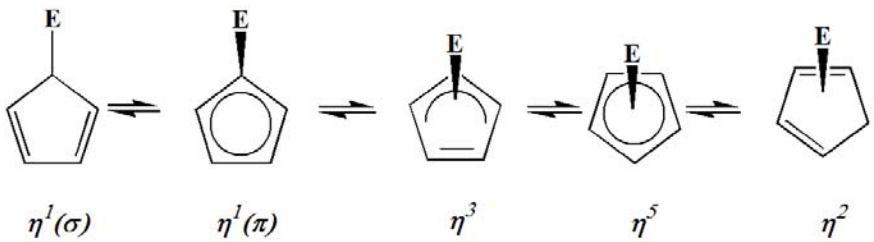

Figure A. Structural alternatives for C_5R_5−E compounds (E is 13–15 group element).

4.1.2 A view into cyclopentadienyl chemistry of bismuth

The bismuth compounds with cyclopentadienyl ligands, $(C_5H_4R)_3Bi$ (R = H, Me) and $(C_5H_5)_2BiCl$ (R = H, Me), have been discovered in 1960 by Fischer and Schreiner.[3] In 1970, Fischer et al. again investigated $(C_5H_4R)_3Bi$ (R = H) and suggested an exist of its two crystalline forms of different colors (red and black).[4] Nearly eighteen years after, Jutzi and Schwartzen were able to observe formation of the pentamethylcyclopentadienyl bismuth dibromide $(C_5Me_5)BiBr_2$ on oxidative addition reaction of bismuth with 5-bromopentamethyl-l,3-cyclopentadiene, Me_5C_5Br.[5] Shortly after that, the two complexes $(C_5H_5)Bi_2Cl_5$ and $(C_5H_5)BiCl_2$ have been reported by Frank.[6] Interesting, a red thermolabile and light sensible $(C_5H_5)BiCl_2$ compound (Figure B, left) became the first structural-characterized bismuth cyclopentadienyl complex by X-ray diffraction. The report, published in 1994 by Sitzmann (picture on the right) and Wolmershäuser in *Chemische Berichte* on bismuth compounds with crowded multiply alkylated cyclopentadienyl ligands, has advanced this chemistry once again (Figure B, center and right).[7] The syntheses and the crystal structures of wide range of orange-red and dark-red cyclopentadienyl-substituted bismuth compounds (C_5R_5 = η^3/η^5-C_5iPr_4H; η^5-$C_5H_2tBu_3$-1,2,4; η^5-$C_5H_2iPr_3$) have been discussed, there.

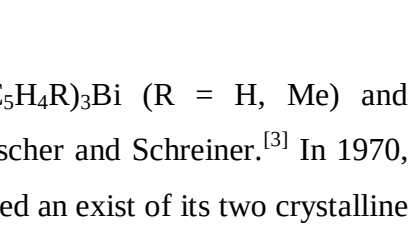

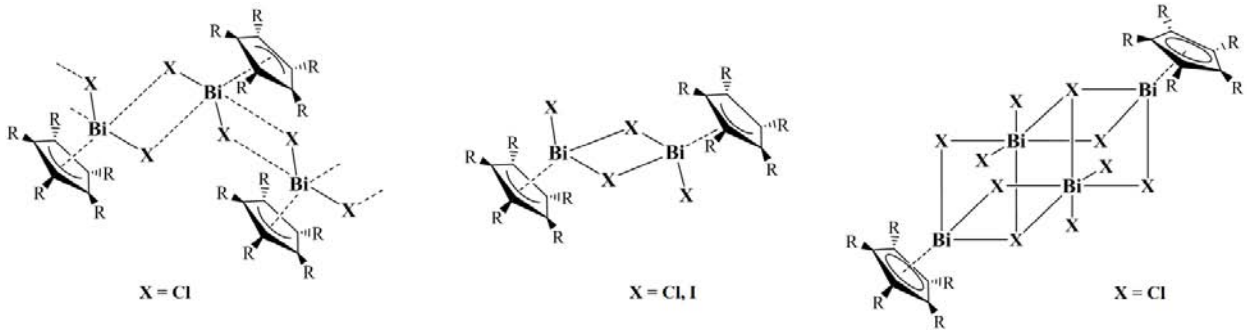

Figure B. Half-sandwich polymeric (left), dimeric (center), and tetrameric (right) bismuth cyclopentadienyl complexes bridged halo ligands, where C_5R_5 = η^2/η^3-C_5H_5, η^3-C_5iPr_4H and η^5-C_5iPr_4H, respectively.

The X-ray crystal structure data for the red crystalline modification of tris(cyclopentadienyl)bismuth $(C_5H_5)_3Bi$ and the different ways to this compound under applied conditions (warming from –70 °C to r.t. during reactions plus a light isolation!) have been reported by Lorberth et al. some time afterwards (in 1995).[8] In the end of the 1990s, Sitzmann et al. reported syntheses and crystal structures of

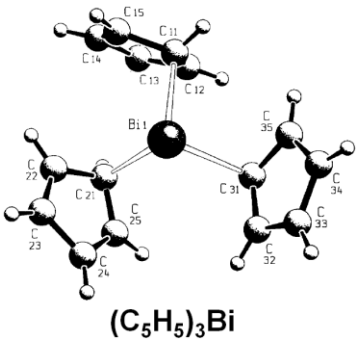

$(C_5H_5)_3Bi$

the first bismocenium ion $[(1,2,4\text{-}t\text{Bu}_3\text{C}_5\text{H}_2)_2\text{Bi}]^+$[9] and the first cationic organobismuth halides.

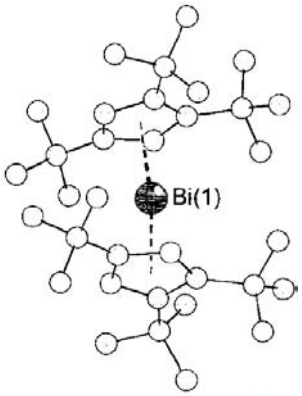

$[(1,2,4\text{-}t\text{Bu}_3\text{C}_5\text{H}_2)_2\text{Bi}]^+$

The latter are dimeric chloro(cyclopentadienyl) bismuthenium cations.[10] The bismocenium ion was observed by halide abstraction from a substituted bis(cyclopentadienyl)bismuth chloride $(1,2,4\text{-}t\text{Bu}_3\text{C}_5\text{H}_2)_2\text{BiCl}$. Furthermore, red crystals of a $(\text{C}_5\text{Me}_5)\text{Bi}$ compound with elevenfold coordinated bismuth atoms have been observed by Schnöckel et al. in 1999 on reaction of BiI_3 with $[(\text{C}_5\text{Me}_5)\text{Al}]_4$ in toluene at room temperature.[11] The solid-state molecular structure of that exhibits a chain-like arrangement of $(\text{C}_5\text{Me}_5)\text{Bi}$ units that are bridged by tetraiodoaluminate ions (Figure C). In addition, bismuth cyclopentadienyl complexes have displayed solution fluxionality where the C_5R_5−Bi bond hapticity changes have been observed.

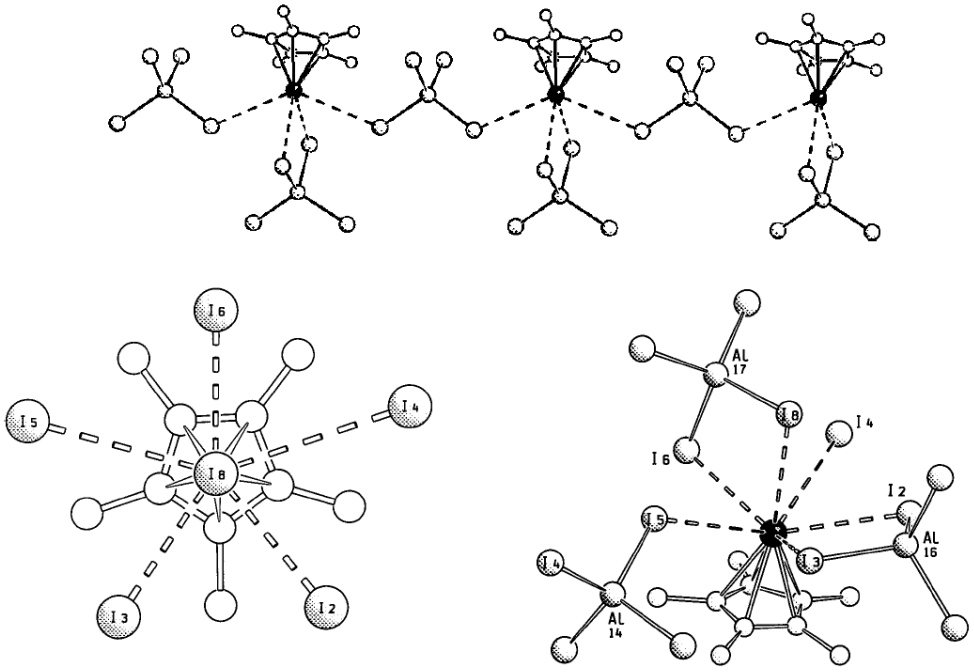

Figure C. Slice of polymeric association of $(\text{C}_5\text{Me}_5)\text{Bi}(\text{AlI}_4)$ units (top) through AlI_4 species in crystal of $[(\text{C}_5\text{H}_5)_2\text{Al}][(\text{C}_5\text{Me}_5)\text{Bi}](\mu\text{-}\text{AlI}_4)(\text{AlI}_4)_2\cdot 2\text{C}_7\text{H}_8$ and bismuth coordination sphere (bottom; top view - left and side view - right).

4.1.3 References

[1] (a) J. Dahlhaus, P. Jutzi, H. J. Fienck, N. Kulisch, *Adv. Mater.* **1993**, *5*, 377; (b) M. Scherer, T. Kruck, *Chem. Vap. Deposition* **1999**, *3*, 33; (c) S. Bensiek, M. Bangel, P. Jutzi, *Organometallics* **2000**, *19*, 1292; (d) A. Klipp, F. Hamelmann, G. Haindl, J. Hartwich, U. Kleineberg, P. Jutzi, U. Heinzmann, *Chem. Vap. Deposition* **2000**, *6*, 63; (e) K. Dittmar, P. Jutzi, J. Schmalhorst, G. Reiss, *Chem. Vap. Deposition* **2001**, *7*, 193; (f) P. Jutzi, *Pure Appl. Chem.* **2003**, *75*, 483.

[2] (a) R. A. Bartlett, A. Cowley, P. Jutzi, M. M. Olmstead, H.-G. Stammler, *Organometallics* **1992**, *11*, 2837; (b) P. Jutzi, N. Burford, *Chem. Rev.* **1999**, *99*, 969; (c) P. Jutzi, G. Reumann, *J. Chem. Soc., Dalton Trans.* **2000**, 2237.

[3] E. O. Fischer, S. Schreiner, *Chem. Ber.* **1960**, *93*, 1417.

[4] B. Deubzer, M. Elian, E. O. Fischer, H. P. Fritz, *Chem. Ber.* **1970**, *103*, 799.

[5] P. Jutzi, K.-H. Schwartzen, *Chem. Ber.* **1989**, *122*, 287.

[6] W. Frank, *J. Organomet. Chem.* **1990**, *386*, 177.

[7] H. Sitzmann, G. Wolmershäuser, *Chem. Ber.* **1994**, *127*, 1335.

[8] J. Lorberth, W. Massa, S. Wocadlo, I. Sarraje, S.-H. Shin, X.-W. Li, *J. Organomet. Chem.* **1995**, *485*, 149.

[9] H. Sitzmann, G. Wolmershäuser, *Z. Naturforsch.* **1997**, *52b*, 398.

[10] H. Sitzmann, G. Wolmershäuser, R. Boese, D. Bläser, *Z. Anorg. Allg. Chem.* **1999**, *625*, 2103.

[11] C. Üffing, A. Ecker, E. Baum, H. Schnöckel, *Z. Anorg. Allg. Chem.* **1999**, *625*, 1354.

4.2 Theoretical study of low-valent bismuth cyclopentadienyl and pentamethylcyclopentadienyl half-sandwich compounds

4.2.1 Introduction

Each discovery of novel cyclopentadienyl bismuth complexes has caused new interesting questions such as why is there a trend to formation of the coordination polymers or why is there a spontaneous phase changing in some cases? Non-integrity of collected experimental data for this class of compounds did not allow finding a clear explanation to above entire questions. Unfortunately, the fifty years after the first report on the bismuth compounds with cyclopentadienyl ligands did not get clear-cut information on the nature of the C_5R_5–Bi bonding, its behavior and the intramolecular interactions in such complexes. Gas phase studies of structure and other molecular properties of cyclopentadienyl-substituted bismuth compounds should be very useful in solving of above-listed problems and give an insight into these topics. Nevertheless, electron diffraction, photoelectron spectra as well as quantum chemical calculations for cyclopentadienyl bismuth complexes have not been available up to now. By contrast, isoelectronic fragments of the groups 13−14 elements of type $(C_5R_5)_aE^{q+}X_b$ (E = Al, Ga, In, Tl, Si, Ge, Sn, Pb; a = 1−2; b = 0, 2, 3; q = 0−1) have been studied more extensively.[1]

For these reasons, this part of thesis is dedicated to a creation of the starting picture for general understanding of the fascinating fluxionality of C_5R_5–bismuth interactions on the basis of their quantum chemical study. Thus, gas phase model structures of the monomeric trivalent bismuth cyclopentadienyl complexes of two types, $(C_5R_5)Bi^{2+}$ (where R = H, Me) and $(C_5R_5)BiX_2$ (where R = H, Me; X = Cl, Br, I) along with an experimentally unknown family of the monovalent bismuth cyclopentadienyl complexes $[(C_5R_5)Bi]_n$ (where R = H, Me; n = 1−4) are investigated with several goals. One is to predict their further synthetic strategies (donor−acceptor properties, etc.), another to give useful information to the understanding of structures and the qualitative and quantitative description of bonding modes and electronic ligand effects. The H and Me substituents at the C_5R_5 ring were chosen because the metal complexes with the strong π-electron donating cyclopentadienyl ligand (R = H) and the more bulky but even stronger donor pentamethylcyclopentadienyl (R = Me) ligand show different properties and behavior (thermal stability, intermolecular interactions, solubility, tendency to form polymeric structures, etc.). In conclusion, an effective adjustment of electronic and bonding situations will open a way to a manipulation of the bismuth-cyclopentadienyl bonds.

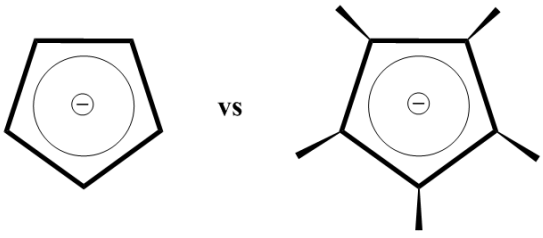

C_5H_5 C_5Me_5

4.2.2 Compounds of the types $(C_5R_5)Bi^{2+}$ and $[(C_5R_5)Bi]_n$ (R = H, Me; n = 1−4)

DFT structure optimizations of molecules of type $[(C_5R_5)Bi]^{q+}$ (R = H, Me; q = 2, 0) are performed. The cationic $(C_5R_5)Bi^{2+}$ complexes display a half-sandwich "open-faced" structure where the pentagonal ligand C_5R_5 is η^5-coordinated to the bismuth center (Figure 2). The carbon−carbon bond lengths in the C_5R_5 ring are 143.4 pm for R = H and 145.1 pm for R = Me. The metal-to-ring centroid distance (Bi−Z) for $(C_5H_5)Bi^{2+}$ is slightly longer than that for the $(C_5Me_5)Bi^{2+}$ complex.

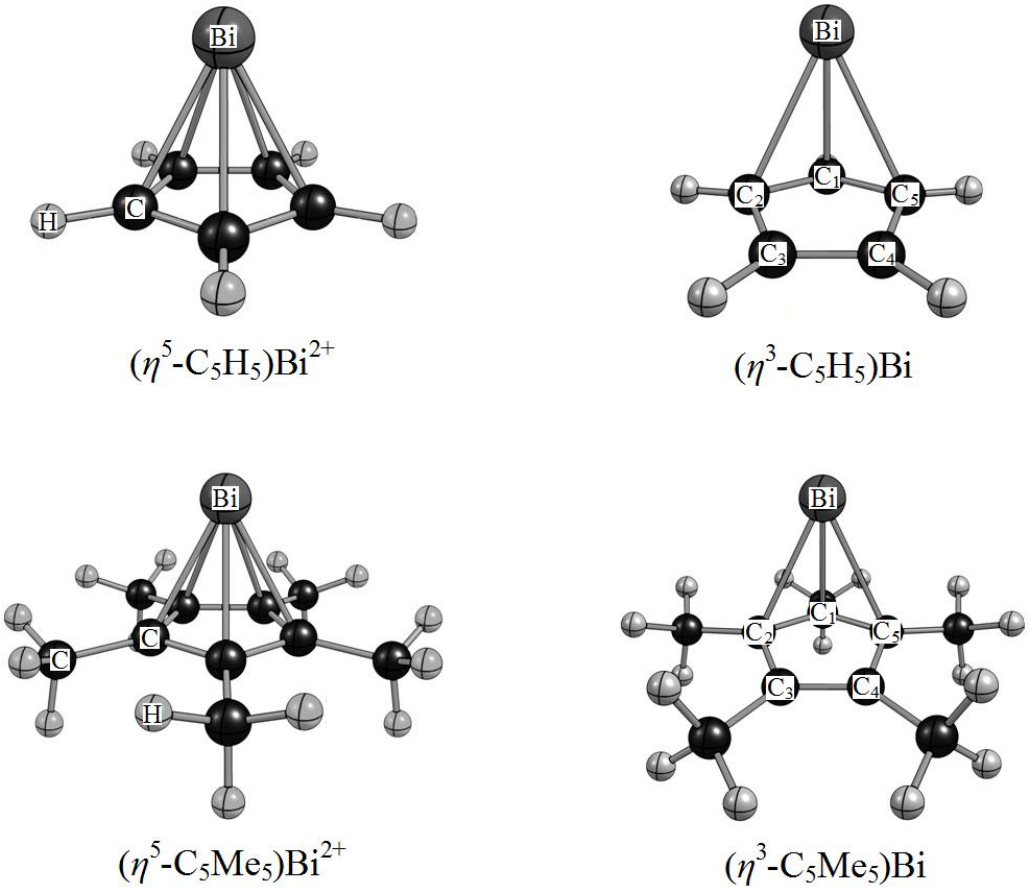

$(\eta^5\text{-}C_5H_5)Bi^{2+}$ $(\eta^3\text{-}C_5H_5)Bi$

$(\eta^5\text{-}C_5Me_5)Bi^{2+}$ $(\eta^3\text{-}C_5Me_5)Bi$

Figure 2. PBE0/BS-I optimized geometries of $[(C_5R_5)Bi]^{q+}$ (R = H, Me; q = 2, 0) molecules where the bismuth atom is bonded to the C_5R_5 ring in a η^5- and η^3-fashion, respectively. Selected computed bond lengths [pm] and angles [deg] of **$(C_5H_5)Bi^{2+}$**: Bi−Z 212.3. **$(C_5Me_5)Bi^{2+}$**: Bi−Z 211.7. **$(C_5H_5)Bi$**: Bi−Z 254.8, Bi−C_1 232.7, Bi−C_2 259.7, Bi−C_5 260.4, Bi−C_3 322.4, Bi−C_4 322.7, C_1−C_2 143.4, C_2−C_3 143.6, C_1−C_5 143.4, C_4−C_5 143.5, C_3−C_4 136.6, Bi−C_2−C_3 102.3, Bi−C_5−C_4 102.2, Bi−C_1−Z 85.6. **$(C_5Me_5)Bi$**: Bi−Z 250.5, Bi−C_1 233.3, Bi−C_2 256.8, Bi−C_5 256.7, Bi−C_3 317.3, Bi−C_4 317.3, C_1−C_2 144.2, C_2−C_3 145.5, C_1−C_5 144.2, C_4−C_5 145.5, C_3−C_4 136.6, Bi−C_2−C_3 100.5, Bi−C_5−C_4 100.5, Bi−C_1−Z 82.9.

Compared to isoelectronic groups 13 and 14 cyclopentadienyl compounds of the types $(C_5R_5)E$

and $(C_5R_5)E^+$, respectively, this distance is slightly longer than in the germanium, aluminum, gallium, and tin compounds (Ge^+: 189.7 pm for R = Me; Al: 203.7 pm for R = H, 206.3 pm for R = Me; Ga: 209.6 pm for R = H, 208.1 pm for R = Me; Sn^+: 211.4 pm for R = Me) but shorter than in the indium, thallium, and lead derivatives (In: 232.2 pm for R = H, 228.8 pm for R = Me; Tl: 241.0 pm for R = H, 237.2 pm for R = Me; Pb^+: 244.4 pm for R = Me).[1a, 1d-1i, 1k, 1n] This indicates that the distances metal−centroid (El−Z) are sensitive to the nature of metal, its environment and type of ligand, thereby the El−Z distance clearly elongates down on the group and shortens left to right on the period, as is expected.

The structure optimizations of $(C_5R_5)Bi$ molecules with bismuth in oxidation state +I reveal distorted half-sandwich structures (bent-conformation) where the C_5R_5 rings exhibit η^3-coordination and monoene distortion C_3−C_4 (Figure 2). The shortest Bi−C distances are d_{Bi-C1} = 232.7 pm for R = H and 233.3 pm for R = Me, respectively. The C_1 carbon atom is slightly displaced from the ring plane toward the bismuth atom. The bond length in the monoene fragment d_{C3-C4} of the C_5R_5 ring is similar for R = H and R = Me (136.6 pm). Other carbon−carbon distances (C_1−C_2, C_1−C_5, C_2−C_3, C_4−C_5) in the C_5R_5 ring are in the region of ~144 pm for R = H and ~145 pm for R = Me. The angle between the Bi−C_1 bond and the center of the C_5R_5 ring (Bi−C_1−Z) is 85.6° for R = H and 82.9° for R = Me. This means, the bismuth atom in the $(C_5H_5)Bi$ complex is shifted from the central axes of the C_5R_5 ring and loses strength of π-bonding to the cyclopentadienyl ring.

The natural population analysis (NPA) shows that the bismuth atom does not have an idealized electronic configuration $6s^26p^0$ (in the ^1S ground state) in $(C_5R_5)Bi^{2+}$ and $6s^26p^2$ (in the ^3P ground state) in $(C_5H_5)Bi$ complexes, but a partial occupied s^ap^b-hybrid (a, $b > 1$ and $a > 1$, $b > 2$, respectively) with increased electron density in the 6p orbitals. In accordance with the natural electronic configuration (NEC) (Table 1) the 6s electrons of both complexes $(C_5R_5)Bi^{2+}$ and $(C_5R_5)Bi$ are almost completely localized; therefore it may be expected that the 6p orbital will give the major contribution to covalent bonding.

The positive partial charge is located on the bismuth atom; it is less than the chemical valence of Bi in the ionic model (+3 and +1, respectively). In the $(C_5R_5)Bi$ complexes, most negative charges in the C_5R_5 ring are located on the carbon atom C_1 [−0.46 (R = H), −0.21 (R = Me)]. The charges on the C_2 and C_5 carbons are −0.38 for R = H, and −0.15 for R = Me. The carbon atoms C_3 and C_4 in the monoene fragment have −0.26 for R = H and −0.04 for R = Me.

The NPA reveals a predominantly ionic character of the Bi−C bonds in $(\eta^5\text{-}C_5R_5)Bi^{2+}$ complexes for R = H (57.6 %, ionic participation) and R = Me (52.9 %), and a predominantly covalent character of the Bi−C bonds in $(\eta^3\text{-}C_5R_5)Bi$ complexes for R = H (41.4 %) and R = Me

(36.5 %). The charge on the metal atoms in the bismuth pentamethylcyclopentadienyl complexes is less than in the bismuth cyclopentadienyl complexes. This is in line with better donor properties of the C_5Me_5 ligand compared to those of the C_5H_5 ligand. The localized NBO Lewis-description (ρ_L) illustrates the high accuracy of the calculation models.

Table 1. Important calculated values for the complexes obtained from the NBO analysis at the MP2(full)/BS-II//PBE0/BS-I level.

Parameter	$(C_5R_5)Bi^{2+}$		$(C_5R_5)Bi$	
	R = H	R = Me	R = H	R = Me
*n*VE[a]	8	8	10	10
NEC[b] of Bi	$6s^{1.93}6p^{1.34}$	$6s^{1.91}6p^{1.50}$	$6s^{1.93}6p^{2.65}$	$6s^{1.92}6p^{2.71}$
Q_{NPA}[c] on Bi	+1.728	+1.587	+0.414	+0.365
$i_{C5R5-Bi}$[d]	57.6	52.9	41.4	36.5
LP_1 NHO[e] at Bi	$s^{95.92\%}p^{4.07\%}$	$s^{94.95\%}p^{5.05\%}$	$s^{95.50\%}p^{4.50\%}$	$s^{94.73\%}p^{5.26\%}$
occupancy[f]	1.998	1.997	1.999	1.997
LP_2 NHO at Bi			$s^{0.24\%}p^{99.74\%}$	$s^{0.58\%}p^{99.40\%}$
occupancy			1.893	1.865
ρ_L[g]	97.1	97.6	98.5	98.7

[a] Number of valence electrons. [b] Natural electron configuration. [c] Natural charge. [d] Degree of ionicity of C_5R_5–Bi bonding [%]. [e] Lone pair natural hybrid orbital. [f] Occupancy of lone pair orbital [*e*]. [g] Accuracy of calculation model [%].

On the basis of NBO analysis, the space-filling lone pair localized on bismuth in the $(C_5R_5)Bi^{2+}$ complexes mainly has s-like-character. In $(C_5R_5)Bi$ one of the lone pairs (LP) is of s-type, while the second one has predominantly p-character. The orbital occupancy of the LP with the s-main contribution is higher than the occupancy of the LP with a more p-like character. The larger contributions of the s- and p-orbital parts in the lone pairs of $(C_5R_5)Bi^{2+}$ and $(C_5R_5)Bi$ complexes indicate that such compounds have a relatively low Lewis basicity. Besides, the acceptor ability of the $(C_5R_5)Bi$ complexes is expressed to a lesser degree compared to $(C_5R_5)Bi^{2+}$, but the donor ability is stronger. Consequently, the $(C_5R_5)Bi$ complexes might act as ditopic ligands. In NBO evaluations, described above, hybrid orbitals are used, which are not eigenfunctions. In an alternative concept, canonical molecular orbitals are taken in account to

get an insight into ligand metal interaction for $[(C_5R_5)Bi]^{q+}$ (R = H, Me; q = 2, 0). Thus, for the MO construction (Table 2, Figure 3) between the C_5R_5 π-system and the {s, p} bismuth set in the $(\eta^5\text{-}C_5R_5)Bi^{2+}$ complexes an approximation in the Lewis structures was used. The $\pi_{sym}(a_2'')$ orbital of C_5R_5 ring interacts with the bismuth s and p_z atomic orbitals (AOs) forming three centrosymmetric MOs: $1a_1$, $2a_1$, and $3a_1$ (high-lying anti-bonding MO). The bonding $1a_1$ orbital is formed as an approximation $\langle s,p_z|a''_2\rangle$: $1a_1 = (\langle s|a_1''\rangle, \langle p_z|a''_1\rangle) = \langle s,p_z|a''_1\rangle_{bonding}$. The non-bonding $2a_1$ MO is classical metal sp_z ($2a_1 = \langle s,p_z\rangle_{non\text{-}bonding}$).

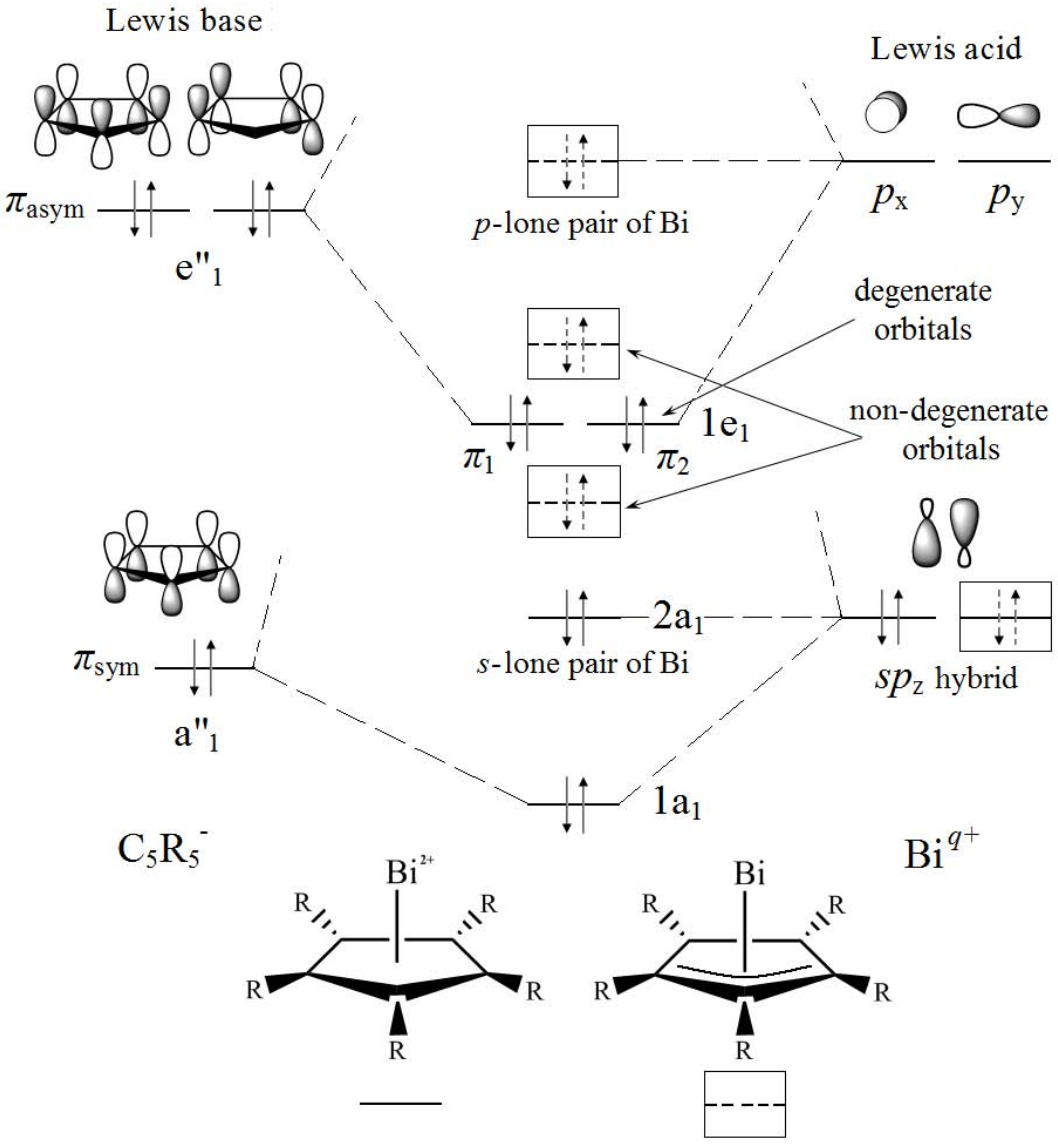

Figure 3. Slice from the qualitative correlation MO-diagram of the filled valence orbital interactions of C_5R_5–Bi in the $(\eta^5\text{-}C_5R_5)Bi^{2+}$ and $(\eta^3\text{-}C_5R_5)Bi$ complexes upon bending. The MO scheme shows the interaction of a''_1 of C_5R_5 with the s and p_z bismuth AOs and the interaction of e''_1 of C_5R_5 with the p_x and p_y bismuth AOs. For $(\eta^3\text{-}C_5R_5)Bi$ the degeneration of the HOMO $1e_1$ orbital is repealed, resulting in a new non-degenerate HOMO.

The two filled $\pi_{asym}(e_1'')$ orbitals of C_5R_5 ring interact with the p_x and p_y bismuth AOs forming two bonding $1e_1$ and two anti-bonding $2e_1$ molecular orbitals. The two bonding $1e_1$ orbitals are formed by the non-axial $\langle p_x,p_y|e_1''\rangle$ interaction $1e_1 = (\langle p_x|e_1''\rangle, \langle p_y|e_1''\rangle) = \langle p_x,p_y|e_1''\rangle_{bonding}$. Thus, the $(C_5R_5)Bi^{2+}$ compounds have 8 valence electrons; all 5 C_5R_5 electrons are involved in bonding to the bismuth center. A similar MO scheme was observed for cyclopentadienyl complexes of the group 13 elements in their oxidation state +I.[1d, 1h, 1m]

The results of the MO approximation indicate that the highest occupied molecular orbital (HOMO) and the lowest unoccupied molecular orbital (LUMO) of the $(\eta^5\text{-}C_5R_5)Bi^{2+}$ complexes are doubly degenerate (e_1 and e_2 symmetries, respectively). The HOMO contains the main contribution of the $\pi(C_5R_5)$-π(Bi) interaction. The HOMO-3 (a_1 symmetry) corresponds to the sp_z-hybridized bismuths lone pair with the major contribution from the bismuth 6s-orbital. In the bismuth(I) cyclopentadienyl complexes the electronic situation changes from 8 to 10 VEs [isoelectronic to groups 13 and 14 cyclopentadienyl compounds of the types $(C_5R_5)EX_2$ and $(C_5R_5)EX$, respectively] and the degeneracy of the HOMO disappears (non-degenerate π-orbitals) and these orbitals become HOMO-1 and HOMO-2, accordingly. The new HOMO is metal centered (LP of p_y type) and has a major contribution from the bismuth 6p-orbital. The sp_z-lone pair of Bi in the $(\eta^3\text{-}C_5R_5)Bi$ complexes lies, similar to that in the $(\eta^5\text{-}C_5R_5)Bi^{2+}$ complexes, under the π_1 and π_2 orbitals. These changes are in line with the haptotropic shifts and a change of coordination of the C_5R_5 ring from η^5 to η^3 (Figure 3). As can be seen, the interpretation via canonical MO theory is in line with the results obtained by the NBO approach with hybridized molecular orbitals for the $[(C_5R_5)Bi]^{q+}$ complexes.

Table 2. Selected computed orbital energies and dipole moments at the MP4(SDQ)/BS-II//PBE0/BS-I level.

Parameter	$(C_5R_5)Bi^{2+}$		$(C_5R_5)Bi$	
	R = H	R = Me	R = H	R = Me
LUMO	−9.46 ($2e_1$)	−8.04 ($2e_1$)	0.19	0.51
HOMO	−20.60 ($1e_1$)	−18.15 ($1e_1$)	−6.06 (p-LP)	−5.67 (p-LP)
HOMO-1	−23.46 ($2a_1$)	−20.60 ($2a_1$)	−8.80 (π_1)	−7.94 (π_1)
HOMO-2			−9.16 (π_2)	−8.36 (π_2)
HOMO-3			−13.12 (s-LP)	−11.77 (s-LP)
$\Delta E_{HOMO-LUMO}$	11.14	10.11	6.25	6.18
μ	4.63	4.92	0.23	1.46

The heterolytic association energies ($\Delta E_{h.a.}$) of the $[(C_5Me_5)Bi]^{q+}$ compounds are slightly more exothermic than $\Delta E_{h.a}$ of $[(C_5H_5)Bi]^{q+}$ (Scheme 1).

$$C_5H_5^- + Bi^{3+} \longrightarrow (C_5H_5)Bi^{2+} \qquad \Delta E_{h.a.} = -2900 \text{ kJ/mol}$$

$$C_5Me_5^- + Bi^{3+} \longrightarrow (C_5Me_5)Bi^{2+} \qquad \Delta E_{h.a.} = -3113 \text{ kJ/mol}$$

$$C_5H_5^- + Bi^{+} \longrightarrow (C_5H_5)Bi \qquad \Delta E_{h.a.} = -837 \text{ kJ/mol}$$

$$C_5Me_5^- + Bi^{+} \longrightarrow (C_5Me_5)Bi \qquad \Delta E_{h.a.} = -881 \text{ kJ/mol}$$

Scheme 1. Heterolytic association energies of the $[(C_5R_5)Bi]^{q+}$ compounds calculated at the MP4(SDQ)/BS-II//PBE0/BS-I level (zero-point energies are given in the appendix to chapter 4.2).

Time-dependent (TD) DFT computations of vertical electronic transitions in the $(C_5R_5)Bi$ complexes show three main excited electronic states S_1, S_2, and S_3 (see the appendix to chapter 4.2). Thus, for the $(C_5R_5)Bi$ bismuth complexes the lowest energy $S_0 \rightarrow S_1$ transition can be described as a HOMO → LUMO excitation (2566 nm for R = H; 1929 nm for R = Me) from the lone pair of p-type localized on bismuth toward its lowest unoccupied p-MO ($n_{Bi(p)} \rightarrow n_{Bi(p)}^*$). This transfer of electrons is the most intense energy transition. The $S_0 \rightarrow S_2$ transition is a HOMO → LUMO+1 excitation with $n_{Bi(p)} \rightarrow n_{Bi(p)}^*$ character, whereas the $S_0 \rightarrow S_3$ transition is mainly a $\pi \rightarrow n_{Bi(p)}^*$ excitation (from a predominantly ligand π-orbital toward the LUMO of metal). The very low energy values (< 1 eV) of the HOMO → LUMO excitation for both derivates of the $(C_5R_5)Bi$ complexes and low values of ΔE ($E_{HOMO} - E_{LUMO}$), which are about 1.5 times lower than these of the $(C_5R_5)BiX_2$ complexes (will be discussed later) indicate that the cyclopentadienyl compounds of monovalent bismuth are much less kinetically stable than these of trivalent bismuth. Finally, the low values of the first ionization potential ($-IP_1 = -E_{HOMO}$) indicate that $(C_5R_5)Bi$ can be easily oxidized. This also explains why the monovalent Bi cyclopentadienyl compounds can hardly exist in their monomer state. The kinetically much more stable group 13 cyclopentadienyl compounds $(C_5R_5)E$, which have the larger HOMO−LUMO gap and higher energy values for the HOMO → LUMO excitation, are only monomers in gas phase and solution.[1d, 1f-1i]

Can the cyclopentadienyl complexes of bismuth be stabilized in its low-oxidation state +I in spite of this? Obviously, such stabilization might come from the formation of homonuclear systems (clusters) of *n*-bonded Bi−Bi atoms or heteronuclear systems in the form of bismuth−metal adducts, when the p-lone pair of bismuth will be localized at one of these bonds.

Therefore, simple "*n*-merized" models of the bismuth cyclopentadienyl complexes of type $[(C_5H_5)Bi]_n$ (n = 2−4) in their *cis*- and *trans*-configurations were studied (Figure 4). DFT structural simulations of molecules show that all of these have bent core geometry with pure $\eta^1(\sigma)$-coordination modes of the C_5H_5 ring. The results from MP2 calculations suggest that *trans*-optimized structures are more stable than *cis* isomers. Therefore, in the following only *trans*-geometries of the $[(C_5H_5)Bi]_n$ complexes are considered.

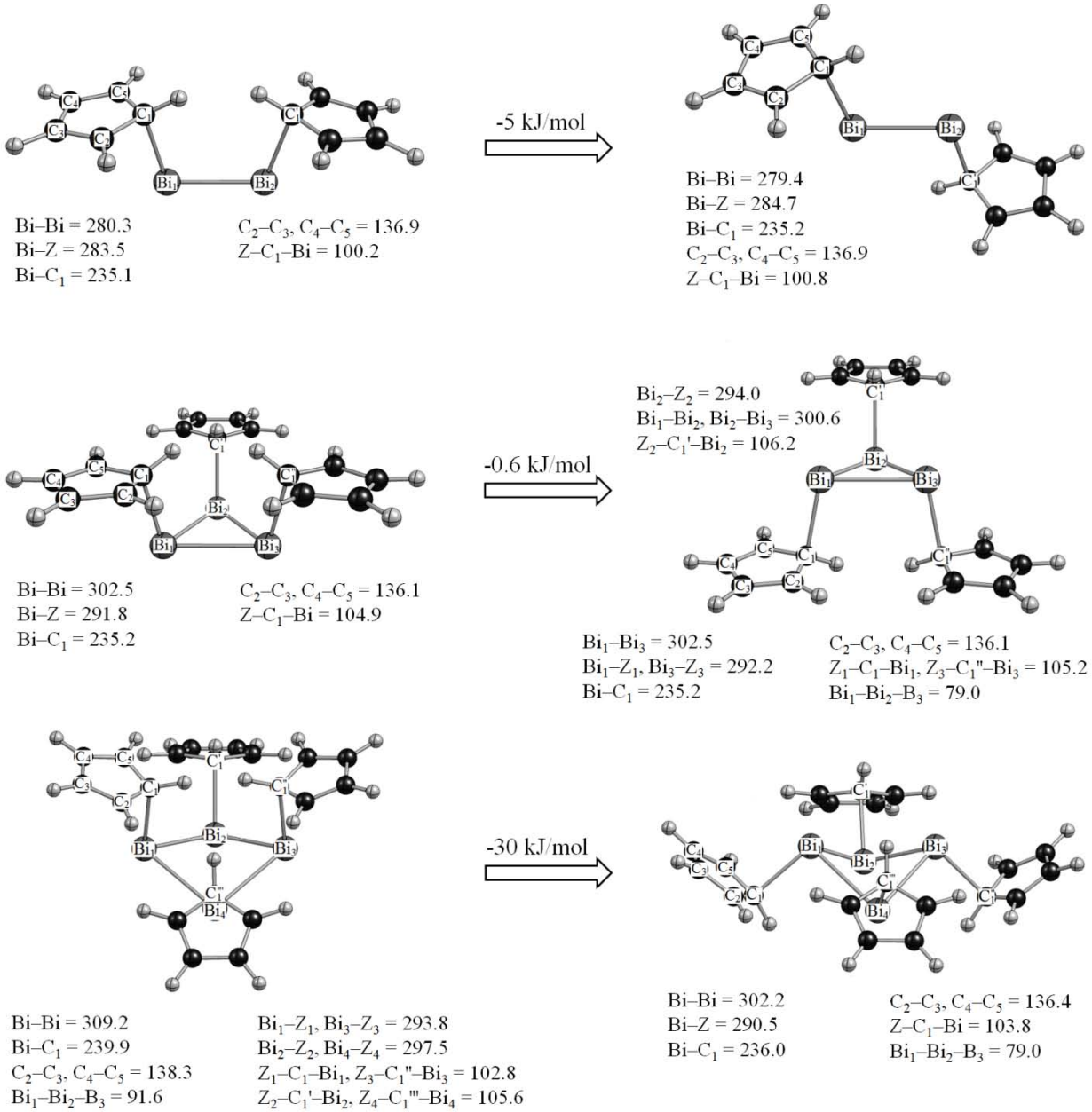

Figure 4. *cis*-bent core (left) and *trans*-bent core (right) optimized structures of the $[(C_5H_5)Bi]_n$ (n = 2−4) complexes and total energy differences between them calculated at the MP2(full)/BS-II//PBE-0/BS-I level. Selected important bond lengths and angles are given in [pm] and [deg], respectively.

Thus, the Bi−Bi distance in the dimeric molecule $[(C_5H_5)Bi]_2$ is of double bond character (279.4 pm). The molecule shows a *trans*-geometry (*anti*-periplanaric) of the C_{ipso}−Bi_1−Bi_2−C_{ipso} core (torsion angle −179.9°) or LP_1−Bi_1−Bi_2−LP_2, where the lone pairs (LP_1 and LP_2) localized on the bismuth atoms are of a predominantly s-type (~ 86 %). This distance corresponds to the Wiberg bond index (WBI) of 1.83, which describes the bond order and can be used as indicator of bond strength. Besides, the value of the Bi=Bi double bond distance indicates that a cyclopentadienyl dibismuthene has more electronic repulsion of the metal centers than the aryl dibismuthene {*trans*-$[(C_6H_5)Bi]_2$: d_{Bi-Bi} = 277.1 pm}.[2] The C−Bi−Bi bond angle of 95.8° deviates from the ideal sp^2 hybridized bond angle (120°), which is connected with the "inert s-pair effect". This "non-hybridization effect" was also observed in aryl dibismuthenes obtained.[3] The Bi−Bi distances in the tribismuthane $[(C_5H_5)Bi]_3$ with a *trans*-bent, nonplanar conformation (C_{ipso}−Bi−Bi−C_{ipso} torsion angle of −167.6°) and in the folded four-membered bismuth ring $[(C_5H_5)Bi]_4$ with a *trans*-geometry (C_{ipso}−Bi−Bi−C_{ipso} torsion angle of ± 118.6°) are of single bond character (d_{Bi-Bi}: over 300 pm; WBI values are approximately 0.95). Examples of a zirconocene-complexed dibismuthene trimeric[4] and tetrameric bismuthanes with alkyl or silyl substituents[5] have been reported with similar bonding parameters.

Thus, the s-character of the lone pairs at bismuth in $[(C_5H_5)Bi]_n$ decreases with "*n*-merization" of the Bi atoms (~ 96 % for n = 1, ~ 86 % for n = 2, ~ 85 % for n = 3, ~ 83 % for n = 4). This leads to an increase of the Lewis basicity. The ionic character of the Bi−C bonds, which are polarized toward carbons (~ 71 %), decreases from n = 2 (45.6 %) via n = 3 (44.0 %) to n = 4 (43.7 %). Besides, "*n*-merization" leads to an increase of the kinetic stability ($\Delta E_{HOMO-LUMO}$: 6.24 for n = 1, 6.35 for n = 2, 7.79 for n = 3, 7.78 for n = 4) and the first ionization potential. Consequently, the result is a decrease of the ability for oxidation (−6.06 for n = 1, −6.54 for n = 2, −7.19 for n = 3, −7.45 for n = 4). Thus, the $S_0 \rightarrow S_1$ transition for $[(C_5H_5)Bi]_n$, describing a HOMO → LUMO excitation with $n_{Bi(p)} \rightarrow n_{Bi(p)}$* character, has now relatively high energies (> 2 eV: 512 nm for n = 2, 471 nm for n = 3, 476 nm for n = 4). The increase in the "*n*-merization" energies and the energy expenses *per* monomer unit $(C_5H_5)Bi$ result from the increased stabilization of corresponding molecules (Scheme 2, Figure 5).

$$2\ (C_5H_5)Bi \longrightarrow [(C_5H_5)Bi]_2 \qquad \Delta E_{di} = -296\ (cis)\ \text{vs.}\ -301\ (trans)\ [kJ/mol]$$

$$3\ (C_5H_5)Bi \longrightarrow [(C_5H_5)Bi]_3 \qquad \Delta E_{tri} = -558\ (cis)\ \text{vs.}\ -559\ (trans)\ [kJ/mol]$$

$$4\ (C_5H_5)Bi \longrightarrow [(C_5H_5)Bi]_4 \qquad \Delta E_{tetra} = -761\ (cis)\ \text{vs.}\ -791\ (trans)\ [kJ/mol]$$

Scheme 2. Di-, tri-, and tetramerization energies of monovalent bismuth cyclopentadienyl complexes $[(C_5H_5)Bi]_n$ (n = 2−4) calculated at the MP2(full)/BS-II//PBE-0/BS-I level.

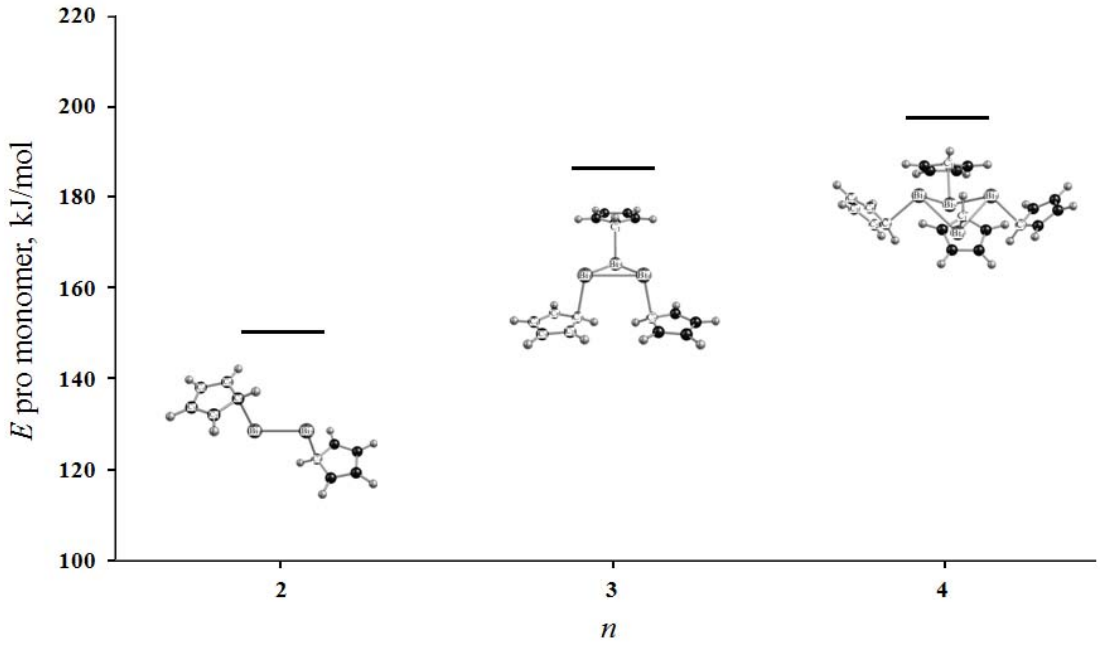

Figure 5. Energy expenses of the *trans*-$[(C_5H_5)Bi]_n$ (n = 2−4) complexes *per* monomer unit calculated at the MP2(full)/BS-II//PBE-0/BS-I level.

To understand the preferred coordination modes of the C_5R_5 ring to Bi in trivalent bismuth cyclopentadienyl complexes, haptotropic rearrangement processes were studied using the example of the cationic $(C_5R_5)Bi^{2+}$ complexes and the relative energies of the haptotropic shifts were calculated for variable bonding modes (η^3, η^2, η^1) of the C_5R_5 ring to the metal center with regard to the η^5-coordinated $(C_5R_5)Bi^{2+}$ (R = H, Me) molecules (Figure 6).

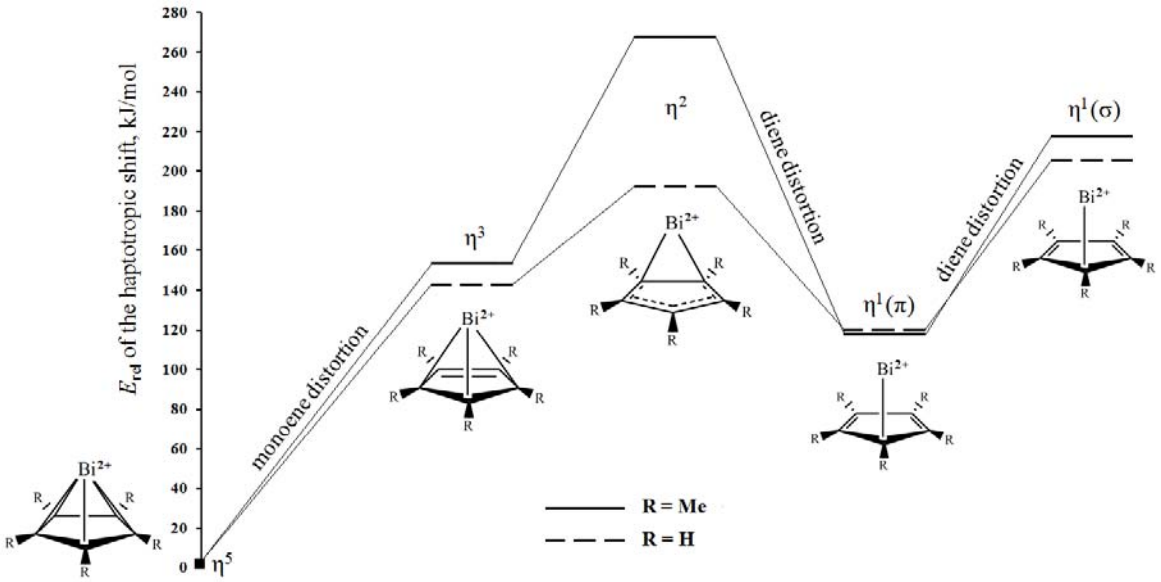

Figure 6. Relative energies of the C_5R_5−Bi bond hapticity changes ($\eta^3 \rightarrow \eta^2 \rightarrow \eta^1$) in the model compounds $(C_5R_5)Bi^{2+}$ (R = H, Me) relatively to η^5-bonded ring C_5R_5 (R = H, Me) to the bismuth center [MP4(SDQ)/BS-II//PBE0/BS-I].

The reaction path clearly shows that $\eta^1(\pi)$-bonded C_5R_5 rings (when Bi resides inside the cylinder) possess the lowest energy barriers (120 kJ/mol for R = H, 118 kJ/mol for R = Me). Such bonding is energetically more favorable than the $\eta^1(\sigma)$- (when Bi resides outside the cylinder; 205 kJ/mol for R = H, 218 kJ/mol for R = Me), η^2- (192 kJ/mol for R = H, 268 kJ/mol for R = Me) or η^3-coordinated modes (142 kJ/mol for R = H, 153 kJ/mol for R = Me). Thus, the MP4(SDQ) calculations suggest that the structures of $(C_5R_5)Bi^{2+}$ are more stabilized in the series $(\eta^5\text{-}C_5R_5)Bi^{2+} > [\eta^1(\pi)\text{-}C_5R_5]Bi^{2+} > (\eta^3\text{-}C_5R_5)Bi^{2+} > [\eta^2/\eta^1(\sigma)\text{-}C_5R_5]Bi^{2+}$.

4.2.3. Cyclopentadienyl bismuth(III) dihalides of the type $(C_5R_5)BiX_2$ (R = H, Me; X = Cl, Br, I)

$(C_5R_5)BiX_2$ compounds usually are oligomers via Bi−Bi bridges. Herein, only monomers were examined. The molecular views resulting from the DFT minima structures indicate that the bismuth atom in the $(C_5R_5)BiX_2$ (R = H, Me; X = Cl, Br, I) complexes display a pyramidal coordination environment (Table 3, Figure 7). The distance of the metal atom to the carbon C_1 is longer than the sum of the covalent Bi−C radii ($\Delta\sum r_{cov}$ = 223 pm). Thus, the Bi−C_1 distances are elongated in the row of the $(C_5Me_5)BiX_2$ compounds from X = Cl via X = Br to X= I. For the $(C_5H_5)BiX_2$ complexes such elongation is expressed very weakly. For both rows of the $(C_5R_5)BiX_2$ compounds an elongation of the Bi−X distances, an increase of the sum of angles at the bismuth center (Bi^{sum}), and an increase in pyramidalization with increasing ring and halogen sizes are observed. The elongation of the Bi−Z distance with increasing halogen size for complexes with R = H in the C_5R_5 ring leads to an increase in the β angle (Table 3) and thus, to a lower (π)-coordination mode (η^1). For the $(C_5Me_5)BiX_2$ complexes such regularity is expressed weakly. Thus, the dihalides show different bismuth-ring coordination than the related dications.

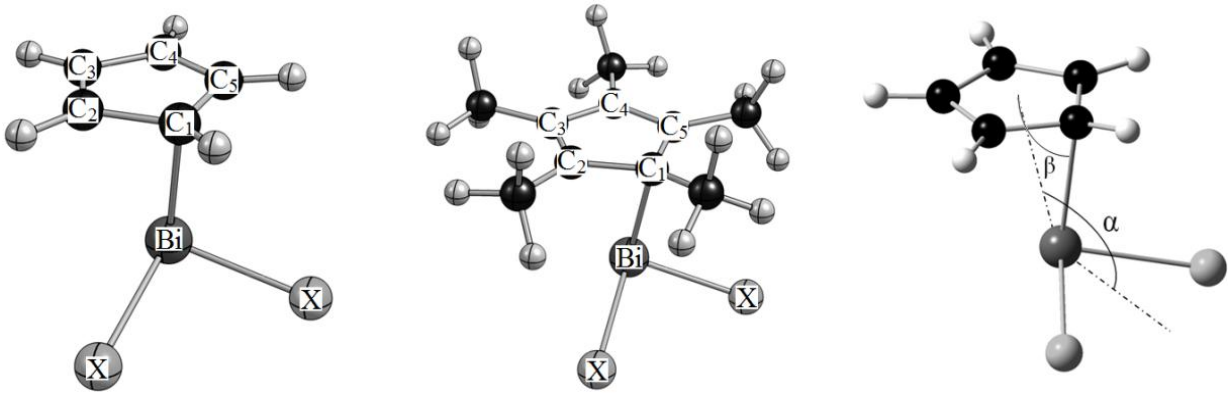

Figure 7. PBE0/BS-I optimized structures of the complexes $(C_5H_5)BiX_2$ (left) and $(C_5Me_5)BiX_2$ (center) in bent conformation where the bismuth atom is bonded to the C_5R_5 ring in a "monohapto" fashion. Right, the angles α and β are mapped on the $(C_5R_5)BiX_2$ complex.

The interactions of the bismuth atom with the C_2 and C_5 carbons are not regarded as bonding. The distances of C_2–C_3 and C_4–C_5 show a slight diene distortion of the C_5R_5 ring. The C_5R_5 rings are attached via a $\eta^1(\pi)$-bonding mode, Bi–C_1. To answer the question "what kind of type is the Bi–C_1 bond: ionic, covalent, or non-bonded?", to get an insight into the electronic influence of halide ions on the bismuth–cyclopentadienyl bonds, and to evaluate the nature of these bonds, the natural bond orbital (NBO) analysis was performed (Table 4).

Table 3. Selected geometrical parameters of $(C_5R_5)BiX_2$ (R = H, Me; X = Cl, Br, I) optimized at the PBE0/BS-I level of theory.[a]

Complex	Bi–Z	Bi–C_1	Bi–$C_{2,5}$	C_1–C_2, C_1–C_5	C_2–C_3, C_4–C_5	C_3–C_4	Bi–X	Bi^{sum}	α	β
$(C_5H_5)BiCl_2$	253.0	237.0	270.1	144.4	138.5	141.9	247.4	293.3	132.2	83.1
$(C_5Me_5)BiCl_2$	247.5	237.3	267.7	145.8	139.3	143.3	250.1	293.5	133.8	80.1
$(C_5H_5)BiBr_2$	253.6	237.1	270.7	144.5	138.4	142.1	263.3	295.7	133.3	83.4
$(C_5Me_5)BiBr_2$	247.2	238.3	267.8	145.8	139.3	143.4	266.4	297.1	135.9	79.5
$(C_5H_5)BiI_2$	256.5	237.1	272.7	144.6	138.2	142.3	284.2	297.5	134.0	84.8
$(C_5Me_5)BiI_2$	248.7	239.2	269.2	145.9	139.2	143.5	287.6	299.1	137.3	79.8

[a] Bond lengths [pm], angles [deg].

The natural population analysis (NPA) of the cyclopentadienyl bismuth(III) dihalides shows that the bismuth atom does not have an idealized $6s^26p^0$ electronic configuration (in the ^1S ground state) but has a partial occupied s^ap^b-hybrid (a, b > 1) with increased electron density in the 6p orbitals. In accordance with the NEC (Table 4) the 6s electrons of Bi are almost completely localized; therefore, the contribution to covalent attraction is mainly due to participation of its 6p orbitals.

The positive partial charge is located on the bismuth atom and is far less than its chemical valence of +3 in the ionic model. Most of the negative charges in C_5R_5 ring are located on the C_1 carbon (~ −0.55 [R = H], ~ −0.30 [R = Me]). It makes the charge transfer between the C_1 carbon atom and the bismuth ion and proves the existence of the sole Bi–C_1 coordination bond. In addition, the natural population analysis reveals a predominantly ionic character of the Bi–C_1 bond for $(C_5R_5)BiCl_2$ (~ 54 % ionic character according to NPA charges) and a predominantly covalent character of the Bi–C_1 bond for the $(C_5R_5)BiX_2$ compounds (~ 47 % [X = Br], ~ 40 % [X = I]).

Table 4. Important calculated values for the complexes obtained from the NBO analysis at the MP2(full)/BS-II//PBE0/BS-I level.

Parameter		$(C_5H_5)BiX_2$			$(C_5Me_5)BiX_2$		
		Cl	Br	I	Cl	Br	I
*n*VE[a]		12	12	12	12	12	12
NEC of Bi[b]		$6s^{1.86}6p^{1.49}$	$6s^{1.87}6p^{1.68}$	$6s^{1.87}6p^{1.90}$	$6s^{1.86}6p^{1.50}$	$6s^{1.88}6p^{1.67}$	$6s^{1.89}6p^{1.87}$
Q_{NPA}[c]	Bi	+1.618	+1.420	+1.189	+1.614	+1.423	+1.203
	C_1	−0.549	−0.543	−0.544	−0.312	−0.296	−0.284
$i_{C5R5-Bi}$[d]		53.9	47.3	39.6	53.8	47.4	40.1
overlap/WBI[e]		0.370/0.476	0.345/0.487	0.352/0.510	0.342/0.490	0.340/0.494	0.337/0.509
NHO at Bi−C_1[f]	Bi		$s^{5.39\%}p^{94.18\%}$	$s^{5.54\%}p^{94.03\%}$			$s^{5.61\%}p^{94.03\%}$
	C_1		$s^{6.60\%}p^{93.34\%}$	$s^{7.01\%}p^{92.94\%}$			$s^{5.77\%}p^{94.18\%}$
occupancy			1.626	1.651			1.637
$100\|C_{Bi}\|^2$[g]			27.03	28.26			29.77
LP NHO[h] at Bi		$s^{90.16\%}p^{9.83\%}$	$s^{90.24\%}p^{9.75\%}$	$s^{90.13\%}p^{9.86\%}$	$s^{90.60\%}p^{9.39\%}$	$s^{91.09\%}p^{8.91\%}$	$s^{91.18\%}p^{8.82\%}$
occupancy		1.997	1.997	1.997	1.995	1.995	1.996
LP NHO at C_1		$s^{4.60\%}p^{95.33\%}$			$s^{4.86\%}p^{95.08\%}$	$s^{5.05\%}p^{94.89\%}$	
occupancy		1.211			1.203	1.189	
E(2)[i]		273.28			277.77	310.58	
E(2)[j]		8.02			7.70	7.51	
ρ_L[k]		99.0	99.4	99.5	99.0	99.2	99.4

[a] Number of valence electrons. [b] Natural electron configuration. [c] Natural charges. [d] Degree of ionicity of C_5R_5−Bi bonding [%]. [e] Atom-atom overlap-weighted NAO bond order and Wiberg bond index for the Bi−C_1 interaction. [f] Natural hybrid orbital at the Bi−C_1 bond. [g] Polarization toward Bi [%]. [h] Lone pair natural hybrid orbital. [i] Delocalization energy of LP_{C1} into bismuth 6p-orbital [kcal/mol]. [j] Delocalization energy of LP_{Bi} into carbon (C_1) LP-orbital [kcal/mol]. [k] Accuracy of calculation model [%].

A bonding population analysis displays overlap populations of approximately 0.35 between the bismuth center and the C_1 carbon atom in these compounds. WBI values for the Bi−C_1 bond indicate the single bond character and comparatively weak covalent interactions (accordingly a

weak overlap population) for the $(C_5R_5)BiX_2$ (X = Cl, Br) compounds. Accordingly, stronger interactions are observed for X = I. Since, the Bi−C_1 bond is polar and strongly polarized toward the C_1 carbon atom (~ 70 %), the bond order should have a value less than one. The localized NBO Lewis-description (ρ_L) illustrates the high accuracy of the calculation models.

On the basis of natural hybrid orbitals (NHO), the Bi−C_1 bond mainly forms from p-orbitals of both atoms. The NBO analysis for $(C_5R_5)BiX_2$ finds the voluminous sp_y-hybridized lone pair orbital localized at the bismuth atom. This lone pair is mostly of s-type and has a high orbital occupancy. The large contribution of the s-orbital in the lone pair indicates that compounds of type $(C_5R_5)BiX_2$ have a relatively low Lewis basicity. In addition, the Lewis base strength slightly increases in the $(C_5Me_5)BiX_2$ complexes from X = I via X = Br to X = Cl with a decrease of the s-character of the bismuth's lone pair. For the $(C_5H_5)BiX_2$ complexes such regularity is not obvious. Also, the lone pair of p-type (~ 95 %) can be found on the C_1 carbon atom for a predominantly ionic character of the Bi−C_1 bond (lone pairs of halogen atoms are not discussed, here). The exception is $(C_5Me_5)BiBr_2$ with a more covalent character of the Bi−C_1 bond. Here, according to a NBO analysis, there is also the lone pair of p-type on the C_1 carbon atom.

In this Bi−C_1 interaction these lone pairs contribute differently. Thus, the lone pair of the C_1 carbon atom interacts with anti-bonding orbitals located at the metal center, which makes the main contribution to the Bi−C_1 interaction: delocalization {$E(2)$} from the lone pair orbital of C_1 into Bi unoccupied 6p-orbitals. Another, more important delocalization could be obtained from the interaction between lone pairs of the bismuth center and the C_1 carbon atom. Other delocalizations have only minor contributions.

To get a clear-cut picture into the electronic interactions and the inter-electronic effects in the $(C_5R_5)BiX_2$ complexes, the valence and frontier molecular orbitals (MOs) of these were studied using the canonical MO theory. In this way, the MO construction of some important orbitals was performed and the inter-electronic effects in the $(C_5R_5)BiX_2$ complexes (R = H, Me; X = Cl, Br, I) were studied (Table 5, Figure 8). Thus, the results of MO approximation indicate that the non-degenerate bonding D and C types of orbitals representing HOMO and HOMO-1 are of π type. They are formed from the contributions of AOs of the C_5R_5−X_2 system and the bismuth valence $6p_{x,z}$ set. The bonding HOMO-3 (denoted as B) has mainly metallic character and corresponds to the space-filling sp_y-hybridized bismuth's lone pair. The major contribution to this comes from the bismuth 6s-MO.

The bonding A MO is formed from the contributions of the C_5R_5−X_2 AOs and the bismuth valence 6s AO. The bonding MOs, in which two electrons, each, are donated from halo ligands,

are not discussed, herein and not shown in Figure 8. As a result, the $(C_5R_5)BiX_2$ compounds with a realized 12 valence electron situation are isoelectronic to groups 13 and 14 cyclopentadienyl compounds of the types $(C_5R_5)_2E^+$ and $(C_5R_5)EX_3$, respectively. In addition, the canonical MO theory evidences results of the NBO analysis for the $[(C_5R_5)Bi]^{q+}$ complexes.

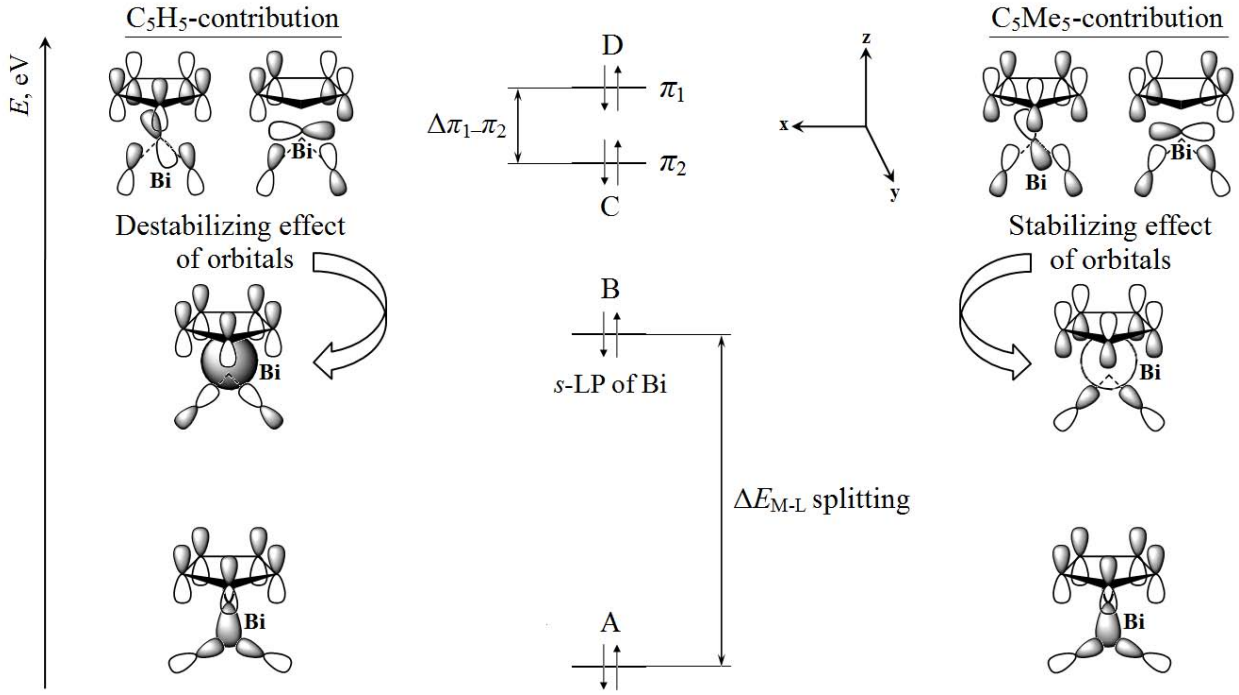

Figure 8. Slice from the qualitative correlation MO-diagram of the filled valence orbital interactions of $X_2Bi{-}C_5R_5$ in the $(\eta^1\text{-}C_5R_5)BiX_2$ complexes.

The testing of the interelectronic behavior of the $(\eta^1\text{-}C_5R_5)BiX_2$ complexes starts with an examination of the interactions of important bonding orbitals (*A*, *B*, *C*, and *D*; Table 5). Thus, the interplane distances $d_{C_5R_5-X_2}$ are much longer than the corresponding sums of the van der Waals (vdW) radii in the $(\eta^1\text{-}C_5R_5)BiX_2$ complexes, that is, vdW repulsion outweighs vdW attraction. The first type of stabilization can be found from the examination of LUMO−B interactions, that is, a low-lying π* orbital of ligands and a MO with metal s-like character, respectively. Thus, the compounds with more covalent $Bi{-}C_1$ bonds have a smaller energy difference (Table 5), which means a stronger mixing and more stabilized B MO (LP of Bi). The B MO is more destabilized in compounds having lone pairs at the Bi and the C_1 carbon atom, which can participate in different delocalizations among themselves.

The ΔE ($E_{HOMO} - E_{LUMO}$) values of the $(\eta^1\text{-}C_5R_5)BiX_2$ complexes, resulting from the Koopman's free-electron molecular-orbital approximation (FE-MO) approach, show the general kinetic stabilization of molecules, which decreases with increasing halogen size. The energy of metal−ligand splitting ΔE_{M-L}, which can be regarded as the energy of Jahn−Teller splitting,

characterizes vdW repulsion energy in molecule. The higher this energy is, the less stable the compound is. The repulsion energy increases with increasing halogen size and decreases with increasing ring size. The different orbital orientation in the (η^1-C_5R_5)BiX_2 complexes with R = H and R = Me clearly expresses this regularity and confirms that the compounds with the sterically better protected C_5Me_5 ligand have less repulsion forces and are more stabilized (Figure 8).

Table 5. Selected important calculated values for the complexes obtained at the MP4(SDQ)/BS-II//PBE0/BS-I level.

Parameter	(C_5H_5)BiX_2			(C_5Me_5)BiX_2		
	Cl	Br	I	Cl	Br	I
E (LUMO)	0.48	0.38	0.12	0.74	0.64	0.40
D (HOMO)	−9.48	−9.34	−9.15	−8.60	−8.54	−8.44
C	−9.80	−9.63	−9.31	−8.93	−8.83	−8.67
B	−11.02	−10.29	−9.57	−10.48	−9.81	−9.12
A	−15.09	−14.85	−14.63	−13.53	−13.33	−13.16
$d_{C5R5-X2}$ [a]	385.9	396.1	411.0	386.2	397.6	414.2
ΔE_{LUMO-B} [b]	11.50	10.67	9.69	11.23	10.45	9.52
$\Delta E_{HOMO-LUMO}$ [c]	9.96	9.72	9.27	9.34	9.18	8.84
ΔE_{M-L} [d]	4.07	4.56	5.06	3.05	3.52	4.04
$\Delta\pi_1$–π_2 [e]	0.32	0.29	0.16	0.33	0.29	0.23
$\Delta E_{h.a}$ [f]	−824	−792	−753	−878	−847	−805
λ [g]*	290	310	351	324	344	372
μ [h]	5.50	5.04	4.65	7.05	6.98	6.97

[a] Interplane distance between the C_5R_5 plane and X−X line [pm]. [b] Stabilization energy between LUMO and B MO [eV]. [c] Energy of the HOMO−LUMO-gap [eV]. [d] Splitting energy with metal contribution [eV]. [e] Stabilization energy between D and C MOs [eV]. [f] Heterolytic association energy [kJ/mol]. [g] *Values of the $S_0 \rightarrow S_1$ transition (HOMO → LUMO excitation) [nm] computed at the TD-PBE0/BS-II//PBE0/BS-I level. [h] Dipole moment [Debye].

Furthermore, the electrostatic attraction between bismuth and the C_5Me_5 ring, obtained from the electric charge difference, provides a stronger stabilizing force than that in the complexes with the unalkylated cyclopentadienyl ring. The smaller energy difference between C and D π orbitals indicates the stronger covalent π(C_5R_5)-π(Bi) interaction. The corresponding decrease of

$\Delta\pi_{1-}\pi_2$ values in a direction of the compounds with a predominantly covalent Bi–C_1 bonding can be observed. Thus, the heterolytic association energies decrease with increasing halogen size and increase with increasing ring size. The dipole moment decreases with increasing halogen size. The peralkylated cyclopentadienyl derivates of the complexes are more polar than unalkylated ones.

TD-PBE0 calculations for the $(C_5R_5)BiX_2$ (X = Cl, Br, I) complexes having the sole hybridized lone pair of s-type localized on bismuth show that the most intense $S_0 \rightarrow S_1$ transition corresponds to a HOMO → LUMO excitation with $\pi \rightarrow n_{Bi(p)}$* character (see the appendix to chapter 4.2). This lowest energy transition can be described as ligand–metal charge transfer (LMCT excitation) arising from the electron move from a predominantly ligand π-orbital to a predominantly metal p-orbital. Such a type of transition promotes the reduction of the bismuth center and a formation of a new type of the lowest-valent bismuth compounds in further synthetic reactions. In addition, the energy of the $S_0 \rightarrow S_1$ transition decreases with increasing ring and halogen sizes.

4.2.4 Outlook of complexes $(C_5R_5)BiX_2$ (R = H, Me; X = Cl, Br, I)

The orientation of the s- and p-lone pairs on the bismuth center in regard to the cyclopentadienyl ring, as well as the valence electron number, is responsible for the η^x-hapticity of the C_5R_5 ligand and determines the structure and stability of the complexes (Figure 9).

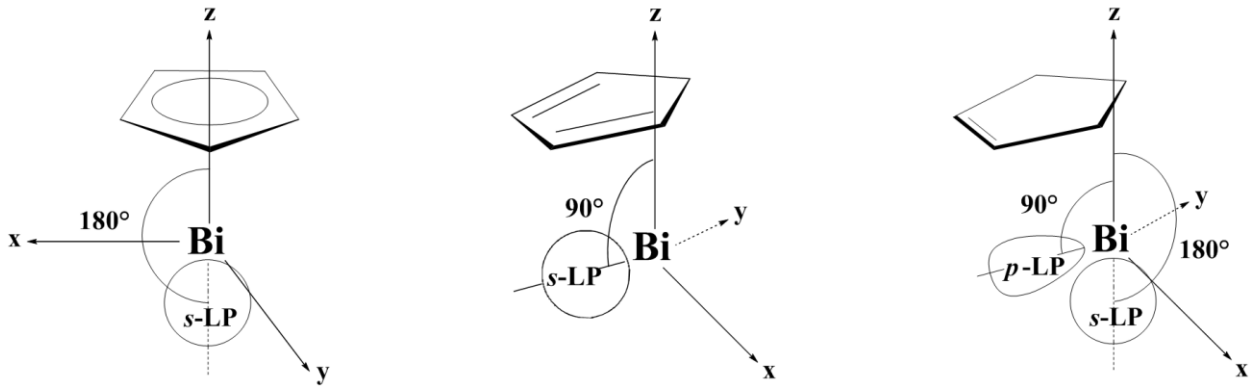

Figure 9. Orientations of the lone pairs in *x*, *y*, *z* dimension coordinates for $(\eta^5\text{-}C_5R_5)Bi^{2+}$ (left), $(\eta^1\text{-}C_5R_5)BiX_2$ (center; X_2 part is not shown), and $(\eta^3\text{-}C_5R_5)Bi$ (right). The lone pairs show the main contribution in their orbitals.

Here, 12 and 8 VE situations correspond to the compounds of type $(\eta^1\text{-}C_5R_5)BiX_2$ and $(\eta^5\text{-}C_5R_5)Bi^{2+}$, respectively, whereas the 10 VE situation corresponds to the kinetically less stable $(\eta^3\text{-}C_5R_5)Bi$ compounds. Besides, the $\eta^1(\pi)$-coordination (LP is of 90° to *z*-axes) of the C_5R_5 ring to Bi in the cyclopentadienyl bismuth(III) dihalides (12 VEs) should be realized mainly in

solution, whereas in solid state such compounds should associate. A haptotropic rearrangement in the η^5-coordination (LP is of 180° to *z*-axes) is possibly due to an equilibrium distribution of electronic density on the metal center (Figure 9, Scheme 3).

The complexes of type $(C_5R_5)BiX_2$ enable three potential regions for an attack: the bismuth center, the halogen X groups, and the C_5R_5 ring (Scheme 3). The reactivity of complexes of this type depends strongly on the nature of both the C_5R_5 and X ligands and the nature of the C_5R_5–Bi bonding. First, the $(C_5R_5)BiX_2$ complexes may react via a space-filling lone pair orbital of s-type localized at the bismuth atom as Lewis base (σ-donor), donating electrons to the empty p-orbitals of trigonal-planar molecules of the group 13 p-elements (ElR_3) or to the empty d-orbitals of transition metal complex fragments, to form Lewis acid–base adducts of type $[(C_5R_5)BiX_2]$–LA (LA = Lewis acid). Here, the covalent C_5R_5–Bi bonding with only one LP on Bi looks more reasonable.

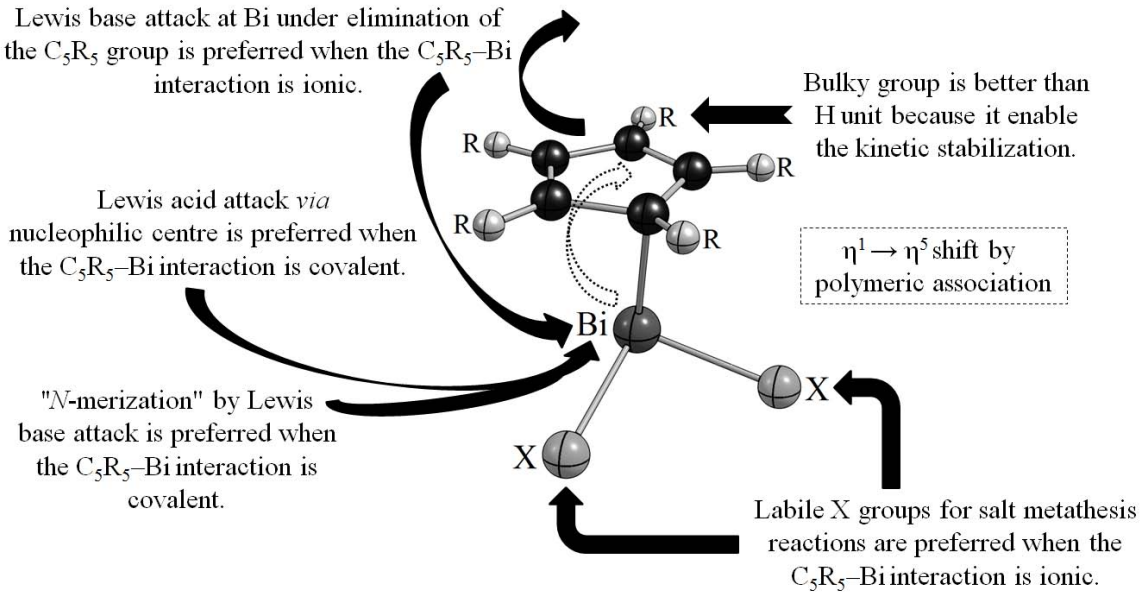

Scheme 3. Further behavior and capabilities of the $(C_5R_5)BiX_2$ complexes.

By Lewis base attack on such covalent bonded molecules "*N*-merization" of the bismuth center can be preferred, resulting, for example, in the dipnictene compounds of type $[(C_5R_5)Bi]_n$. Corresponding terphenyl derivatives have already been characterized.[6] Second, the $(C_5R_5)BiX_2$ complexes may react via valence p-orbitals as Lewis acids (π-acceptor), exchanging the chlorine electrons for the electrons of the incoming groups (salt metathesis reactions), to form the molecules of type $(C_5R_5)Bi(IG)_2$ (IG = incoming group). The alkyl or silyl ligands of the alkali metal (M) coordination compounds $[MR_a(R_b)_3$, where R_a = C, Si, Ge; R_b = organic group] can act as incoming groups. For these aims, the ionic C_5R_5–Bi bonding with two LPs localized on

bismuth and C_1 carbon of the C_5R_5 ring looks more reasonable. Besides, here the C_5R_5-group allows for a possibility of its exchange [$-(C_5R_5)M$, $-MX$] for the nucleophilic incoming group of the Lewis base to form the compounds of type $Bi_x(IG)_y$. Finally, it is necessary to remark that the ionic C_5R_5−Bi bonding can work as one of the reasons of forming associated structures.

4.2.5 References

[1] (a) P. Jutzi, F. Kohl, P. Hofmann, C. Krüger, Y. H. Tsay, *Chem. Ber.* **1980**, *113*, 757; (b) J. L. Atwood, W. E. Hunter, A. H. Cowley, R. A. Jones, C. A. Stewart, *Chem. Commun.* **1981**, 925; (c) A. Haaland, B. E. R. Schilling, *Acta Chem. Scand.* **1984**, *38A*, 217; (d) M. Lattman, A. H. Cowley, *Inorg. Chem.* **1984**, *23*, 241; (e) P. Jutzi, D. Kanne, C. Krüger, *Angew. Chem. Int. Ed.* **1986**, *25*, 164; (f) O. T. Beachley, Jr., J. C. Pazik, T. E. Glassman, M. R. Churchill, J. C. Fettinger, R. Blom, *Organometallics* **1988**, *7*, 1051; (g) O. T. Beachley, Jr., R. Blom, M. R. Churchill, K. Faegri, Jr., J. C. Fettinger, J. C. Pazik, L. Victoriano, *Organometallics* **1989**, *8*, 346; (h) D. Loos, H. Schnöckel, J. Gauss, U. Schneider, *Angew. Chem. Int. Ed.* **1992**, *31*, 1362; (i) D. Loos, E. Baum, A. Ecker, H. Schnöckel, A. J. Downs, *Angew. Chem. Int. Ed.* **1997**, *36*, 860; (j) D. R. Armstrong, M. J. Duer, M. G. Davidson, D. Moncrieff, C. A. Russell, C. Stourton, A. Steiner, D. Stahlke, D. S. Wright, *Organometallics* **1997**, *16*, 3340; (k) J. G. Winter, P. Portius, G. Kociok-Kohn, R. Steck, A. C. Filippou, *Organometallics* **1998**, *17*, 4176; (l) J. D. Smith, T. P. Hanusa, *Organometallics* **2001**, *20*, 3056; (m) G. Frenking, K. Wichmann, N. Fröhlich, C. Loschen, M. Lein, J. Frunzke, V. M. Rayón, *Coord. Chem. Rev.* **2003**, *238−239*, 55; (n) J. N. Jones, J. A. Moore, A. H. Cowley, C. L. B. Macdonald, *Dalton Trans.* **2005**, 3846; (o) C. Schenk, A. Schnepf, *Organometallics* **2006**, *25*, 2378.

[2] The *trans*-$[(C_6H_5)Bi]_2$ molecule was optimized at the PBE0/def2-TZVP level of theory using the Turbomole program.

[3] (a) N. Tokitoh, Y. Arai, R. Okazaki, S. Nagase, *Science* **1997**, *277*, 78; (b) N. J. Hardman, B. Twamley, P. P. Power, *Angew. Chem. Int. Ed.* **2000**, *39*, 2771.

[4] Y. Wang, B. Quillian, X. J. Yang, P. Wei, Z. Chen, C. S. Wannere, P. v. R. Schleyer, G. H. Robinson, *J. Am. Chem. Soc.* **2005**, *127*, 7672.

[5] (a) H. J. Breunig, R. Rösler, E. Lork, *Angew. Chem. Int. Ed.* **1998**, *37*, 3175; (b) G. Linti, W. Köstler, *Z. Anorg. Allg. Chem.* **2002**, *628*, 63; (c) G. Linti, W. Köstler, H. Pritzkow, *Eur. J. Inorg. Chem.* **2002**, 2643; (d) G. Balázs, L. Balázs, H. J. Breunig, E. Lork, *Organometallics* **2003**, *22*, 2919.

[6] (a) B. Twamley, C. D. Sofield, M. M. Olmstead, P. P. Power, *J. Am. Chem. Soc.* **1999**, *121*, 3357; (b) R. Wolf, J. Fischer, R. C. Fischer, J. C. Fettinger, P. P. Power, *Eur. J. Inorg. Chem.* **2008**, 2515.

4.3 Molecular self-assemblies based on Cp^*BiX_2 units ($Cp^* = C_5Me_5$; X = halogen)

4.3.1 Syntheses and spectroscopic characterization of pentamethylcyclopentadienyl bismuth complexes

The reactions of bismuth(III) halides BiX_3 (X = Cl, Br, I) with pentamethylcyclopentadienyl-lithium LiCp* in a 1:1 ratio in the solvent thf yield the pentamethylcyclopentadienyl-substituted bismuth halide complexes **1** – **4** (Scheme 4). Thus, upon treatment of BiX_3 with LiCp* under the applied conditions (warming from –78 °C to r.t. during the reactions), a quick color deepening of the reaction mixtures to dark-red was observed. Workup of resulting mixtures allows isolation of **1** – **4** as red or deep-red crystals.

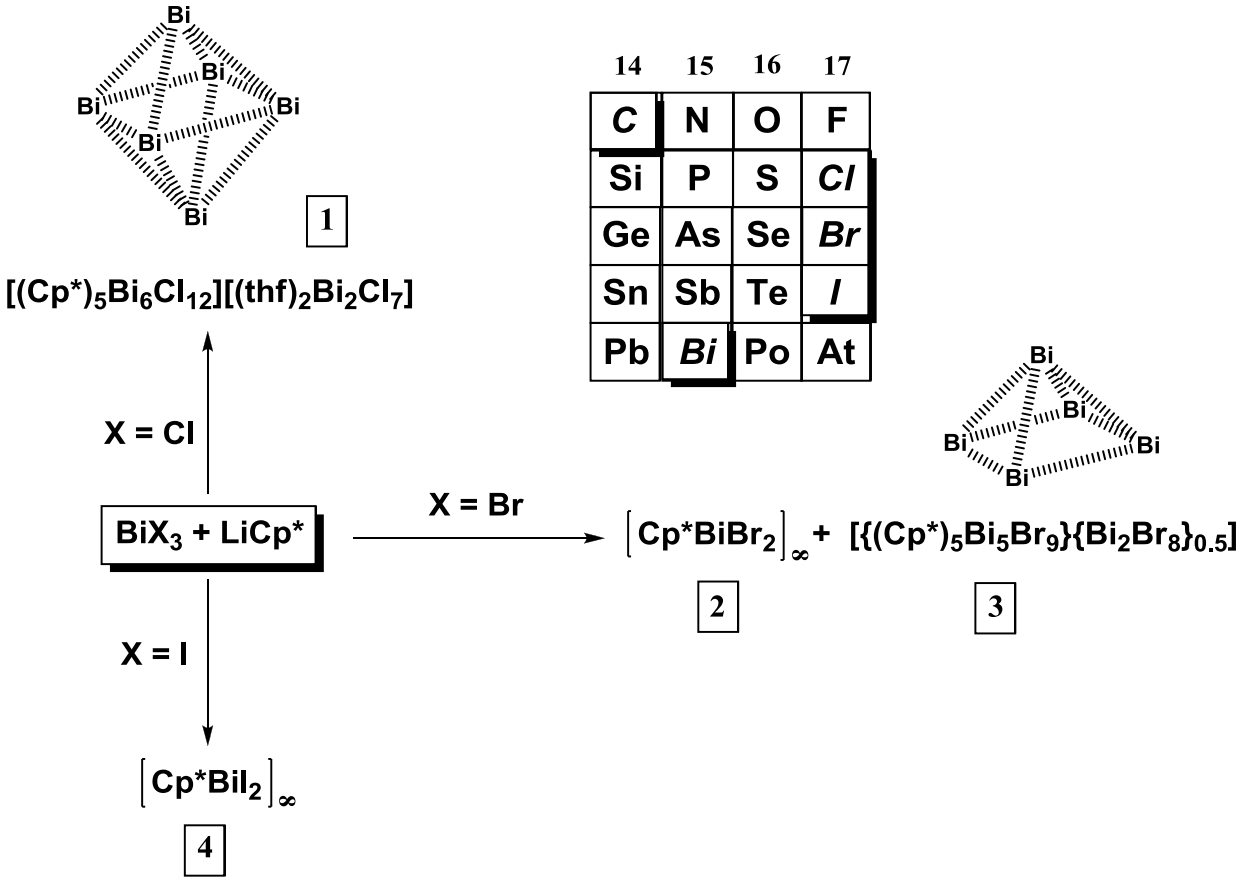

Scheme 4. Reaction pathways leading to the formation of bismuth pentamethylcyclopentadienyl compounds **1** – **4** under the applied conditions (–78°C → r.t.).

In the ^1H and ^{13}C NMR spectra, compounds **2** and **4** show five sets of singlets, each, for the methyl groups and the ring carbon atoms. Thus, the obtained data indicate that the Cp* rings in solutions are attached to the Bi atoms unsymmetrically, i.e. not η^5. But the pattern suggests a η^1 coordination mode. The ^{13}C-NMR spectra of **2** and **4** also reveal an influence of corresponding

halide atoms on the shift of the C1 carbon atom that is bonded to the Bi center in a η^1 fashion. Here, the carbon (C1) resonances of $(\eta^1\text{-Cp*})BiX_2$ complexes were observed at 58.8 (X = Br) and 60.2 (X = I) ppm. Other ring carbons are strong deshielded and their resonances appear at lower field in the range of 120 – 145 ppm. In contrast to **2** and **4**, the ^1H and ^{13}C NMR spectra of **1** and **3** show only one type of Cp* groups. For **1**, the proton resonance was observed at 2.37 ppm (singlet) and the carbon ones at 9.3 (s, Me) and 126.1 (s, C_{ring}) ppm. For **3**, the proton resonance was observed at 2.63 ppm (singlet) and the carbon ones at 10.8 (s, Me) and 125.3(s, C_{ring}) ppm. The obtained data thus evidence, that the Cp* rings are bonded in a η^5 coordination mode.

4.3.2 X-ray crystal structure of $[(Cp^*)_5Bi_6Cl_{12}][(thf)_2Bi_2Cl_7]$

Single crystals of $[(Cp^*)_5Bi_6Cl_{12}][(thf)_2Bi_2Cl_7]$ (**1**) suitable for X-ray structure determination were isolated from a thf/toluene mixture at –20°C. Compound **1** crystallizes in the monoclinic crystal system, space group *Cc*, *Z* = 4 (Figure 10).

The $[(thf)_2Bi_2Cl_7]^-$ anion is the counterion for the cation $[(Cp^*)_5Bi_6Cl_{12}]^+$ (**1a**). The structure of **1a** may be described as a distorted Bi_6 octahedron with a Cl atom in the center (denoted as Cl_{center}) (Figure 11). The Bi–Cl_{center} bond lengths are $d_{Bi-Cl_{center}}$ = 300.7 – 373.7 pm. The Bi···Bi distances in the Bi_6 octahedron are $d_{Bi\cdots Bi}$ = 423.3 – 511.8 pm. These are outside of the sum of the covalent radii for two Bi atoms ($\Delta\Sigma r_{cov}$ = 304 pm). Thus, the Bi···Bi distances are essentially non-bonding. On the other hand, these Bi···Bi distances lie with one exception in the range of van der Waals interactions ($\Delta\Sigma r_{vdW}$ = 480 pm). In this manner, only one Bi···Bi distance ($d_{Bi\cdots Bi}$ = 511.8 pm), corresponding to connection between Cp*Bi and $BiCl_3$ fragments in the Bi_6 octahedron, is too elongated, whereas the other five ($d_{Bi\cdots Bi}$ = 423.3 – 470.7 pm) are inside of the sum of van der Waals radii ($\Delta\Sigma r_{vdW}$ = 480 pm). Consequently, the Bi_6 octahedron can be considered as an open-faced octahedron.

While five octahedron's apexes are bonded to the Cp* rings in a η^5-fashion, resulting in square pyramidal $(Cp^*)_5Bi_5$ shape (Figure 11), the sixth one is bonded to three μ_1-coordinated chlorine atoms. The Cp* ring centroid–metal bond distances (denoted as Bi–Z where Z is ring centroid) are d_{Bi-Z} = 222.2 – 227.4 pm, here.

Furthermore, whereas the four faces of square pyramidal $(Cp^*)_5Bi_5$ part are capped by μ_3-Cl atoms ($d_{Bi-\mu3\text{-}Cl}$ = 292.7 – 302.6 pm), the interaction between resulting $(\eta^5\text{-Cp*})_5Bi_5(\mu_3\text{-Cl})_4$ and the sixth Bi atom in the $BiCl_3$ fragment ($d_{Bi-\mu1\text{-}Cl}$ = 245.9 – 248.4 pm) is via four remaining chlorine atoms. The latter are μ^2-coordinated ($d_{Bi-\mu2\text{-}Cl}$ = 278.4 – 299.7 pm) to Bi_4 ground of $(\eta^5\text{-Cp*})_5Bi_5(\mu_3\text{-Cl})_4$. These four chlorine atoms interact to $BiCl_3$ to be in a μ_3-fashion ($d_{Cl_3Bi-\mu3\text{-}Cl}$ = 306.9 – 387.9 pm). The Bi–μ_3-Cl distances are longer than Bi–μ_1-Cl ones, as expected.

A total of eight chlorine atoms are μ_3-coordinated, three chlorine atoms are terminal (μ_1) and one chlorine atom is interstitial.

Thus, $[(Cp^*)_5Bi_6Cl_{12}]^+$ ion can compare as far as possible with weak associated hexameric structures $(ECp^*)_6$ of the group 13 elements (see E = Ga or In, for example).[1]

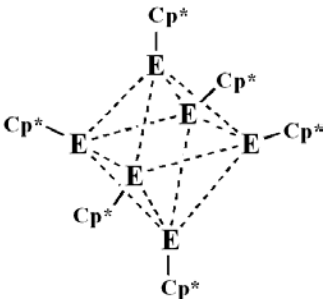

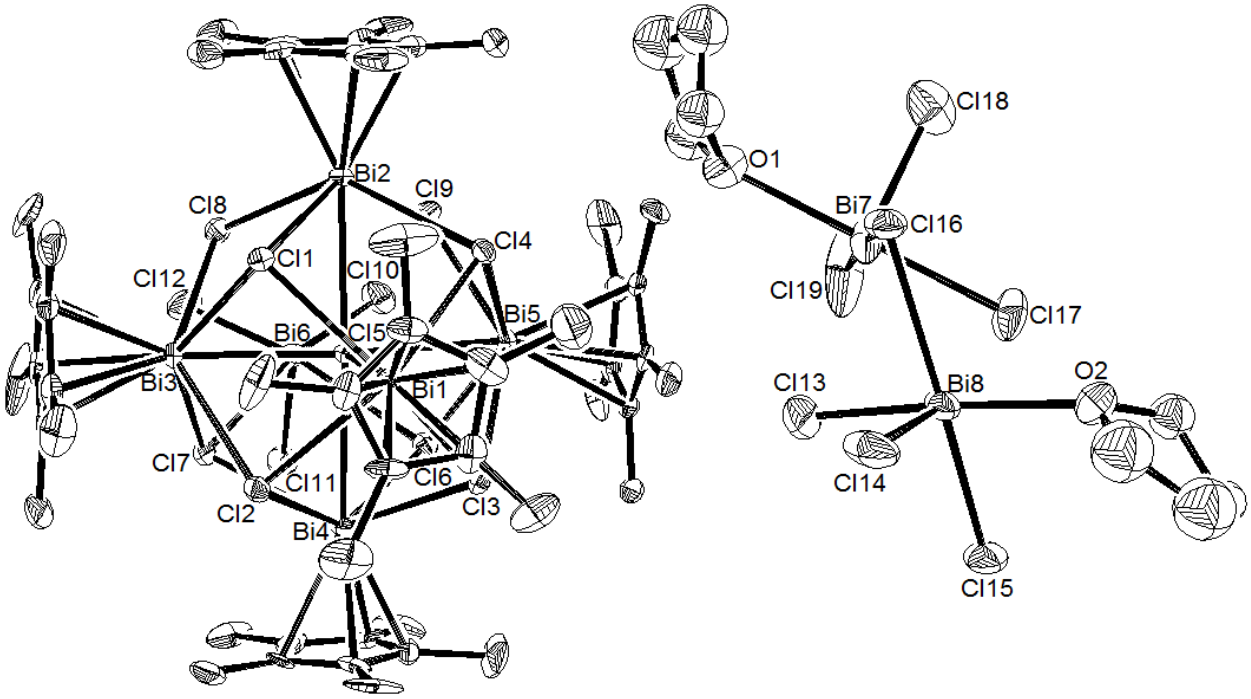

Figure 10. Solid-state molecular structure of **1** (crystal; the thermal ellipsoids are given at the 30% probability level; hydrogen atoms are omitted for clarity). Selected bond lengths [pm]: Bi1–Bi2 440.0(1), Bi1–Bi3 438.7(1), Bi1–Bi4 435.3(1), Bi1–Bi5 438.5(1), Bi2–Bi3 423.3(2), Bi2–Bi5 425.7(2), Bi2–Bi6 511.8(1), Bi3–Bi4 434.4(2), Bi3–Bi6 467.7(1), Bi4–Bi5 437.6(2), Bi4–Bi6 442.2(2), Bi5–Bi6 470.7(2), Bi1–Z 224.7(8), Bi2–Z 227.4(9), Bi3–Z 225.3(1), Bi4–Z 225.4(7), Bi5–Z 222.2(1), Bi1–Cl5 303.9(5), Bi2–Cl5 308.4(5), Bi3–Cl5 301.9(5), Bi4–Cl5 306.8(5), Bi5–Cl5 300.7(5), Bi6–Cl5 373.7(5), Bi6–Cl10 246.4(8), Bi6–Cl11 245.9(5), Bi6–Cl12 248.4(8), Bi1–Cl1 295.1(5), Bi2–Cl1 304.8(5), Bi3–Cl1 304.9(5), Bi1–Cl2 302.6(5), Bi3–Cl2 304.3(5), Bi4–Cl2 300.0(55), Bi3–Cl7 287.8(5), Bi4–Cl7 299.7(5), Bi6–Cl7 306.9(5), Bi2–Cl8 284.8(5), Bi3–Cl8 294.1(5), Bi6–Cl8 351.9(6), Bi4–Cl6 291.2(5), Bi5–Cl6 292.8(5), Bi6–Cl6 308.2(5), Bi2–Cl9 278.4(6), Bi5–Cl9 285.5(5), Bi6–Cl9 387.9(5), Bi1–Cl4 292.7(5), Bi2–Cl4 309.9(5), Bi5–Cl4 308.9(5), Bi1–Cl3 294.0(5), Bi4–Cl3 297.7(5), Bi5–Cl3 318.8(5).

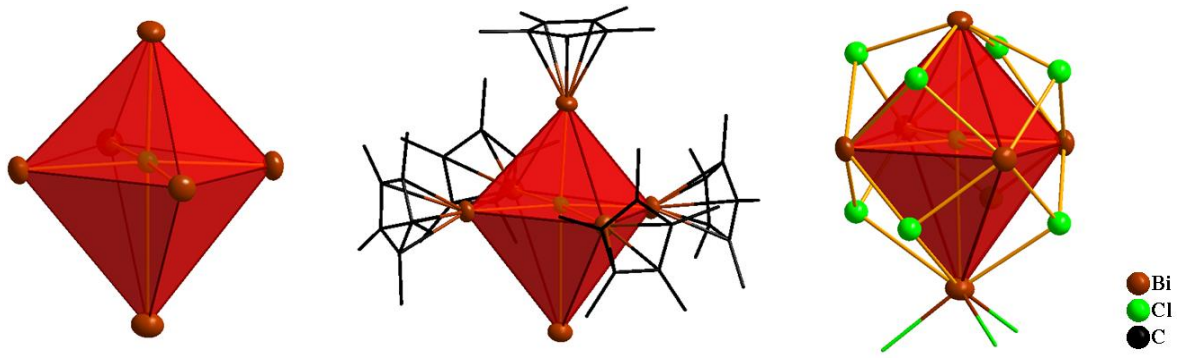

Figure 11. A perspective view of structural arrangements of $[(Cp^*)_5Bi_6Cl_{12}]^+$.

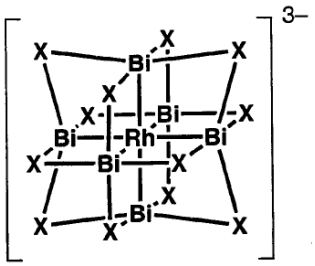

$[RhBi_6(\mu\text{-}X)_{12}]^{3-}$

The octahedral cluster $[RhBi_6(\mu\text{-}X)_{12}]^{3-}$ (X = Br, I) has been reported as a d^6 Rh(III) complex containing six equivalent BiX_2^- ligands with interligand halogen bridging but no direct bismuth–bismuth bonding.[2] A closely related $RuBi_6(\mu\text{-}Br)_{12}$ structural unit is also found in the phase $Ru_3Bi_{24}Br_{20}$ in addition to discrete $BiBr_4$ groups and $Ru_2Bi_{17}Br_4$ stacks.[3] The Bi_6 octahedra are centered by an metal atom and the halogen atoms are μ_2 bridging on the edges.

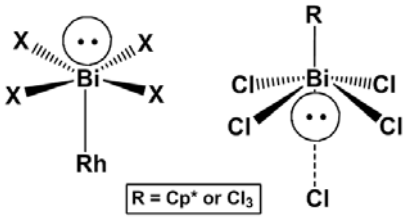

Interesting, some main structural features of $[(Cp^*)_5Bi_6Cl_{12}]^+$ and $[RhBi_6(\mu\text{-}X)_{12}]^{3-}$ are different. Thus, the six bismuth atoms in $[RhBi_6(\mu\text{-}I)_{12}]^{3-}$ anion are equivalent and exhibit square pyramidal coordination, which can be regarded as a Bi(III) pseudooctahedron with the lone electron pair required for Bi(III) *trans* to the Rh atom (on the outside of Bi_6; $d_{Bi–Rh}$ = 271 pm). In contrast to $[RhBi_6(\mu\text{-}I)_{12}]^{3-}$, the six bismuth atoms of $[(Cp^*)_5Bi_6Cl_{12}]^+$ exhibit octahedral coordination where the lone pairs are placed inside of the Bi_6 octahedron, *cis* to the Cl_{center} atom (internal lone pairs of s character).

4.3.3 X-ray crystal structure of $[\{(Cp^*)_5Bi_5Br_9\}\{Bi_2Br_8\}_{0.5}]$

Single crystals of $[\{(Cp^*)_5Bi_5Br_9\}\{Bi_2Br_8\}_{0.5}]$ (**3**) suitable for X-ray structure determination were isolated from a CH_2Cl_2 solution at –20°C. Compound **3** crystallizes in the triclinic crystal system, space group $P\bar{1}$, Z = 2 (Figure 12).

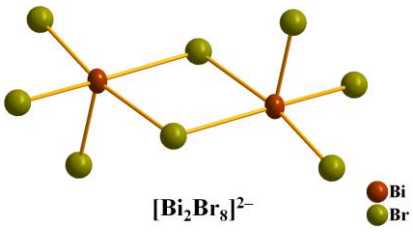

$[Bi_2Br_8]^{2-}$

The $\{Bi_2Br_8\}^{2-}$ anion is the counterion for the cations $\{(Cp^*)_5Bi_5Br_9\}^+$ (**3a**). The Bi–Br bond lengths in $\{Bi_2Br_8\}^{2-}$ are $d_{Bi–\mu2\text{-}Br}$ = 302.6 – 312.8 pm and $d_{Bi–\mu1\text{-}Br}$ = 267.3 – 271.4 pm.

The structure of **3a** may be described as a Bi_5 square pyramid with a Br_1 atom in the center (denoted as Br_{center}) (Figure 13). The Bi–Br_{center} bond lengths are $d_{Bi–Br_{center}}$ = 318.8 – 323.3 pm. The Bi···Bi distances in the Bi_5 square pyramid are $d_{Bi\cdots Bi}$ = 446.3 – 460.2 pm. These are

outside of the sum of the covalent radii for two Bi atoms ($\Delta\Sigma r_{cov}$ = 304 pm). Thus, the Bi···Bi distances are essentially non-bonding. On the other hand, these Bi···Bi distances lie in the range of van der Waals interactions ($\Delta\Sigma r_{vdW}$ = 480 pm).

All five octahedron's apexes are bonded to the Cp* rings in a η^5-fashion (Figure 13). The Cp* ring centroid–metal bond distances are d_{Bi-Z} = 228.7– 231.8 pm, here.

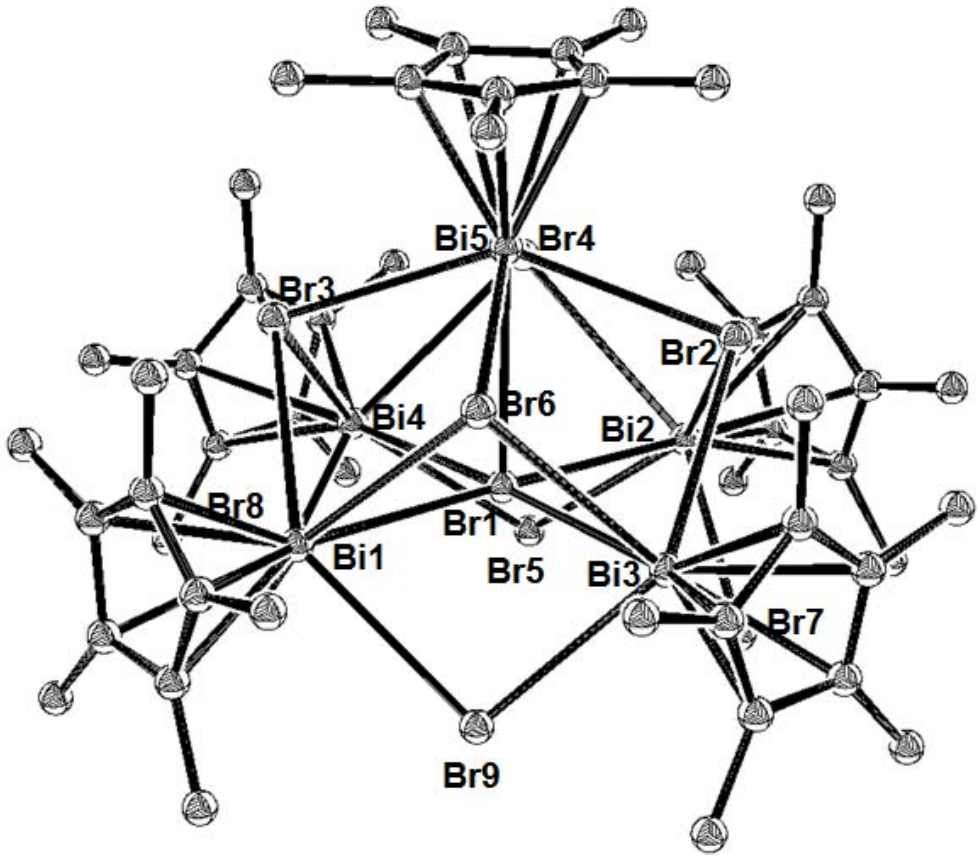

Figure 12. Molecular structure of **3a** (crystal; the ellipsoids are given at the 30% probability level; hydrogen atoms are omitted for clarity). Selected bond lengths [pm]: Bi1–Bi4 457.2(2), Bi4–Bi2 458.5(2), Bi2–Bi3 446.3(2), Bi3–Bi1 451.2(2), Bi1–Bi5 457.9(2), Bi4–Bi5 459.5(2), Bi2–Bi5 456.3(2), Bi3–Bi5 460.2(2), Bi1–Z 231.8(8), Bi2–Z 230.7(8), Bi3–Z 230.4(7), Bi4–Z 229.7(8), Bi5–Z 228.7(9), Bi1–Br1 320.5(2), Bi2–Br1 318.8(2), Bi3–Br1 323.3(2), Bi4–Br1 320.2(2), Bi5–Br1 319.4(2), Bi1–Br3 329.5(2), Bi1–Br8 300.9(2), Bi4–Br3 325.5(2), Bi4–Br8 311.2(2), Bi4–Br4 321.6(2), Bi4–Br5 300.1(2), Bi2–Br4 325.8(2), Bi2–Br5 316.4(2), Bi2–Br2 313.0(2), Bi2–Br7 298.8(2), Bi3–Br2 326.0(2), Bi3–Br7 296.5(2), Bi3–Br6 325.1(2), Bi3–Br9 307.3(2), Bi1–Br6 328.9(2), Bi1–Br9 292.5(2), Bi5–Br3 310.0(2), Bi5–Br4 316.0(2), Bi5–Br2 314.9(2), Bi5–Br6 305.2(2).

The four faces of Bi_5 square pyramid are capped by μ_3-Br atoms where $d_{Bi-\mu3-Br}$ = 305.2 – 329.5 pm (Figure 13). Four remaining bromine atoms are μ_2-bridges ($d_{Bi-\mu2-Br}$ = 292.5 – 316.4 pm)

between the Bi atoms in Bi_4 ground of the square pyramid.

The five Bi atoms of **3a** exhibit octahedral coordination (similar to **1a**) where the lone pairs are placed inside of the Bi_5 square pyramid, *cis* to the Br_{center} atom (internal lone pairs of s character). These lone pairs are stereochemically inert, obviously, because the Bi–Br_{center} bond lengths are equivalent. Hence, the main structural difference between cations **3a** and **1a** is a BiX_3 unit complexated to the $\{(Cp^*)_5Bi_5Cl_9\}^+$ part of the latter.

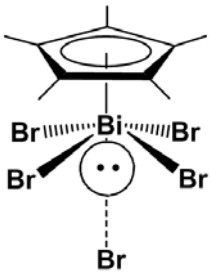

The distances between the Cp* centroids of Bi1 and Bi2 as well as Bi3 and Bi4 in **3a** are 1 nm. The vertical distance between Br_{center} and the Cp* centroid of Bi5 is 547.9 pm.

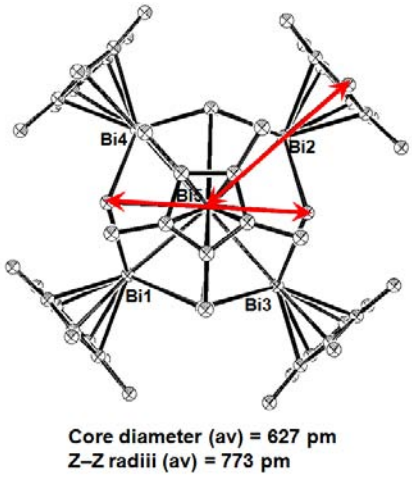

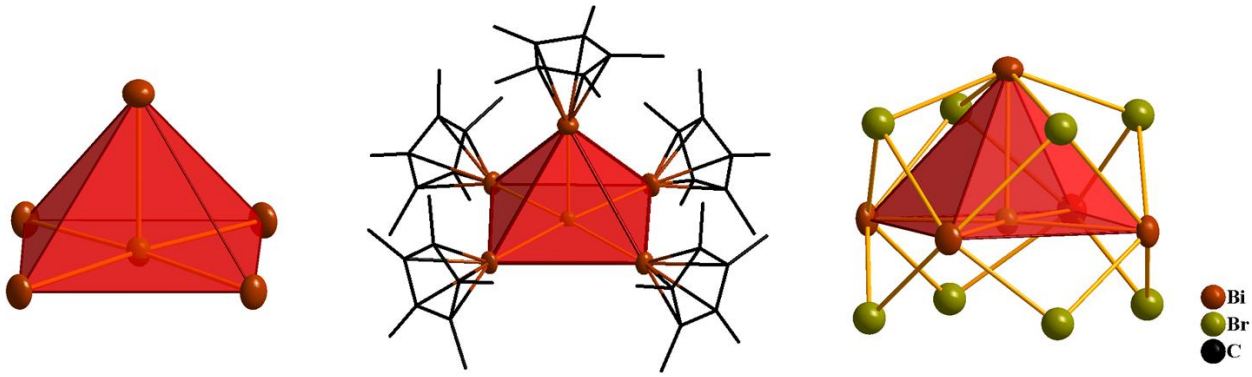

Figure 13. A perspective view of structural arrangements of $\{(Cp^*)_5Bi_5Br_9\}^+$.

The solid-state molecular structure of **3** shows a unique supramolecular architecture! Its system is organized by intermolecular CH···X-mediated interactions via $[(CH_2Cl_2)(BiBr_4)]_2$ chain linking three-dimensional square pyramidal bromine-centered bismuth cage structures $\{(Cp^*)_5Bi_5Br_9\}^+$ through Cp* fragments (Figures 14 and 15).

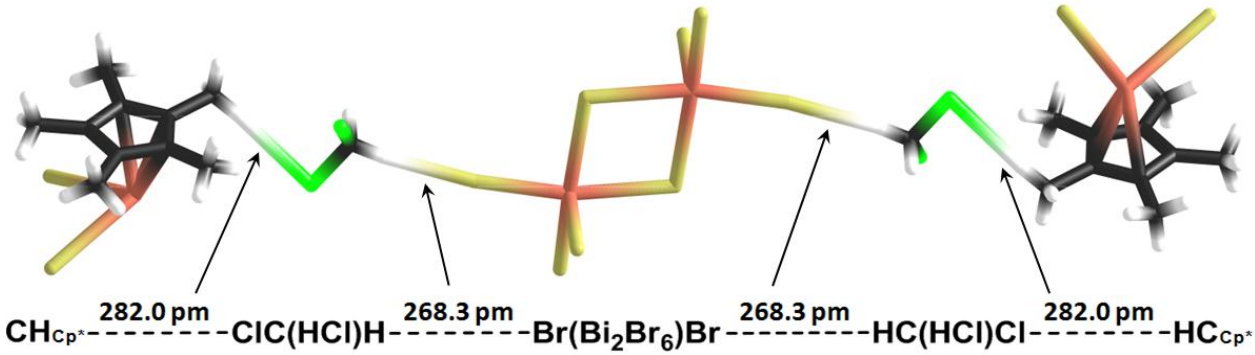

Figure 14. Intermolecular $[(CH_2Cl_2)(BiBr_4)]_2$ chain linking Cp* fragments of **3a**.

The weak hydrogen bonds were thus established, here. The nanosized **3** is an unprecedented example in organobismuth chemistry!

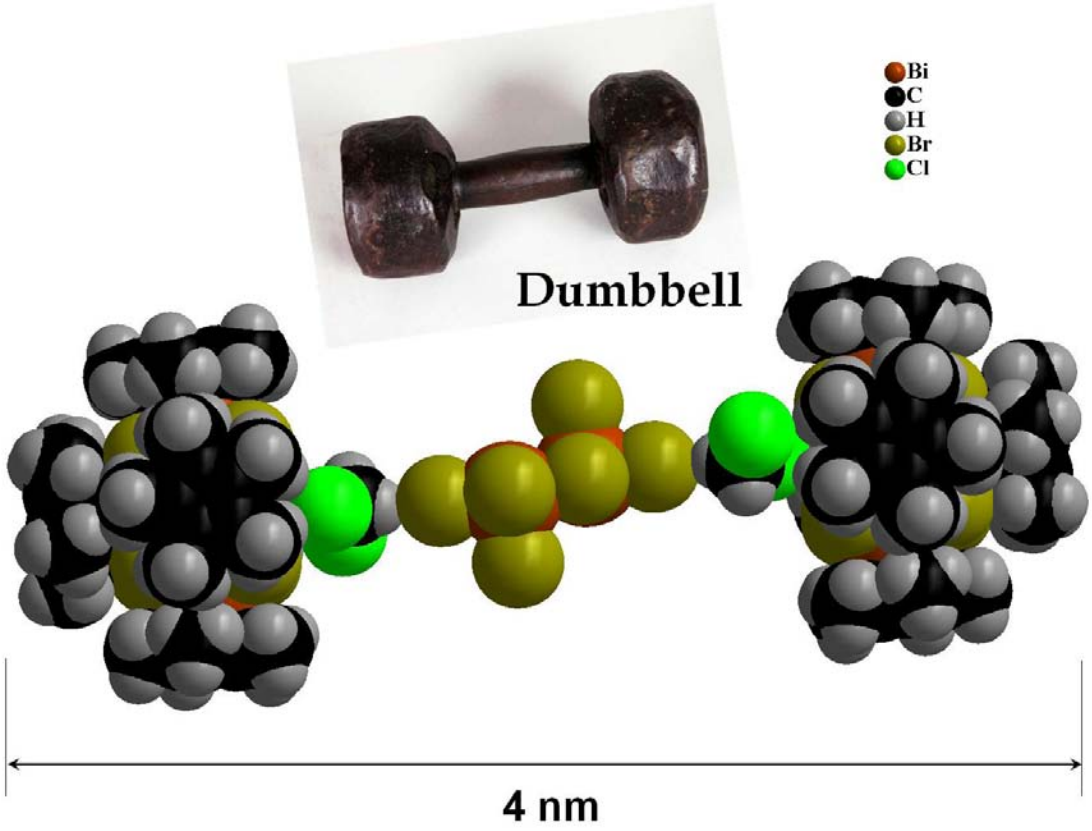

Figure 15. Space-filling model of 3D cages linking via intermolecular chain in the solid-state molecular structure of **3** (4 nm is diameter, calculated between Z–Z).

Figure 14 shows intermolecular H···Cl and H···Br contacts where the chlorine atoms of CH_2Cl_2 are involved in contacts with the hydrogen atoms of the Cp* substituents and the bromine atoms of $(Bi_2Br_8)^{2-}$ are involved in contacts with the hydrogen atoms of CH_2Cl_2. The H···Cl distances of 282.0 pm are shorter than the sum of van der Waals radii for H and Cl ($\Delta\Sigma r_{vdW}$ = 295 pm) and can thus be classified as belonging to the intermediate contacts according to the classification, published by Brammer, Orpen and co-workers in 1998.[4] They established that the intermolecular H···Cl contacts lie in the range of 180 – 315 pm. The H···Br distances of 268.3 pm in the intermolecular chain are significantly shorter than the sum of van der Waals radii for H and Br ($\Delta\Sigma r_{vdW}$ = 305 pm) and can also be classified as belonging to the intermediate contacts.

The first characterization of weak hydrogen bonds in organoantimony compounds was done by V. Chandrasekhar et al. in 2001, only. A C–H···Cl–Sb-mediated, zig-zag, supramolecular polymeric architecture in $[Ph_2Sb(Cl)\{S_2C_2(CN)_2\}]$ was reported (Figure 16). Thus, the X-ray

crystal structure analysis of $[Ph_2Sb(Cl)\{S_2C_2(CN)_2\}]$ has shown an existence in the latter of four different types of secondary interaction: (a) C–H···Cl intramolecular contacts (271.1 and 281.5 pm), (b) C–H···Cl intermolecular contacts (279.7 and 311.2 pm), (c) C–H···S intramolecular contacts (278.3 and 278.9 pm), and (d) intermolecular C–H···π interactions (302.8 pm).[5]

Also, the comparable H···Cl distances have been observed by Jones and Freytag for C–H···Cl–Au contacts in a Au(I) complex.[6]

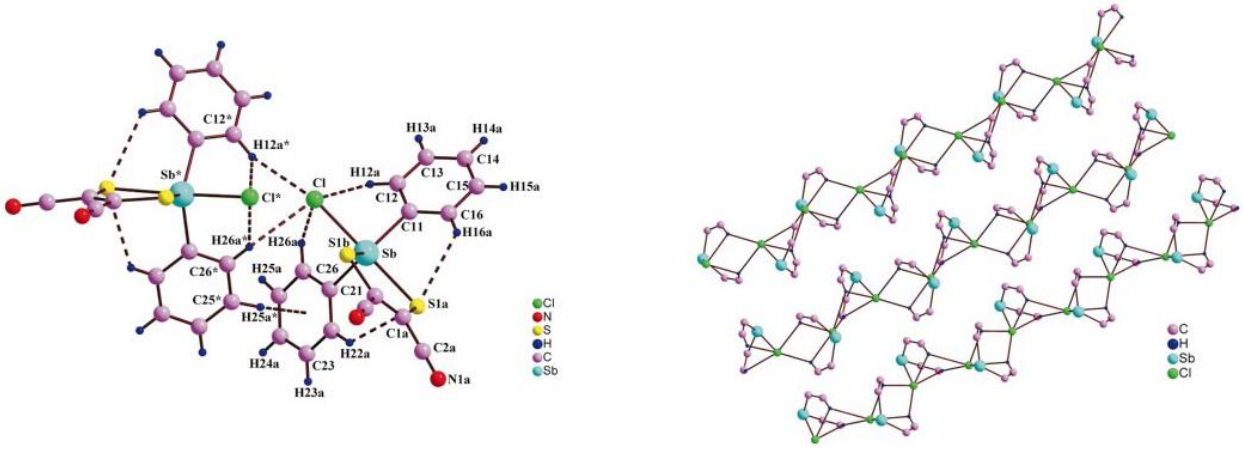

Figure 16. Left: molecular structure of $[Ph_2Sb(Cl)\{S_2C_2(CN)_2\}]$ showing all the intra- and intermolecular C–H···Cl, C–H···S and C–H···π contacts by considering a dimeric unit. Right: the zig-zag polymeric network of $[Ph_2Sb(Cl)\{S_2C_2(CN)_2\}]$ in a ball-and-stick model.

As an example, weak intramolecular coordinations of the pendant CH_2NMe_2 groups to the bismuth atom have been established for a few low-valent organobismuth compounds such as *cyclo*-R_4Bi_4, $RBi[W(CO)_5]_2$, and R_4Bi_2 [R = 2-$(Me_2NCH_2)C_6H_4$].[7] The 2-$(Me_2NCH_2)C_6H_4$ groups act as bidentate chelating ligands with weak N↔Bi intramolecular interactions.

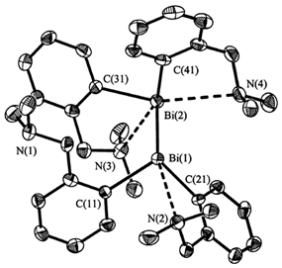

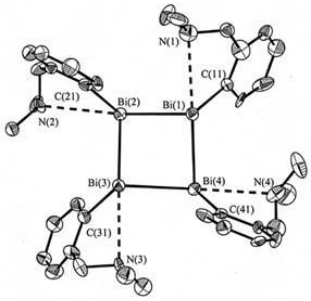

"*The importance of weak hydrogen bonds in the context of crystal engineering, molecular recognition and supramolecular chemistry have been well recognized in recent years.*[8] *Also, these secondary interactions have ramifications in the systematic design of new materials processing novel chemical, magnetic, optical or electronic properties.*[8b,c] *Such studies are still in their infancy with respect to heavier main group compounds involving Groups 14 and 15 elements...*"

V. Chandrasekhar et al., *CrystEngComm*, 2001

4.3.4 X-ray crystal structures of [Cp*BiBr$_2$] and [Cp*BiI$_2$]

Single crystals of [Cp*BiBr$_2$] (**2**) and [Cp*BiI$_2$] (**4**) suitable for X-ray structure determination were isolated from a CH_2Cl_2 solution and a toluene/thf mixture at –20°C, respectively. The compounds **2** and **4** crystallize in the orthorhombic crystal systems, space groups $P2_12_12_1$, $Z = 4$. **2** and **4** are polymers in the crystal state and contain no solvent molecules. The molecular units Cp*BiBr$_2$ and Cp*BiI$_2$ in the solid state structures of **2** and **4**, respectively, are illustrated in Figures 17 – 18 and shall be discussed first.

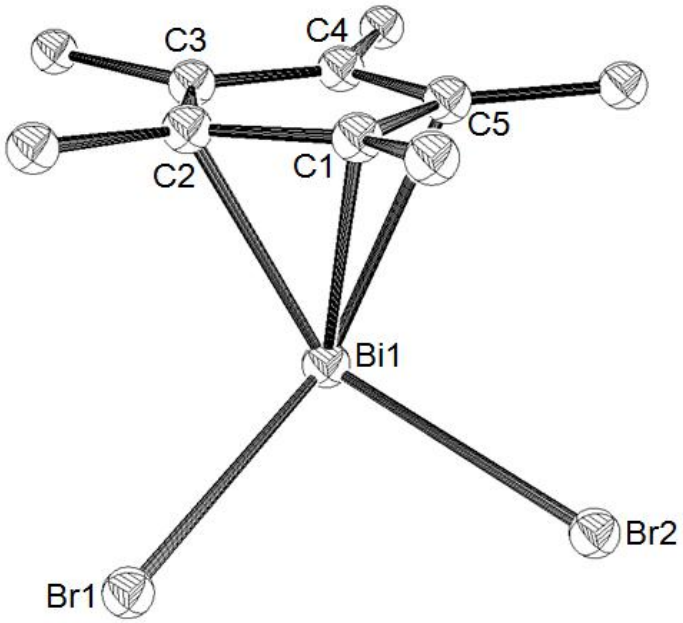

Figure 17. Molecular structure of Cp*BiBr$_2$ (**2**; crystal; the ellipsoids are given at the 30% probability level; hydrogen atoms are omitted for clarity). Selected bond lengths [pm] and angles [°]: Bi1–Br1 286.4(1), Bi1–Br2 281.5(1), Bi1–C1 246.6(8), Bi1–C2 258.4(8), Bi1–C3 277.1(8), Bi1–C4 275.4(8), Bi1–C5 256.0(8), Bi1–Z 233.4(4), Z–(Br1–Br2)$_{line}$ 400.3(5), Br1–Bi1–Br2 84.6(6), Z–Bi1–(Br1–Br2)$_{line}$ 129.0(1).

The most interesting features of discrete Cp*BiBr$_2$ and Cp*BiI$_2$ is that the BiX$_2$ (X = Br, I) group is π bonded to the Cp* ring. Although the pentamethylcyclopentadienyl bismuth complexes in solutions (according to the NMR data) and in the gas phase (according to the quantum chemical calculations) are η^1-bonded Cp* compounds, on the basis of the observed Bi–C_{ring} distances lying outside of the sum of the covalent radii for these two elements ($\Delta\Sigma r_{cov}$ = 229 pm), the Cp*–Bi bonding in Cp*BiX$_2$ can be regarded here as weak π-interaction in η^3 coordination mode for X = Br and η^2 this one for X = I.

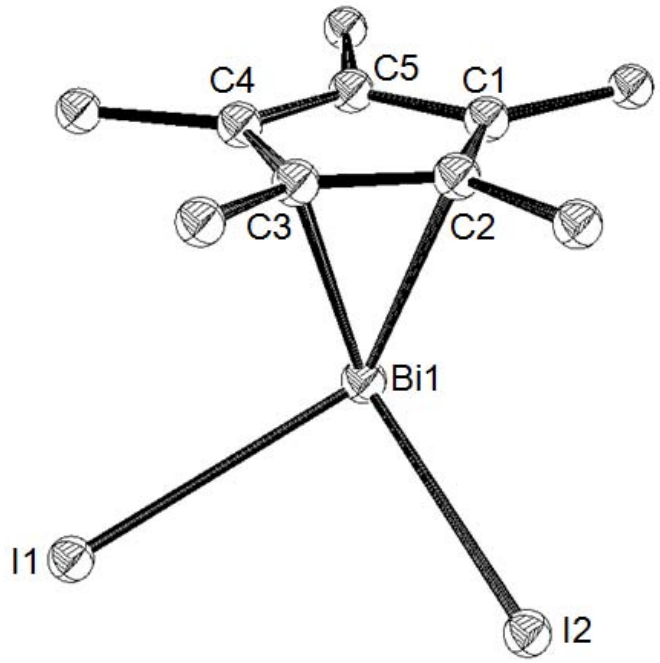

Figure 18. Molecular structure of Cp*BiI_2 (**4**; crystal; the ellipsoids are given at the 30% probability level; hydrogen atoms are omitted for clarity). Selected bond lengths [pm] and angles [°]:Bi1–I1 315.9(4), Bi1–I2 301.8(4), Bi1–C1 268.6(4), Bi1–C2 254.1(4), Bi1–C3 253.1(4), Bi1–C4 266.8(5), Bi1–C5 274.2(3), Bi1–Z 235.0(3), Z–$(I1–I2)_{line}$ 416.9(5), I1–Bi1–I2 85.7(3), Z–Bi1–$(I1–I2)_{line}$ 129.2(5).

The determination of η^x-coordination in these compounds is in line with a concept of Sitzmann et al. for the cyclopentadienyl-substituted bismuth halides.[9] According to this concept, an approximately symmetric position of the Bi atom straight below the top corner can be regarded as η^3 coordination, whereas a significant shift of the central atom to one side indicates η^2 coordination (Figure 19). Thus, the distance patterns in Cp*$BiBr_2$ molecular units of **2** with three shorter and two longer distances may be interpreted as η^3 coordinations, whereas the distance pattern in Cp*BiI_2 unit of **4** with two shorter and three longer distances resembles η^2 coordination. The Cp* ring centroid–metal bond distances (Bi–Z) are 233.4 pm (unit of **2**) for X = Br and 235.0 pm for X = I.

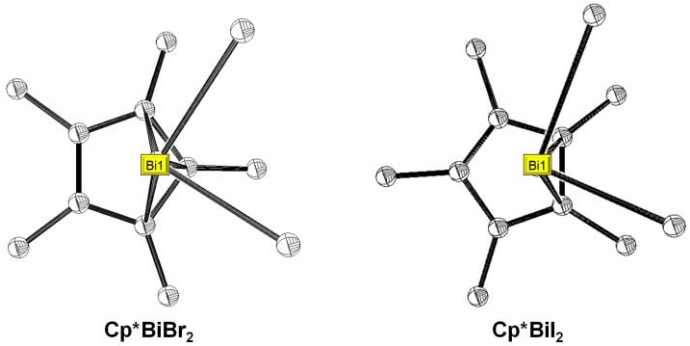

Figure 19. Projection of the central bismuth atom on the five-membered ring plane for compounds Cp*BiX_2.

One more interesting feature of Cp^*BiI_2 is its Bi–I bond lengths. Thus, two Bi–I bond distances, where $d_{Bi1–I1}$ = 315.9 pm and $d_{Bi1–I2}$ = 301.8 pm, are not equivalent (Figure 18). This is a consequence of formation of the polymer sheets.

The $\eta^1 \rightarrow \eta^2$ haptotropic phase shift (gas phase/solution → solid state) as well as non-equivalent Bi–I distances in Cp^*BiI_2 molecular unit is related to that the crystals of **4** consist of Cp^*BiI_2 molecules that are associated into $[Cp^*BiI_2]_\infty$ zig-zag chain built through intermolecular interactions of Cp^*BiI_2 units via Bi–I···Bi bridges involving both iodine atoms of the molecular unit (Figure 20). Furthermore, the Bi–I bond lengths are related also to those of the corresponding Bi···I semibonding distances in the Bi–I···Bi connectivities, i.e. shorter Bi–I bonds correspond to longer Bi···I distances and vice versa.

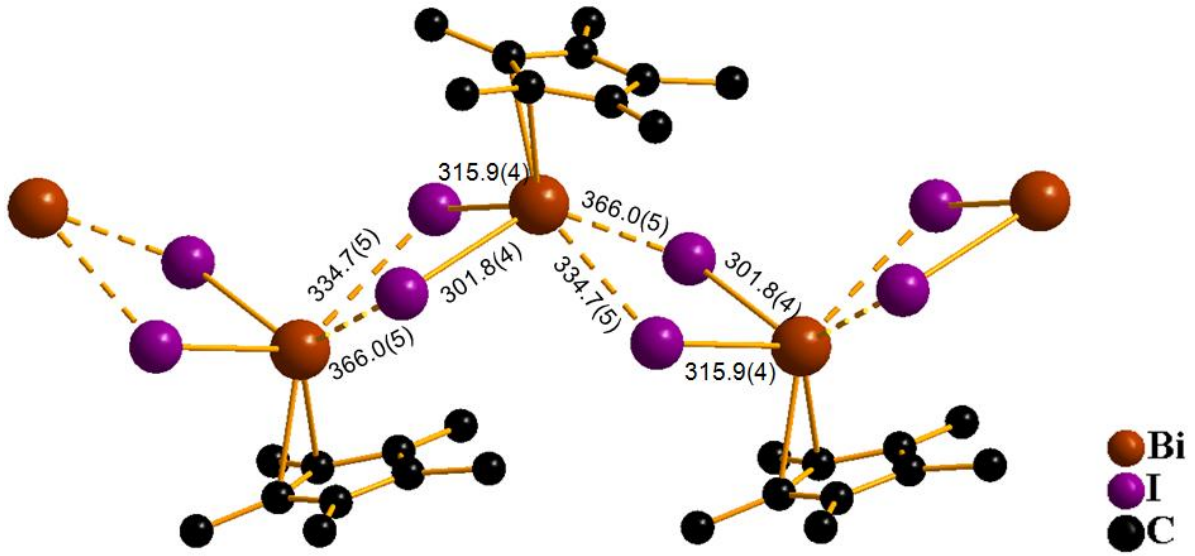

Figure 20. Slice of polymeric association in the crystal of **4** (hydrogen atoms are omitted for clarity).

Such behavior of **4** can compare as far as possible with that one of $[(C_5iPr_4H)BiI_2]$ complex observed by Sitzmann et al.[10] where the latter displays dimeric structure with two bridging and two terminal halogeno ligands and η^3-coordination of the cyclopentadienyl rings. The coordination geometry around Bi can be described as distorted tetrahedral, there. The Bi–I bond distance is shorter for the terminal ligand than for the bridging one. Thus, the Bi–μ_1-I distance in $[(C_5iPr_4H)BiI_2]$ is 291.1 pm and the Bi–μ_2-I distances are 301.7 and 345.6 pm, there. The Bi–μ_2-I distances in **4** are pointed in Figure 20.

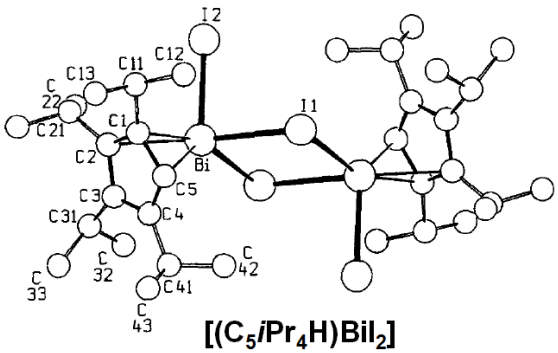

$[(C_5iPr_4H)BiI_2]$

The similar behavior to **4** can be found in complex [$(C_5H_5)BiCl_2$] observed by Frank (Figure 21).[11] However, the main structural features of **4** and [$(\eta^2/\eta^3\text{-}C_5H_5)BiCl_2$] are different. These differences are expressed in η-bonding modes the cyclopentadienyl ligands and coordination environment around the bismuth centers. The latter seems to be very interesting feature of such zig-zag chain compounds. Here, whereas **4** displays distorted square pyramidal coordination polyhedron around the Bi atom, [$(C_5H_5)BiCl_2$] exhibits ψ-octahedral this one. Thus, the solid-state structures of **4** and [$(C_5H_5)BiCl_2$] can be considered as 1D coordination polymer network.

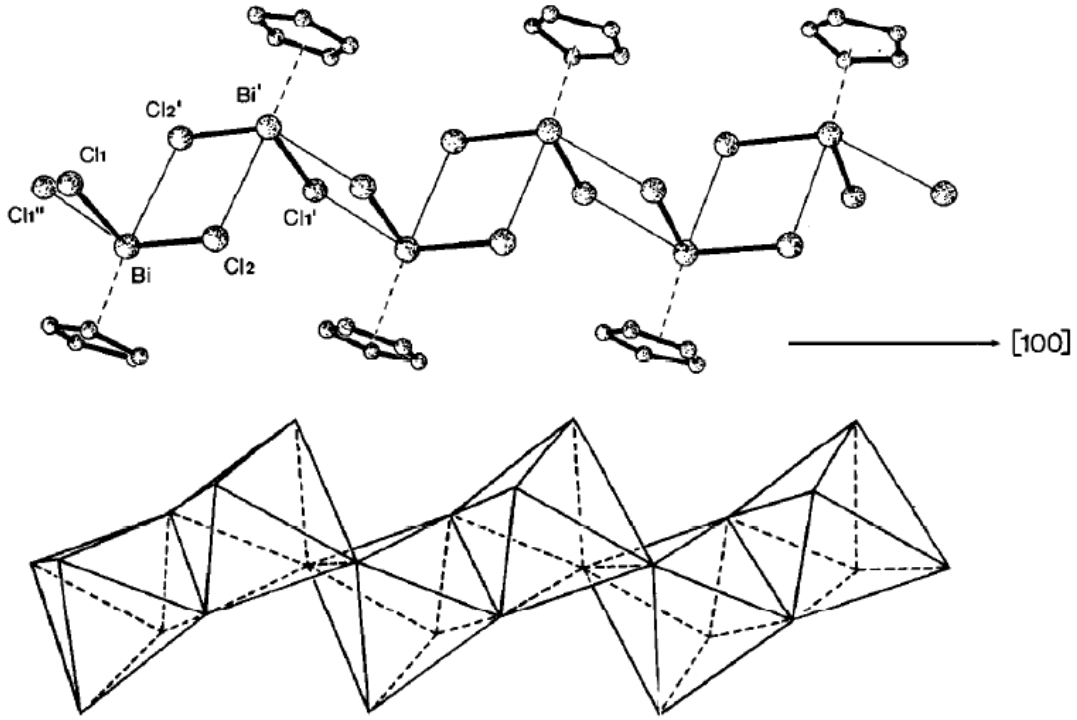

Figure 21. Slice of polymeric association in the crystal of [$(C_5H_5)BiCl_2$] (hydrogen atoms are omitted for clarity). [Reprinted from ref. 11.]

The solid-state molecular structure of **2** shows zig-zag polymeric network based on two different types of intermolecular interaction. Here, the linking chains $[Cp^*BiBr_2]_\infty$ are built through (i) intermolecular interactions of Cp^*BiBr_2 units via Bi–Br···Bi bridges involving both bromine atoms of the molecular unit and (ii) intermolecular CH···Br interactions where one bromine atom of Cp^*BiBr_2 is involved in contact with one hydrogen atom of the Cp* substituent at $BiBr_2$ ion of another unit (Figure 22). The H···Br distances of 286.5 pm are shorter than the sum of the van der Waals radii for H and Br ($\Delta\Sigma r_{vdW}$ = 305 pm) and can thus be classified as belonging to the intermediate contacts (see 4.3.5). In addition, the $\eta^1 \rightarrow \eta^3$ haptotropic phase shifts (gas phase/solution → solid state) in Cp^*BiBr_2 units are directly related to two above-described types of polymeric association in the crystal of **2**.

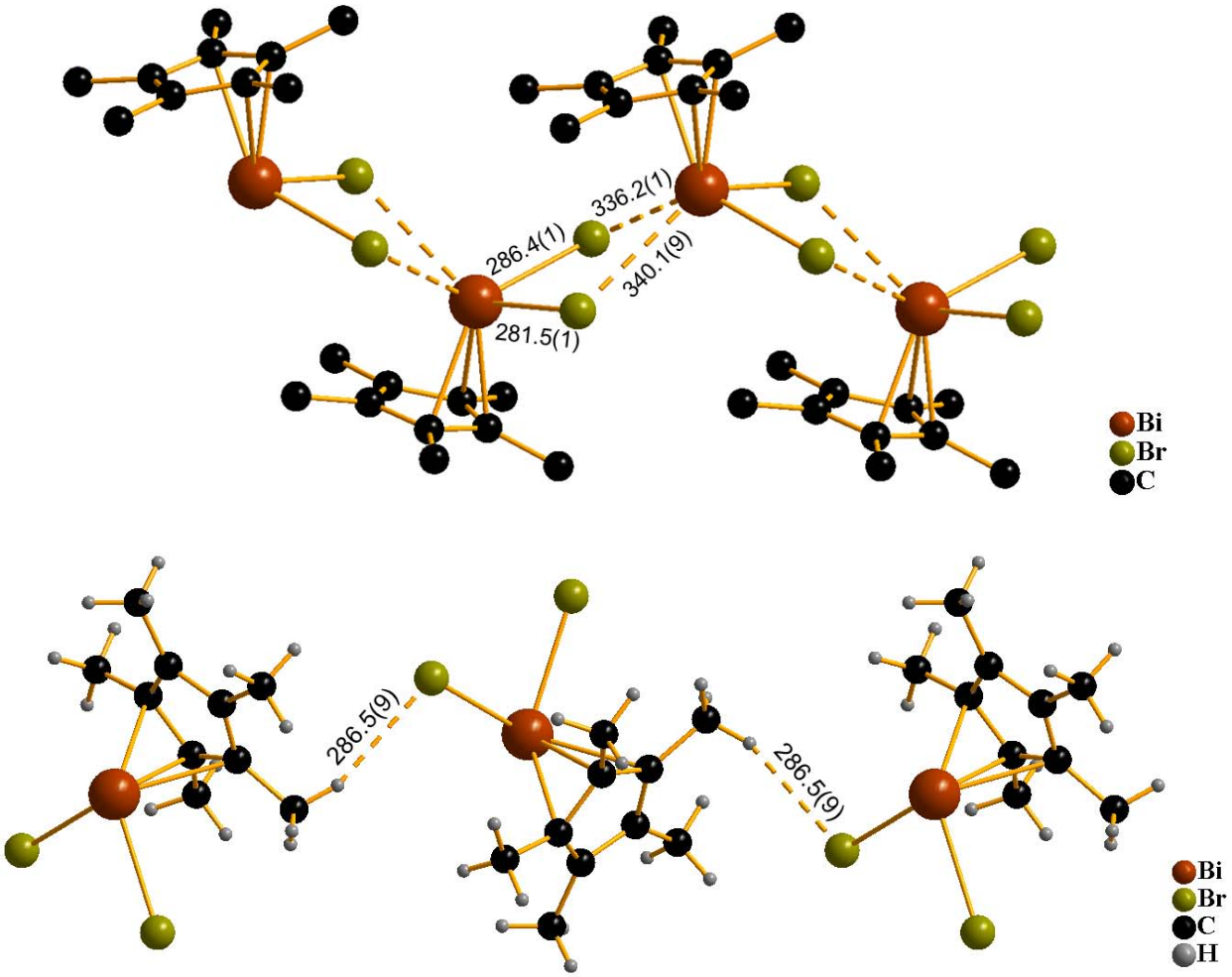

Figure 22. Slice of arrangements of zig-zag polymeric network in the crystal of **2**: intermolecular interactions of Cp^*BiBr_2 units via Bi–Br···Bi bridges (top; hydrogen atoms are omitted for clarity) and intermolecular CH···Br interactions (bottom).

The space-filling models of polymeric association in the crystals of $[Cp^*BiX_2]$ complexes (X = Br, I) are depicted in Figures 23 – 24.

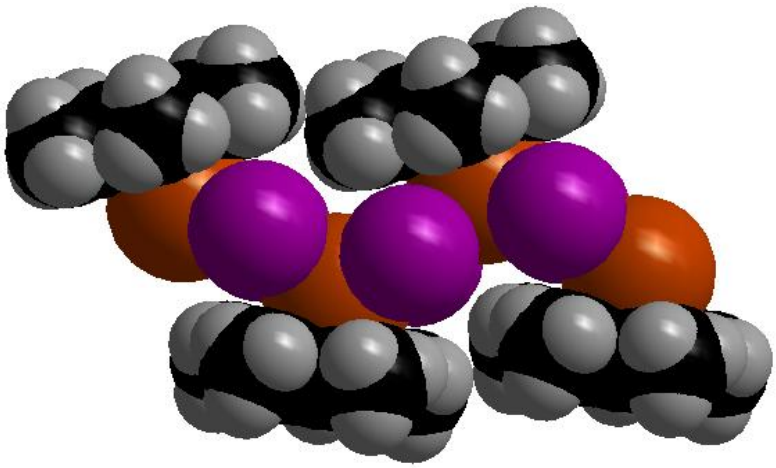

Figure 23. Space-filling model slice of polymeric association in the crystal of **4**.

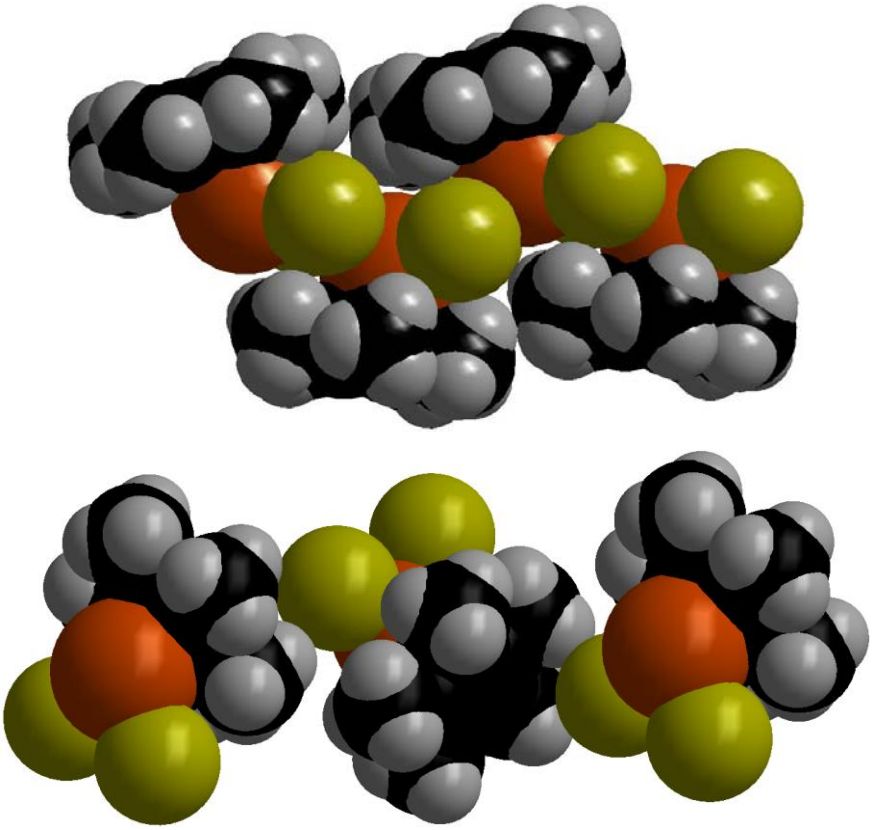

Figure 24. Space-filling model slice of arrangements of zig-zag polymeric network in the crystal of **2**: intermolecular interactions of Cp^*BiBr_2 units via Bi–Br···Bi bridges (top) and intermolecular CH···Br interactions (bottom).

4.3.5 Quantum chemical description of Cp^*BiX_2 units (X = F, Cl, Br, I)

Herein, an additional computational study on Cp^*BiX_2 units was performed. The nature of the chemical bonding in a series of pentamethylcyclopentadienyl bismuth(III) dihalides Cp^*BiX_2 (X = F, Cl, Br, I) was examined with DFT and *ab initio* methods to give a more reach insight into the causes of formation of solid state molecular structures of pentamethylcyclopentadienyl bismuth complexes **1** – **4**. Thus, Cp^*BiX_2 (X = F, Cl, Br, I) units were considered as the building blocks of all observed complexes. DFT minima structures of those indicate that their bismuth atoms display a pyramidal coordination environment with η^1-coordination of Cp* (Table 6, Figure 25).

The Bi–C_1 and Bi–X distances are elongated upon traveling downward within group X. An increase of the sum of angels at the bismuth centre (Bi^{sum}) and an increase in pyramidalization with increasing halogen size are observed. The regularity in elongation of the Bi–Z distance and decrease in the β angle are broken by Cp^*BiBr_2 unit. The distances of C_2–C_3 and C_4–C_5 (~ 139 pm) show a slight diene distortion of the Cp* ring. Therefore, the interactions of the bismuth atom with the C_2 and C_5 carbons are not regarded as bonding. In this manner, the Cp* ring is

attached via a $\eta^1(\pi)$-bonding mode, Bi–C_1. To evaluate the nature of these Bi–C_1 bonds in Cp*BiX_2 units, the natural bond orbital (NBO) analysis was performed (Table 6).

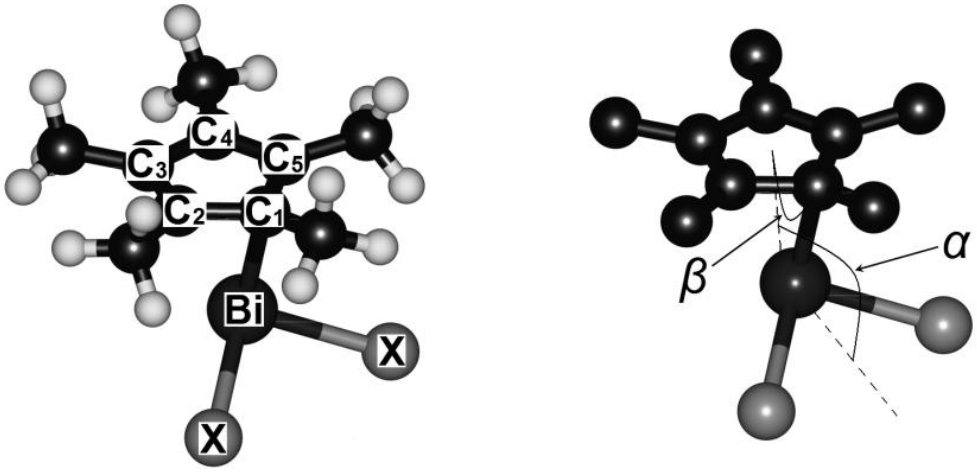

Figure 25. PBE0/TZVP optimized structures of the complexes Cp*BiX_2 (X = F, Cl, Br, I) in bent conformation where the bismuth atom is bonded to the Cp* ring in a "monohapto" fashion. Right the angels α and β are mapped on the model complex (Me atoms are omitted for clarity).

Table 6. Selected structural parameters (bond lengths in pm and bond angles in degrees) of the complexes Cp*BiX_2 (C_s symmetry) calculated at the PBE0/BS-I level of theory.

Parameter	Cp*BiX_2, X =			
	F	Cl	Br	I
Bi–Z	246.6	247.8	247.2	248.8
Bi–C_1	234.8	236.7	238.1	238.9
Bi–$C_{2,5}$	265.9	267.8	267.9	269.3
Bi–X	204.4	250.1	266.4	287.5
Bi^{sum}	283.7	293.1	297.2	299.1
α	127.8	133.3	136.0	137.3
β	80.7	80.5	79.6	80.0
$d_{Cp^*-X_2}$[a]	352.1	385.5	397.5	414.3

[a] Interplane distance between the Cp* plane and X–X line.

The natural population analysis (NPA) for the pentamethylcyclopentadienyl bismuth(III) dihalides shows that the bismuth atom has not an idealized $6s^26p^0$ electronic configuration (in the ^1S ground state), but a partial occupied sp-hybrid with increased electron density in the 6p orbitals upon travelling downward within group X. In accordance with the NEC (Table 7) the 6s electrons of Bi are almost completely localized; therefore, the contribution to covalent attraction

is mainly due to participation of its 6p orbitals. This result lies in line with the charge distribution within the complexes.

Thus, the positive partial charge is located on the bismuth atom and is far less than its chemical valence of +3 in the ionic model. Most of the negative charge in the Cp* ring is located on the C_1 carbon (~ –0.3), whereas the other four exhibit the same charge values (~ –0.1). It makes the charge transfer between the C_1 carbon atom and the bismuth ion and proves the existence of the sole Bi–C_1 coordination bond. This bond becomes stronger with increasing halogen size according to the WBI values. As consequence, the ionic character of the Bi–C_1 bond decrease in the same direction, according to the NPA charges (Table 7). The NBO analysis for Cp*BiX_2 (X = F, Cl, Br, I) finds one sp-hybridized lone pair orbital localized at the bismuth atom. This lone pair is predominantly of s type (~ 90 %). The large contribution of the s orbital part in the lone pair indicates a low basicity of the bismuth coordination centre via this one. The bonding nature of the Bi–C_1 bond determines a presence or an absence of the lone pair on the C_1 carbon atom. According to the NBO analysis (Table 7) for the complexes where this lone pair is appeared, it is of p type (~ 95 %). A presence of the lone pair on C_1 does not quite affect diene distortion in the Cp* ring. Furthermore, the lone pairs of Bi and C_1 contribute in the Bi–C_1 interaction. Thus, the lone pair of the C_1 carbon atom interacts with antibonding orbitals located at the bismuth centre. Such delocalization of the lone pair orbital of C_1 into unoccupied 6p orbitals of Bi makes the main contribution to the Bi–C_1 interaction. Not less important delocalization in the Bi–C_1 relation region comes from the interaction between the lone pairs of Bi and C_1 (Table 7). Such above-described Bi–C_1 relations are characteristic for the complexes Cp*BiX_2 (X = Cl, Br). A predominantly ionic character of the Bi–C_1 bonding (X = Cl) provides a forming the ionic complex in the solid state, whereas equilibrated nature of Cp*–$BiBr_2$ bonding makes available the formation of charge-neutral and ionic species (Scheme 5). On the base of the NBO analysis, the strong ionic Bi–C_1 bond (70.2 %) in the Cp*BiF_2 complex suggests another mechanism of the Bi–C_1 interaction and namely radical. For the Cp*BiI_2 complex with a predominantly covalent character of the Bi–C_1 bonding, the latter mainly forms from p orbitals of both Bi atoms, according to the natural hybrid orbitals (NHOs). As a consequence, this results in the charge-neutral complex in the solid state, only (Scheme 5).

It is necessary to remark that a presence of the high degree of ionicity in all of these complexes may be related to van der Waals (vdW) interactions between ligand parts of those. The inter-plane distances $d_{Cp^*–X_2}$ are much longer than the corresponding sums of vdW radii that reveals that vdW repulsions outweigh vdW attractions.

Table 7. Selected data obtained from the NBO analysis at the MP2(full)/BS-III//PBE0/BS-I level.

Parameter		$(C_5Me_5)BiX_2$, X =			
		F	Cl	Br	I
NEC[a] of Bi		$6s^{1.83}6p^{1.04}$	$6s^{1.86}6p^{1.47}$	$6s^{1.87}6p^{1.60}$	$6s^{1.88}6p^{1.83}$
Q_{NPA}[b]	on Bi	+2.107	+1.641	+1.495	+1.247
	on C_1	–0.351	–0.319	–0.302	–0.290
i_{C1-Bi}[c]		70.2	54.7	49.8	41.6
WBI_{C1-Bi}[d]		0.417	0.474	0.477	0.492
LP NHO at Bi[e]		$s^{89.41\%}p^{10.56\%}$	$s^{90.07\%}p^{9.91\%}$	$s^{90.95\%}p^{9.04\%}$	$s^{90.75\%}p^{9.24\%}$
LP NHO at C_1[e]			$s^{4.82\%}p^{95.04\%}$	$s^{4.92\%}p^{94.95\%}$	
$E_{deloc}(LP_{C1} \rightarrow p_{Bi})$[f]			260.90	281.05	

[a] Natural electron configuration. [b] Natural charges [e]. [c] Degree of ionicity of Cp*–Bi bonding [%]. [d] Value of Wiberg bond index for Bi–C_1 bonding. [e] Lone pair natural hybrid orbital at the Bi and C_1 atoms. [f] Delocalization energy of LP_{C1} into Bi 6p orbital [kcal/mol].

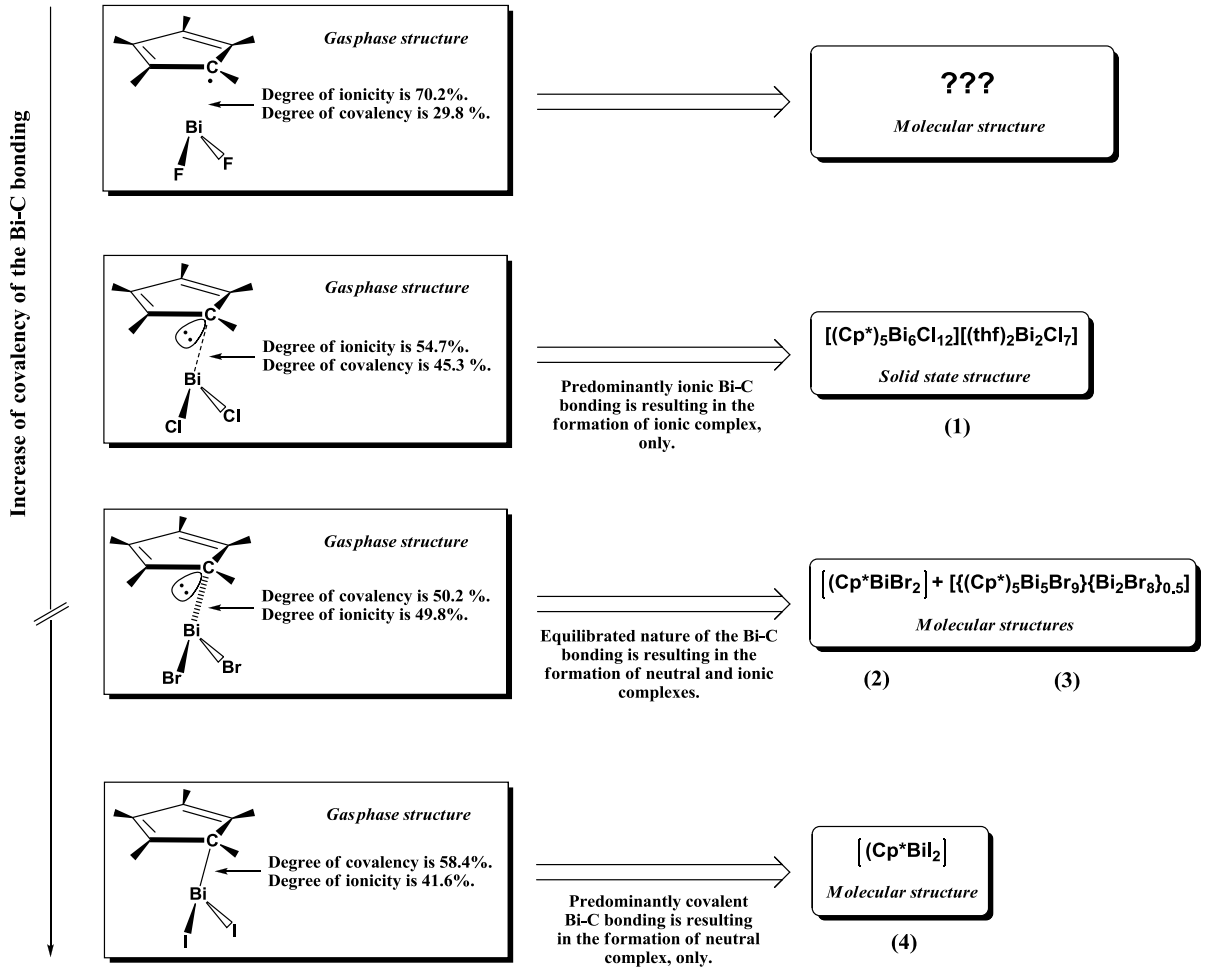

Scheme 5. Principles of forming complexes **1** – **4** with the dual nature of the chemical bonding.

4.3.6 Conclusions

By the reaction of BiX_3 (X = Cl, Br, I) with LiCp* in a 1:1 ratio, the formation of unprecedented pentamethylcyclopentadienyl-substituted bismuth halide complexes **1** – **4** was observed. Each of these displays unique structural and bonding features which generate the considerable interest in terms of polynuclear bismuth chemistry, supramolecular chemistry and crystal engineering. The high fluxionality of all of these compounds depending on halogen X atom was observed. It was well-demonstrated that the bromine as a substituent at the Bi atom is a real "star" in the cyclopentadienyl bismuth chemistry. The Cp*−BiX_2 bond hapticity changes were established in solutions, in the solid states and in the gas phases. The units Cp*BiX_2 (X = Br, I) can be regarded as very useful synthons for syntheses of novel organobismuth compounds and polynuclear bismuth complexes. The integrity of collected experimental and theoretical data for this class of compounds allows answering many questions in this area of chemistry concerning the geometric and electronic structure, the chemical bonding and the intramolecular and intermolecular interactions. The bismuth cage chemistry has taken one step forward once again.

4.3.7 References

[1] (a) D. Loos, E. Baum, A. Ecker, H. Schnöckel, A. J. Downs, *Angew. Chem. Int. Ed.* **1997**, *36*, 860; (b) O. T. Beachley, Jr., R. Blom, M. R. Churchill, K. Faegri, Jr., J. C. Fettinger, J. C. Pazik, L. Victoriano, *Organometallics* **1989**, *8*, 346.

[2] (a) M. Ruck, *Z. Anorg. Allg. Chem.* **2000**, *626*, 14; (b) R. B. King, *Dalton Trans.* **2003**, 395.

[3] M. Ruck, *Z. Anorg. Allg. Chem.* **1997**, *623*, 1591.

[4] G. Aullon, D. Bellamy, L. Brammer, E. A. Bruton, A. G. Orpen, *Chem. Commun.* **1998**, 653.

[5] V. Chandrasekhar, V. Baskar, S. Kingsley, S. Nagendran, R. J. Butcher, *CrystEngComm.* **2001**, *17*, 1.

[6] M. Freytag, P. G. Jones, *Chem. Commun.* **2000**, 277.

[7] L. Balázs, H. J. Breunig, E. Lork, C. Silvestru, *Eur. J. Inorg. Chem.* **2003**, 1361.

[8] (a) J. M. Lehn, *Supramolecular Chemistry*; VCH, Weinheim, **1995**; (b) D. Braga, F. Grepioni, G. R. Desiraju, *Chem. Rev.* **1998**, *98*, 1375; (c) G. R. Desiraju, *Angew. Chem. Int. Ed.* **1995**, *34*, 2311.

[9] H. Sitzmann, G. Wolmershäuser, R. Boese, D. Bläser, *Z. Anorg. Allg. Chem.* **1999**, *625*, 2103.

[10] H. Sitzmann, G. Wolmershäuser, *Chem. Ber.* **1994**, *127*, 1335.

[11] W. Frank, *J. Organomet. Chem.* **1990**, *386*, 177.

4.4 Appendix to chapter 4.2

4.4.1 ZPE corrections to the energies of the compounds $(C_5R_5)Bi$ and $(C_5R_5)BiX_2$ (R = H, Me; X = Cl, Br, I)

Table A. Zero-point corrections to the energies (ZPE) computed at the HF/BS-II//PBE0/BS-I level.

Fragment	ZPE correction, E_o [Hartree]	Fragment	ZPE correction, E_o [Hartree]
$(\eta^5\text{-}C_5H_5)Bi^{2+}$	0.088807	$(C_5H_5)Bi$	0.087287
$(\eta^5\text{-}C_5Me_5)Bi^{2+}$	0.236448	$(C_5Me_5)Bi$	0.235198
$(\eta^3\text{-}C_5H_5)Bi^{2+}$	0.087234	$(C_5H_5)BiCl_2$	0.090592
$(\eta^3\text{-}C_5Me_5)Bi^{2+}$	0.234788	$(C_5Me_5)BiCl_2$	0.238712
$(\eta^2\text{-}C_5H_5)Bi^{2+}$	0.086950	$(C_5H_5)BiBr_2$	0.089960
$(\eta^2\text{-}C_5Me_5)Bi^{2+}$	0.233207	$(C_5H_5)BiBr_2$	0.238003
$[\eta^1(\pi)\text{-}C_5H_5]Bi^{2+}$	0.087386	$(C_5H_5)BiI_2$	0.089657
$[\eta^1(\pi)\text{-}C_5Me_5]Bi^{2+}$	0.234982	$(C_5Me_5)BiI_2$	0.237670
$[\eta^1(\sigma)\text{-}C_5H_5]Bi^{2+}$	0.086640	$C_5H_5^-$	0.084060
$[\eta^1(\sigma)\text{-}C_5Me_5]Bi^{2+}$	0.233343	$C_5Me_5^-$	0.230140
$Bi_2(C_5H_5)_2$	0.176890 (*cis*)	Cl_2Bi^+	0.002093
	0.176804 (*trans*)		
$Bi_3(C_5H_5)_3$	0.266064 (*cis*)	Br_2Bi^+	0.001410
	0.266030 (*trans*)		
$Bi_4(C_5H_5)_4$	0.350410 (*cis*)	I_2Bi^+	0.001080
	0.354806 (*trans*)		

4.4.2 Vertical excitation energies of the compounds $(C_5R_5)Bi$ and $(C_5R_5)BiX_2$

Table B. Vertical excitation energies [nm] computed at the TD-PBE0/BS-II//PBE0/BS-I level.

Complex	Transition	Energy (osc. str.[a])	Orbitals	Description
$(C_5H_5)Bi$	$S_0 \rightarrow S_1$	2566 (0.0001)	H → L	$n_{Bi(p)} \rightarrow n_{Bi(p)}^*$
	$S_0 \rightarrow S_2$	532 (0.0167)	H → L+1	$n_{Bi(p)} \rightarrow n_{Bi(p)}^*$
	$S_0 \rightarrow S_3$	369 (0.0260)	H–1 → L	$\pi \rightarrow n_{Bi(p)}^*$
$(C_5Me_5)Bi$	$S_0 \rightarrow S_1$	1929 (0.0001)	H → L	$n_{Bi(p)} \rightarrow n_{Bi(p)}^*$
	$S_0 \rightarrow S_2$	518 (0.0127)	H → L+1	$n_{Bi(p)} \rightarrow n_{Bi(p)}^*$
	$S_0 \rightarrow S_3$	404 (0.0002)	H–2 → L	$\pi \rightarrow n_{Bi(p)}^*$
$(C_5H_5)BiCl_2$	$S_0 \rightarrow S_1$	290 (0.0035)	H → L	$\pi \rightarrow n_{Bi(p)}^*$
	$S_0 \rightarrow S_2$	272 (0.0165)	H–1 → L	$\pi \rightarrow n_{Bi(p)}^*$
			H → L+2	$\pi \rightarrow n_{Bi(p)}^*$
	$S_0 \rightarrow S_3$	259 (0.0023)	H → L+1	$\pi \rightarrow n_{Bi(p)}^*$
$(C_5Me_5)BiCl_2$	$S_0 \rightarrow S_1$	324 (0.0038)	H → L	$\pi \rightarrow n_{Bi(p)}^*$
	$S_0 \rightarrow S_2$	300 (0.0061)	H–1 → L	$\pi \rightarrow n_{Bi(p)}^*$
			H → L+1	$\pi \rightarrow n_{Bi(p)}^*$
	$S_0 \rightarrow S_3$	281 (0.0060)	H → L+2	$\pi \rightarrow n_{Bi(p)}^*$
$(C_5H_5)BiBr_2$	$S_0 \rightarrow S_1$	310 (0.0009)	H → L	$\pi \rightarrow n_{Bi(p)}^*$
	$S_0 \rightarrow S_2$	289 (0.0244)	H–1 → L	$\pi \rightarrow n_{Bi(p)}^*$
			H → L+2	$\pi \rightarrow n_{Bi(p)}^*$
	$S_0 \rightarrow S_3$	274 (0.0005)	H → L+1	$\pi \rightarrow n_{Bi(p)}^*$
			H–2 → L	$n_{Bi(s)} \rightarrow n_{Bi(p)}^*$
$(C_5Me_5)BiBr_2$	$S_0 \rightarrow S_1$	344 (0.0004)	H → L	$\pi \rightarrow n_{Bi(p)}^*$
	$S_0 \rightarrow S_2$	313 (0.0150)	H–1 → L	$\pi \rightarrow n_{Bi(p)}^*$
			H → L+1	$\pi \rightarrow n_{Bi(p)}^*$
	$S_0 \rightarrow S_3$	289 (0.0080)	H–2 → L	$n_{Bi(s)} \rightarrow n_{Bi(p)}^*$
			H → L+2	$\pi \rightarrow n_{Bi(p)}^*$
$(C_5H_5)BiI_2$	$S_0 \rightarrow S_1$	351 (0.0021)	H → L	$\pi \rightarrow n_{Bi(p)}^*$
	$S_0 \rightarrow S_2$	330 (0.0165)	H–1 → L	$\pi \rightarrow n_{Bi(p)}^*$
			H → L+2	$\pi \rightarrow n_{Bi(p)}^*$
	$S_0 \rightarrow S_3$	322 (0.0162)	H–3 → L+2	$n_{Bi(s)} \rightarrow n_{Bi(p)}^*$
$(C_5Me_5)BiI_2$	$S_0 \rightarrow S_1$	372 (0.0007)	H → L	$\pi \rightarrow n_{Bi(p)}^*$
	$S_0 \rightarrow S_2$	339 (0.0201)	H–1 → L	$\pi \rightarrow n_{Bi(p)}^*$
			H → L+1	$\pi \rightarrow n_{Bi(p)}^*$
	$S_0 \rightarrow S_3$	337 (0.0073)	H–3 → L+1	$n_{Bi(s)} \rightarrow n_{Bi(p)}^*$

[a] Oscillator strengths are given in parentheses.

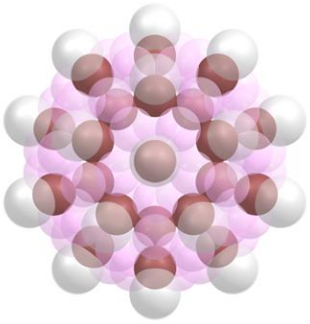

$[H_{32}Bi_{32}Li_{60}]^{4-}$

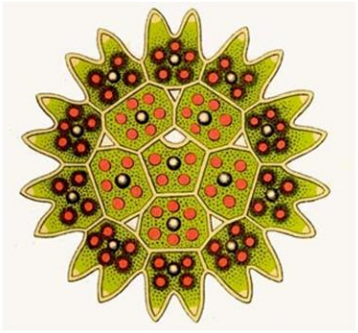

Pediastrum selenaea

Chapter 5. Icosahedral and Macroicosahedral Bismuthanediide Oligomers

5.1 Introduction

Capability of the heaviest element of the group 15 elements (bismuth) to form polyhedral cage molecules is a unique phenomenon and development in the chemistry of this main group element. Synthetic pathways to such compounds and their theoretical characterization are the main points, which excite many scientists working in this area. Although bismuth cage chemistry has been an object of intensive studies for the last two and a half decades for purely academic and practical reasons, this area is still extremely underdeveloped.

Thus, the number of bismuth compounds displaying polyhedral-cage-like shapes is rare up to now. These can be separated into two general classes, bismuth cluster polycations (examples are given in Scheme A, appendix to chapter 5) isolated in intermetallic phases (Bi_5^{3+}, Bi_5^{+}, Bi_6^{2+}, Bi_8^{2+}, Bi_9^{5+}, Bi_{10}^{4+})[1] and their ligand-stabilized forms. The latter generate the considerable interest in terms of the metal-cluster catalysis and the advanced material science (e.g. hybrid materials, drug carriers, molecular reactors, superconductors etc.).

The compounds, where the bismuth atoms are placed in such a manner to form a polyhedral cage (tetrahedron or other polyhedra), are mostly stabilized by d-transition-metal (d-TM) organometallic fragments or d-TM along with halo ligands.[2] Some polyhedral bismuth cages stabilized by organic and inorganic ligands are reported within this thesis (see chapter 4).

A few examples of the clusters, as is observed by X-ray diffraction, contain Bi_4 tetrahedra as building blocks, even though the bare tetrahedral cluster Bi_4 is a high temperature modification, which exists only in liquid or in the gas phase.[2] An octahedral Bi_6 cage stabilized by halo ligands and interstitial d-TM atom has been also observed.[3] For the bismuth's pentagonal bipyramidal (Bi_7) cage, stabilized by halo ligands and interstitial d-TM atom, Möbius aromaticity has been observed.[4] New examples of a Bi_4 stabilized by d-TM groups as well as bismuth's square pyramidal (Bi_5) *nido*-polyhedron-like and octahedral (Bi_6) deltahedron-like cages stabilized by C_5Me_5 and halo ligands in the crystal state are described herein in chapters 3 and 4. All of these above-mentioned compounds, where polyhedral bismuth cages are stabilized by inorganic and organic ligands amaze by the beauty and the difficulty to properly explain their complicated structures in terms of classic concepts of chemical bonding.

However, one of the most important developments that occurred in this area, is an observation of the bismuthanediide $[Na_x@\{(t\text{Bu}_3\text{Si})_{12}Bi_{12}Na_{20}\}]^{3-}$ (Figure 1), consisting of an endohedral ball-like $Bi_{12}Na_{20}$ cage where a Bi_{12} (I_h) icosahedron, covered by lipophilic Si*t*Bu$_3$ groups, is face-capped by 20 sodium atoms (Figure 2). This molecular assembly has been observed by Linti et al. as one of the reaction products of conversion of $BiBr_3$ with bulky sodium silanide $Na(thf)_2Sit\text{Bu}_3$.[5]

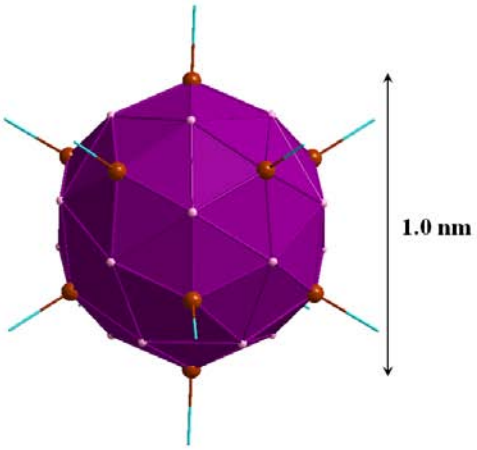

Figure 1. A perspective space-filled spherical view of the bismuthanediide-ball-like $[Na_x@\{(t\text{Bu}_3\text{Si})_{12}Bi_{12}Na_{20}\}]^{3-}$.

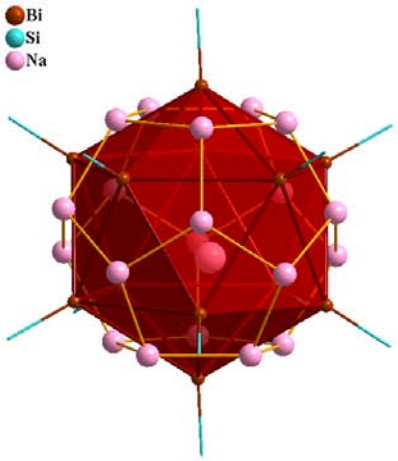

Figure 2. Topological representation of the endohedral cluster $[Na_x@\{(t\text{Bu}_3\text{Si})_{12}Bi_{12}Na_{20}\}]^{3-}$ where icosahedral $Bi_{12}(Sit\text{Bu}_3)_{12}$ subunit is capped by alkali metal shell (Na_{20}) in pentagon dodecahedral arrangement (*t*Bu-groups are omitted from the plot for clarity).

The compound $[Na_3(thf)_{14}][(t\text{Bu}_3\text{Si})_{12}Bi_{12}Na_{21}]$ is the sodium salt of an RBi^{2-} ion, which means that a highly aggregated structure can be expected. In fact, this forms an RBi dodecamer (Figure 1) in which 12 bismuth atoms and 20 sodium atoms form a ball-like cage. Of the

remaining four sodium atoms two show up as $[Na(thf)_4]^+$ and one as $[Na(thf)_6]^+$. In the structural model applied, the fourth is in a disordered position in the center of the $Bi_{12}Na_{20}$ cage (Figure 2). The disordered sodium atom takes the positions of an internal icosahedron. In the cage, 12 Bi atoms form an icosahedron ($d_{Bi–Bi}$ = 527 – 536 pm), whose faces are capped by 20 sodium atoms (Figure 2). These sodium atoms themselves form a pentagonal dodecahedron ($d_{Na–Na}$ = 351 – 363 pm). All Bi atoms are bonded to the central silicon atom of a Si*t*Bu$_3$ substituent ($d_{Bi–Si}$ = 263.7 pm on average), which is severely disordered, as usual.

As a result, this bismuthanediide displaying a sphere-like structure (!) and consisting of the largest bismuth deltahedral cage known up to now is unique in the chemistry of Bi and can be regarded as nanoscopic intermediate between molecular cluster and solid-state compound.[6]

It is necessary to remark that $(R'P)_{12}Li_{20}$ and $(R'As)_{12}R_{20}$ (R = Li, Na) compounds with an analogous arrangement of the pnicogen and alkali metal atoms as in the bismuthanediide are already known, too.[6] However, in most cases, these molecules are filled by M_nO (n = 2, 4, 6) units in the center of the cages.

Furthermore, one more unique feature of the bismuthanediide in term of «mimicry»,[7] i.e. its structural similarity with circogonia icosahedra, depicted in Ernst Haeckel's «Art Forms in Nature» (Figure 3), was observed.[8]

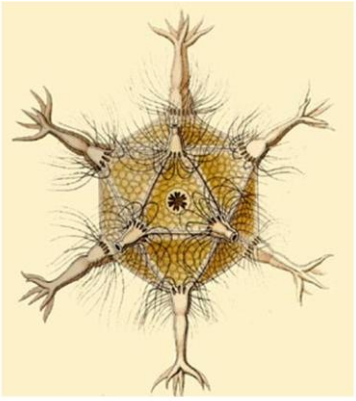

Figure 3. Circogonia icosahedra, having rigid siliceous skeletons and spicules (the image is taken from Ernst Haeckel's «Art Forms in Nature»).

The discovery of the bismuthanediide trianion $[Na_x@\{(tBu_3Si)_{12}Bi_{12}Na_{20}\}]^{3–}$ opened a new chapter in the chemistry of highly symmetric bismuth cage molecules. That is the reason why the icosahedral and macroicosahedral bismuthanediides, having a high potential to exhibit unique physical-chemical properties, are a main topic for this chapter.

5.2 A theoretical analysis of structure and electronic properties of the bismuthanediides $[H_nBi_nM_{2n–4}]^{4–}$ (n = 12, 32; R = H; M = Li) and their bismuth polycation precursors

On the basis of Wade's electron count rules and principles of isolobality and isoelectronicity, the structural and electronic relationships between highly symmetric bismuth deltahedra with I_h point symmetry and borane deltahedra as well as the fullerene polyhedra were established (Scheme 1).

Here, icosahedral Bi_{12}^{10+} of the cluster family $Bi_n^{(n–2)+}$ (see the appendix to chapter 5) is isolobal to the $B_{12}H_{12}^{2–}$ dianion and dual with a E_{20} dodecahedron, for example C_{20} [polyhedra are called

duals, where the number of vertices of one polyhedron corresponds to the number of faces of another and vice versa; see Scheme 1]. On the basis of duality of polyhedrons, Wade's electron count rules and principles of isolobality and isoelectronicity the ligand–stabilized I_h compounds $[R_nBi_nM_{2n-4}]^{4-}$ are obtained (R is an anionic $2e^-$-donor ligand; M is an alkali metal) where n = 12, 32, 92, … etc. (Scheme 1). The next members in this row are put forward by the rule for I_h symmetrical bismuthanediides, $n_{x+1} = 3n_x - 4$ where index «x» corresponds to the ordinal number of the deltahedron in the icosahedral row with the vertices 12 (x = 1), 32 (x = 2), 92 (x =3), …etc. Index «x+1» corresponds to the next member in this icosahedral row 12 (n_1) → 32 (n_2) → 92 (n_3). Thus, the experimentally unknown macroicosahedral deltahedron $[R_{32}Bi_{32}M_{60}]^{4-}$ isoelectronic to $B_{92}H_{92}^{8-}$ is the first possible this one after $[R_{12}Bi_{12}M_{20}]^{4-}$ (isoelectronic to $B_{32}H_{32}^{8-}$) to have icosahedral (I_h) symmetry. While the dualities of the truncated icosahedrons of C_{60} and C_{180} are the $B_{32}H_{32}^{8-}$ and $B_{92}H_{92}^{8-}$ octaanions,[9] respectively, the analogous structural relationships of these molecules with the macroicosahedral bismuthanediides $[R_nBi_nM_{2n-4}]^{4-}$ (n = 32, 92,… etc.) were not observed, unfortunately (Scheme 1). This is due to chemical bonding reasons where the Bi···Bi distances have clearly non-bonding character (will be discussed later), there.

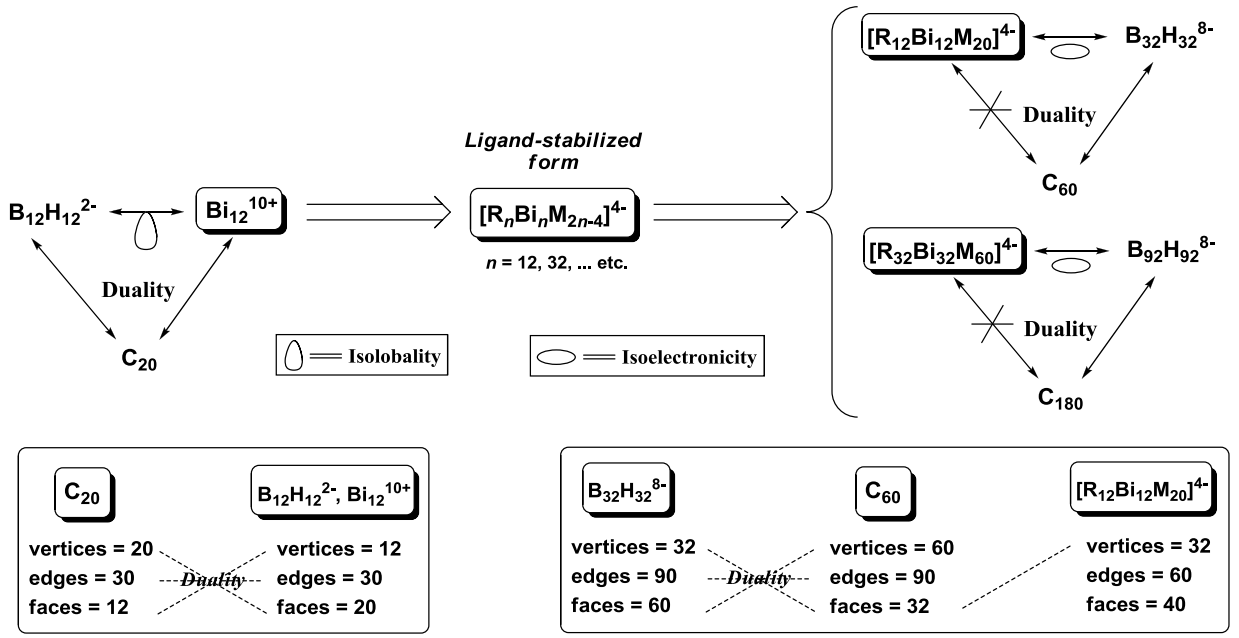

Scheme 1. Structural and electronic relationships between boron, carbon and bismuth deltahedral and polyhedral molecules.

All bismuth molecular systems, described herein, were examined theoretically using density functional theory (DFT). Although, the simplified models of $[R_nBi_nM_{2n-4}]^{4-}$ (n = 12, 32) where R is hydrogen (H) and M is lithium (Li) were used, there were shallow potential energy surfaces

that made geometry optimizations very expensive. For an explanation of the DFT optimized geometries of the bismuth polycations and their ligand-stabilized forms $[H_nBi_nLi_{2n-4}]^{4-}$ (n = 12, 32) multiple shell description[6] was applied.

According to the Wade's electron counting rule, skeletal electron count (SEC) for Bi_{12}^{10+} is 26. Hence, with 13 skeletal electrons pairs the shape of this bare polycation corresponds to a *closo*-polyhedral cluster (n+1 bonding orbitals where n = 12). As a consequence, the Bi_{12}^{10+} cluster displays an icosahedral *closo*-structure. Its ligand-stabilized form, $[H_{12}Bi_{12}Li_{20}]^{4-}$ display a sphere-like structure with 36 skeletal electrons pairs (Figure 4). The Bi···Bi distances in the latter are slightly longer than the sum of the van der Waals radii ($\Delta\Sigma r_{vdW}$ = 480 pm) and can be regarded as non-bonding. The Bi–Li contacts are longer than the sum of the covalent radii ($\Delta\Sigma r_{cov}$ = 280 pm) (Table 1) and have mostly ionic character of bonding. The Li···Li distances lie in the range of van der Waals interactions between the Li atoms ($\Delta\Sigma r_{vdW}$ = 364 pm) within Li_{20} shell. The HOMO–LUMO gaps for these two types of compounds reveal that the Bi_{12}^{10+} polycation is slightly more stable than its ligand-stabilized form (Table 1). It may be related to magnetic deshielding of latter, resulting in a positive NICS value.

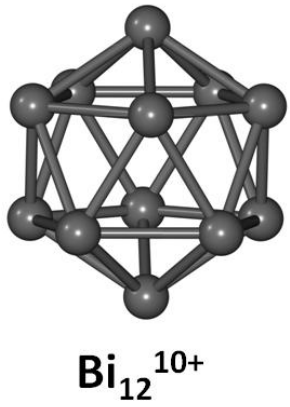

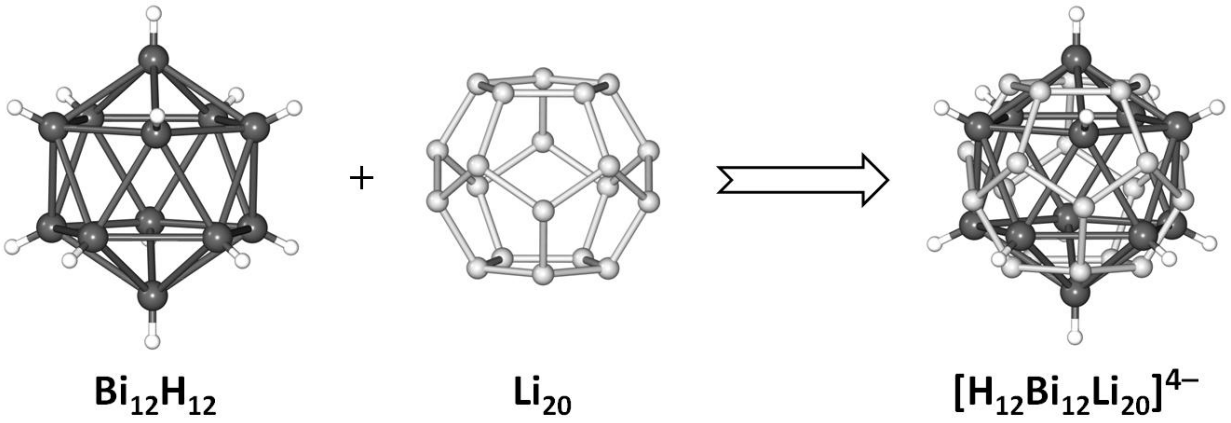

Figure 4. Topological representation of the $[H_{12}Bi_{12}Li_{20}]^{4-}$ bismuthanediide where icosahedral $Bi_{12}H_{12}$ subunit is capped by alkali metal shell (Li_{20}) in pentagon dodecahedral arrangement.

As was established by the rule for I_h symmetrical bismuthanediides, the first possible macroicosahedral deltahedron after above-considered icosahedral $[H_{12}Bi_{12}Li_{20}]^{4-}$ is the experimentally unknown $[H_{32}Bi_{32}Li_{60}]^{4-}$ with 96 skeletal electrons pairs. On the basis of multiple shell description for such structures, $[H_{32}Bi_{32}Li_{60}]^{4-}$ can be built from I_h Bi_{32} macroicosahedron, Li_{60} shell and 32 hydrogen atoms covering this deltahedron (Figure 5). The latter is a precedent for the discussion.

As is already known, the polycationic precursors for the bismuthanediides $[R_nBi_nM_{2n-4}]^{4-}$ should be submitted to the formula $Bi_n^{(n-2)+}$. Thus, Bi_{12}^{10+} is a precursor for its ligand-stabilized form $[H_{12}Bi_{12}Li_{20}]^{4-}$. A precursor for macroicosahedral $[H_{32}Bi_{32}Li_{60}]^{4-}$ should be Bi_{32}^{30+}, accordingly. However, the latter with its large delocalized charge cannot exist as isolated ion, which was confirmed by DFT optimization analysis. To reduce this charge, the twelve tops of the Bi_{32} deltahedron (built from C_{20} or $B_{32}H_{32}$) were capped by oxygen atoms to give $Bi_{32}O_{12}^{6+}$ polycation. The DFT optimized geometry of latter displayed a unique structure type, the icosahedral metalloid $Bi_{32}O_{12}^{6+}$ cluster! The Bi–Bi distances of $Bi_{32}O_{12}^{6+}$ as well as these ones of Bi_{12}^{10+} lie between the sum of the covalent radii and the sum of the van der Waals radii for the bismuth atoms. But, the bismuth-bismuth interactions in the hexacation are much stronger than these in the decacation and, as consequence the Bi–Bi distances are much shorter. Although, the negative NICS value (–13.4 ppm) at the cage center of the $Bi_{32}O_{12}^{6+}$ cluster proofs its aromaticity, this bismutoxid polycation is less stable than Bi_{12}^{10+} on the basis of calculated HOMO –LUMO gaps for these clusters (Table 1).

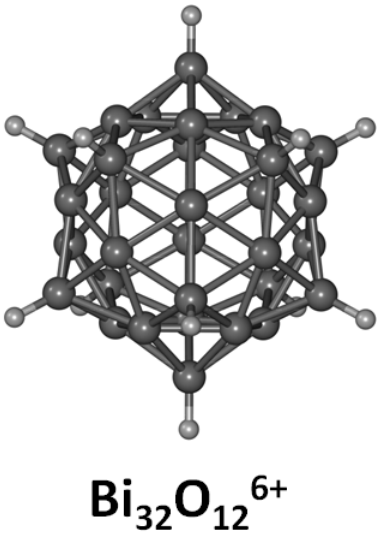

Table 1. Results for *closo*-polycations $Bi_n^{(n-2)+}$ (n = 12, 32) and non-filled *closo*-deltahedra $[H_nBi_nM_{2n-4}]^{4-}$ (n =12, 32; M = Li) with I_h point symmetry.

	Bi_{12}^{10+}	$[H_{12}Bi_{12}Li_{20}]^{4-}$	$Bi_{32}O_{12}^{6+}$	$[H_{32}Bi_{32}Li_{60}]^{4-}$
d(Bi–Bi)[a]	374.7	483.3	330.4–339.2	486.4–507.0
d(Li···Li)[a]		318.1		283.8–303.9
d(Bi–Li)[a]		290.4		277.6–296.2
Height[b]	712.7	919.3	1115.7	1578.8
Diameter[b]	606.2	782.0	949.1	1343.0
HLG[c]	2.51	2.23	1.03	2.75
Deg. of H/L[d]	3/4	3/1	3/3	3/1
NICS[e]	–0.8	+1.7	–13.4	+0.3
α[f]	85.8	197.1	283.1	376.3

[a] Bond lengths [pm] computed at the PBE0/BS-I level. [b] Height and diameter of the compounds [pm]. [c] HOMO–LUMO gap [eV] computed at the MPW1PW91/BS-II level. [d] Degeneracy of HOMO/LUMO. [e] NICS value [ppm] computed at the cage center of compound at the MPW1PW91/BS-II level. [f] Static polarizability of cage [Å^3].

The DFT optimized geometry of the nanosized macroicosahedral bismuthanediide $[H_{32}Bi_{32}Li_{60}]^{4-}$ (Figure 5) displays a relatively similar structural situation to icosahedral $[H_{12}Bi_{12}Li_{20}]^{4-}$ in regard to the chemical bonding in the sphere-like cage (Table 1). Although, the nonbonding Bi···Bi distances in deltahedron Bi_{32} of $[H_{32}Bi_{32}Li_{60}]^{4-}$ are more elongated and its Bi–Li contacts lie in limits and outside of the sum of the covalent radii for these two elements ($\Delta\Sigma r_{cov}$ = 280 pm). The Li···Li distances in the macroicosahedral bismuthanediide are more reduced in comparison to those in icosahedral $[H_{12}Bi_{12}Li_{20}]^{4-}$. One interesting feature of nonaromatic $[H_{32}Bi_{32}Li_{60}]^{4-}$ (according to the positive NICS value) is its relatively high stability (according to the HOMO–LUMO gap) (Table 1). Among all of the investigated species macroicosahedral $[H_{32}Bi_{32}Li_{60}]^{4-}$ is the most stable! Thus, an increase of this stability can be expected in the icosahedral row (the number of vertices n = 12, 32, 92, … etc.) by an enlargement of the molecular bismuthanediide system, i.e. an increase in the spherical size of Bi_nM_{2n-4} shell.

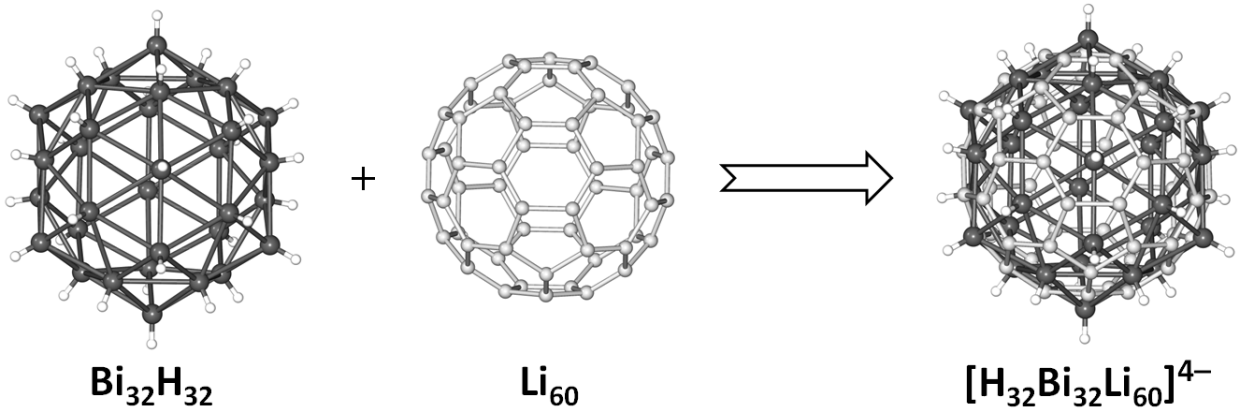

Figure 5. Topological representation of the $[H_{32}Bi_{32}Li_{60}]^{4-}$ bismuthanediide where icosahedral $Bi_{32}H_{32}$subunit is capped by alkali metal shell (Li_{60}) in pentagon dodecahedral arrangement.

One of the most important characteristics of the «empty» icosahedral and macroicosahedral bismuthanediides (as well as the I_h bismuth polycations) is their large polarizabilities, which much higher values than these ones for C_{60} (73.8 Å^3),[10] for example! On this basis, these molecular systems were tested regarding their capability to trap atoms and small molecules to generate endohedral complexes.

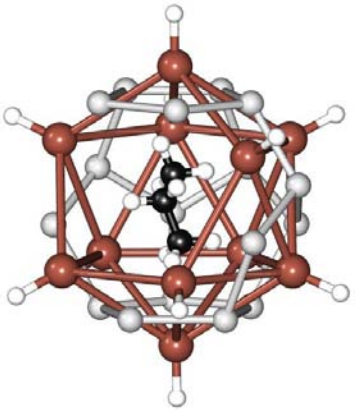

Thus, Li^+, Li_nO (n = 2, 4, 6) and propane C_3H_8 were considered as the guest molecules for icosahedral $[H_{12}Bi_{12}Li_{20}]^{4-}$ and molecular hydrogen H_2 was a guest for macroicosahedral $[H_{32}Bi_{32}Li_{60}]^{4-}$. The

DFT optimized structures of all of these endohedral complexes have shown that all encapsulated atoms or small molecules either are placed in the center of Bi_nLi_{2n-4} shell or are displaced out of the center of the shell (in case of Li^+ ion)! Some distortions of Bi_n and Li_{2n-4} shells were observed for encapsulated Li_nO (n = 4, 6). Besides, the size of the $Bi_{12}Li_{20}$ shells for the icosahedral bismuthanediide tetraanions decreases upon an encapsulation of Li^+ to give endohedral $Li@[H_{12}Bi_{12}Li_{20}]^{3-}$ trianion and increases upon an encapsulation of neutral guest molecules such as Li_2O and C_3H_8 (Table 2).

Table 2. Results[a] for endohedral complexes $\{Guest\}@[H_nBi_nLi_{2n-4}]^{q-}$ (n =12, 32; Guest = Li^+, Li_2O, $[Li_4O]^{2+}$, $[Li_6O]^{4+}$, C_3H_8, H_2).

Size of cage	*Height* [pm]	*Diameter* [pm]
$Li@[H_{12}Bi_{12}Li_{20}]^{3-}$	902.6	767.0
$Li_2O@[H_{12}Bi_{12}Li_{20}]^{4-}$	963.1	805.0
$Li_4O@[H_{12}Bi_{12}Li_{20}]^{2-}$	921.7	776.2
$Li_6O@[H_{12}Bi_{12}Li_{20}]$	936.7	746.7
$C_3H_8@[H_{12}Bi_{12}Li_{20}]^{4-}$	953.3	796.4
$H_2@[H_{32}Bi_{32}Li_{60}]^{4-}$	1576.0	1340.9

[a] Height and diameter [pm] were obtained from the calculations at the PBE0/BS-I level.

The space-filling representations of non-filled («empty») $[H_{32}Bi_{32}Li_{60}]^{4-}$ and endohedral $H_2@[H_{32}Bi_{32}Li_{60}]^{4-}$, where the encapsulated H_2 guest-molecule is placed in the center of the $Bi_{32}Li_6$ shell, are shown in Figure 6. The size of the $Bi_{32}Li_{60}$ shell slightly decreases upon an encapsulation of nonpolar H_2 molecule.

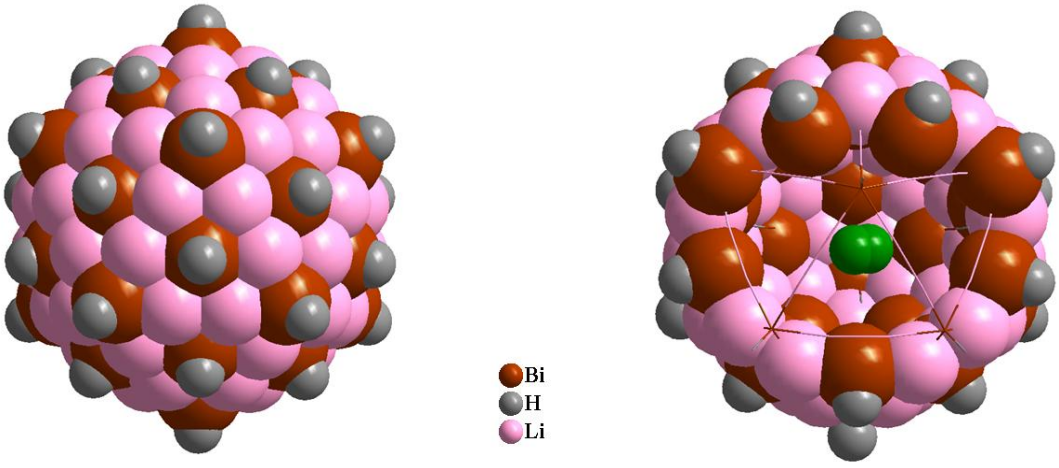

Figure 6. Space-filling model of non-filled $[H_{32}Bi_{32}Li_{60}]^{4-}$ (left) and space-filling model slice of endohedral $H_2@[H_{32}Bi_{32}Li_{60}]^{4-}$ with encapsulated H_2 (green) molecule inside the $Bi_{32}Li_{60}$ cage.

5.3 Conclusions

The synthetic availability of herein represented nanoscale molecular systems is a challenge not only in the chemistry of bismuth, but also in the chemistry of the main group elements. The obtained theoretical results, based on a discovered rule for I_h symmetrical bismuthanediides, are a good starting point to inspire the realization of such compounds experimentally and to develop efficient synthetic approaches to those.

The icosahedral and macroicosahedral bismuthanediides have a good chance to become perspective molecular containers. Their capability to trap atoms and small molecules to generate endohedral complexes should be further tested in the future. The first performed calculations already demonstrated that the icosahedral and macroicosahedral bismuthanediides act as highly polarizable spheres that may trap Li^+, Li_nO (n = 2, 4, 6), C_3H_8, and H_2 inside the cages. One experimental example of similar endohedral complex is already known, $[Na_x@\{(t\text{Bu}_3\text{Si})_{12}\text{Bi}_{12}\text{Na}_{20}\}]^{3-}$.[5] Furthermore, the capability of the highly polarizable spheres of the «empty» icosahedral and macroicosahedral bismuthanediides to trap atoms and small molecules can compare with that one of the fullerenes spheres[10,11] to generation of their endohedral complexes.

Of course, more accurate understanding structure–bonding–properties relationships of their geometric and electronic structures, chemical bonding, and electronic, spectroscopic and energy properties should be based on high-precision computational analysis, where all relativistic effects would be treated. This could lead to the development of new multifunctional materials in term of molecular containers as well as an important step forward in the questions of recognizing general bonding concepts and endohedral chemistry. In addition, it should help to identify their potential as new agents and materials for molecular electronics, nanoprobes, superconductors, and nonlinear optics. However, it is necessary to remark here that the bismuthanediide $[Na_x@\{(t\text{Bu}_3\text{Si})_{12}\text{Bi}_{12}\text{Na}_{20}\}]^{3-}$ (as an example) is a highly air-sensitive species and quickly decomposes upon exposure to moisture.

5.4 References

[1] (a) A. Hershaft, J. D. Corbett, *Inorg. Chem.* **1963**, *2*, 979; (b) S. Ulvenlund, K. Stahl, L. Bengtsson-Kloo, *Inorg. Chem.* **1996**, *35*, 223; (c) J. Beck, C. J. Brendel, L. Bengtsson-Kloo, B. Krebs, M. Mummert, A. Stankowski, S. Ulvenlund, *Chem. Ber.* **1996**, *129*, 1219; (d) M. Ruck, *Z. Anorg. Allg. Chem.* **1998**, *624*, 521; (e) M. Ruck, V. Dubenskyy, T. Söhnel, *Angew. Chem. Int. Ed.* **2003**, *42*, 2978; (f) B. Wahl, M. Ruck, *Z. Anorg. Allg. Chem.* **2009**, *636*, 337.

[2] (a) K. H. Whitmire, T. A. Albright, S.-K. Kang, M. R. Churchill, J. C. Fettinger, *Inorg. Chem.* **1986**, *25*, 2799; (b) G. Ciani, M. Moret, A. Fumagalli, S. Martinengo, *J. Organomet. Chem.* **1989**, *362*, 291; (c) M. Ruck, *Z. Anorg. Allg. Chem.* **1997**, *623*, 1591; (d) J. L. Stark, B. Harms, I. Guzman-Jimenez, K. H. Whitmire, R. Gautier, J.-F- Halet, J.-Y. Saillard, *J. Am. Chem Soc.* **1999**, *121*, 4409; (e) T. Gröer, M. Scheer, *Organometallics* **2000**, *19*, 3683; (f) M. Ruck, S. Hampel, *Polyhedron* **2002**, *21*, 651; (g) R. B. King, *Inorg. Chem.* **2003**, *42*, 8755.

[3] M. Ruck, *Z. Anorg. Allg. Chem.* **2000**, *626*, 14.

[4] (a) M. Ruck, *Angew. Chem. Int. Ed.* **1997**, *36*, 1971; (b) Z. Xu and Z. Lin, *Angew. Chem. Int. Ed.* **1998**, *37*, 1686; (c) R. B. King, *Dalton Trans.* **2003**, 395.

[5] G. Linti, W. Köstler, H. Pritzkow, *Eur. J. Inorg. Chem.* **2002**, 2643.

[6] M. Driess, *Acc. Chem. Res.* **1999**, *32*, 1017.

[7] R. C. King, W. D. Stansfield, P. K. Mulligan, *A dictionary of genetics* **2006**, 7th ed. Oxford. p. 278.

[8] E. Haeckel, *Kunstformen der Natur* **1899**, p. 396.

[9] (a) Z.-X. Wang, P. v. R. Schleyer, *J. Am. Chem Soc.* **2003**, *125*, 10484; (b) Z. Chen, R. B. King, *Chem. Rev.* **2005**, *105*, 3613.

[10] Y. H. Hu, E. Ruckenstein, *J. Am. Chem Soc.* **2005**, *127*, 11277.

[11] (a) J. Cioslowski, E. D. Fleischmann, *J. Chem Phys.* **1991**, *94*, 3730; (b) J. Cioslowski, *J. Am. Chem. Soc.* **1991**, *113*, 4139; (c) J. Cioslowski, Q. Lin, *J. Am. Chem. Soc.* **1995**, *117*, 2553.

5.5 Appendix to chapter 5

Table A. Cluster family of the bare polyhedral bismuth polycations $Bi_n^{(n-2)+}$.

$Bi_n^{(n-2)+}$	Typ of structure	Symmetry	SEC	*d*(Bi–Bi) [pm][a]	NICS [ppm][a]
Bi_4^{2+}	tetrahedron	*nido* (T_d)	10	309.0	+59.0
Bi_6^{4+}	octahedron	*closo* (O_h / D_{2d})	14	323.1	+7.7
Bi_8^{6+}	bisdisphenoid	*closo* (D_{2d})	18	315.9 – 350.5	–7.5
Bi_{10}^{8+}	bicapped square	*closo* (D_{4d})	22	345.0 – 363.1	–5.8

[a] Calculations, performed in the framework of this thesis.

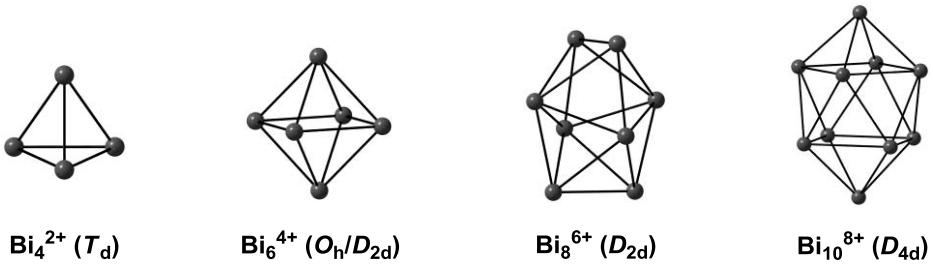

Figure A. View of the DFT optimized geometries of $Bi_n^{(n-2)+}$ clusters and their symmetries.

Some *ab initio* calculations on bismuth cluster polycations in order to investigate their general properties and the applicability of Wade's rules on bismuth polycations as well as study of the electronic excitations for the cations Bi_5^{3+}, Bi_8^{2+}, and Bi_9^{5+} have been performed relatively recently.[1]

Table B. Cluster family of the bare polyhedral bismuth polycations $Bi_n^{q\pm}$.

Bi_n	Typ of structure	Symmetry	SEC	Bond lenghts [pm]		Ref.
				PBE0/SV(P)[a]	exptl.	to exp.
Bi_4	tetrahedron	*nido* (T_d)	12	298.9		
Bi_5^+	square-pyramid	*nido* (C_{4v})	14	297.5 – 311.6	315 – 317	[2]
Bi_5^-	trigonal bipyramid	*closo* (D_{3h})	16	303.9 – 317.3		
Bi_5^{3+}	trigonal bipyramid	*closo* (D_{3h})	12	305.3 – 331.3	301 – 332	[3]
Bi_6	trigonal prism	*arachno* (D_{3h})	18	302.2 – 306.1		
Bi_6^{2+}	octahedron	*nido* (C_{2v})	16	293.3 – 326.3	317[b]	[2]
Bi_6^{2+}	pentagonal pyramid	*nido* (C_{5v})	16	294.0 – 323.2		
Bi_7^{5+}	pentagonal bipyramid	*closo* (D_{5h})	16	314.7 – 339.5		
Bi_7^+	seven-vertex	*arachno* (C_{3v})	14	302.1 – 326.9		
Bi_7^{3-}	seven-vertex	*arachno* (C_{3v})	18	291.1 – 310.4		
Bi_8	cuboid	*arachno* (O_h)	24	305.9		
Bi_8^{2+}	square antiprism	*arachno* (D_{4d})	22	308.2 – 316.1	309 – 311	[4]
Bi_9^{5+}	tricapped trigonal prism	*nido* (C_{4v})	22	319.4 – 347.3	310 – 321[c]	[5]

[a] Calculations, performed in the framework of this thesis. [b] O_h. [c] D_{3h}.

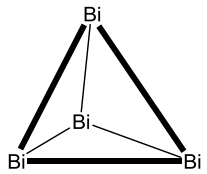

Bi_4 (T_d)

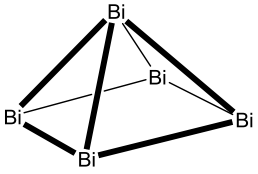

Bi_5^+ (C_{4v})

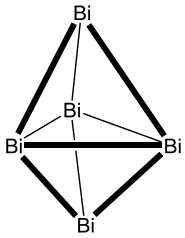

Bi_5^- (D_{3h})

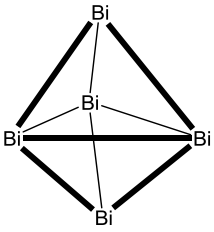

Bi_5^{3+} (D_{3h})

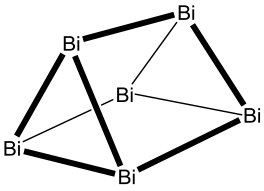

Bi_6 (D_{3h})

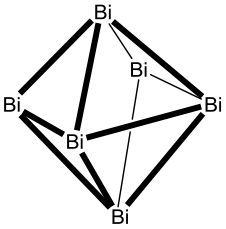

Bi_6^{2+} (C_{2v})

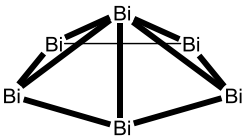

Bi_6^{2+} (C_{5v})

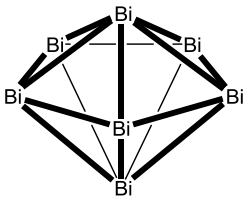

Bi_7^{5+} (D_{5h})

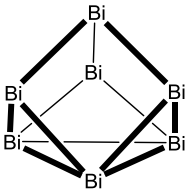

Bi_7^+ (C_{3v})

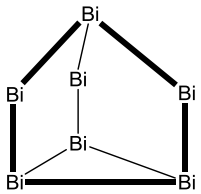

Bi_7^{3-} (C_{3v})

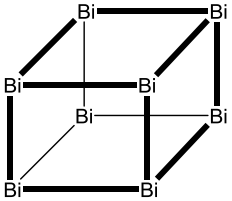

Bi_8 (O_h)

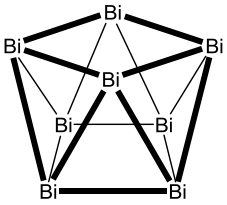

Bi_8^{2+} (D_{4d})

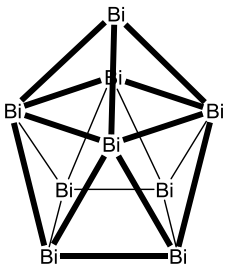

Bi_9^{5+} (C_{4v})

Scheme A. View of the DFT optimized geometries of $Bi_n^{q\pm}$ clusters.

5.6 References

[1] (a) A. N. Kuznetsov, L. Kloo, M. Lindsjö, J. Rosdahl, H. Stoll, *Chem. Eur. J.* **2001**, *7*, 2821; (b) G. M. Day, R. Glaser, N. Shimomura, A. Takamuku, K. Ichikawa, *Chem. Eur. J.* **2000**, *6*, 1078.

[2] M. Ruck, *Z. Anorg. Allg. Chem.* **1998**, *624*, 521.

[3] S. Ulvenlund, K. Stahl, L. Bengtsson-Kloo, *Inorg. Chem.* **1996**, *35*, 223.

[4] J. Beck, C. J. Brendel, L. Bengtsson-Kloo, B. Krebs, M. Mummert, A. Stankowski, S. Ulvenlund, *Chem. Ber.* **1996**, *129*, 1219.

[5] (a) A. Hershaft, J. D. Corbett, *Inorg. Chem.* **1963**, *2*, 979; (b) R. M. Friedman, J. D. Corbett, *Inorg. Chem.* **1973**, *12*, 1134.

Summary and Conclusions

Aim of this thesis was to study bismuth–silicon and bismuth–iron bonded molecules as well as bismuth cyclopentadienyl complexes and alkali metal-rich bismuth compounds experimentally and theoretically.

(A) On reaction of $BiBr_3$ with $Li(thf)_3SiPh_2tBu$ (**1**) in the corresponding ratios redox/metathesis reactions were observed, yielding dibismuthane $(tBuPh_2Si)_4Bi_2$ (**2**) and disilylbismuth halide $(tBuPh_2Si)_2BiBr$ (**3**). The latter is a reaction intermediate in the formation of the dark-red **2**. The X-ray crystal structures of **1** – **3** were determined by low-temperature X-ray diffraction. The $Si_2Bi–BiSi_2$ core of **2** is in the semi-eclipsed conformation. No oligomerization of "nonthermochromic" **2** was observed. Compound **3** is a mixed substituted monomer with a pyramidal environment around the bismuth center. On the basis of quantum chemical calculations, the formation of tertiary bismuthane $(tBuPh_2Si)_3Bi$ is not expected for steric reasons.

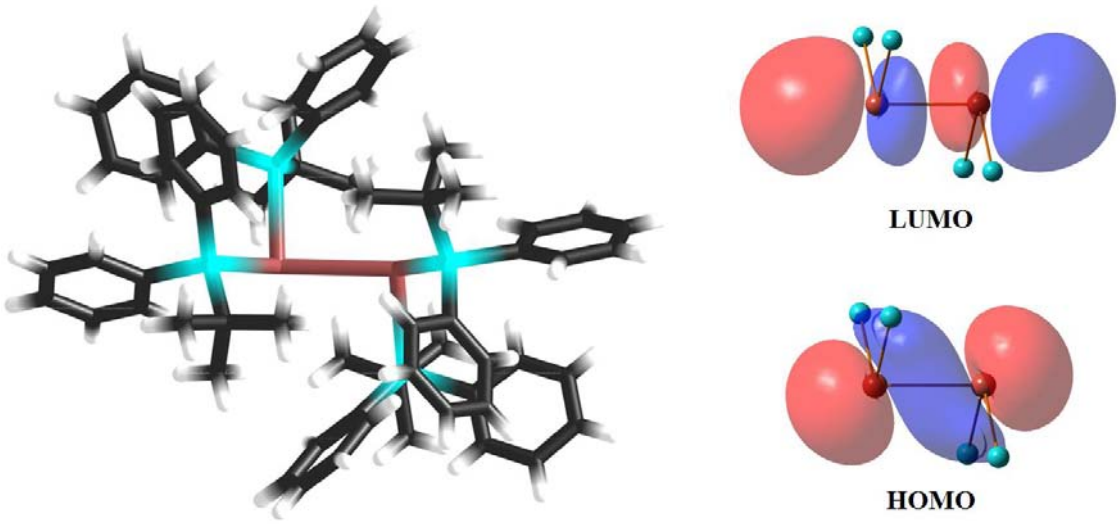

According to DFT-optimized geometries of the simplified model systems $n[(H_3Si)_2Bi]_2$ (n = 1–3), the closed-shell attraction between intermolecular Bi centers in the chain provides a moderate elongation of the intramolecular Bi–Bi bond in the dibismuthane unit and a shortening of the intermolecular Bi···Bi contacts. According to the MP4(SDQ) computations, such oligomerization is carried out by intermolecular interaction of s lone pairs that are bound together and p-type orbitals of the Bi–Bi bonds in the bismuth chain. An increase in the number of $[(H_3Si)_2Bi]_2$ molecules *per* chain results in a decrease in the HOMO–LUMO gap and leads to a bathochromic shift. TD-PBE0 computations suggest that the lowest energy electron transition in **2** is metal-metal charge transfer. In addition, the attractive contributions in the chain $[(H_3A)_2Bi]_2\cdots[Bi(AH_3)_2]_2$ with silyl groups (A = Si) outweigh the repulsion of the Bi···Bi

centers, whereas for the alkyl-substituted bismuth chain (A = C) the repulsive van der Waals force dominates. This fact makes the rectangle oligomerization model more preferred for $n[(H_3A)_2Bi]_2$ (A = C; n = 2), while for A = Si chain formation is favored in the gas phase.

(B) Reaction of *cyclo*-$Bi_4[Si(SiMe_3)_3]_4$ (**1**) with $Na_2[Fe(CO)_4]$ in the presence of nBu$_4$NCl leads to the formation of the cage compound $[n\text{Bu}_4\text{N}]_4[Bi_4Fe_8(CO)_{28}]$ (**2**). According to X-ray single-crystal structure analysis the faces of the tetrahedral Bi_4 core are capped by $Fe(CO)_3$ moieties in a μ_3 fashion to give a cubanoid Bi_4Fe_4 framework. The four $Fe(CO)_4$ fragments are μ_1-coordinated to bismuth, each. With 12 skeletal electron pairs the $[Bi_4Fe_8(CO)_{28}]^{4-}$ anion (**2a**) is a Bi_4Fe_4 cubane. The negative charge is localized within cluster **2a** according to the NBO analysis of its derivates. The strength of metal-ligand interactions Bi–μ_3-$Fe(CO)_3$ is responsible for the size of the cluster's cubic core. NICS computations at the cage centers of considered molecules show that **2a** has paratropic character, whereas removal of four μ_1-$Fe(CO)_4$ fragments from latter causes spherical aromaticity of the modified clusters $[Bi_4Fe_4(CO)_{12}]^{4-}$ (**2aa**) and $[Bi_4Fe_4(CO)_{12}]^{2+}$ (***arachno*-2ab**), mediated by a Bi_4 cluster π orbital.

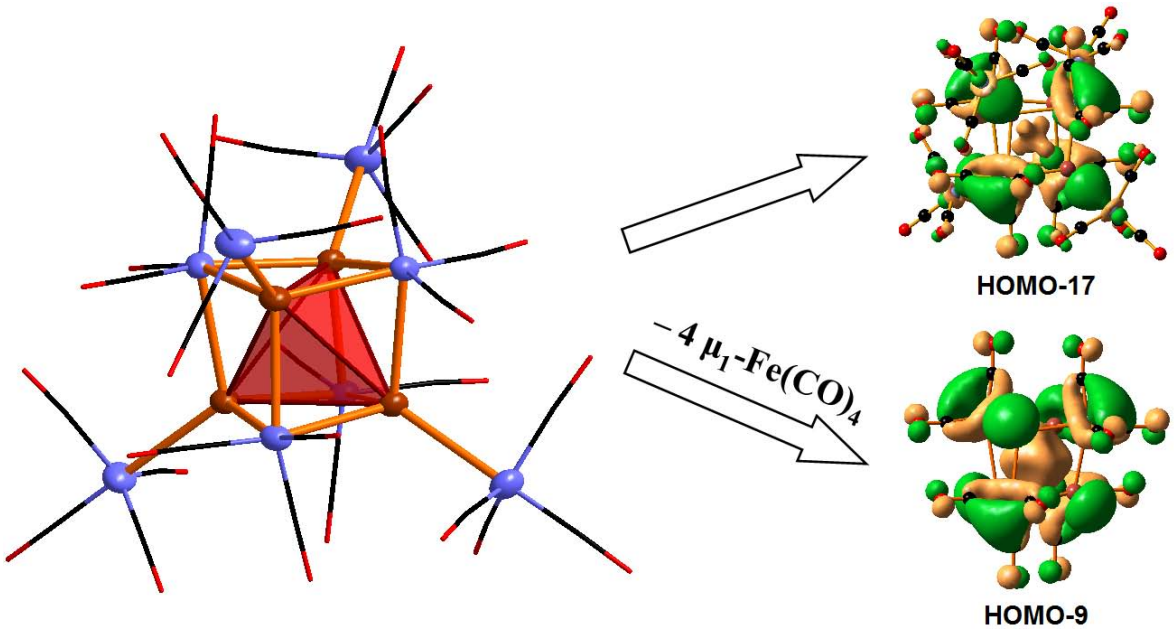

(C) The reactions of $BiBr_3$ and $(C_5Me_5)BiI_2$ with $Na_2[Fe(CO)_4]$ lead to the formation of the cluster $[Bi_4Fe_3(CO)_9]$ (**1**). According to X-ray single-crystal structure analysis, three of the four faces of the tetrahedral Bi_4 core in **1** are capped by $Fe(CO)_3$ moieties in a μ_3 fashion; the fourth is left bare. Bismuth–arene π-complexations ($d_{Bi\cdots Arene}$ = 324.8 and 342.6 pm), where two toluene molecules are attached to two Bi's tops of Bi_4 via $\eta^6(\pi)$ coordination mode [**1**·2(C_6H_5Me)], and inverted sandwich behavior in the crystal cell of latter were observed. As a result, it is one of few examples of weak intermolecular interactions of bismuth with the aromatic hydrocarbon established for its cluster compounds in the solid state. With 9 skeletal electrons pairs the cluster

1 corresponds to a *nido*-polyhedral cluster and, as consequence, displays the seven-vertex *nido*-structure derived from a disphenoid. NICS computation at the cage center of **1** shows that the cluster provides spherical aromaticity, mediated by a Bi_4 cluster π orbital. This aromaticity slightly decreases upon coordination of two C_6H_5Me molecules.

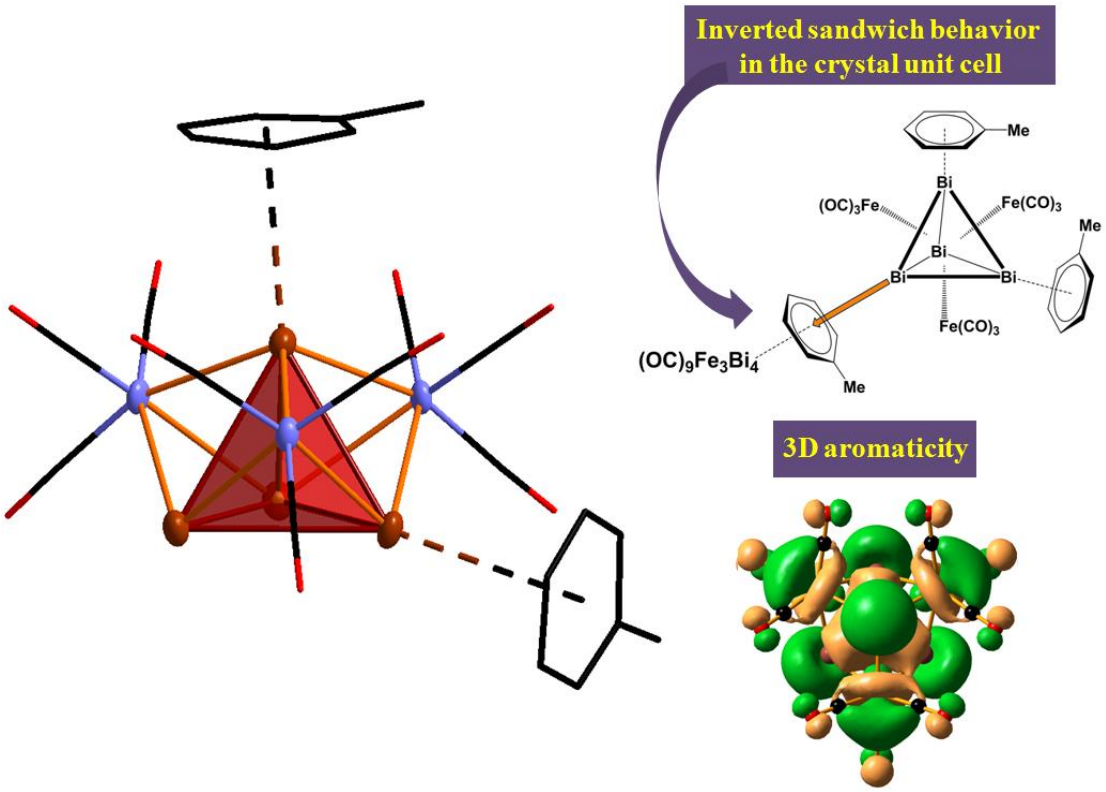

(D) The correlations between structural and electronic properties of the bismuth cyclopentadienyl complexes of the types $[(C_5R_5)_nBi_n]^{q+}$ (where R = H, Me; n = 1, q = 2; n = 1−4, q = 0) and $(C_5R_5)BiX_2$ (where R = H, Me; X = Cl, Br, I) were studied with quantum chemical calculations.

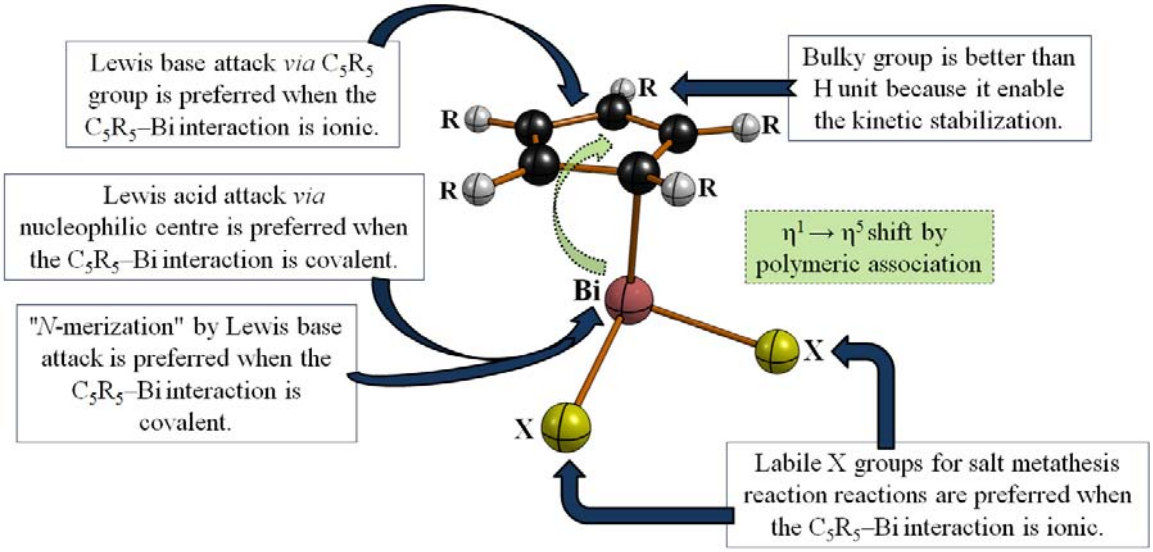

The electronic ligand effects, significant variations in the Bi−C bond lengths, haptotropic shifts providing distortion of the C_5R_5 rings, Jahn−Teller splitting, interstabilization effects, and the role of the lone pairs on "p-block element−unalkylated or peralkylated cyclopentadienyl ring" interactions were examined to obtain qualitative and quantitative pictures of the intramolecular C_5R_5−Bi interactions and the intramolecular packing effects. The theoretical investigations of monovalent and trivalent bismuth cyclopentadienyl complexes give an insight into the geometric and electronic structures, the relative stabilities and further behavior of this kind of compounds.

(E) A series of pentamethylcylcopentadienyl-substituted bismuth halide complexes was prepared by the reactions of bismuth(III) halides BiX_3 (X = Cl, Br, I) with $Li(C_5Me_5)$ in a 1:1 ratio. The observed X-ray crystal structures of the reaction products amaze by their structural diversity and shapes. The cation portions of $[(C_5Me_5)_5Bi_6Cl_{12}][(thf)_2Bi_2Cl_7]$ (**1**) and $[\{(C_5Me_5)_5Bi_5Br_9\}\{Bi_2Br_8\}_{0.5}]$ (**3**) compounds display polyhedral-like bismuth cages capped by halo ligands and η^5-Cp* groups. The distorted octahedral Bi_6 and square pyramidal Bi_5 structural shapes were found there, respectively. The solid-state molecular structure of **3** shows an unprecedented nanoscopic supramolecular architecture $[\{(C_5Me_5)_5Bi_5Br_9\}\{(CH_2Cl_2)(BiBr_4)\}]_2$. Along with **1** and **3** complexes, zig-zag polymers $[(C_5Me_5)BiBr_2]_\infty$ (**2**) and $[(C_5Me_5)BiI_2]_\infty$ (**4**) were observed in the crystal state. The C_5Me_5−BiX_2 bond hapticity changes were established in solutions (on the basis of ^1H and ^{13}C NMR spectra), in the solid states (on the basis of X-ray diffraction) and in the gas phases (on the basis of quantum chemical calculations). The weak hydrogen bonds were observed for compounds containing bromine.

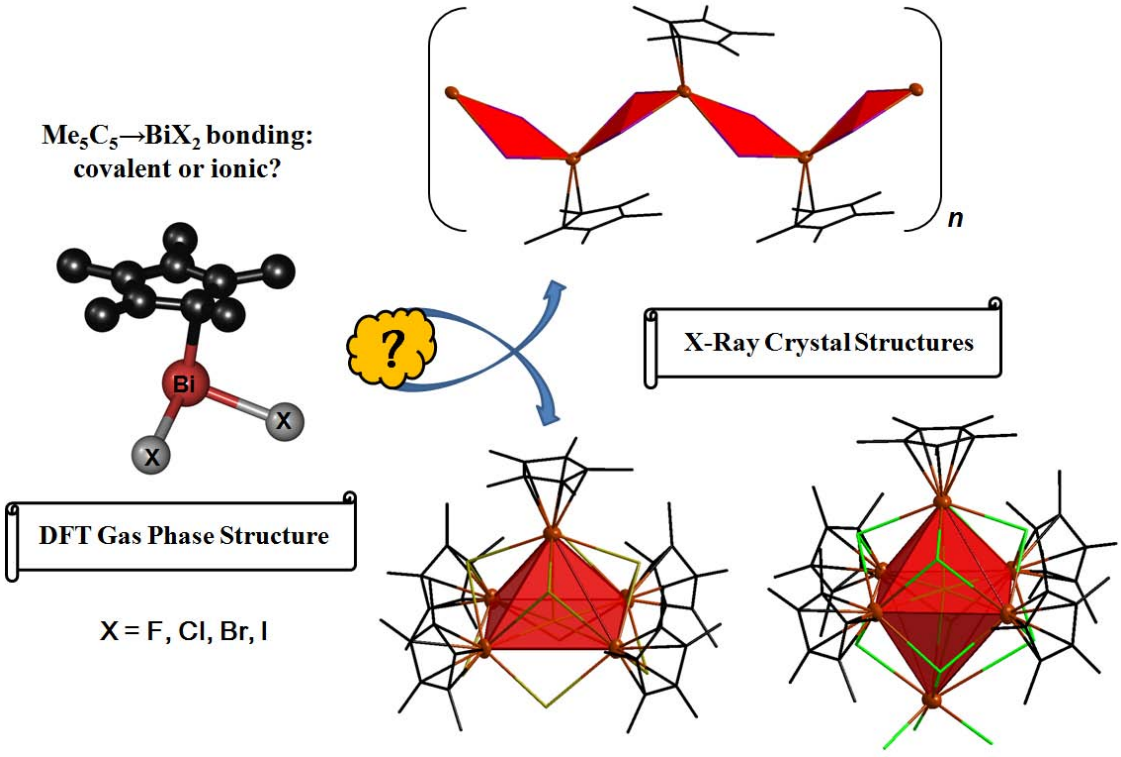

(F) A theoretical analysis of structure and electronic properties of the unique icosahedral and macroicosahedral bismuthanediides $[R_nBi_nM_{2n-4}]^{4-}$ (n = 12, 32; R = H; M = Li) and their family of the polyhedral bismuth polycations was performed. Thus, a rule «$n_{x+1} = 3n_x - 4$» providing a determination and a finding of I_h symmetrical bismuthanediides was discovered. The structural and electronic relationships between highly symmetric bismuth deltahedra with I_h point symmetry and borane deltahedra as well as the fullerene polyhedra were established on the basis of Wade's electron count rules and principles of isolobality and isoelectronicity. According to DFT geometry optimizations, the bismuthanediides display sphere-like structures (I_h) and can be regarded as nanoscopic intermediates between molecular clusters and solid-state compounds. On the basis of the large polarizabilities of the icosahedral and macroicosahedral bismuthanediides, these were tested regarding their capability to trap atoms and small molecules such as H_2, C_3H_8, Li^+ and Li_nO (n = 2, 4, 6) to generate endohedral complexes. The obtained theoretical results are a good starting point to inspire the realization of such compounds experimentally and through further computational studies.

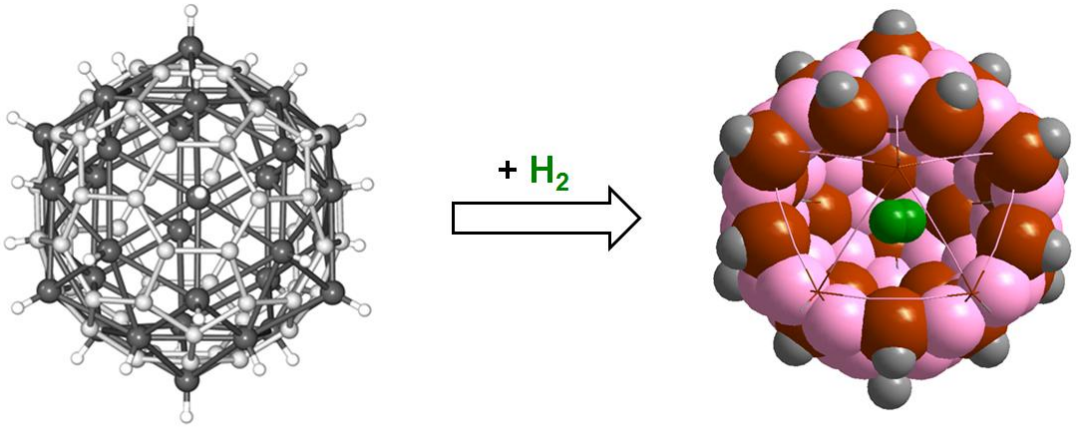

Experimental and Computational Part

A. General remarks, measurement methods and instrumentations

All manipulations were carried out with the use of standard Schlenk techniques under an oxygen-free and water-free argon atmosphere and in vacuum. All organic solvents were distilled, dried and degassed according to standard procedures.

Elemental analysis

Elemental analyses were recorded by the Micro Analytical Laboratory of the Institute of Inorganic Chemistry, Heidelberg. The measured samples were embedded in two micro aluminum containers and put in the machine. A Vario EL Elemental analysis apparatus was used.

NMR spectroscopy

The NMR spectra were recorded using three different spectrometers: Bruker ARX 200, Bruker Advance II 400 and Bruker Advance III 600. All chemical shifts were reported in δ units and referenced to internal solvent resonance and external standard of tetramethylsilane (TMS) $SiMe_4$ as δ 0.00.

Infrared spectroscopy

The IR spectra in solution and in the solid state were recorded from 4000 to 450 cm^{-1} with a Perkin-Elmer Spectrum 100 FT-IR instrument.

Mass spectrometry

The EI mass spectra were recorded on a JEOL JMS-700 (EI) machine. For all EI mass spectra, 70 eV electron beam energy was operated. The electrospray mass spectra (ESI-MS) were recorded on a Bruker Apex-Qe 9.4 T FT-ICR operating in the negative ion mode with full scanning in the range [200.0 – 2500.0]. All the samples were directly brought in the ionization field using a glass tube. The LIFDI mass spectra were recorded on a JEOL JMS-700 operating in the positive ion mode with full scanning in the range [100 – 2000]; samples were supplied as dilute solutions at about 0.2 mg ml^{-1}.

Ultraviolet-visible spectrophotometry

Electronic spectra were measured at r.t. under argon atmosphere with a Tidas II J&M spectrophotometer, using respective solvent.

X-ray crystal structure analysis

Suitable single crystals were mounted with perfluorated polyether oil on the tip of a glass fiber and cooled immediately on the goniometric head. Data were collected on an STOE IPDS I diffractometer equipped with an image plate area detector, using a graphite monochromator Mo(Kα) (λ = 71.073 pm). The structures were refined against all F^2 data by full-matrix least squares techniques (SHELXT 5.01; PC Version, Siemens, Bruker AXS). The non-hydrogen

atoms were given anisotropic displacement parameters. All hydrogen atoms bonded to carbon atoms were included in calculated positions and refined using a *riding model* with fixed isotropic U's in the final refinement. All the crystal structures were solved by Direct Methods and refined by full-matrix least-squares against F^2. The positions of other hydrogen atoms were taken from a difference Fourier map and refined isotropically. For supplementary details, see appendices on crystallographic data, without structure factors, or see the Cambridge Crystallographic Data Center where have been deposited the structures reported in chapters 2 and 3 of this thesis. These data can be obtained free of charge from via www.ccdc.cam.ac.uk/data_request/cif, or on application to CCDC, 12 Union Road, Cambridge CB 2 1 EZ, UK [Fax: int. code +44(1223)336-033; E-mail: deposit@ccdc.cam.ac.uk]. The data for the structures reported in chapter 4 of this thesis are deposited at Prof. Dr. Gerald Linti, University of Heidelberg, Institute of Inorganic Chemistry, Im Neuenheimer Feld 270, D-69120 Heidelberg, Germany, Fax: +49-6221-546617, e-mail: gerald.linti@aci.uni-heidelberg.de

Quantum chemical calculations

The computations were carried out using HPC-Cluster: Quad-Xeon Server + 65 Dual and Quad-Core Opteron and Xeon Nodes as well as dual-core notebook as personal workstation.

Chemicals used

The following chemicals were of commercial reagent grade and used without any further purification directly as purchased: Li (granulate), MeLi in Et_2O, *n*BuLi in hexane, Na (pieces), $SiCl_4$, $ClSiMe_3$, $ClSiPh_2tBu$, C_4H_8O, C_5Me_5H, $C_{10}H_8$, nBu_4NCl, $Fe(CO)_5$, $InCl_3$, $BiCl_3$, $BiBr_3$, BiI_3, C_6D_6, CD_2Cl_2, Et_2O, hexane, toluene.

The following reagents were prepared as described in the literature: $Li(C_5Me_5)$[1], $Li(thf)_3SiPh_2tBu$,[2] $Li(thf)_3Si(SiMe_3)_3$,[3] $C_{10}H_8Na$,[4] $Na_2[Fe(CO)_4]$[5], $Bi_4[Si(SiMe_3)_3]_4$[6].

[1] O. T. Beachley, Jr., R. Blom, M. R. Churchill, K. Faegri, Jr., J. C. Fettinger, J. C. Pazik, L. Victoriano, *Organometallics* **1989**, *8*, 346.

[2] B. K. Campion, R. H. Heyn, T. D. Tilley, *Organometallics* **1993**, *12*, 2584.

[3] (a) H. Gilman, C. L. Smith, *J. Organomet. Chem.* **1968**, *14*, 91; (b) A. Heine, R. Herbst-Irmer, G. M. Sheldrick, D. Stalke, *Inorg. Chem.* **1993**, *32*, 2694.

[4] E. J. Corey, A. W. Gross, *Organic Syntheses* **1993**, *8*, 93.

[5] (a) H. Strong, P. J. Krusic, J. San Filippo Jr., S. Keenan, R. G. Finke in *Inorganic Syntheses*, **1990**, *28*, 203; (b) H. B. Chin, R. Bau, *J. Am. Chem. Soc.* **1976**, *98*, 2434.

[6] G. Linti, W. Köstler, *Z. Anorg. Allg. Chem.* **2002**, *628*, 63.

B. Experimental section of chapter 2

B.1) Synthesis and characterization of $Li(thf)_3SiPh_2tBu$

The compound was synthesized by starting from the reaction of tBuPh$_2$SiCl with lithium granulate in thf solution according to the literature procedure (see *chemicals used*). It was crystallized from a *n*-hexane/thf mixture at –20 °C to give pale yellow-green crystals of $Li(thf)_3SiPh_2tBu$.

^{29}Si NMR (C_6D_6, eTMS): δ = 7.26 (s, tBuPh$_2$*Si*).

B.2) Synthesis and characterization of $(tBuPh_2Si)_4Bi_2$

A suspension of (2.93 g, 6.34 mmol) $Li(thf)_3SitBuPh_2$ in toluene (20 ml) was added dropwise to a stirred solution of (0.95 g, 2.11 mmol) $BiBr_3$ in toluene (40 ml) at –78 °C. The dark-colored reaction mixture was stirred for additional 3 h at low temperature and was then slowly warmed to ambient temperature. Initially, a green solution was observed. After stirring for 16 h, all volatile reaction components were removed in oil pump vacuum. The residue was extracted with hexane (60 ml) and then with toluene (60 ml). After filtration, dark-red solutions were obtained. The hexane and toluene fractions show similar ^{29}Si NMR signals. The toluene and hexane solutions were reduced to a volume of 15 ml and cooled to –20 °C, resulting in the formation of dark-red crystals of $(tBuPh_2Si)_4Bi_2$. Yield: 0.88 g (60.5 %; with reference to Bi). The compound is soluble in organic solvents and stable in the range –30-100 °C.

$C_{64}H_{76}Bi_2Si_4$ (1374.46): calcd. C 55.88, H 5.57; found C 55.69, H 6.05.

^{1}H NMR (399.89 MHz, C_6D_6, iTMS): δ = 1.12 (s, C*Me*$_3$, 1), 7.58 (m, *o*-Ph), 7.67 (m, *p*-Ph), 7.79 (m, *m*-Ph).

^{13}C NMR (100.55 MHz, C_6D_6, iTMS): δ = 26.8 (s, *C*Me$_3$), 30.4 (s, C*Me*$_3$), 129.7 (*m*-Ph), 132.6 (*p*-Ph), 136.0 (*o*-Ph), 138.2 (*i*-Ph).

^{29}Si NMR (79.44 MHz, C_6D_6, eTMS): δ = 15.9 (s, *Si*Ph$_2$*t*Bu).

UV/Vis (toluene): λ_{max} (ε, L mol^{-1} cm^{-1}) = 465 (2132) nm.

LIFDI-MS (toluene): *m*/*z* (%) = 1374.6 (100) $[M]^+$, 1135.4 (13) $[M^+ - SiPh_2tBu]$, 687.3 (18) $[(tBuPh_2Si)_2Bi]^+$, 447.3 (5) $[(tBuPh_2Si)Bi]^+$.

B.3) Synthesis and characterization of $(tBuPh_2Si)_2BiBr$

A suspension of $Li(thf)_3SitBuPh_2$ (3.06 g, 6.63 mmol) in toluene (20 ml) was added dropwise to a stirred solution of (1.49 g 3.31 mmol) $BiBr_3$ in toluene (40 ml) at −78 °C. The dark-colored reaction mixture was stirred for additional 3 h at low temperature and was then slowly warmed to ambient temperature. After stirring for 16 h, all volatile reaction components were removed in

oil pump vacuum, and the residue was extracted first with hexane (60 ml) and then with toluene (60 ml). After filtration of the hexane and toluene fractions, the dark-green (denoted "***DGS***") and red (denoted "***RS***") solutions were obtained, respectively. Hexane and toluene solutions were reduced to a volume 15 ml and cooled to −20 °C, resulting in the formation of only red crystals of $(t\text{BuPh}_2\text{Si})_2\text{BiBr}$. ^{29}Si NMR spectra for both solutions contain the silicon signals of $(t\text{BuPh}_2\text{Si})_2\text{BiBr}$ and disilane, too. Yield of ***DGS***: 0.91 g (35.7 %; with reference to Bi). Yield of ***RS***: 0.48 g (19.0 %; with reference to Bi). After short periods of time at −20 °C or at r.t., both solutions decompose with formation of elemental bismuth. The crystals of **2** (which form predominantly) also were obtained by this reaction in a 1:1 ratio (^{29}Si NMR signals of **2** and disilane were observed, too).

DGS: The signals of **2** and disilane are omitted.

^{1}H NMR (399.89 MHz, C_6D_6, iTMS): δ = 7.87 (m, *m*-Ph), 7.71 (m, *p*-Ph), 7.49 (m, *o*-Ph), 1.21 (s, C*Me*$_3$).

^{13}C NMR (100.55 MHz, C_6D_6, iTMS): δ = 138.5 (*i*-Ph), 137.1 (*o*-Ph), 133.3 (*p*-Ph), 130.0 (*m*-Ph), 31.2 (s, C*Me*$_3$), 27.0 (s, *C*Me$_3$).

^{29}Si NMR (79.44 MHz, C_6D_6, eTMS): δ = −4.2 (s, *Si*Ph$_2$*t*Bu).

RS: The signals of **2**, disilane, and ***DGS*** are omitted.

^{1}H NMR (400 MHz, C_6D_6, iTMS): δ = 7.74 (m, *m*-Ph), 7.63 (m, *p*-Ph), 7.29 (m, *o*-Ph), 1.14 (s, C*Me*$_3$).

^{13}C NMR (100.55 MHz, C_6D_6, iTMS): δ = 138.3 (*i*-Ph), 136.3 (*o*-Ph), 132.7 (*p*-Ph), 129.9 (*m*-Ph), 31.1 (s, C*Me*$_3$), 27.6 (s, *C*Me$_3$).

^{29}Si NMR (79.44 MHz, C_6D_6, eTMS): δ = −6.1 (s, *Si*Ph$_2$*t*Bu).

B.4) Synthesis and characterization of $\text{In(SiPh}_2t\text{Bu)}_3$

A suspension of $\text{Li(thf)}_3\text{SiPh}_2t\text{Bu}$ (7.0 g, 15.2 mmol) in 15 ml thf was added dropwise to a stirred solution of 1.12 g (5.07 mmol) $InCl_3$ in 35 ml thf at −78 °C. The dark-coloured reaction mixture was stirred for additional 3 h at low temperature and was then slowly warmed to ambient temperature. After stirring for 16 h all volatile reaction components were removed in oil pump vacuum and the residue was extracted with 60 ml of toluene. After filtration a reddish-brown solution was obtained, from which $[\text{In(SiPh}_2t\text{Bu)}_3]$ was isolated as brownish powder. The powder was dissolved in the mixture of 20 ml toluene and 10 ml hexane, reduced to a volume 15 ml and cooled to −20 °C, resulting in the formation of pale yellow crystals. Yield: 0.93 g (22.1%; with reference to In).

$InSi_3C_{48}H_{57}$ (832.1): calcd. C 69.22 %, H 6.85 %; found C 69.78 %, H 7.04.

^{1}H NMR (399.89 MHz, C_6D_6, iTMS): δ = 1.04 (s, C*Me*$_3$), 7.5 (m, *o*-Ph), 7.7 (m, *p*-Ph), 7.8 (m, *m*-Ph).

^{13}C NMR (100.55 MHz, C_6D_6, iTMS): δ = 27.7 (s, *C*Me$_3$), 31.9 (s, C*Me*$_3$), 129.7 (*m*-Ph), 134.1 (*p*-Ph), 136.5 (*o*-Ph), 139.7 (*i*-Ph).

^{29}Si{^{1}H}-NMR (79.44 MHz, C_6D_6, eTMS): δ = 24.5 (s, *Sit*BuPh$_2$, complex), −2.19 (s, *Sit*BuPh$_2$, disilane).

MS (EI, 70 eV): *m*/*z* = 593 {[In(Si*t*BuPh$_2$)$_2$]$^+$, 26.4 %}, 478 ([Si*t*BuPh$_2$]$_2$$^{+\cdot}$, 7.9 %), 239 ([Si*t*BuPh$_2$]$^+$, 100 %), 115 (In$^+$, 18 %).

C. Computational section of chapter 2

C.1) Details and theory

DFT structure optimizations were performed with the Turbomole program,[1] adopting the multiple "M3" grid size for the density fitting and a SCF convergence criterion of 1×10^{-7} E_h. The initial geometries were fully optimized with the hybrid exchange-correlation functional PBE0.[2] As Gaussian AO basis for all atoms, all-electron split valence SV(P) sets of def2-type[3] were employed (Basis Set System I, which is denoted as BS-I). The vibrational frequencies were evaluated at the same level of theory on all DFT-optimized geometries to verify their status as true global and local minima on the potential energy surfaces and to obtain zero-point corrections to the energies (ZPE) without scaling. All other computations were carried out on PBE0 optimized geometries using the Gaussian 03 program package.[4] The Los Alamos National Laboratory 2 (LANL2) relativistic effective core potentials (RECPs) to describe the core electrons of In, P, As, Sb, Bi, and Br atoms and employed split-valence (double-ζ) quality basis sets to describe their s and p valence electrons were used. For P, As, Sb, Bi, and Br atoms, the LANL2DZ basis set was augmented by adding one set of polarization and one set of diffuse functions.[5] For Si, C, and H atoms, all-electron split-valence 6-311+G(d,p) basis sets supplemented with a single set of diffuse functions on carbon and silicon atoms were employed.[6] The combination of LANL2DZdp and 6-311+G(d,p) is denoted as Basis Set System II (BS-II). The nature of the chemical bonding was analyzed by the NBO approach with the second-order Møller-Plesset perturbation theory, including all valence electrons in the configuration space [MP2(full)]. The atomic charges were computed within the natural population analysis (NPA). Wiberg indexes were evaluated and used as bond strength indicators. NBO analyses were performed with NBO Version 3.1[7] incorporated in the Gaussian 03 program. To gain insight into the vertical singlet electronic states, time-dependent functional theory[8] (TD-PBE0 method) calculations were performed. Energies reported herein were

evaluated using the fourth-order Møller-Plesset perturbation theory [MP4(SDQ)] in combination with PBE0 parameterization.

C.2) References

[1] R. Ahlrichs, M. Bär, M. Häser, H. Horn, C. Kölmel, *Chem. Phys. Lett.* **1989**, *162*, 165.

[2] C. Adamo, V. Barone, *J. Chem. Phys.* **1999**, *110*, 6158.

[3] (a) B. Metz, H. Stoll, M. Dolg, *J. Chem. Phys.* **2000**, *113*, 2563; (b) F. Weigend, **R**. Ahlrichs, *Phys. Chem. Chem. Phys.* **2005**, *7/18*, 3297.

[4] M. J. Frisch, G. W. Trucks, H. B. Schlegel, G. E. Scuseria, M. A. Robb, J. R. Cheeseman, J. A. Montgomery Jr., T. Vreven, K. N. Kudin, J. C. Burant, J. M. Millam, S. S. Iyengar, J. Tomasi, V. Barone, B. Mennucci, M. Cossi, G. Scalmani, N. Rega, G. A. Petersson, H. Nakatsuji, M. Hada, M. Ehara, K. Toyota, R. Fukuda, J. Hasegawa, M. Ishida, T. Nakajima, Y. Honda, O. Kitao, H. Nakai, M. Klene, X. Li, J. E. Knox, H. P. Hratchian, J. B. Cross, V. Bakken, C. Adamo, J. Jaramillo, R. Gomperts, R. E. Stratmann, O. Yazyev, A. J. Austin, R. Cammi, C. Pomelli, J. W. Ochterski, P. Y. Ayala, K. Morokuma, G. A. Voth, P. Salvador, J. J. Dannenberg, V. G. Zakrzewski, S. Dapprich, A. D. Daniels, M. C. Strain, O. Farkas, D. K. Malick, A. D. Rabuck, K. Raghavachari, J. B. Foresman, J. V. Ortiz, Q. Cui, A. G. Baboul, S. Clifford, J. Cioslowski, B. B. Stefanov, G. Liu, A. Liashenko, P. Piskorz, I. Komaromi, R. L. Martin, D. J. Fox, T. Keith, M. A. Al-Laham, C. Y. Peng, A. Nanayakkara, M. Challacombe, P. M. W. Gill, B. Johnson, W. Chen, M. W. Wong, C. Gonzalez, and J. A. Pople, *Gaussian 03*, Revision E. 01, Gaussian, Inc., Wallingford CT, **2004**.

[5] (a) P. J. Hay, W. R. Wadt, *J. Chem. Phys.* **1985**, *82*, 270; (b) P. J. Hay, W. R. Wadt, *J. Chem. Phys.* **1985**, *82*, 284; (c) P. J. Hay, W. R. Wadt, *J. Chem. Phys.* **1985**, *82*, 299; (d) C. E. Check, T. O. Faust, J. M. Bailey, B. J. Wright, T. M. Gilbert, L. S. Sunderlin , *J. Phys. Chem. A* **2001**, *105*, 8111.

[6] (a) R. Krishnan, J. S. Binkley, R. Seeger, J. A. Pople, *J. Chem. Phys.* **1980**, *72*, 650; (b) T. Clark, J. Chandrasekhar, P. v. R. Schleyer, *J. Comput. Chem.* **1983**, *4*, 294.

[7] (a) E. D. Glendening, A. E. Reed, J. E. Carpenter, F. Weinhold, *NBO program*, vers. 3.1; (b) A. E. Reed, L. A. Curtiss, F. Weinhold, *Chem. Rev.* **1988**, *88*, 899.

[8] M. E. Casida, C. Jaorski, K. C. Casida, D. R. Salahub, *J. Chem. Phys.* **1998**, *108*, 4439.

D. Experimental section of chapter 3

D.1) Synthesis and characterization of $[n\mathrm{Bu_4N}]_4[\mathrm{Bi_4Fe_8(CO)_{28}}]$

A suspension of 0.17 g (0.8 mmol) $Na_2[Fe(CO)_4]$ in 10 ml of thf was added dropwise to a stirred dark-red solution of 0.18 g (0.1 mmol) $Bi_4[Si(SiMe_3)_3]_4$ (1) in 15 ml of thf at –78°C. After the addition was complete, the reaction mixture was warmed for additional 2 h to ambient temperature. 16 fold excess (ca. 1.6 mmol) of $n\mathrm{Bu_4NCl}$ in 20 ml thf was then introduced to the reaction mixture. After stirring for further 16 h at ambient temperature all volatile reaction components were removed in oil pump vacuum. The dark residue was extracted with 20 ml of thf. After filtration a dark-brown solution was obtained. The thf solution was removed; the dark residue was washed with some amount of hexane and re-crystallized again in 15 ml of thf. The thf solution was reduced to a volume of 5 ml and cooled to –20°C. Black crystals of $[n\mathrm{Bu_4N}]_4[\mathrm{Bi_4Fe_8(CO)_{28}}]$ were obtained after some months. Yield: 54 mg (18 %; with reference to Bi). $Bi_4Fe_8C_{92}O_{28}H_{144}N_4$ (M = 3036.4).

IR (thf, cm^{-1}): 2004w, 1977s, 1957s, 1934m, 1919m, 1899m ($\tilde{\nu}_{CO}$).

IR (KBr, cm^{-1}): 2008w, 1994w, 1976m, 1915s, 1895s, 1878s ($\tilde{\nu}_{CO}$).

ESI-MS (thf): unspecific decomposition of the compound; m/z 349 $[BiFe(CO)_3]^-$, 474 $[Bi_2Fe]^-$, 502 $[Bi_2Fe(CO)]^-$, 530 $[Bi_2Fe(CO)_2]^-$, 586 $[Bi_2Fe_2(CO)_2]^-$, 642 $[Bi_2Fe_2(CO)_4]^-$, 879 $[Bi_3Fe_2(CO)_5]^-$.

D.2) Synthesis and characterization of $[\mathrm{Bi_4Fe_3(CO)_9}]\cdot 2(\mathrm{C_6H_5Me})$

(i) A suspension of 0.27 g (1.28 mmol) $Na_2[Fe(CO)_4]$ in 20 ml of thf was added dropwise to a stirred solution of 0.38 g (0.85 mmol) $BiBr_3$ in 20 ml of thf at –78°C. After the addition was complete, the reaction mixture was warmed for additional 2 h to ambient temperature. After stirring for further 16 h at ambient temperature, the color change of the mixture from dark-green (initially) to dark-brown was observed. All volatile reaction components were removed in oil pump vacuum. The dark residue was extracted with 40 ml of toluene. After filtration, a dark-red-brown solution was obtained. The toluene solution was reduced to a volume of 8 ml and cooled to –20°C, resulting in the formation of dark-red-brown crystals of $[Bi_4Fe_3(CO)_9]\cdot 2(C_6H_5Me)$ after some weeks. Yield: 0.109 g (35.8 %, with reference to Bi).

(ii) A suspension of 0.068 g (0.32 mmol) $Na_2[Fe(CO)_4]$ in 10 ml of thf was added dropwise to a stirred solution of 0.191 g (0.32 mmol) $(C_5Me_5)BiI_2$ in 10 ml of thf at –78°C. After the addition was complete, the reaction mixture was warmed for an additional 2 h to ambient temperature. After stirring for further 16 h at ambient temperature, the color change of the mixture from dark-green (initially) to dark-brown was observed. All volatile reaction components were removed in

oil pump vacuum. The dark residue was extracted with 20 ml of toluene. After filtration, a dark-red-brown solution was obtained. The toluene solution was reduced to a volume of 5 ml and cooled to –20°C, resulting in the formation of dark-red-brown crystals of $[Bi_4Fe_3(CO)_9]\cdot 2(C_6H_5Me)$ after one week. Yield: 0.067 g (58.3 %, with reference to Bi).

IR (thf, cm^{-1}): 2132w, 2097w, 2000m, 1991m, 1967s ($\tilde{\nu}_{CO}$).

IR (KBr, cm^{-1}): 2054w, 2040m, 2002s, 1950s, 1934s ($\tilde{\nu}_{CO}$).

LIFDI-MS (toluene): *m*/*z* (%) = 1393.3 (100) $[M^+ - OMe_2]$, 1256.3 (22) $[Bi_4Fe_3(CO)_9]^+$, 1172.1 (49) $[Bi_4Fe_3(CO)_6]^+$, 1115.9 (18) $[Bi_4Fe_2(CO)_6]^+$, 767.1 (28) $[Bi_3Fe(CO)_3]^+$, 502.8 (47) $[Bi_2FeCO]^+$, 474.0 $[Bi_2Fe]^+$.

E. Computational section of chapter 3

E.1) Details and theory

All of the calculations were carried out using the Gaussian 03 program package. Electron correlation for geometry optimizations was treated within the Local Spin Density Approximation denoted as LSDA.[1] SCF convergence criterion of 10^{-7} was used. The LSDA density functional was employed with the double-ζ quality plus polarization SV(P) basis set of def2 type (Basis Set System I, which is denoted as BS-I) for all atoms.[2,3] The vibrational frequencies were evaluated at the same level of theory on all optimized geometries of the clusters to verify their status as true global and local minima on the potential energy surfaces and to obtain zero-point corrections to the energies (ZPE). As a result of true minima, there were no imaginary vibrational frequencies (negative signs) for all optimized geometries. To evaluate nature of the chemical bonding, energies and Nucleus Independent Chemical Shifts (NICS) values of the clusters, the hybrid MW1PW91 density functional[4] was employed with the Hay-Wadt relativistic effective core potentials (RECPs) plus LANL08 basis sets (correspond to triple-ζ valence orbital quality), augmented by adding one set of polarization *d* and *f* functions [denoted as LANL08(d)[5] for Bi and LANL08(f)[6] for Fe, respectively] and the split-valence basis sets 6-311G(d)[7] for C, O and H atoms. The combination of these basis sets is denoted as Basis Set System II (BS-II). Nature of the chemical bonding was analyzed by means of Natural Bond Orbital (NBO) approach. The atomic charges were computed within the Natural Population Analysis (NPA). Wiberg bond indexes (WBI) were evaluated and used as bond strength indicators. NBO analyses were performed with NBO Version 3.1[8] incorporated in the Gaussian 03 program[9]. NICS-computations[10] were carried out at the cage centers of clusters on their DFT optimized geometries.

E.2) References

[1] S. H. Vosko, L. Wilk, M. Nusair, *Can. J. Phys.* **1980**, 58, 1200.

[2] B. Metz, H. Stoll, M. Dolg, *J. Chem. Phys.* **2000**, *113*, 2563.

[3] F. Weigend, R. Ahlrichs, *Phys. Chem. Chem. Phys.* **2005**, *7/18*, 3297.

[4] (a) J. P. Perdew, In *Electronic Structure of Solids '91*; P. Ziesche, H. Eschig, Eds.; Akademie Verlag: Berlin, **1991**, 11; (b) C. Adamo, V. Barone, *J. Chem. Phys.* **1998**, *108*, 664; (c) B. J. Lynch, Y. Zhao, D. G. Truhlar, *J. Phys. Chem. A* **2003**, *107*, 1384.

[5] (a) P. J. Hay, W. R. Wadt, *J. Chem. Phys.* **1985**, *82*, 284; (b) C. E. Check, T. O. Faust, J. M. Bailey, B. J. Wright, T. M. Gilbert, L.S. Sunderlin, *J Phys. Chem. A* **2001**, *105*, 8111; (c) L. E. Roy, P. J. Hay, R. L. Martin, *J. Chem. Theory Comput.* **2008**, *4*, 1029.

[6] (a) P. J. Hay, W. R. Wadt, J. Chem. Phys. **1985**, *82*, 299; (b) A. W. Ehlers, M. Bohme, S. Dapprich, A. Gobbi, A. Hollwarth, V. Jonas, K. F. Kohler, R. Stegmann, A. Veldkamp, G. Frenking, *Chem. Phys. Lett.* **1993**, *208*, 111; (c) L. E. Roy, P. J. Hay, R.L. Martin, *J. Chem. Theory Comput.* **2008**, *4*, 1029.

[7] R. Krishnan, J. S. Binkley, R. Seeger, J. A. Pople, *J. Chem. Phys.* **1980**, *72*, 650.

[8] (a) E. D. Glendening, A. E. Reed, J. E. Carpenter, F. Weinhold, *NBO program*, ver. 3.1; (b) A. E. Reed, L. A. Curtiss, F. Weinhold, *Chem. Rev.* **1988**, *88*, 899.

[9] M. J. Frisch, G. W. Trucks, H. B. Schlegel, G. E. Scuseria, M. A. Robb, J. R. Cheeseman, J. A. Montgomery, Jr., T. Vreven, K. N. Kudin, J. C. Burant, J. M. Millam, S. S. Iyengar, J. Tomasi, V. Barone, B. Mennucci, M. Cossi, G. Scalmani, N. Rega, G. A. Petersson, H. Nakatsuji, M. Hada, M. Ehara, K. Toyota, R. Fukuda, J. Hasegawa, M. Ishida, T. Nakajima, Y. Honda, O. Kitao, H. Nakai, M. Klene, X. Li, J. E. Knox, H. P. Hratchian, J. B. Cross, V. Bakken, C. Adamo, J. Jaramillo, R. Gomperts, R. E. Stratmann, O. Yazyev, A. J. Austin, R. Cammi, C. Pomelli, J. W. Ochterski, P. Y. Ayala, K. Morokuma, G. A. Voth, P. Salvador, J. J. Dannenberg, V. G. Zakrzewski, S. Dapprich, A. D. Daniels, M. C. Strain, O. Farkas, D. K. Malick, A. D. Rabuck, K. Raghavachari, J. B. Foresman, J. V. Ortiz, Q. Cui, A. G. Baboul, S. Clifford, J. Cioslowski, B. B. Stefanov, G. Liu, A. Liashenko, P. Piskorz, I. Komaromi, R. L. Martin, D. J. Fox, T. Keith, M. A. Al-Laham, C. Y. Peng, A. Nanayakkara, M. Challacombe, P. M. W. Gill, B. Johnson, W. Chen, M. W. Wong, C. Gonzalez, and J. A. Pople, *Gaussian 03*, Revision E.01, Gaussian, Inc., Wallingford CT, **2004**.

[10] NICS-Nucleus Independent Chemical Shifts: P. von R. Schleyer, C. Maerker, A. Dransfeld, H. Jiao, N. J. R. van Eikema Hommes, *J. Am. Chem Soc.* **1996**, *118*, 6317.

F. Experimental section of chapter 4

All pentamethylcyclopentadienyl-substituted bismuth halide complexes described herein are extremely unstable compounds. However, these can be stored at –20 °C for some time under an oxygen-free and water-free argon atmosphere.

The ^{1}H and ^{13}C NMR data are assigned according to the numbering depicted in Figure A, here. In the ^{1}H NMR spectra, the sequence of the chemical shifts for the methyl groups is δ (2,5-*Me*) > δ (3,4-*Me*) > δ (1-*Me*) [in a 2 : 2 : 1 ratio]. The C_5Me_5 ligand is abbreviated as Cp*.

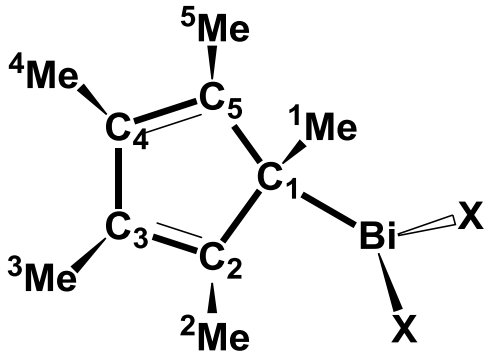

Figure A.

F.1) Synthesis and characterization of $[(Cp^*)_5Bi_6Cl_{12}][(thf)_2Bi_2Cl_7]$

A stirred suspension of 1.0 g (7 mmol) LiCp* in 20 ml of thf was added dropwise to a stirred solution of 2.21 g (7 mmol) $BiCl_3$ in 50 ml of thf at –78°C. The reaction mixture got quickly a pale yellow color which deepened with sequential addition of LiCp*. The deep-red-colored reaction mixture was stirred for additional 3 h at low temperature and was then slowly warmed to ambient temperature. After stirring for 16 h a red solution and a brown powder were obtained. All volatile reaction components were removed in oil pump vacuum and the residue was extracted two times with 60 ml of CH_2Cl_2. After centrifugation a deep-red solution of $[(Cp^*)_5Bi_6Cl_{12}][(thf)_2Bi_2Cl_7]$ (**1**) together with a green-gray powder was obtained and filtrated. The solvent was removed and **1** was isolated as orange-red crystal powder, which was washed five times with 20 ml Et_2O at 0°C. Yield: 1.1 g (39.7 %; with reference to Bi). The powder was dissolved in the mixture of 20 ml thf and 20 ml toluene, reduced to a volume 10 ml and cooled to –20°C, resulting in the formation of red crystals.

^{1}H NMR (399.89 MHz, CD_2Cl_2, iTMS): δ = 1.87 (m, thf-C*H*$_2$), 2.37 (s, C_5*Me*$_5$), 3.76 (m, thf-OC*H*$_2$).

^{13}C NMR (100.55 MHz, CD_2Cl_2, iTMS): δ = 9.3 (s, C_5*Me*$_5$), 24.8 (s, thf-*C*H$_2$), 67.1 (s, thf-OCH$_2$), 126.1 (s, *C*$_5$Me$_5$).

F.2) Syntheses and characterization of [Cp*BiBr$_2$] and [{(Cp*)$_5$Bi$_5$Br$_9$}{Bi$_2$Br$_8$}$_{0.5}$]

A stirred suspension of 1.0 g (7 mmol) LiCp* in 20 ml of thf was added dropwise to a stirred solution of 3.14 g (7 mmol) $BiBr_3$ in 50 ml of thf at –78°C. The reaction mixture got quickly a pale yellow color which deepened with sequential addition of LiCp*. The deep-red-colored reaction mixture was stirred for additional 3 h at low temperature and was then slowly warmed to ambient temperature. After stirring for 16 h a red solution and a gray-brown powder were obtained. All volatile reaction components were removed in oil pump vacuum and the residue was extracted two times with 50 ml of CH_2Cl_2. After centrifugation a deep-red solution was obtained and filtrated. The resulting solution was reduced to a volume ~ 15 ml and cooled to –20°C, resulting in the formation of red crystals of [Cp*BiBr$_2$] (**2**) and dark-red crystals of [{(Cp*)$_5$Bi$_5$Br$_9$}{Bi$_2$Br$_8$}$_{0.5}$] (**3**). For powders **2** and **3** – yield of **2**: 2.17 g (61.6 %; with reference to Bi); yield of **3**: 1.26 g (36.4 %; with reference to Bi).

2: ^{1}H NMR (600.13 MHz, CD_2Cl_2, iTMS): δ = 1.03 (s, 1-*Me*); 1.29, 1.65 (s, 3,4-*Me*); 1.90, 2.51 (s, 2,5-*Me*).

^{13}C NMR (150.90 MHz, CD_2Cl_2, iTMS): δ = 8.8, 10.5 (s, 2,5-*Me*); 10.6, 10.8 (s, 3,4-*Me*); 19.2 (s, 1-*Me*); 58.8 (s, C1); 123.9, 133.5 (s, C-3–4); 138.5, 142.7 (s, C-2–5).

3:^{1}H NMR (399.89 MHz, CD_2Cl_2, iTMS): δ = 2.63 (s, C_5Me_5).

^{13}C NMR (100.55 MHz, CD_2Cl_2, iTMS): δ = 10.8 (s, C_5Me_5), 125.3 (s, C_5Me_5).

F.3) Synthesis and characterization of [Cp*BiI$_2$]

A stirred suspension of 1.0 g (7 mmol) LiCp* in 20 ml of thf was added dropwise to a stirred solution of 4.13 g (7 mmol) BiI_3 in 50 ml of thf at –78°C. The deep-red-colored reaction mixture was stirred for additional 3 h at low temperature and was then slowly warmed to ambient temperature. After stirring for further 16 h all volatile reaction components were removed in oil pump vacuum and the gray residue was extracted two times with 50 ml of CH_2Cl_2. After centrifugation a deep-red solution was obtained and filtrated. The solvent was removed and [Cp*BiI$_2$] (**4**) was isolated as dark-orange-red crystal powder. Yield: 3.45 g (82.4 %; with reference to Bi). The powder was dissolved in the mixture of 30 ml of toluene and 10 ml of thf, reduced to a volume ~ 20 ml and cooled to –20°C, resulting in the formation of dark-red crystals.

^{1}H NMR (399.89 MHz, CD_2Cl_2, iTMS): δ = 1.09 (s, 1-*Me*); 1.28, 1.69 (s, 3,4-*Me*); 1.96, 2.40 (s, 2,5-*Me*).

^{13}C NMR (100.55 MHz, CD_2Cl_2, iTMS): δ = 9.4, 11.0 (s, 2,5-*Me*); 11.3, 12.7 (s, 3,4-*Me*); 19.6 (s, 1-*Me*); 60.2 (s, C1); 122.5, 133.5 (s, C-3–4); 138.1, 142.2 (s, C-2–5).

G. Computational section of chapter 4

G.1) Details and theory

The electron structure calculations were performed by means of density functional theory (DFT) based on Kohn−Sham theory and Møller−Plesset perturbation theory based on Rayleigh−Schrödinger perturbation theory (RS-PT), and using Hartree−Fock (HF) theory.

In part 4.2, the initial geometries were fully optimized with the hybrid exchange-correlation functional PBE0,[1] which uses a 1:3 mixture of DFT, 25% of the exact exchange from Hartree−Fock, and 75% correlation weighting from PBE for the exchange part with a generalized-gradient approximation, $E_{XC} = 0.25E_X(HF) + 0.75E_X(PBE) + E_C(mPW91)$. DFT structure optimizations were performed with the Turbomole program,[2] adopting the multiple "M3" grid size for the density fitting and a self-consistent field (SCF) convergence criterion of 1×10^{-7} E_h. Coulomb interactions were considered within the resolution of the identity (RI) approximation. As Gaussian AO basis for all atoms, large all-electron triple ζ split valence (TZVP) sets of def2-type[3] were employed (Basis Set System I, which is denoted BS-I). In standard notation these are [6s, 5p, 3d, 2f] for Bi, [5s, 3p, 2d, 1f] for C, [5s, 5p, 2d, 1f] for Cl, [6s, 5p, 4d, 1f] for Br, [6s, 5p, 3d, 2f] for I, and [3s, 1p] for H.

The post-Hartree−Fock *ab initio* methods of second- and fourth-order Møller−Plesset perturbation theory [MP2 and MP4(SDQ), respectively] were applied to account for high electron correlation effects in molecules and to obtain more accurate energies and charges. Los Alamos National Laboratory 2 (LANL2) relativistic effective core potentials (ECPs) were used to describe the core electrons of Bi, Cl, Br, and I atoms and split-valence (double-ζ) basis sets were used to describe s- and p-valence electrons of Bi, Cl, Br, and I. The LANL2DZ basis set was augmented by adding one set of polarization functions on all atoms and one set of diffuse functions on all non-hydrogen atoms.[4] For C and H atoms, all-electron split-valence 6-31+G(d,p) basis sets, supplemented with a single set of diffuse functions on carbon atoms, were employed.[5] The combination of LANL2DZdp and 6-31+G(d,p) is denoted Basis Set System II (BS-II). The vibrational frequencies were evaluated on all DFT-optimized geometries using the HF method to verify their status as true global and local minima on the potential energy surfaces and to obtain zero-point corrections to the energies (ZPE) without scaling. The nature of the chemical bonding was analyzed by the Natural Bond Orbital (NBO) approach with the second-order Møller−Plesset perturbation theory, including all valence electrons in the configuration space [MP2(full)/BS-II]. The atomic charges were computed within the Natural Population Analysis (NPA). Second order perturbative analysis of donor−acceptor interactions is available, labeled as $E(2)$ energies. Wiberg indexes were evaluated and used as bond strength indicators.

NBO analysis was performed with NBO Version 3.1[6] incorporated in the Gaussian 03 program. The vertical singlet electronic states were studied using the extended Koopman's theorem with time-dependent PBE0 density functional method (TD-PBE0/BS-II). Energies and dipole moments reported herein were evaluated using the second- and fourth-order Møller−Plesset perturbation theory [MP2(full)/BS-II or MP4(SDQ)/BS-II] in combination with PBE0 parametrization [PBE0/BS-I]. All of these computations were carried out using the Gaussian 03 program package.[7]

In part 4.3, the initial geometries were fully optimized with the hybrid exchange-correlation functional PBE0,[1]. DFT structure optimizations were performed with the Turbomole program,[2] adopting the multiple "M3" grid size for the density fitting and a self-consistent field (SCF) convergence criterion of 1×10^{-7} E_h. As Gaussian AO basis for all atoms, large all-electron triple ζ split valence (TZVP) sets of def2-type[3] were employed (Basis Set System I, which is denoted BS-I).

The nature of the chemical bonding was analyzed by the Natural Bond Orbital (NBO) approach with the second-order Møller−Plesset perturbation theory, including all valence electrons in the configuration space [MP2(full)]. The Hay-Wadt relativistic effective core potential (RECP) for Bi plus LANL08 basis sets (correspond to triple-ζ valence orbital quality), augmented by adding one set of polarization and one set of diffuse functions, were used.[8] For C and H atoms, all-electron split-valence basis sets 6-311+G(d,p) was supplemented with a single set of diffuse functions on carbon atoms.[9] For halogen atoms (F, Cl, Br, I), all-electron split-valence basis sets 6-311G(d,p) were employed.[10] The combination of all of these basis sets is denoted as Basis Set System III (BS-III). These computations were carried out using the Gaussian 03 program package.[7]

G.2) References

[1] C. Adamo, V. J. Barone, *Chem. Phys.* **1999**, *110*, 6158.

[2] R. Ahlrichs, M. Bär, M. Häser, H. Horn, C. Kölmel, *Chem. Phys. Lett.* **1989**, *162*, 165

[3] (a) B. Metz, H. Stoll, M. Dolg, *J. Chem. Phys.* **2000**, *113*, 2563; (b) F. Weigend, R. Ahlrichs, *Phys. Chem. Chem. Phys.* **2005**, *7/18*, 3297.

[4] (a) P. J. Hay, W. R. Wadt, *J. Chem. Phys.* **1985**, *82*, 270; (b) P. J. Hay, W. R. Wadt, *J. Chem. Phys.* **1985**, *82*, 284; (c) P. J. Hay, W. R. Wadt, *J. Chem. Phys.* **1985**, *82*, 299; (d) C. E. Check, T. O. Faust, J. M. Bailey, B. J. Wright, T. M. Gilbert, L. S. Sunderlin, *J. Phys. Chem. A* **2001**, *105*, 8111.

[5] (a) W. J. Hehre, R. Ditchfield, J. A. Pople, *J. Chem. Phys.* **1972**, *56*, 2257; (b) T. Clark, J. Chandrasekhar, P.v.R. Schleyer, *J. Comput. Chem.* **1983**, *4*, 294.

[6] (a) E. D. Glendening, A. E. Reed, J. E. Carpenter, F. Weinhold, *NBO program*, ver. 3.1; (b) A. E. Reed, L. A. Curtiss, F. Weinhold, *Chem. Rev.* **1988**, *88*, 899.

[7] M. J. Frisch, G. W. Trucks, H. B. Schlegel, G. E. Scuseria, M. A. Robb, J. R. Cheeseman, J. A. Montgomery, Jr., T. Vreven, K. N. Kudin, J. C. Burant, J. M. Millam, S. S. Iyengar, J. Tomasi, V. Barone, B. Mennucci, M. Cossi, G. Scalmani, N. Rega, G. A. Petersson, H. Nakatsuji, M. Hada, M. Ehara, K. Toyota, R. Fukuda, J. Hasegawa, M. Ishida, T. Nakajima, Y. Honda, O. Kitao, H. Nakai, M. Klene, X. Li, J. E. Knox, H. P. Hratchian, J. B. Cross, V. Bakken, C. Adamo, J. Jaramillo, R. Gomperts, R. E. Stratmann, O. Yazyev, A. J. Austin, R. Cammi, C. Pomelli, J. W. Ochterski, P. Y. Ayala, K. Morokuma, G. A. Voth, P. Salvador, J. J. Dannenberg, V. G. Zakrzewski, S. Dapprich, A. D. Daniels, M. C. Strain, O. Farkas, D. K. Malick, A. D. Rabuck, K. Raghavachari, J. B. Foresman, J. V. Ortiz, Q. Cui, A. G. Baboul, S. Clifford, J. Cioslowski, B. B. Stefanov, G. Liu, A. Liashenko, P. Piskorz, I. Komaromi, R. L. Martin, D. J. Fox, T. Keith, M. A. Al-Laham, C. Y. Peng, A. Nanayakkara, M. Challacombe, P. M. W. Gill, B. Johnson, W. Chen, M. W. Wong, C. Gonzalez, and J. A. Pople, *Gaussian 03*, Revision E.01, Gaussian, Inc., Wallingford CT, **2004**.

[8] (a) P. J. Hay, W. R. Wadt, *J. Chem. Phys.* **1985**, *82*, 284; (b) C. E. Check, T. O. Faust, J. M. Bailey, B. J. Wright, T. M. Gilbert, L.S. Sunderlin, *J Phys. Chem. A* **2001**, *105*, 8111; (c) L. E. Roy, P. J. Hay, R. L. Martin, *J. Chem. Theory Comput.* **2008**, *4*, 1029.

[9] (a) R. Krishnan, J. S. Binkley, R. Seeger, J. A. Pople, *J. Chem. Phys.* **1980**, *72*, 650; (b) T. Clark, J. Chandrasekhar, P. v. R. Schleyer, *J. Comput. Chem.* **1983**, *4*, 294.

[10] (a) R. Krishnan, J. S. Binkley, R. Seeger, J.A. Pople, *J. Chem. Phys.* **1980**, *72*, 650; (b) A. D. McLean, G. S. Chandler, *J. Chem. Phys*. **1980**, *72*, 5639; (c) L. A. Curtiss, M. P. McGrath, J-P. Blandeau, N. E. Davis, R. C. Binning, Jr., L. Radom, *J. Chem. Phys.* **1995**, *103*, 6104; (d) M. N. Glukhovstev, A. Pross, M. P. McGrath, L. Radom, *J. Chem. Phys.* **1995**, *103*, 1878.

H. Computational section of chapter 5

H.1) Details and theory

DFT structure optimizations were performed with the Turbomole program,[1] adopting the multiple "M3" grid size for the density fitting and a SCF convergence criterion of 1×10^{-7} E_h. The initial geometries were fully optimized with the hybrid exchange-correlation functional PBE0.[2] As Gaussian AO basis for all atoms, all-electron split valence SV(P) sets of def2-type[3] were employed (Basis Set System I, which is denoted as BS-I). The vibrational frequencies were evaluated on the DFT-optimized geometries at the same method of theory to verify their status as true minima on the potential energy surfaces.

All other computations were carried out on PBE0 optimized geometries using the Gaussian 03 program package.[4] The energies, the Nucleus Independent Chemical Shifts (NICS) and the polarizabilities of the molecular systems were calculated using the hybrid MW1PW91 density functional[5] employed with Los Alamos National Laboratory 2 (LANL2) relativistic effective core potential (RECP) and the split-valence (double-ζ) quality basis sets. The LANL2DZ basis set was augmented by adding one set of a polarization d function [LANL2DZd].[6] For O, C, Li and H atoms, all-electron split-valence 6-311G(d,p) basis sets were employed.[7] The combination of LANL2DZd and 6-311G(d,p) is denoted as Basis Set System II (BS-II). NICS-computations[8] were carried out at the cage centers of compounds on their DFT optimized geometries.

H.2) References

[1] R. Ahlrichs, M. Bär, M. Häser, H. Horn, C. Kölmel, *Chem. Phys. Lett.* **1989**, *162*, 165.

[2] C. Adamo, V. Barone, *J. Chem. Phys.* **1999**, *110*, 6158.

[3] (a) B. Metz, H. Stoll, M. Dolg, *J. Chem. Phys.* **2000**, *113*, 2563; (b) F. Weigend, R. Ahlrichs, *Phys. Chem. Chem. Phys.* **2005**, *7*/*18*, 3297.

[4] M. J. Frisch, G. W. Trucks, H. B. Schlegel, G. E. Scuseria, M. A. Robb, J. R. Cheeseman, J. A. Montgomery, Jr., T. Vreven, K. N. Kudin, J. C. Burant, J. M. Millam, S. S. Iyengar, J. Tomasi, V. Barone, B. Mennucci, M. Cossi, G. Scalmani, N. Rega, G. A. Petersson, H. Nakatsuji, M. Hada, M. Ehara, K. Toyota, R. Fukuda, J. Hasegawa, M. Ishida, T. Nakajima, Y. Honda, O. Kitao, H. Nakai, M. Klene, X. Li, J. E. Knox, H. P. Hratchian, J. B. Cross, V. Bakken, C. Adamo, J. Jaramillo, R. Gomperts, R. E. Stratmann, O. Yazyev, A. J. Austin, R. Cammi, C. Pomelli, J. W. Ochterski, P. Y. Ayala, K. Morokuma, G. A. Voth, P. Salvador, J. J. Dannenberg, V. G. Zakrzewski, S. Dapprich, A. D. Daniels, M. C. Strain, O. Farkas, D. K. Malick, A. D. Rabuck, K. Raghavachari, J. B. Foresman, J. V. Ortiz, Q. Cui, A. G. Baboul, S.

Clifford, J. Cioslowski, B. B. Stefanov, G. Liu, A. Liashenko, P. Piskorz, I. Komaromi, R. L. Martin, D. J. Fox, T. Keith, M. A. Al-Laham, C. Y. Peng, A. Nanayakkara, M. Challacombe, P. M. W. Gill, B. Johnson, W. Chen, M. W. Wong, C. Gonzalez, and J. A. Pople, *Gaussian 03*, Revision E.01, Gaussian, Inc., Wallingford CT, **2004**.

[5] (a) J. P. Perdew, In *Electronic Structure of Solids '91*; P. Ziesche, H. Eschig, Eds.; Akademie Verlag: Berlin, **1991**, 11; (b) C. Adamo, V. Barone, *J. Chem. Phys.* **1998**, *108*, 664; (c) B. J. Lynch, Y. Zhao, D. G. Truhlar, *J. Phys. Chem. A* **2003**, *107*, 1384.

[6] (a) P. J. Hay, W. R. Wadt, *J. Chem. Phys.* **1985**, *82*, 270; (b) P. J. Hay, W. R. Wadt, *J. Chem. Phys.* **1985**, *82*, 284; (c) P. J. Hay, W. R. Wadt, *J. Chem. Phys.* **1985**, *82*, 299; (d) C. E. Check, T. O. Faust, J. M. Bailey, B. J. Wright, T. M. Gilbert, L. S. Sunderlin , *J. Phys. Chem. A* **2001**, *105*, 8111.

[7] R. Krishnan, J. S. Binkley, R. Seeger, J. A. Pople, *J. Chem. Phys.* **1980**, *72*, 650.

[8] NICS-Nucleus Independent Chemical Shifts: P. von R. Schleyer, C. Maerker, A. Dransfeld, H. Jiao, N. J. R. van Eikema Hommes, *J. Am. Chem Soc.* **1996**, *118*, 6317.

Crystals Data and Structure Refinement Details

Table 1. Crystallographic data of $Li(thf)_3SiPh_2tBu$ (CCDC-742475)

Empirical formula	$C_{28}H_{43}LiO_3Si$
Formula weight [g/mol]	462.32
Temperature [K]	200
Crystal color	pale yellow-green
Crystal size [mm^3]	0.37 × 0.35 × 0.24
Crystal system	monoclinic
Space group	$P2_1/n$
a [pm]	1018.6(2)
b [pm]	1711.3(3)
c [pm]	4808(1)
β [°]	90.08(3)
V [$Å^3$]	8381(3)
Z	12
D_{calc} [Mg/m^3]	1.099
μ (Mo-*K*α) [mm^{-1}]	0.109
F(000)	3020
θ-range [°]	2.04 – 26.13
Numerical absorption correction	T_{min} = 0.9618, T_{max} = 0.9832
Index ranges	$-12 \le h \le 12$ $-21 \le k \le 21$ $-59 \le l \le 59$
Reflections collected	36694
Independent reflections	14556
Observed refl. [$I > 2\sigma(I)$]	6160
Data/restraints/parameters	14556/0/912
Goodness-of-fit (S) on F^2	0.842
Final *R* indices [$I > 2\sigma(I)$]	$R1$ = 0.0630 wR_2 = 0.1291
R indices (all data)	$R1$ = 0.1463 wR_2 = 0.1553
Largest diff. peak/hole [e $Å^{-3}$]	0.214/–0.192

Table 2. Crystallographic data of (tBuPh$_2$Si)$_4$Bi$_2$·2(C$_6$H$_5$Me) (CCDC-742476)

Empirical formula	$C_{78}H_{92}Bi_2Si_4$
Formula weight [g/mol]	1559.84
Temperature [K]	200
Crystal color	dark red
Crystal size [mm^3]	0.30 × 0.16 × 0.07
Crystal system	triclinic
Space group	$P\bar{1}$
a [pm]	1368.8(3)
b [pm]	1421.5(3)
c [pm]	1848.0(4)
α [°]	96.01(3)
β [°]	92.84(3)
γ [°]	101.42(3)
V [Å^3]	3496(1)
Z	2
D_{calc} [Mg/m^3]	1.482
μ (Mo-$K\alpha$) [mm^{-1}]	5.137
F(000)	1564
θ-range [°]	2.52 – 30.63
Numerical absorption correction	T_{min} = 0.255, T_{max} = 0.674
Index ranges	$-19 \le h \le 19$ $-20 \le k \le 19$ $-26 \le l \le 26$
Reflections collected	42336
Independent reflections	19419
Observed refl. [$I > 2\sigma(I)$]	9297
Data/restraints/parameters	19419/0/757
Goodness-of-fit (S) on F^2	0.774
Final R indices [$I > 2\sigma(I)$]	$R1$ = 0.0515, wR_2 = 0.1055
R indices (all data)	$R1$ = 0.1249, wR_2 = 0.1235
Largest diff. peak/hole [e Å^{-3}]	0.258/–0.307

Table 3. Crystallographic data of (tBuPh$_2$Si)$_2$BiBr (CCDC-742477)

Empirical formula	$C_{32}H_{38}BiBrSi_2$
Formula weight [g/mol]	767.69
Temperature [K]	200
Crystal color	red
Crystal size [mm^3]	0.41 × 0.14 × 0.06
Crystal system	orthorhombic
Space group	$P2_12_12_1$
a [pm]	1044.1(2)
b [pm]	1150.9(2)
c [pm]	2526.2(5)
V [Å^3]	3035(1)
Z	4
D_{calc} [Mg/m^3]	1.680
μ (Mo-$K\alpha$) [mm^{-1}]	7.223
F(000)	1504
θ-range [°]	2.11 – 28.15
Numerical absorption correction	T_{min} = 0.1945, T_{max} = 0.5230
Index ranges	$-13 \le h \le 13$ $-15 \le k \le 14$ $-33 \le l \le 33$
Reflections collected	29770
Independent reflections	7354
Observed refl. [$I > 2\sigma(I)$]	6592
Data/restraints/parameters	7354/0/326
Goodness-of-fit (S) on F^2	0.923
Final R indices [$I > 2\sigma(I)$]	$R1$ = 0.0248, wR_2 = 0.0509
R indices (all data)	$R1$ = 0.0307, wR_2 = 0.0521
Largest diff. peak/hole [e Å^{-3}]	0.112/–0.548

Table 4. Crystallographic data of $In(SiPh_2tBu)_3$ (CCDC-728998)

Empirical formula	$C_{48}H_{57}InSi_3$
Formula weight [g/mol]	833.0
Temperature [K]	153
Crystal size [mm^3]	0.42 × 0.23 × 0.22
Crystal system	triclinic
Space group	$P\bar{1}$
a [pm]	999.9(2)
b [pm]	1189.3(2)
c [pm]	1865.1(4)
α [°]	87.01(3)
β [°]	86.06(3)
γ [°]	78.24(3)
V [$Å^3$]	2164.8(8)
Z	2
D_{calc} (mg/m^3)	1.278
μ (Mo Kα) (mm^{-1})	0.66
F(000)	872
θ-range [°]	2.5 – 27.5
Index ranges	$-12 \le h \le 12$,
	$-15 \le k \le 15$,
	$-24 \le l \le 24$
Reflections collected	20 226
Data/restraints/parameters	9234/0/478
Goodness-of-fit (S) on F^2	0.834
Final *R* indices [$I > 2\sigma(I)$]	$R_1 = 0.0378$,
	$wR_2 = 0.0788$
R indices (all data)	$R_1 = 0.0584$,
	$wR_2 = 0.0827$
Largest diff. peak and hole [e $Å^{-3}$]	0.64/−0.64

Table 5. Crystallographic data of (tBuPh$_2$Si)$_2$ (CCDC-742909)

Empirical formula	$C_{32}H_{38}Si_2$
Formula weight [g/mol]	478.80
Temperature [K]	200(2)
Crystal size [mm^3]	0.34 × 0.15 × 0.13
Crystal system	monoclinic
Space group	$P2_1/c$
a [pm]	857.20(17)
b [pm]	1016.2(2)
c [pm]	1550.1(3)
β [º]	95.83(3)
V [Å^3]	1343.2(5)
Z	2
D_{calc} (Mg/m^3)	1.184
μ (Mo Kα) (mm^{-1})	0.151
F(000)	516
θ-range [°]	2.39 − 24.14
Index ranges	$-9 \le h \le 9$,
	$-11 \le k \le 11$,
	$-17 \le l \le 17$
Reflections collected	8504
Numerical absorption correction	T_{min} = 0.9652,
	T_{max} = 0.9827
Data/restraints/parameters	2093/0/154
Goodness-of-fit (S) on F^2	0.880
Final R indices [$I > 2\sigma(I)$]	$R1$ = 0.0433
	$wR2$ = 0.0960
R indices (all data)	$R1$ = 0.0714
	$wR2$ = 0.1020
Largest diff. peak and hole [e Å^{-3}]	0.427/−0.186

Table 6. Crystallographic data of $[n\mathrm{Bu_4N}]_4[\mathrm{Bi_4Fe_8(CO)_{28}}]\cdot 6(\mathrm{thf})$ (CCDC-767166)

Empirical formula	$C_{92}H_{144}Bi_4Fe_8O_{28}N_4\cdot(C_4H_8O)_6$
Formula weight [g/mol]	3469.46
Crystal size [mm^3]	0.52 × 0.38 × 0.35
Crystal system	orthorhombic
Space group	*Pba*2
a [pm]	2184.1(4)
b [pm]	2269.3(5)
c [pm]	1513.3(3)
V [$Å^3$]	7501(3)
Z	4
D_{calc} (g/cm^3)	1.536
μ (Mo Kα) (mm^{-1})	5.49
F(000)	3456
θ-range [°]	2 – 28
Index ranges	$-27 \le h \le 27$,
	$-29 \le k \le 29$,
	$-19 \le l \le 11$
Reflections collected	37959
Numerical absorption correction	T_{min} = 0.151,
	T_{max} = 0.241
Data/restraints/parameters	14007/31/748
Goodness-of-fit (S) on F^2	0.96
Final *R* indices [$I > 2\sigma(I)$]	R_1 = 0.053,
	wR_2 = 0.130
R indices (all data)	R_1 = 0.075,
	wR_2 = 0.141
Largest diff. peak and hole [e $Å^{-3}$]	3.40/–2.59

Table 7. Crystallographic data of $[Bi_4Fe_3(CO)_9]\cdot 2(C_6H_5Me)$

Empirical formula	$C_{23}H_{16}Bi_4Fe_3O_9$
Formula weight [g/mol]	1439.83
Crystal size [mm^3]	0.22 × 0.20 × 0.12
Crystal system	monoclinic
Space group	$P2_1/n$
a [pm]	1144.5(2)
b [pm]	1819.0(4)
c [pm]	1464.7(3)
β [º]	95.14(3)
V [$Å^3$]	3037.2(10)
Z	4
D_{calc} (g/cm^3)	3.149
μ (Mo Kα) (mm^{-1})	24.528
F(000)	2544
θ-range [°]	2.64 – 26.00
Index ranges	$-14 \le h \le 14$
	$-22 \le k \le 22$
	$-18 \le l \le 18$
Reflections collected	24143
Numerical absorption correction	T_{min} = 0.994,
	T_{max} = 0.997
Data/restraints/parameters	5679/0/352
Goodness-of-fit (S) on F^2	0.915
Final *R* indices [$I > 2\sigma(I)$]	R_1 = 0.066,
	wR_2 = 0.152
R indices (all data)	R_1 = 0.089,
	wR_2 = 0.160
Largest diff. peak and hole [e $Å^{-3}$]	7.658/–7.545

Table 8. Crystallographic data of $[(Cp^*)_5Bi_6Cl_{12}][(thf)_2Bi_2Cl_7]$

Empirical formula	$C_{58}H_{91}O_2Bi_8Cl_{19}$
Formula weight [g/mol]	3165.70
Temperature [K]	200(2)
Crystal size [mm^3]	0.20 × 0.20 × 0.06
Crystal system	monoclinic
Space group	*Cc*
a [pm]	2609.2(5)
b [pm]	1231.3(3)
c [pm]	2828.2(6)
β [°]	91.95(3)
V [$Å^3$]	9080(3)
Z	4
D_{calc} (g/cm^3)	2.316
μ (Mo Kα) (mm^{-1})	16.038
Transmission factors	T_{min} = 0.1818,
	T_{max} = 0.2034
F(000)	5768
θ-range [°]	2.31 – 26.00
Index ranges	$-32 \le h \le 32$
	$-15 \le k \le 15$
	$-31 \le l \le 34$
Reflections collected	32329
Independent reflections	16979
Observed refl. [$I > 2\sigma(I)$]	13778
Data/restraints/parameters	16979/2/770
Goodness-of-fit (S) on F^2	0.987
Final *R* indices [$I > 2\sigma(I)$]	0.0623
	0.1461
R indices (all data)	0.0739
	0.1512
Largest diff. peak and hole [e $Å^{-3}$]	3.794 /–3.093

Table 9. Crystallographic data of [Cp*$BiBr_2$]

Empirical formula	$C_{10}H_{15}BiBr_2$
Formula weight [g/mol]	504.02
Temperature [K]	200(2)
Crystal size [mm^3]	0.22 × 0.16 × 0.14
Crystal system	orthorhombic
Space group	$P2_12_12_1$
a [pm]	831.25(17)
b [pm]	964.93(19)
c [pm]	1612.7(3)
V [$Å^3$]	1293.6(4)
Z	4
D_{calc} [$g \cdot cm^{-3}$]	2.588
μ (Mo Kα) [mm^{-1}]	19.767
F(000)	912
θ-range [°]	2.76 – 27.49
Numerical absorption correction	T_{min} = 0.0686,
	T_{max} = 0.1609
Index ranges	$-10 \leq h \leq 10$
	$-12 \leq k \leq 12$
	$-20 \leq l \leq 20$
Reflections collected	12075
Independent reflections	2974
Observed refl. [$I > 2\sigma(I)$]	2788
Data/restraints/parameters	2974/0/123
Goodness-of-fit (S) on F^2	1.024
Final *R* indices [$I > 2\sigma(I)$]	$R1$ = 0.0330,
	wR_2 = 0.0768
R indices (all data)	$R1$ = 0.0359,
	wR_2 = 0.0777
Largest diff. peak/hole [e $Å^{-3}$]	3.367/–1.740

Table 10. Crystallographic data of $[\{(Cp^*)_5Bi_5Br_9\}\{Bi_2Br_8\}_{0.5}]\cdot 3(CH_2Cl_2)$

Empirical formula	$C_{53}H_{82}Bi_6Br_{13}Cl_6$
Formula weight [g/mol]	3224.60
Temperature [K]	200(2)
Crystal size [mm^3]	0.28 × 0.13 × 0.07
Crystal system	triclinic
Space group	$P\bar{1}$
a [pm]	1484.4(3)
b [pm]	1493.5(3)
c [pm]	2289.4(5)
α [°]	75.71(3)
β [°]	76.26(3)
γ [°]	88.72(3)
V [$Å^3$]	4774.2(17)
Z	2
D_{calc} [$g\cdot cm^{-3}$]	2.243
μ (Mo Kα) [mm^{-1}]	16.653
F(000)	2910
θ-range [°]	2.52 – 30.46
Index ranges	$-21 \le h \le 21$
	$-20 \le k \le 21$
	$-32 \le l \le 30$
Reflections collected	57237
Independent reflections	26323
Observed refl. [$I > 2\sigma(I)$]	12300
Data/restraints/parameters	26323/76/757
Goodness-of-fit (S) on F^2	0.846
Final *R* indices [$I > 2\sigma(I)$]	0.0623
	0.1501
R indices (all data)	0.1424
	0.1767
Largest diff. peak/hole [e $Å^{-3}$]	3.892/–3.448

Table 11. Crystallographic data of [Cp*BiI_2]

Empirical formula	$C_{10}H_{15}BiI_2$
Formula weight [g/mol]	598.00
Temperature [K]	200(2)
Crystal size [mm^3]	0.37 × 0.05 × 0.05
Crystal system	orthorhombic
Space group	$P2_12_12_1$
a [pm]	843.64(17)
b [pm]	986.0(2)
c [pm]	1695.6(3)
V [$Å^3$]	1410.4(5)
Z	4
D_{calc} [$g \cdot cm^{-3}$]	2.816
μ (Mo Kα) [mm^{-1}]	16.841
F(000)	1056
θ-range [°]	2.39 – 27.93
Numerical absorption correction	T_{min} = 0.3344,
	T_{max} = 0.5206
Index ranges	$-10 \leq h \leq 10$
	$-12 \leq k \leq 12$
	$-22 \leq l \leq 22$
Reflections collected	13516
Independent reflections	3286
Observed refl. [$I > 2\sigma(I)$]	2090
Data/restraints/parameters	3286/6/119
Goodness-of-fit (S) on F^2	0.802
Final *R* indices [$I > 2\sigma(I)$]	$R1$ = 0.0382,
	wR_2 = 0.0738
R indices (all data)	$R1$ = 0.0707,
	wR_2 = 0.0790
Largest diff. peak/hole [e $Å^{-3}$]	1.333/–2.809

Eidesstattliche Erklärung gemäß § 8 Abs. 3 b) und c) der Promotionsordnung:

Ich erkläre hiermit, dass ich die vorliegende Dissertation selbst verfasst und mich dabei keiner anderen als der von mir ausdrücklich bezeichneten Quellen und Hilfen bedient habe. Ich erkläre weiterhin, dass ich an keiner anderen Stelle ein Prüfungsverfahren beantragt bzw. die Dissertation in dieser oder anderer Form bereits anderweitig als Prüfungsarbeit verwendet oder einer anderen Fakultät als Dissertation vorgelegt habe.

Heidelberg, den 20. Mai 2010

_____

(Kirill Yu. Monakhov)